1-1-2012

Linear and non-linear deformations of a wind turbine blade considering warping and all aeroelastic load couplings

Fouad Mohammad Mohammad
Wayne State University,

LINEAR AND NON-LINEAR DEFORMATIONS OF A WIND TURBINE BLADE CONSIDERING WARPING AND ALL AEROELASTIC LOAD COUPLINGS

by

FOUAD MOHAMMAD MOHAMMAD

DISSERTATION

Submitted to the Graduate School

of Wayne State University,

Detroit, Michigan

in partial fulfillment of the requirements

for the degree of

DOCTOR OF PHILOSOPHY

2012

MAJOR: MECHANICAL ENGINEERING

Approved by

Advisor	**Date**

DEDICATION

Dedicated to

GOD

(The Reason of Everything)

then to

… my parents,

my wife & my kids,

my country: Canada,

my motherland: Palestine,

& in loving memory of my grandparents

ACKNOWLEDGEMENTS

I would like to express my deepest gratitude to my professor, Dr. Emmanuel Ayorinde, without whom this work would not be possible, for giving me this opportunity, for all his teachings, his insight, warm advice and guidance.

I thank the members of my PhD dissertation committee: Prof. Xin Wu, Prof. Tawfik Khalil and Prof. Hwai-Chung Wu for their guidance and suggestions. I also thank Prof. Trilochan Singh for all his advice and support.

I am grateful to all my students of the ME-7020 class for their encouragement and to all my friends at Wayne State University for being the surrogate family during the many years I stayed there. To mention few: from the department staff: Ms. Stephanie A. Sepko and Ms. Rosalind Willis and from the engineering library: Ms Sherry Barclay.

Special thanks go to Prof. Ronald M Barron at University of Windsor for answering my questions on some numerical iteration schemes, to Dr. Alan Wright at NREL for directing me to many great wind turbine references and to Mr. Marshall L. Buhl Jr. at NREL for answering my questions on some NREL wind turbine codes such as FAST and Precomp.

Finally, I am forever indebted to: My parents (Jawhara Mansour and Mohammad Mohammad) for their endless encouragement. My wife (Nariman Al-Attal) for her endless care and support- at all times. My kids (Mohammad, Jawhara, Zakareya and Taha) for their endless patience when it was most needed.

PREFACE

A wind turbine blade similar to a helicopter rotor blade has the structure of a pretwisted beam of a variable airfoil asymmetrical cross-section. A number of approximate theories have been developed by different researchers to study the dynamic behavior of the blade of a horizontal axis wind turbine that reacts due to axial, torsional and flexural aerodynamic loadings and to the coupling interactions among all of these loadings. The new contribution in this present research is the consideration of all the extensional, torsional and flexural loadings with their couplings, variable airfoil cross sections with warping effects, shear deflection, rotary inertia and with or without blade's pretwist for both the linear small deformation case and the nonlinear large deformation case. To the best knowledge of the author the simultaneous inclusion of all these factors has not been done before. The mass matrix, linear and nonlinear stiffness matrices and the load vector (function of time step) of the dynamic equations of motion are deduced from the Lagrange equations of motion that were derived step by step.

The steps of the linear and nonlinear Newmark implicit iteration schemes used for solving the dynamic equations of motion respectively were explained in detail. Numerical implementation examples for both linear and nonlinear cases were demonstrated for a 14m long blade with and without pretwisting that has specific material and geometrical properties and a decreasing NACA4415 airfoil cross section from hub to tip. For both of the linear and nonlinear examples, the aerodynamic loadings (lift, drag and pitch moment) and the nonlinear stiffness matrices were computed at each time step utilizing a time dependent set of parameters such as angle of attack, material and air density, wind and blade speed, flow angle, yaw and pitch angles. Then the unknown displacements $u,\ v$ *and* w in the directions of x, y and z axes respectively, the bending rotations θ_1 *and* θ_2 about the y and z axes respectively and the torsional rotation ϕ about the x axis, were solved using the linear and nonlinear Newmark implicit iteration schemes.

TABLE OF CONTENTS

LIST OF TABLES

LIST OF FIGURES & CHARTS

NOTATIONS USED

$\dot{(\ )}$ denotes differentiation with respect to time t

$(\ )'$ denotes differentiation with respect to x

$m,\ \rho$ mass per unit length and material density respectively

g gravitational acceleration

A, L area at any cross section and length of the beam respectively

$E,\ G$ effective Young's and Shear Modulii at any cross section respectively

x coordinate distance measured along the length of the blade from root

$\bar{u}$ bulk or logitudinal displacement on line of centre-of-flexure where y and z equal to zero

u_c longitudinal displacement of particles on the line of centroids

u, v, w displacements in x, y and z directions respectively

u_i displacement field

$y\ , y_1$ dynamic displacement of flexure centre & centroid respectively in yx plane

z, z_1 dynamic displacement of flexure centre & centroid respectively in zx plane

$y\ y,\ z\ z;\ y_1\ y_1,\ z_1\ z_1$ coordinate axes through centre of flexure and centroid respectively

$\dot{y}\ \dot{z}\ ;\ \dot{y}_1\ \dot{z}_1$ coordinates measured from centre of flexure and centroid respectively

$I_{yy},\ I_{zz}$ second moment of area of cross section about $y_1\ y_1$ and $z_1\ z_1$ axes respectively

I_{yz} product moment of area of cross section about $y_1\ y_1$ and $z_1\ z_1$ axes respectively

$I_{\phi s}$ polar mass moment of inertia per unit length about centre-of-flexure axis

I_ϕ or I_α polar mass moment of inertia per unit length about centroid axis

$y_\alpha,\ z_\alpha$ distance between centre-of-flexure and centroid in y, z direction respectively

β	beam pre-twisted angle
$\theta_1,\ \theta_2$	bending rotation about the y, z axes (or in zx, zy planes) respectively
β	blade pre-twist angle at $x = L$
ϕ	dynamic torsional deflection
ς	stagger angle
K	rate of pre-twist assumed along the beam length
C	centroid center of mass axis (loci of the mass centre of the cross section)
O	center of elasticity or flexure axis (loci of the shear center of the cross section)
$EI_{yy},\ EI_{zz}$	bending (flexural) rigidities
$EI_{yz},\ \ GJ$	coupled bending (flexural) rigidity and torsional rigidity respectively
$K_1,\ K_2$	coupled flexure-torsional rigidities
$k,\ kGA$	cross section shear or shape correction factor and shear rigidity respectively
ψ, φ	cross sectional warping and Prandtl stress function respectively
η	displacement of centroid in η direction
$\eta\eta, \xi\xi$	coordinate axes through the centroid of the blade at root, tangential and normal to the plane of disc rotation respectively
ω	angular velocity
R	disc radius
$\overline{R}, etc$	$R/L, etc$
ext	external
m,n,k,l	integers that vary between 1 & M,N,K,L respectively
B.C.	boundary condition

Chapter 1

Literature Review on Blade Design & Research Objectives

1.1 Introduction

The sizes of wind turbine mills have increased significantly over the last two decades [1], as shown in Fig. 1.1.1, and will continue to do so in the coming few years to reach soon a rated power output in the range of 8–10MW and a rotor diameter about 180 m. Nowadays, the largest wind turbines have a rated power output of 5MW and rotor diameters of 126 m.

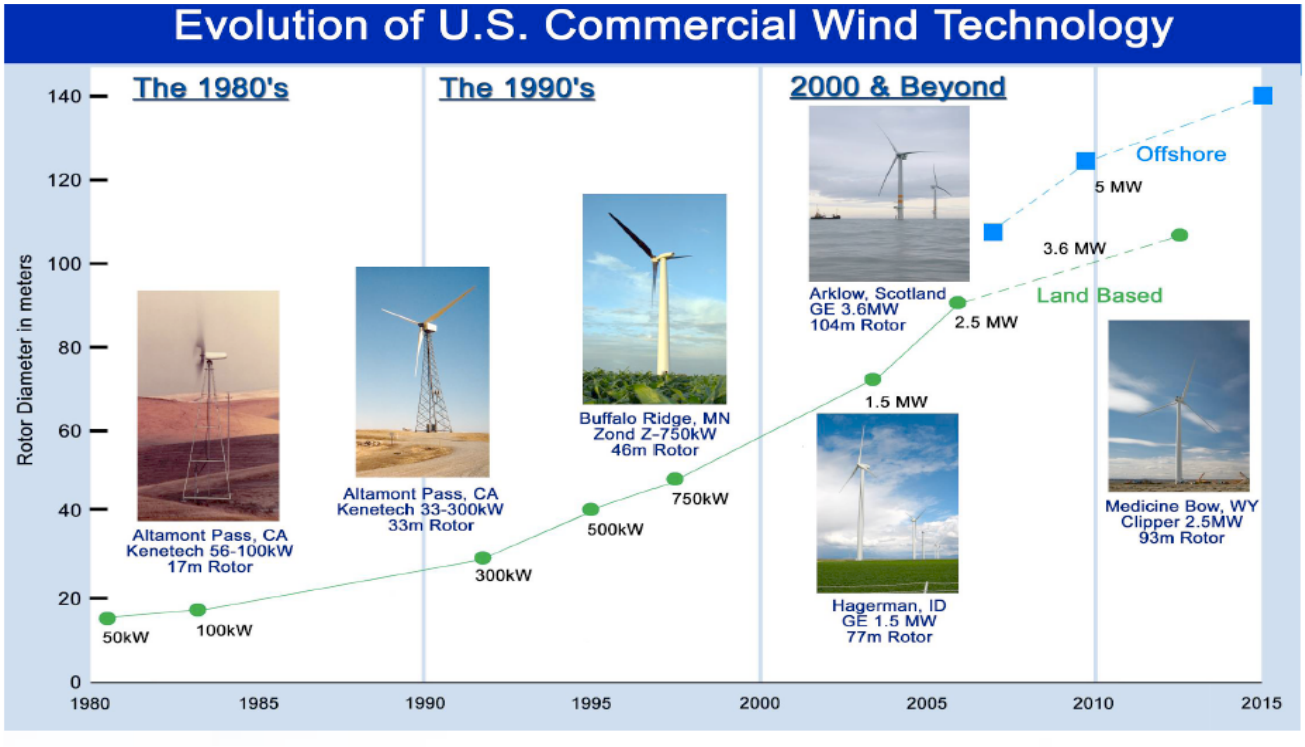

Fig. 1.1.1: The wind turbine growth [1].

The driving motivation behind this size increase is that larger wind turbines have larger energy output per unit rotor area due to increased mean wind velocity with height. Moreover, even though larger wind turbines are more expensive than smaller ones, the general trend is that the total production cost per kilowatt hour of electricity produced decreases with increasing

wind turbine size. Present design methods and the available components and materials do not allow up-scaling of wind turbine size as quoted by many designers, and to achieve the necessary up-scaling, a need exists to address a number of areas that are considered critical in achieving this, including innovative materials with a sufficient strength-to-mass ratio and structural and material design of rotors. Among the materials used in wind turbine blades manufacturing are polymer matrix composite materials, in a combination of monolithic (single skin) and sandwich composites (a special type of composite laminate where two (or more) thin, stiff, strong and relatively dense faces are separated by a thick, lightweight and compliant core material. Such sandwich composites have gained widespread acceptance as an excellent way to obtain extremely lightweight components and structures with very high bending stiffness, high strength, and high buckling resistance. Glass fiber reinforced composites (GFRP) are in use now, but for very large blades carbon fiber-reinforced composites have to be used, in addition to GFRP, to reduce the weight.

1.2 Structural Layout Design and Aerodynamic Loads

1.2.1 Design Factors

Wind turbine mills that have between two and four aerodynamically efficient rotor blades give better results than using many of them. Today's mills have three-blade rotors which are now the general trend. Similar to the wings of a plane, wind turbine blades use the airfoil shape to create lift. As shown in Fig. 1.2.1.1, the lift force is perpendicular to the direction of the motion. We want this force as big as possible. And the drag force is parallel to the direction of the motion. We want this force as small as possible.

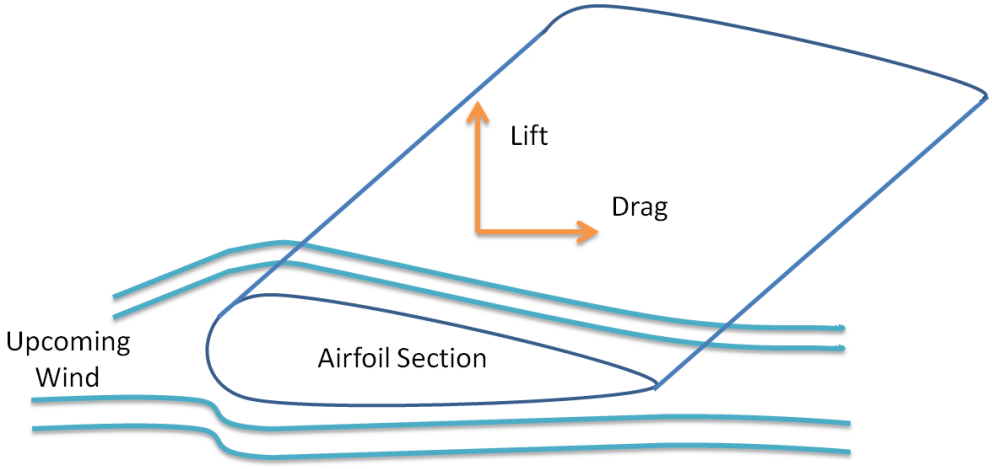

Fig. 1.2.1.1: The wind turbine airfoil (adapted from [2]).

The following are necessary design factors that should taken into consideration when designing a new blade:

1) Pretwisting of the blade:

Pretwisting Blade should be twisted and tapered since speed through the air of a point on the blade that changes along the distance from hub to tip. As shown in Fig. 1.2.1.2, the tip speed ratio varies along the blade length to optimize the angle of attack along blade length, where the blade should be twisted from root to tip. Tip-speed ratio (TSR) is the ratio of the speed of the rotating blade tip to the speed of the free stream wind. There is an optimum angle of attack which creates the highest lift to drag ratio.

$$\mathrm{TSR} = \Omega R / V$$

where,

Ω : rotational speed in radians /sec

R : Rotor Radius

V : Wind “Free Stream” Velocity

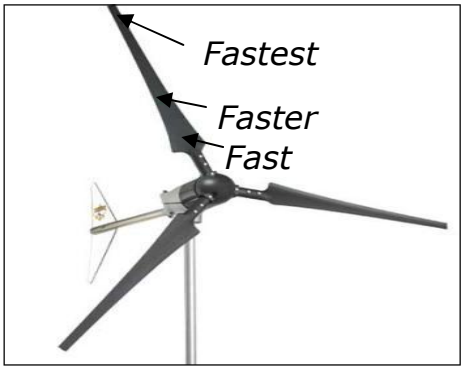

Fig. 1.2.1.2: Wind turbine blade tip-speed ratio [2].

Because the angle of attack depends on the wind speed and direction, there is an optimum tip-speed ratio.

2) Power Coefficient (Cp):

Power Coefficient (Cp) which characterize the wind turbine performance varies with the Tip Speed Ratio as shown in Fig. 1.2.1.3.

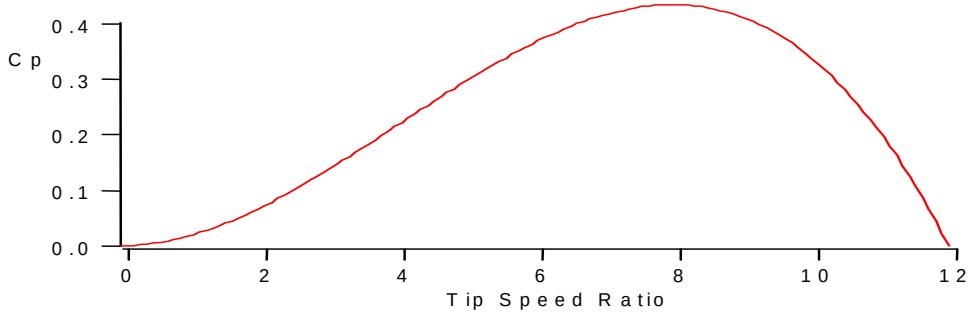

Fig. 1.2.1.3: Power coefficient versus tip-speed ratio [2].

Not all of the wind power captured by the blade rotor which lead to have some air still behind the blade rotor and not allow more wind to pass through after that. Theoretical limit (Betz limit) of rotor efficiency is 59% while most modern wind turbines [2] are in the 35 – 45% range.

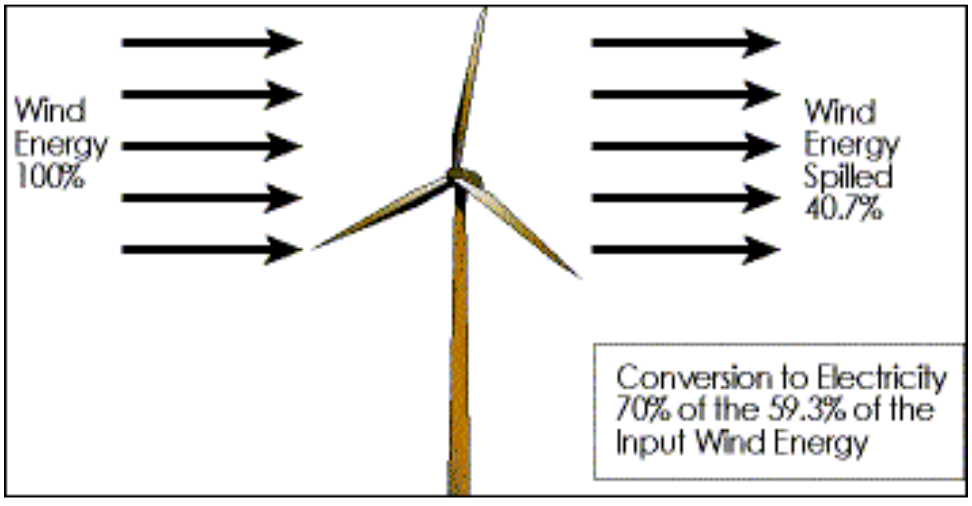

Fig. 1.2.1.4: The wind turbine efficiency [2].

Wind turbine blades should be placed on high towers of steel and / or concrete due to the fact that wind velocity and constancy increase with more height above ground. Rotors are on the upwind side of the tower, in the less turbulent air.

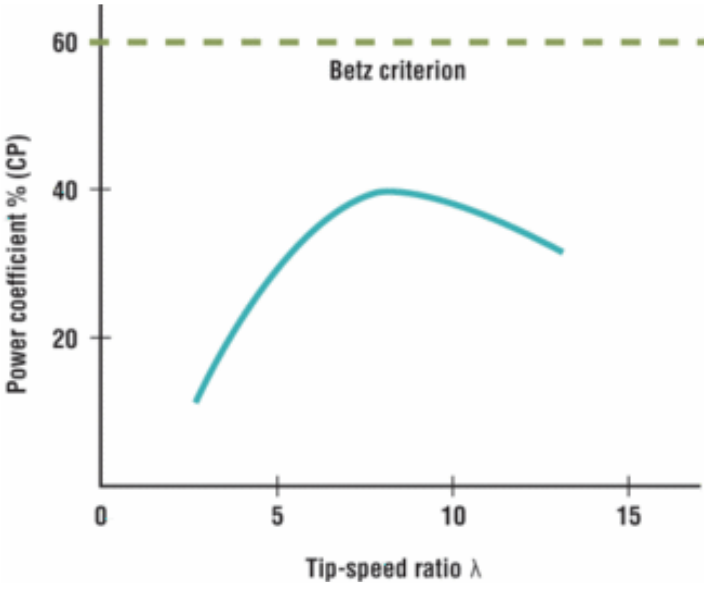

Fig. 1.2.1.5: The Betz criterion [2].

3) Minimizing the blade weight:

Power extractable from the wind is proportional to the swept area A of the rotor:

$$P = \frac{1}{2} \rho A V^2$$

where,

V: is the Wind speed

ρ: is the Air density

A: is equal to πR^2

This brings challenges that power increases with the square of blade length. The blade mass and hence bending loads are more closely related to the cube of the blade length. Since mass rises with rotor size faster than wind energy extracted, minimizing weight becomes increasingly important as turbine size increases. This implies that we can win this challenge only if we build the rotor blades with lighter composites materials including carbon fiber composite to beat the squared-cubed law. Decreasing the blade mass is also important in wind turbine design due to decreasing the load on the hub and shaft, and because the bending loads reverse at every rotational cycle, the blade structure being alternately in compression (blade vertically above the hub) and in tension (blade below). So decreasing the blade weight will decrease these forces and the fatigue-inducing effect of the continual cycling. Another load cycle is experienced due to wind gradient and the passage of blades from the bottom of the disc sweep to an area of higher wind speed at the top. Horizontal axis wind turbines would avoid this wind speed difference, but are less efficient.

4) Utilizing stiff materials:

Long blades can have large deformations with a big chance to strike the wind turbine tower as they bend backwards in response to the wind aerodynamic loadings. In addition to the aerodynamic loadings effect, the blades have an additional structural fatigue loading created by the back pressure that generated by the eddies turbulence as the blades pass

by the wind support tower. Carefully engineered composites of great performance are needed to provide fatigue resistance over design lives of 20 years or more.

Therefore, stiffness is another issue that blade manufacturers need to be met. This can be countered by incorporating both high form stiffness and stiff materials, or in some cases by 'prebending' the blades in the toward-wind direction during manufacturing.

5) Blades with controlled twisting capabilities:

Blades can also fail due to excessive loadings during severe gust winds. To avoid failing, blades are either automatically turn edgewise into wind to offer less resistance (pitch control), or are shaped so that air stops flowing smoothly across the blade surface and, on reaching a certain speed, breaks away destroying blade lift and dissipating energy (stall control).

An emerging possibility is to utilize the tailorability of composite properties to achieve bend-twist coupling, such that when a blade bends away from the direction of an applied load it also tends to twist. Given sufficient twist, this could provide an effective passive means of spilling wind. In other scenarios, some adaptive blades are made to twist when actively signalled to do so. Such mechanisms enable wind turbines to survive up to a wind gust of up to 100 mph by preventing rotors from over speeding by rotating the blade tip to act as an aerodynamic rotor brake.

6) Blade bending mode:

Another critical design issue is the frequency of blade excitation at which the blade can damage and our need to avoid coincidence between this and blade rotational frequency. Any such frequency convergence could lead to a damaging resonance condition under which bending energy is amplified. Blades are usually configured to achieve a first blade bending mode at least 1.5 times the rotational frequency of the rotor. As stiffening the blade increases

its natural (bending) frequency, over-stiffening must be avoided. Damping systems are sometimes included to reduce the effects of any incipient modal vibration.

Endurance quality of materials are also important because blades must be out in the weather, subject to wind, rain, salt, sand and dust erosion plus ultraviolet (UV). They may have to endure thermal and humidity extremes and cycling. As they are high and exposed, blades could attract lightning strikes, so effective protection is needed.

7) Acoustic issue:

Another factor, at least in well-populated developed countries, is acoustic footprint. Most of the sound is emitted by the generators, by blade tips (which on the larger blades can experience high airflow rates), and by insufficiently tapered blade trailing edges. Reinforced plastics can be used for sound-absorbent housings and nacelle covers, and they are readily molded into specific low-noise tip shapes. Environmental objectors also focus on the claimed effects of wind turbines on birds, while blades can adversely affect air traffic control radars. (In the UK, the Ministry of Defense reportedly rejects third party wind farm developments because of the radar interference.

1.2.2 Structural Design

Considering the layout of wind turbine blades [3] as shown in Fig. 1.2.2.1, Fig. 1.2.2.2 and Fig. 1.2.2.3, the following design aspects are typically adopted:

- Wing shells: The composite sandwich laminates are used towards leading and trailing edges to increase the buckling resistance (edgewise loading). For the traditional blade design, see Fig. 1.2.2.2 and Fig. 1.2.2.3 (top), the sandwich shell parts are transferred

into relatively thin monolithic composite laminates in the areas where the shells are adhesively bonded to the main spar.

- Main spar: The main spar usually extends from the root of the blade to a position close to the tip. As mentioned, the primary function of the main spar is to transfer the bladewise bending load, and thus it has to perform as a beam.
- Spar cap: The primary function of the spar cap section is to carry the flapwise bending moment, and it is usually made as a thick monolithic composite laminate, which for some large blades could be a hybrid glass/carbon composite.
- Spar flange: The primary function of these flanges are to carry the flapwise bending moment, and they are usually made as thick monolithic composite laminates, which for some large blades is made using hybrid glass/carbon composites. The main spar lay-up usually include UD-layers to provide for the bending stiffness as well as off-axis or angle-ply layers (often biaxial) to provide for the buckling resistance of the flange loaded in compression (suction side of airfoil).
- Internal webs/stiffeners: They carry the flapwise shear forces, and they are usually made as composite sandwich plates with polymeric or balsa core and relatively with biax laminate thin composite face sheets.

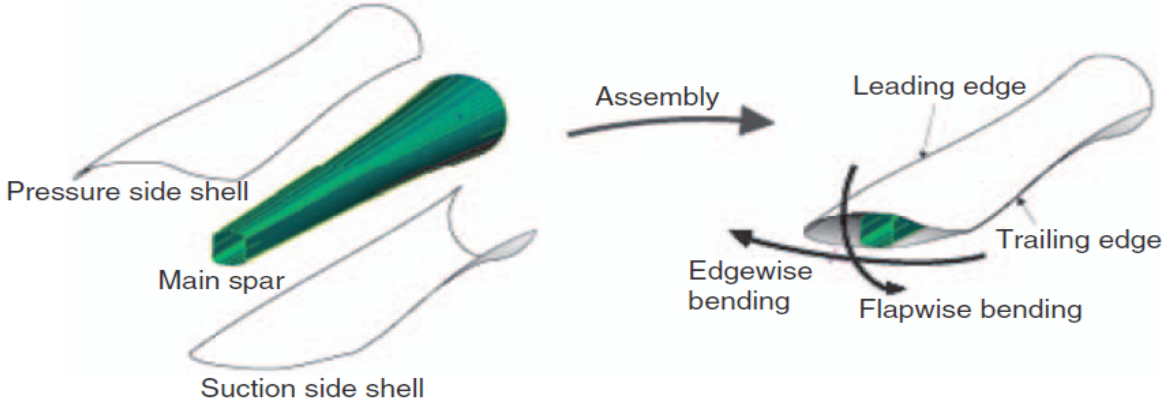

Fig. 1.2.2.1: The wind turbine blade components [3].

The sandwich design is chosen in order to enhance the resistance against in-plane shear buckling. The rotational stiffness of the corners between the flanges and the webs for the 'main spar design' is of significant importance to accommodate for sufficient buckling resistance of the flanges as well as to suppress the tendency of ovalization, the so-called Brazier effect, of the blade and main spar cross sections during flapwise bending.

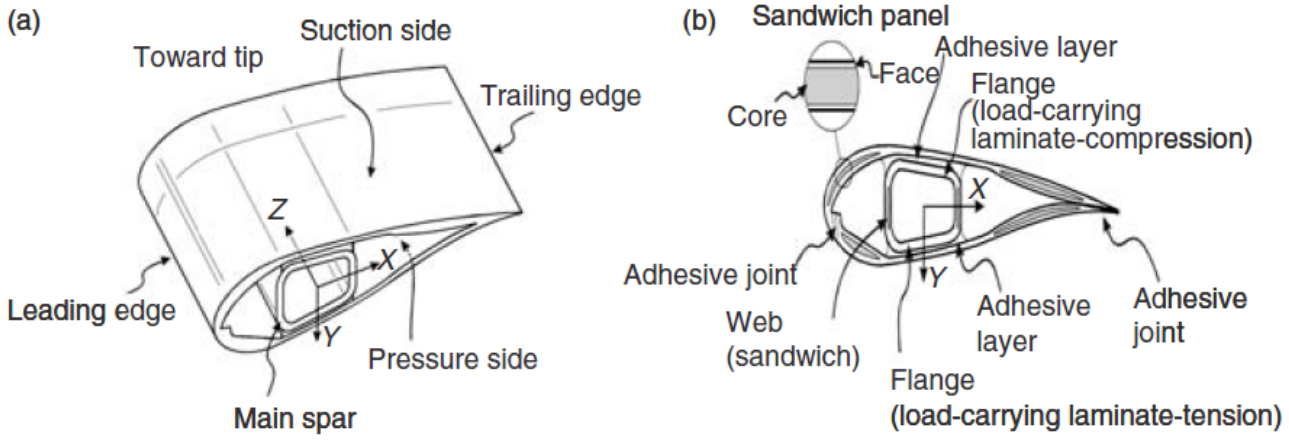

Fig. 1.2.2.2: (a) The wind turbine blade airfoil section [3].
(b) Design details of typical blade [3].

The same goes for the rotational stiffness of the joints between the spar cap and the internal webs/stiffeners for the 'spar cap/internal stiffener design', however, to a somewhat lesser degree. Various manufacturers use different design and manufacturing concepts. Alternative designs, as compared with Fig. 1.2.2.1 and Fig. 1.2.2.2, may involve that the two wing shells are joined with two or more internal webs (stiffeners) as shown schematically in Fig. 1.2.2.3.
In this conceptual design, the wing shells are manufactured with relatively thick so-called spar-caps, which are usually monolithic composite laminates. Other wind turbine manufacturers have adopted a manufacturing technique, where the entire blade structure including internal webs/stiffeners is manufactured in one single process.

Irrespective of each of the below design concepts shown in Fig. 1.2.2.3 are used, the main structural principles described earlier apply, i.e. the flapwise bending load is carried by a main spar or a 'main spar-like' structure (constituted by the spar caps and internal webs/stiffeners), and the edgewise load is carried by the shells.

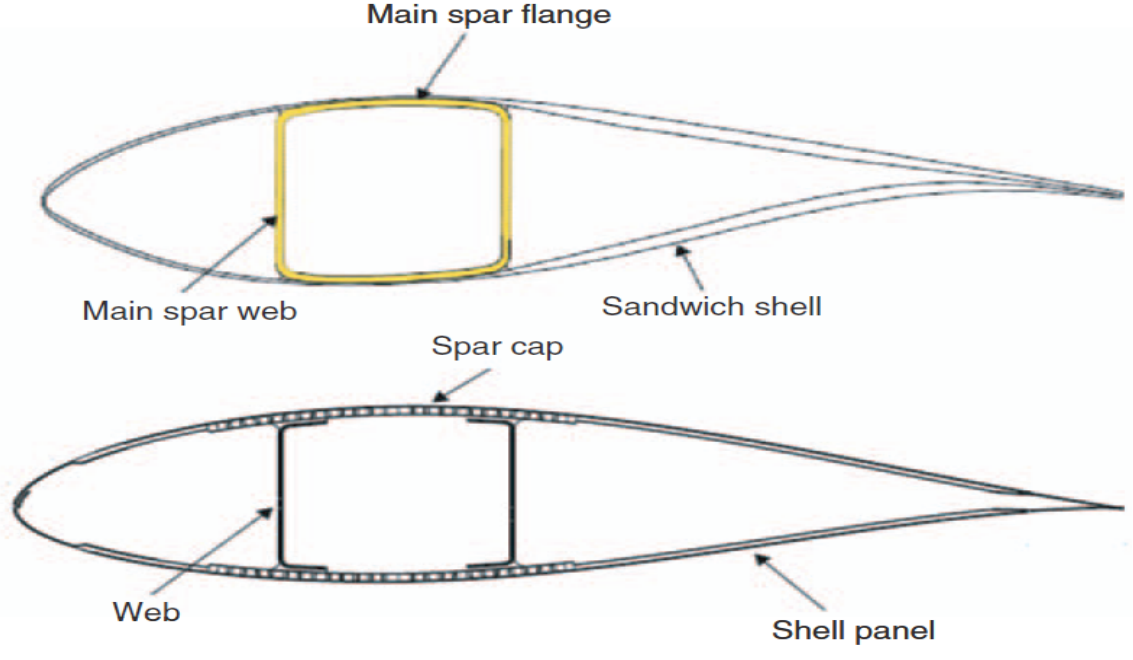

Fig. 1.2.2.3: The different blade design concepts [3]

1.2.3 Barriers in Scaling up Conventional Blade Designs

Many fundamental barriers have been analyzed for the cost-effective scaling of the current commercial blade designs and manufacturing methods over the size range of 100 m to120 m diameter. The most substantial constraint is transportation costs, and these rise sharply for lengths above 50 m (156 ft) and become prohibitive for long blades such as 60 m (187 ft). It is expected that environmental considerations will prohibit the continued use of processes with high emissions of volatile gasses, such as the open-mold wet lay-up that has been the wind industry norm.

Another manufacturing issue for large blade is the bonding compounds. As blade size becomes larger, it is natural for the gaps between bonded parts to grow also. However, the bonding materials used for smaller blades do not scale well to increasing gap sizes, and blade tooling and production costs for large blades increase rapidly as dimensional tolerances are decreased. Gravity loading is not a barrier to scaling-up of the current conventional materials and therefore blade designs over the size range are considered. However, materials and designs that reduce blade weight will be of benefit for large scale megawatt blades, as this facilitate the cost-effective of the scaling and reduce the need for reinforcements in the regions of the trailing edge and at the blade root where transitions occur.

Another issue for turbine design is the use of larger rotors at a given turbine system rating. A trend toward decreasing the power output per the unit rotor swept area (specific rating). It is expected that turbine designs with low specific rating will be of continued interest for deployment in the low wind speed sites of the Midwest United States. As specific rating is decreased (i.e. blade lengths increase at a given rating), blade stiffness and the associated tip deflections become increasingly critical for cost-effective blade design.

1.2.4 Blade Lift, Drag, Pitch Moment and Stall Phenomena

Lift, Drag and Pitch Moment

The two primary aerodynamic forces that act on wind turbine blade airfoil as shown in Fig. 1.2.4.1 are:

- The lift, which acts perpendicular to the direction of wind flow.
- The drag, which acts parallel to the direction of wind flow.
- The pitch moment around the blade length axis.

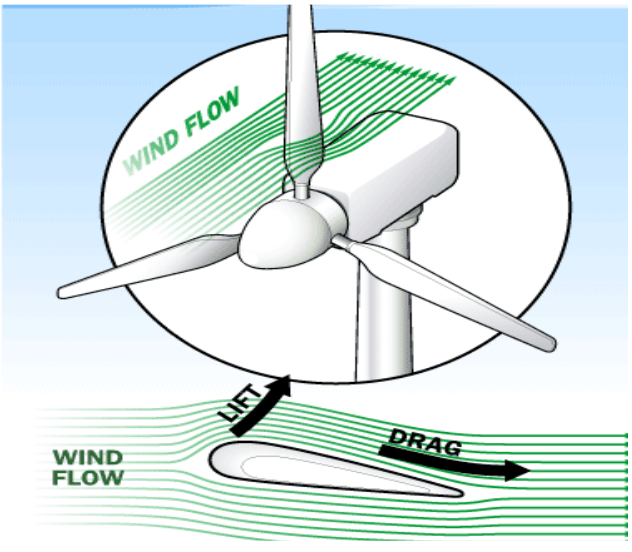

Fig. 1.2.4.1: The lift and drag forces [4].

Wind turbine blade are shaped a lot like an airplane wing. They use an airfoil design where one surface of the blade is somewhat rounded, while the other is relatively kind of flat. In one simplified explanation of lift, when wind travels over the rounded, downwind face of the blade, it has to move faster to reach the end of the blade in time to meet the wind traveling over the flat, upwind face of the blade (facing the direction from which the wind is blowing). Since faster moving air tends to rise in the atmosphere, the downwind, curved surface ends up with a low-pressure pocket just above it. The low-pressure area sucks the blade in the downwind direction, an effect known as "lift." On the upwind side of the blade, the wind is moving slower and creating an area of higher pressure that pushes on the blade, trying to slow it down. Like in the design of an airplane wing, a high lift-to-drag ratio is essential in designing an efficient turbine blade. Turbine blades are twisted so they can always present an angle that takes advantage of the ideal lift-to-drag force ratio.

Stall Phenomena

This phenomenon of stall is what happened when the wind's speed angle of attack is climbed to reach a value where all the sudden the air flow on the upper surface stops sticking to the

surface of the airfoil as shown in Fig. 1.2.4.2. Instead the air whirls around in an irregular vortex (a condition which is also known as turbulence). All of a sudden the lift from the low pressure on the upper surface of the airfoil disappears.

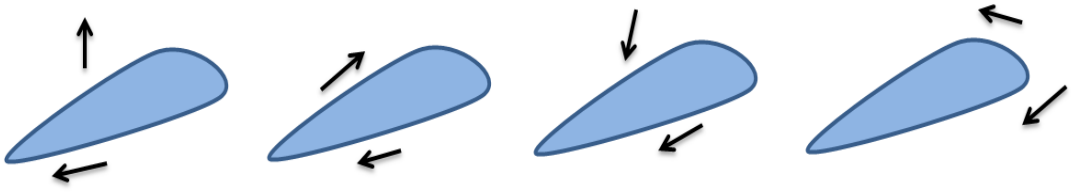

Fig. 1.2.4.2: The Flow around an Airfoil

Therefore, it is not easy to have an accurate selection of the required wind turbine blade airfoils based on the wind tunnel testing data because:

1) Most wind tunnel data sets do not contain airfoil performance in stall, which is commonly experienced by turbines operating in the field.
2) These wind tunnels have different operating conditions.

Also wind turbines are often roughened by soiling, for which there is very little data. Some recent tests have shown that dynamic stall is a common occurrence for most wind turbines operating in yawed, stalled, or turbulent conditions. Little dynamic stall data exists for the airfoils of interest to a wind turbine designer. In summary, very little airfoil performance data exits that is appropriate for wind turbine design.

These data should include airfoil performance at high angles of attack, rough leading edges (bug simulation), and steady and unsteady angles of attack. The unsteady angles of attack are a result of the blade deflections due the changes in the applied aerodynamical load. To illustrate more, let us look at below Fig.1.2.4.3 where we have taken one rotor blade off its hub, and then looking from the hub towards the tip, at the back side (the lee side) of the rotor blade.

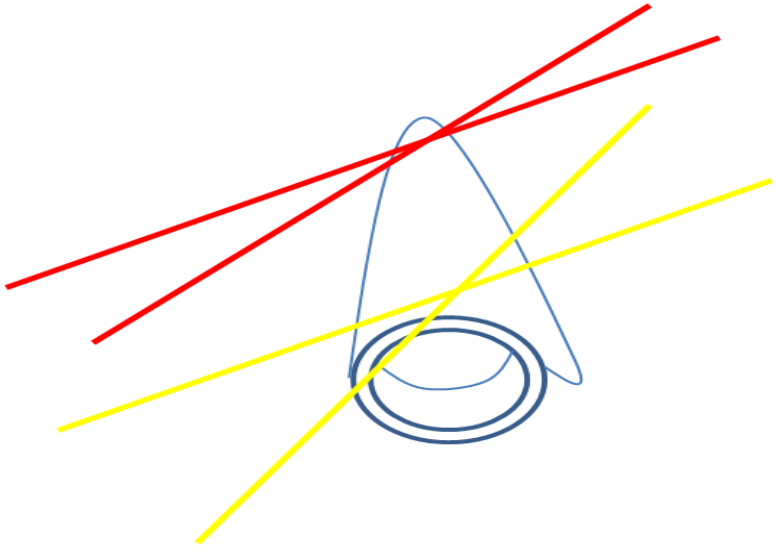

Fig. 1.2.4.3: The variation of the Angle of attack at hub and tip.

For example, consider a typical wind blowing say at 8 m/s and 16 m/s from the bottom of Fig. 1.2.4.3, the tip of the blade rotates towards the left side of the Fig. 1.2.4.3. In this Figure, we can see how the angle of attack of the wind changes much more dramatically at the root of the blade (yellow line) than at the tip of the blade (red line), as the wind changes. If the wind becomes powerful enough to make the blade stall, it will start stalling at the root of the blade.

1.2.5 Wind Turbine Blade Materials

Historically, wind turbine blades have been constructed using different materials including wood, fiberglass . But recently, most of these blades are made of fiberglass with the use of carbon fiber for some critical areas that need local reinforcement. Also the use of carbon fiber in the load-bearing spar structure of the blade has been identified as a substantial promise for cost effective weight reductions beside the increased stiffness. Analyses performed earlier by some researchers predicted mass reductions of approximately up to 30% and a cost decrease up to 15% when use the carbon fiber compared the baseline fiberglass blade. This study

assumed that the fiberglass / carbon hybrid material extended the entire length of the blade spar. Stitched hybrid fabrics and other automated technologies also have potential benefit in this area.

1.2.5.1 Different Blades Composites Manufacturing Processes

Maintaining fiber straightness (see Fig. 1.2.5.1.1) is critical to achieve desirable compressive strength properties from composite materials [1]. While carbon fibers tend to have excellent stiffness and tensile strength properties, realizing the full benefits from carbon fibers will require fabric/preform architectures that also result in good compressive strength. MSU has been testing coupons of large-tow carbon to determine compressive static strength, fatigue strength, and effect of fiber waviness on material performance.

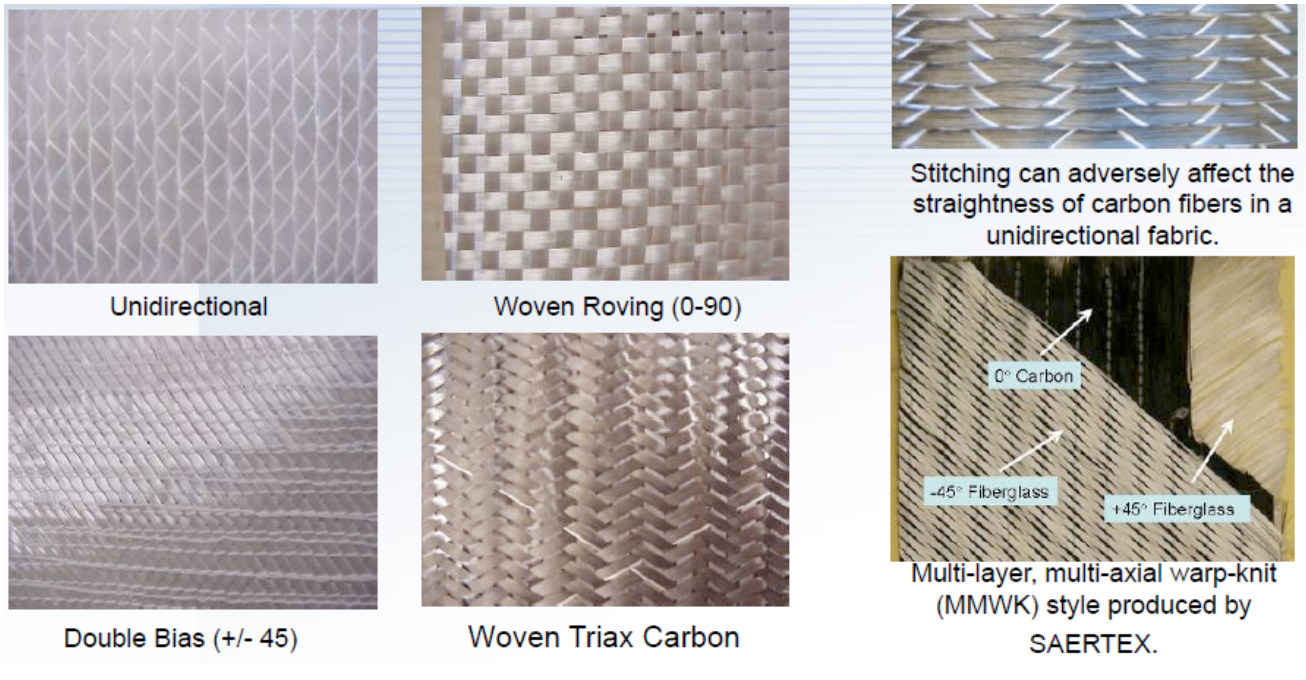

Fig. 1.2.5.1.1: Composite materials [1].

The primary bending loads shown in Fig. 1.2.5.1.2 are from aerodynamic forces, and are carried by a structural spar. In North America wind turbine design community, the spar flanges are termed “spa caps”, while European designers tend to use the term “griders”. For megawatt-scale blades, two shear webs are common, forming a box beam as shown in Figure1. Smaller blades, and some MW-scale designs, use a single shear web, or I-beam configuration. The structural spar is enclosed in two shells (skins) which form the aerodynamic profile. The skins and shear webs are typically sandwich-style laminate. The composites laminated parts are either glass or carbon fiber-reinforced polymers, while the sandwich core materials may be polymeric foams (PVC or BMI), balsa wood core or less frequently of honeycomb type.

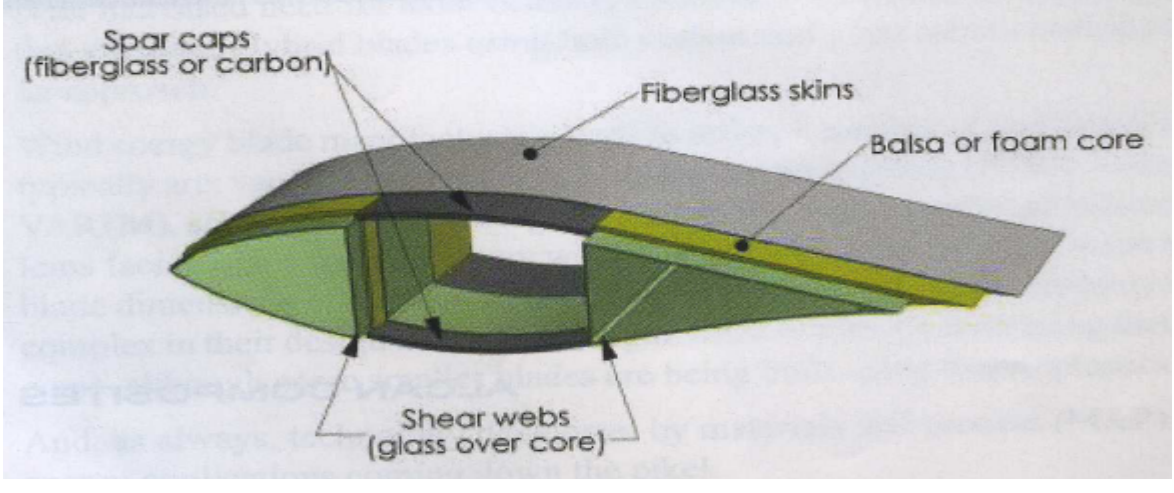

Fig. 1.2.5.1.2: The typical wind turbine blade structural layout [5].

For blade sizes up to 30 m, the most common manufacturing approach has been open mold, wet lay-up. The most notable exception to that approach is Vestas Wind Systems, which has experience in using the prepreg fiberglass for their blade manufacturing. Despite that several manufacturers are using open-mold, wet lay-up processes, become more and more stringent environmental restrictions to move manufacturers toward processes that have lower emissions.

Currently, the most common replacement for traditional methods use one of the following two methods: A) Preimpregnated materials and B) Resin infusion, with VARTM (most common infusion method). Both prepreg and VARTM materials have particular design challenges for manufacturing the relatively thick laminate that typical for large wind turbine blades. For VARTM processes, the permeability of the dry preform determines the rate of resin penetration through the material thickness. For prepreg material, sufficient bleeding is required to avoid resin-rich areas and eliminate voids from trapped gasses.

Another alternative is the partially preimpregnated fabric, marketed by SP Systems and Hexcel Composites under the name of SPRINT and HexFIT respectively. When laid-up, the dry fabric regions provide paths for air to flow, and vacuum can be used to evacuate the part prior to heating. Under heat and pressure, the resin flows into the dry fabric regions to complete the impregnation. High temperature post-cure is desirable for both prepreg and VARTM processes. Current prepreg materials require higher cure temperatures (90℃– 110℃) than epoxies used in VARTM processes (60℃–65℃). Heati ng and temperature control / monitoring becomes increasingly difficult as the laminate thickness is increased.

Mold and tooling costs are also strongly affected by the heat requirements of the cure cycle. In all cases, achieving the desired laminate quality requires a trade-off between the extent of fiber compaction, fabric/ preform architecture, resin viscosity, and the time/temperature profile of the infusion and cure cycles.

The use of automated preforming and lay-up technologies are potential alternatives to hand lay-up in the blade molds. Advantages could include improved quality control in fiber/fabric placement and a decrease in both hand labor and production cycle times. The overwhelming majority of turbine original equipment manufacturers (OEMs) and third-party blade manufacturers use a VARTM process. It is notable that the OEMs with the #1 (Vestas) and #3 (Gamesa) shares of the 2007 global market primarily use prepreg material which is the

standard process for carbon current commercial blades. The differences between the composite prepreg technology and the vacuum assisted vacuum infusion (VARTM or variations of this process) are shown below in Table 1.2.5.1.1.

Prepreg Materials	Infusion	RTM
Advantages	**Advantages**	**Advantages**
Homogeneous distribution of resin content & higher fiber volume than any other process.	Lower raw material prices.	Higher production rates.
Quality & controlled process.	Curing cycles at 60-70 C.	It is becoming an alternative for semi-structural parts.
	Improving process control every year	
Disadvantages	**Disadvantages**	**Disadvantages**
Raw material prices increase more than 30%	Difficulties to guarantee Resin flow through thick laminates and wet-out of carbon fibers.	Resin content higher-lower mechanical properties.
Logistic and storage under restrictive T/RH conditions controlled		
Long curing cycles at 120 C.	Quality- skilled labor required.	Blade surface areas are too large for one shot processes.

Table 1.2.5.1.1: The comparison between Prepreg, Infusion and RTM [1].

1.2.5.2 The Fiber Alignment in Fiber Carbon

The small Business Innovation Research (SBIR) is currently looking on alternatives to prepreg materials, by evaluating different materials with a unidirectional carbon fabric that would achieve good structural properties in a VARTM infusion process. In one scenario, the fabric may infuse well, but waviness in the fibers is a restriction for the carbon to achieve its

potential strength, particularly in compression. In the other scenario, the fabric architecture may have very good fiber alignment, but not allow resin penetration through the thickness.

For most fabric architectures, it is generally true that any feature that promotes through-the – thickness infusion will result in fiber misalignment and corresponding reductions in compressive strength. Fig. 1.2.5.2.1 shows a typical stitched unidirectional fabric using large-tow carbon fibers.

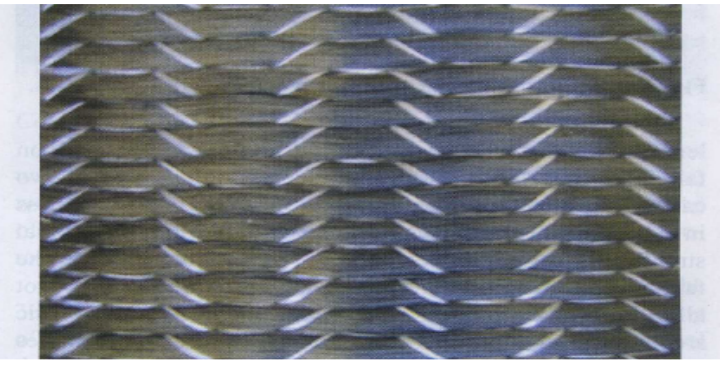

Fig. 1.2.5.2.1: Stitched unidirectional carbon fabric with induced waviness [5].

1.2.6 Varying Properties along the Blade

Wind turbine blades are built from orthotropic materials (where the material parameters are direction dependent) that are made of two or more distinct materials put together such as sandwich plates. Fiber composites are built of several layers, where each layer is composed of fiber reinforcements embedded in a continuous phase termed the matrix. In general, all layers can be made of different materials. Moreover, the direction of the fibers in each layer, according to common axes, influences on the properties of the whole composite. This makes the expressions for the effective material properties for the fiber composite more complicated, and more than two material coefficients are required.

Material Stiffness Matrix for a Single Layer

In the same way as for the isotropic thin plate, lets us assume plane stress conditions to prevail. Thus, for a single layer of unidirectional, continuous fibers, referred to local axes for the layer, it can be shown that the material stiffness matrix may be expressed as:

$$\boldsymbol{Q}_k = \begin{bmatrix} Q_{11} & Q_{12} & 0 \\ Q_{12} & Q_{22} & 0 \\ 0 & 0 & Q_{66} \end{bmatrix}, \tag{1.2.6.1}$$

where k is the layer number, and

$$\begin{aligned} Q_{11} &= \frac{E_L}{1-\nu_{LT}\nu_{TL}}, \\ Q_{22} &= \frac{E_T}{1-\nu_{LT}\nu_{TL}}, \\ Q_{12} &= \frac{\nu_{LT}E_T}{1-\nu_{LT}\nu_{TL}} = \frac{\nu_{TL}E_L}{1-\nu_{LT}\nu_{TL}}, \\ Q_{66} &= G_{LT}\,. \end{aligned} \tag{1.2.6.2}$$

The fiber direction is called the longitudinal direction (L), and the direction normal to the fibers is the transverse direction (T), see Fig. 1.2.6.1.

where,

E_L and E_T : are the elastic moduli in the longitudinal and the transverse directions, respectively

υ_{LT} : is the major Poisson ratio (give transverse strain caused by longitudinal stress)

υ_{TL} : is the minor Poisson's ratio (give the longitudinal strain resulting from a transverse stress)

G_{LT} : is the shear modulus.

These four material constants are related through this relation:

$$\frac{\nu_{LT}}{E_L} = \frac{\nu_{TL}}{E_T}$$

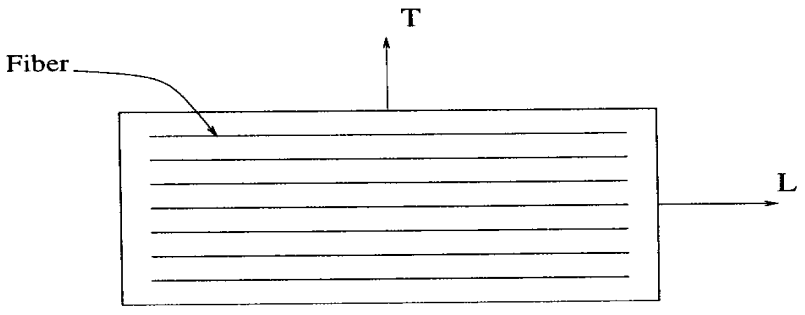

Fig. 1.2.6.1: The fiber direction in a composite build of unidirectional, continuous fibers [6].

Therefore, four independent material parameters (for each layer) are required for such orthotropic problems in 2D. Using transformation matrices, it can be shown that the matrix for a single layer, referred to global ( ) axes, is:

$$\bar{Q}_k = \begin{bmatrix} \bar{Q}_{11} & \bar{Q}_{12} & \bar{Q}_{16} \\ \bar{Q}_{12} & \bar{Q}_{22} & \bar{Q}_{26} \\ \bar{Q}_{16} & \bar{Q}_{26} & \bar{Q}_{66} \end{bmatrix} \tag{1.2.6.3}$$

where,

$$\begin{aligned}
\bar{Q}_{11} &= Q_{11}\cos^4\theta + Q_{22}\sin^4\theta + 2(Q_{12}+2Q_{66})\sin^2\theta cos^2\theta, \\
\bar{Q}_{22} &= Q_{11}\sin^4\theta + Q_{22}\cos^4\theta + 2(Q_{12}+2Q_{66})\sin^2\theta\cos^2\theta, \\
\bar{Q}_{66} &= (Q_{11}+Q_{22}-2Q_{12}-2Q_{66})\sin^2\theta\cos^2\theta + Q_{66}(\cos^4\theta+\sin^4\theta), \\
\bar{Q}_{12} &= (Q_{11}+Q_{22}-4Q_{66})\sin^2\theta\cos^2\theta + Q_{12}(\cos^4\theta+\sin^4\theta), \\
\bar{Q}_{16} &= (Q_{11}-Q_{12}-2Q_{66})\cos^3\theta\sin\theta - (Q_{22}-Q_{12}-2Q_{66})\cos\theta\sin^3\theta, \\
\bar{Q}_{26} &= (Q_{11}-Q_{12}-2Q_{66})\cos\theta\sin^3\theta - (Q_{22}-Q_{12}-2Q_{66})\cos^3\theta\sin\theta\,.
\end{aligned} \tag{1.2.6.4}$$

In these expressions ɵ is the angle between the positive global xbar axis and positive local x axis for the layer and k is the layer number. The stress-strain relation for one single layer of the composite can then be expressed as:

$$\sigma_k = \bar{Q}_k \epsilon \tag{1.2.6.5}$$

To get the material properties for the whole laminate, we sum up for all the layers i.e. integrate over the plate thickness:

$$\begin{aligned} \boldsymbol{D}_{orto} &= \sum_{k=1}^{n} \left(\begin{bmatrix} \bar{Q}_{11} & \bar{Q}_{12} & \bar{Q}_{16} \\ \bar{Q}_{12} & \bar{Q}_{22} & \bar{Q}_{26} \\ \bar{Q}_{16} & \bar{Q}_{26} & \bar{Q}_{66} \end{bmatrix}_k \int_{h_{k-1}}^{h_k} z^2 dz \right) \\ &= \frac{1}{3} \sum_{k=1}^{n} (\bar{Q}_{ij})_k (h_k^3 - h_{k-1}^3), \end{aligned} \tag{1.2.6.6}$$

where (h_k - h_{k-1}) is the thickness of layer number k. By the way, the stiffness matrix for the whole matrix is:

$$\boldsymbol{A}^{(e)} = \int_{\partial \Omega_e} \boldsymbol{B}^T \boldsymbol{D}_{orto} \boldsymbol{B} d\Gamma, \tag{1.2.6.7}$$

1.3 Research Motivation and Objectives

1.3.1 Research Motivation

Over the last two decades, continually growing energy demands as well as global warming and other pollution concerns have drawn considerable attention to the need for alternative and renewable sources of energy including the wind energy. The cutting edge technological development of wind turbine, in recent years, has been focused on the following research areas:

- Developing the blade composite materials to have more stiff but less weight blades.

- Developing new advanced methods to optimize the blade aerodynamic structure.
- Computing the aerodynamic loadings that act on the blade structure using CFD codes.

Also a number of approximate theories used for the pre-twisted beam (that is similar to helicopter rotor blades) have been developed by different researchers to analyze its complex geometry. A carefully selected sample of the relevant literature on the wind turbine blade (as explained in Chapter 4 Introduction), show that there is a need to expand the wind blade research to include more of these research factors that were taken separately in a one complete research, such factors will include:

- *Computing the load vector at each time step and the mass, stiffness matrices of the dynamic equation of motion utilizing an analytical solution and considering all the extensional, torsional and flexural loadings acting on the blade with their couplings.*
- *Variable airfoil cross-sections.*
- *Warping effects.*
- *Shear deflection, rotary inertia and with or without blade's pretwist.*
- *Formulations should include both the linear small deformation case and the nonlinear large deformation case.*

To the best knowledge of the author the simultaneous inclusion of all these factors has not been done before.

1.3.2 Research Objectives

The objective of the present work is to conduct the following research on the wind turbine blade, using an analytical energy approach:

1) New approach for computation of the aerodynamic loading that is not based on CFD codes and considering *all the extensional, torsional and flexural loadings and their couplings acting on the blade at every given time step. This approach utilize the blade airfoils wind tunnel data to compute the aerodynamic parameters from the given angle of attack(s) at each time step.*
2) *Derivation of the total strain energy, total kinetic energy and external work assuming that variable airfoil cross sections with warping effects, shear deflection, rotary inertia and with or without blade's pretwist for small and large deformations cases.*
3) *Then Lagrange equations of motion where derived using the total strain energy, total kinetic energy and external work and then deduce the mass, stiffness (linear and nonlinear) and damping matrices of the linear or the nonlinear dynamic equations of motion(depending whether considering small or large deformation) .*
4) *Use the "assumed modes method", in which displacements are assumed to be a product of a time dependent constant and a polynomial function of x (along the lengthwise of the blade) that satisfies the boundary conditions.*
5) *The aerodynamic parameters (Cl, Cd and Cm) values versus angle of attack for a NACA airfoil profile where plotted and interpolated (expanded) to make sure we have aerodynamic values for any given angle of attack.*
6) *Calculation of the aerodynamic lift, drag and pitch moment loadings were calculated at each time step for a 14m blade that has a linear decreasing NACA4415 airfoil cross section utilizing a time dependent set of parameters such as aerodynamic parameters (Cl, Cd and Cm), air density, wind and blade speed, flow angle, yaw and pitch angles.*
7) Then the centrifugal force, modified pitch moment(due to the coordinate differences between centroid and center of elasticity), thrust and torque forces at some selected

airfoil stations were calculated using the Airfoil wind tunnel aerodynamical parameters data (Cl, Cd and Cm).

8) Create a MATLAB code to contain all the above Mathematical Formulations including the interpolation of all the stations' forces and moments to obtain them as a function of x, using a built-in interpolation algorithm within this code .
9) Using the MATLAB code, compute the six degree of freedom at any point on the blade, for both linear and nonlinear cases (small and large deformations respectively).
10) For the linear small deformation case, compare the MATLAB code displacement result plots with Younsi et al. for the same blade example.
11) Create an ls-dyna code that has the same blade inputs of geometrical and material properties and aerodynamic loadings.
12) For the linear small deformation case, compare its displacement result plots with those of the MATLAB code (since the nonlinear case is not found in the literature to compare).
13) Establish the mathematical relationship for the coupling between the blade twist around the blade and the angle of attack at every time step to update the angle of attack on the next time step by adding or subtracting the twist angle from the angle of attack.

1.4 Aerodynamics Loads

1.4.1 Airfoil's Load Layout

The analysis of the state of load on the wind turbine blade is intended to verify whether the turbine will withstand the action of load within appropriate safety range. Various cases of load

on the blade, resulting from the action of various external factors on the turbine, have to be considered. The following types of states of loadings on a wind turbine blade can be distinguished:

- *The aerodynamic loads* of a wind turbine blade are shown in Fig.1.4.1.1.
- *The mass loads*, as the wind turbine blade is slender, the loads associated with its inertia are limited to the loads generated by its weight, which causes sinusoidal loads the frequency of which corresponds to the rotor. Both mass and aerodynamic loads were investigated.

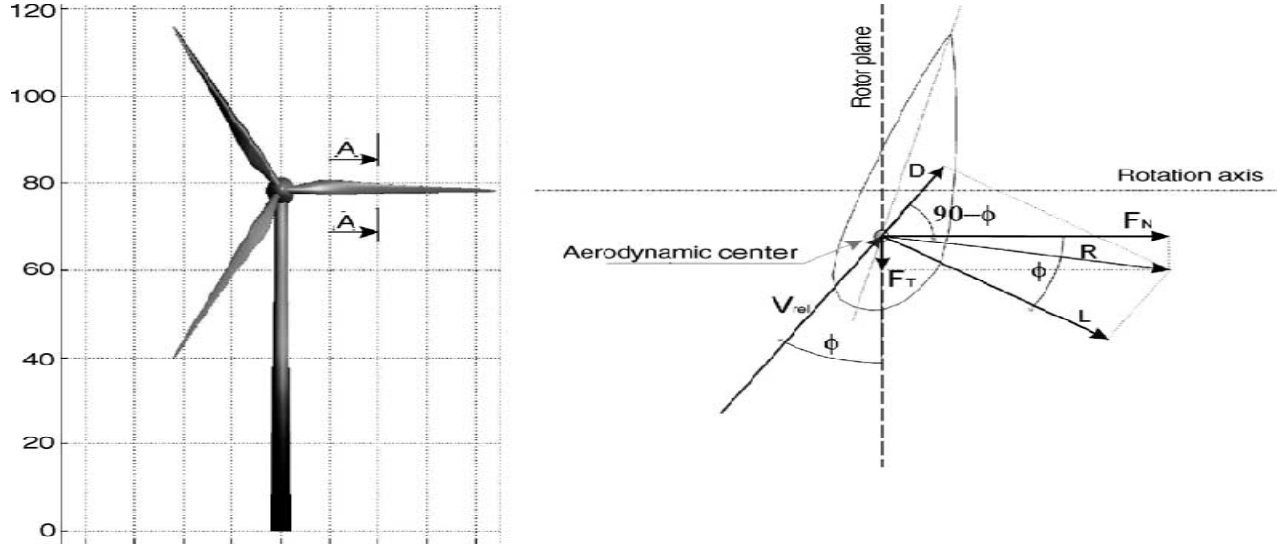

Fig. 1.4.1.1: The local forces on the blade [7]

1.4.2 Simple Load Formulas / Model

The loading on a wind turbine blade as shown in the below Fig.1.4.2.1 consist of the following:

- The flapwise and edgewise bending due to the loadings on the blade (skew bending).

- The gravitational loads, which change direction during the rotation of the blade, and which mainly generate edgewise bending loading.
- The torsional loading because the shear resultants of the flap- and edgewise loads do not go through the shear centre of the blade section.
- The normal loading due to the rotation of the blade (inertia forces).
- The relative small loads due to pitch de-accelerations and accelerations.

The latter three have very little influence on the design loads, and it is the flapwise and edgewise loads that determine the structural design and the blade cross sections. The spar carries most of the flapwise bending, while the edgewise bending primarily is carried of by the leading and trailing edges of the aerodynamic profile, which are strengthened due to this. Below Figure1.4.2.1 illustrates the components of airspeed and force acting on an airfoil section on a wind turbine blade. at a radial distance *r* from the axis of rotation. The view in these schematic diagrams is from the blade hub toward the tip. According to the BEM theory, airloads on a section of an airfoil are proportional to the dynamic pressure at only that section.

Lift and Drag Forces

CL and *CD* coefficients are proportionality constants that is required for the calculation of the *L* and *D* forces as shown in Fig. 1.4.2.1:

$$L = CL \; pd \; C \qquad (1.4.2.1)$$

$$D = CD \; pd \; C \qquad (1.4.2.2)$$

$$pd = 0.5 \; \rho \; V_{rel}^{\,2} \qquad (1.4.2.3)$$

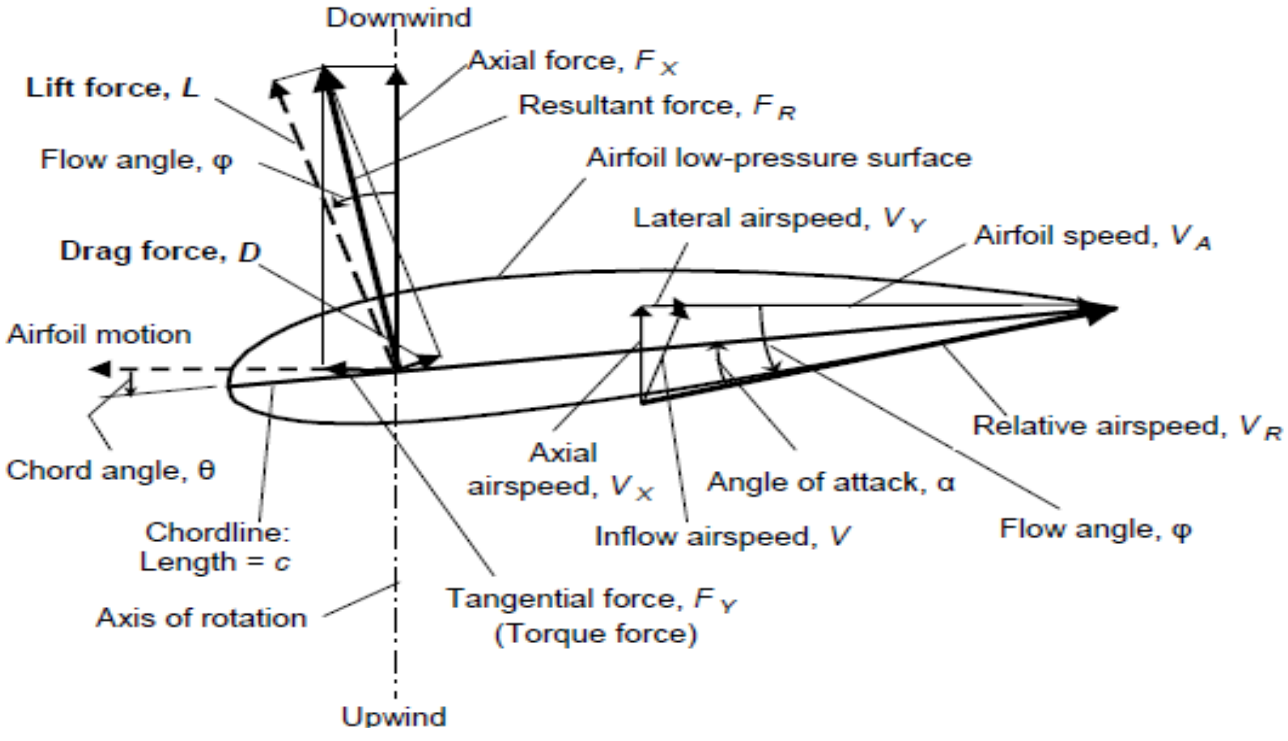

Fig. 1.4.2.1: The wind and force vectors acting on an airfoil [7].

which implies that:

$$\textbf{Lift Force:} \quad L = 0.5\ \rho\ V_{rel}^{\ 2}\ C\ CL \tag{1.4.2.6}$$

$$\textbf{Drag Force:} \quad D = 0.5\ \rho\ V_{rel}^{\ 2}\ C\ CD \tag{1.4.2.7}$$

$$\textbf{Thrust Force:} \quad FN = L\cos\varphi + D\sin\varphi \tag{1.4.2.8}$$

$$\textbf{Torque Force:} \quad FT = L\sin\varphi - D\cos\varphi \tag{1.4.2.9}$$

where,

***L*:** is the lift force per unit span; intensity of force perpendicular to relative airspeed (lb/ft)

***D*:** is the drag force per unit span; intensity of force parallel to relative airspeed (lb/ft)

***CL, CD*:** are the lift and drag coefficients of the section respectively

***C*:** is the chord length of aerodynamic profile (ft)

***pd*:** is the aerodynamic pressure (lb/ft^2)

ρ: is the air density (slugs/ft^2)

***φ*:** is the wind flow angle

1.5 Blade Element Momentum Theory

Blade Element Momentum Theory relates two methods to examine how a wind turbine operates. The first method is to use a momentum balance on a rotating annular stream tube passing through a turbine and the second method is to examine the forces generated by the aerofoil lift and drag coefficients at various sections along the blade as explained in [8].

Momentum Theory

Consider the stream tube around a wind turbine shown in Fig. 1.5.1 and explained in reference [8]. Four stations are shown in the diagram 1, some way upstream of the turbine, 2 just before the blades, 3 just after the blades and 4 some way downstream of the blades. Between 2 and 3 energy is extracted from the wind and there is a change in pressure as a result. Apply Bernoulli's equation, assuming that $p_1 = p_4$ and that $V_2 = V_3$.

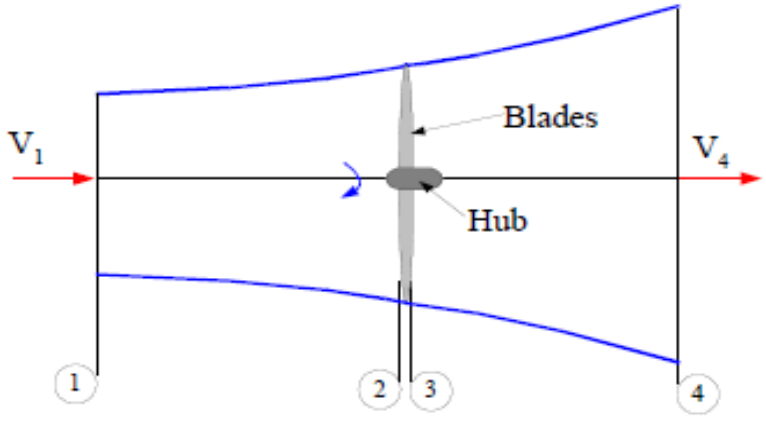

Fig. 1.5.1: Axial stream tube around a wind turbine [8].

We can also assume that between 1 and 2 and between 3 and 4 the flow is frictionless:

$$p_2 - p_3 = \frac{1}{2}\rho(V_1^2 - V_4^2) \tag{1.5.1}$$

Noting that force is pressure multiplied by area:

$$dF_x = (p_2 - p_3)dA \tag{1.5.2}$$

or,

$$dF_x = \frac{1}{2}\rho(V_1^2 - V_4^2)dA \tag{1.5.3}$$

Define a as the axial induction factor:

$$a = \frac{V_1 - V_2}{V_1} \tag{1.5.4}$$

It can also be shown that:

$$V_2 = V_1(1 - a) \tag{1.5.5}$$

$$V_4 = V_1(1 - 2a) \tag{1.5.6}$$

Substitute, implies:

$$dF_x = \frac{1}{2}\rho V_1^2[4a(1 - a)]2\pi r dr \tag{1.5.7}$$

Rotating Annular Stream tube

Applying the conservation of angular momentum in the annular stream tube shown in Fig.1.5.2, where between 2 and 3 the rotation of the turbine imparts a rotation onto the blade wake. Considering that the blade wake rotates with an angular velocity ω and the blades rotate with an angular velocity of Ω. From basic physics, as explained in reference [8], the following equations can be obtained:

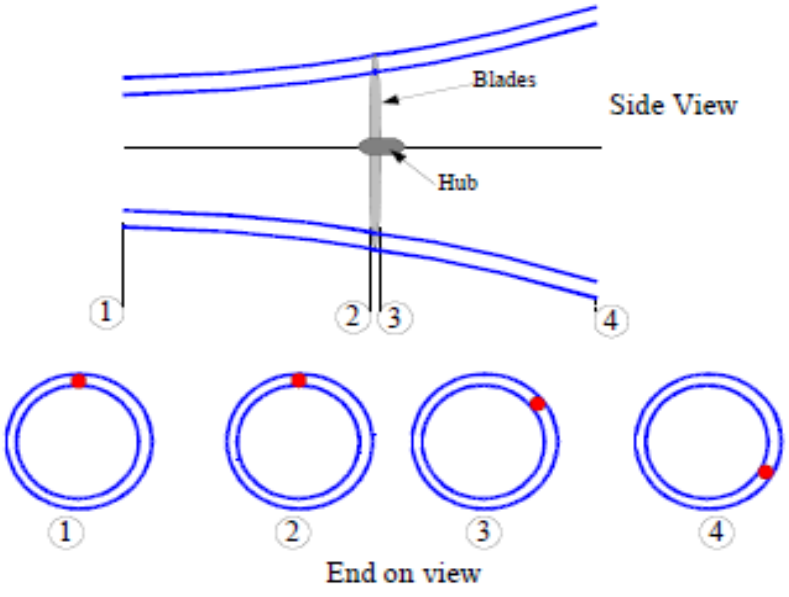

Fig. 1.5.2: Rotating annular stream tube [8].

$$\text{Moment of Inertia of an annulus}, I = mr^2 \tag{1.5.8}$$

$$\text{Angular Moment}, L = I\omega \tag{1.5.9}$$

$$\text{Torque}, T = \frac{dL}{dt} \tag{1.5.10}$$

$$\Rightarrow T = \frac{dI\omega}{dt} = \frac{d(mr^2\omega)}{dt} = \frac{dm}{dt}r^2\omega \tag{1.5.11}$$

So for a small element the corresponding torque will be:

$$dT = d\dot{m}\omega r^2 \tag{1.5.12}$$

For the rotating annular element:

$$d\dot{m} = \rho A V_2 \tag{1.5.13}$$

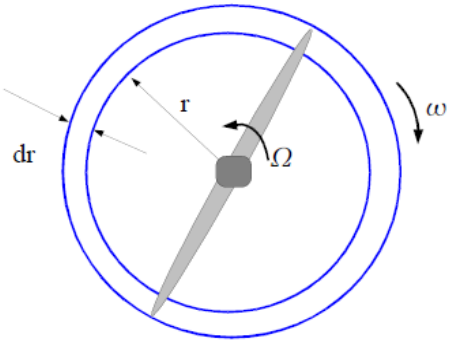

Fig. 1.5.3: Rotating annular stream tube notation [8].

$$d\dot{m} = \rho 2\pi r dr V_2 \tag{1.5.14}$$

$$\Rightarrow dT = \rho 2\pi r dr V_2 \omega r^2 = \rho V_2 \omega r^2 2\pi r dr \tag{1.5.15}$$

Define angular induction factor a' :

$$a' = \frac{\omega}{2\Omega} \tag{1.5.16}$$

Recall that $V_2 = V(1-a)$ so:

$$dT = 4a'(1-a)\rho V \Omega r^3 \pi dr \tag{1.5.17}$$

Momentum theory has therefore yielded equations for the axial (Eqn 1.5.17) and tangential force (Eqn 1.6.1.17) on an annular element of fluid.

Blade Element Theory

Blade element theory relies on the following two key assumptions [8]:

1) There are no aerodynamic interactions between different blade elements.
2) The forces on the blade elements are solely determined by the lift and drag coefficients.

Consider a blade divided up into *N* elements as shown in Fig. 1.5.4. Each of the blade elements will experience a slightly different flow as they have a different rotational speed Ωr, a different chord length *c* and a different twist angle β. Blade element theory involves dividing up the blade into a sufficient number (usually between ten and twenty) of elements and calculating the flow at each one. Overall performance characteristics are determined by numerical integration along the blade span.

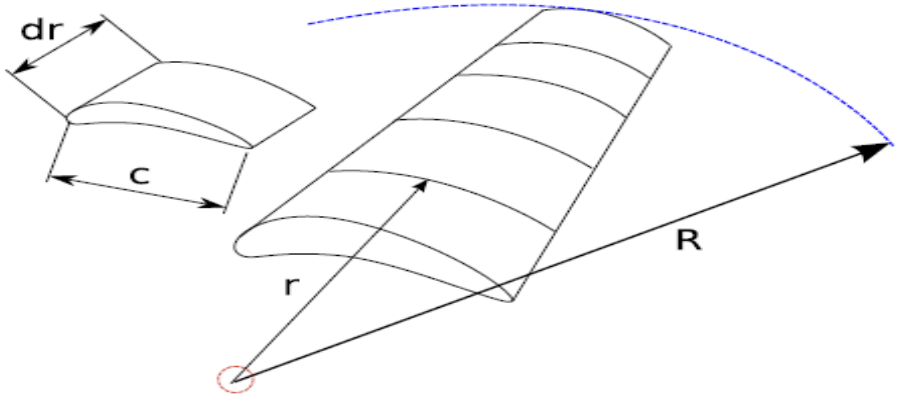

Fig. 1.5.4: The blade different stations [8]

Relative Flow

Lift and drag coefficient data area available for a variety of aerofoils from wind tunnel data. Since most wind tunnel testing is done with the aerofoil stationary we need to relate the flow over the moving aerofoil to that of the stationary test. To do this we use the relative velocity over the aerofoil. In practice the flow is turned slightly as it passes over the aerofoil so in order to obtain a more accurate estimate of aerofoil performance an average of inlet and exit flow conditions is used to estimate performance. The flow around the blades starts at station 2 in Fig. 1.5.2. and Fig. 1.5.1. and ends at station 3. At inlet to the blade the flow is not rotating, at

exit from the blade row the flow rotates at rotational speed ω. That is over the blade row wake rotation has been introduced.

The average rotational flow over the blade due to wake rotation is therefore ω/2. The blade is rotating with speed Ω which lead that the average tangential velocity of the blade is $\Omega r + 0.5\omega r$ as shown in Fig. 1.5.5.

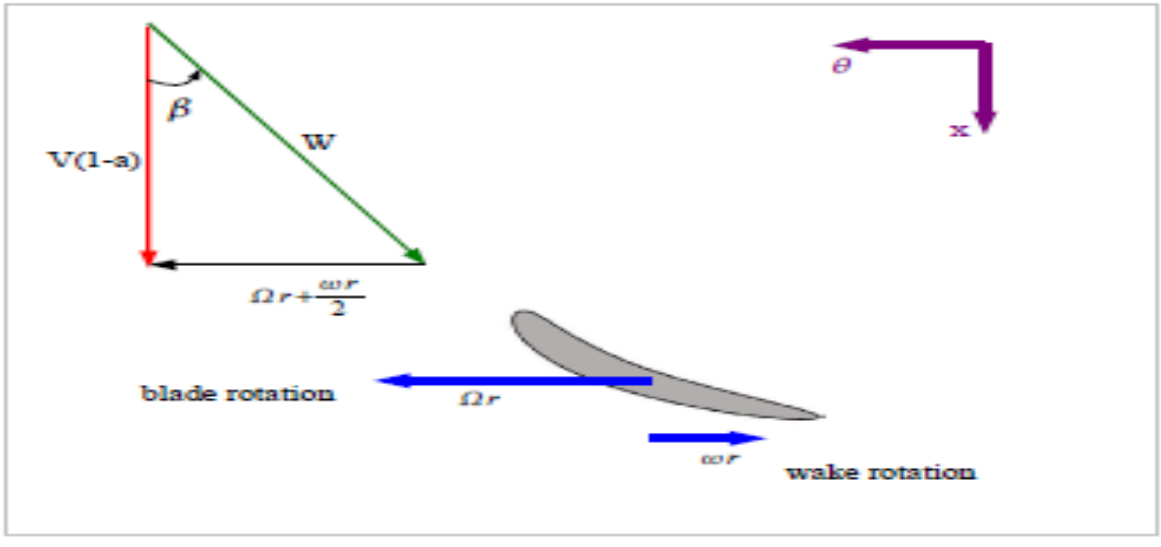

Fig. 1.5.5: Flow onto the turbine blade [8].

Examining Fig. 1.5.5, we can immediately note that:

$$\Omega r + \frac{\omega r}{2} = \Omega r(1 + a') \tag{1.5.18}$$

but since $V_2 = V_1$ $V(1-a)$, implies:

$$\tan\beta = \frac{\Omega r(1 + a')}{V(1 - a)} \tag{1.5.19}$$

where V is used to represent the incoming flow velocity V_1.

The value of β will vary from blade element to blade element. But the local tip speed ratio λ_r is defined as:

$$\lambda_r = \frac{\Omega r}{V} \tag{1.5.20}$$

This leads to a further simplification for tanβ :

$$\tan\beta = \frac{\lambda_r(1+a')}{(1-a)} \tag{1.5.21}$$

From Fig. 1.5.5 the following relation is obvious:

$$W = \frac{V(1-a)}{\cos\beta} \tag{1.5.22}$$

Blade Elements

The forces on the blade element are shown in Fig. 1.5.6, note that by definition the lift and drag forces are perpendicular and parallel to the incoming flow. For each blade element one can conclude:

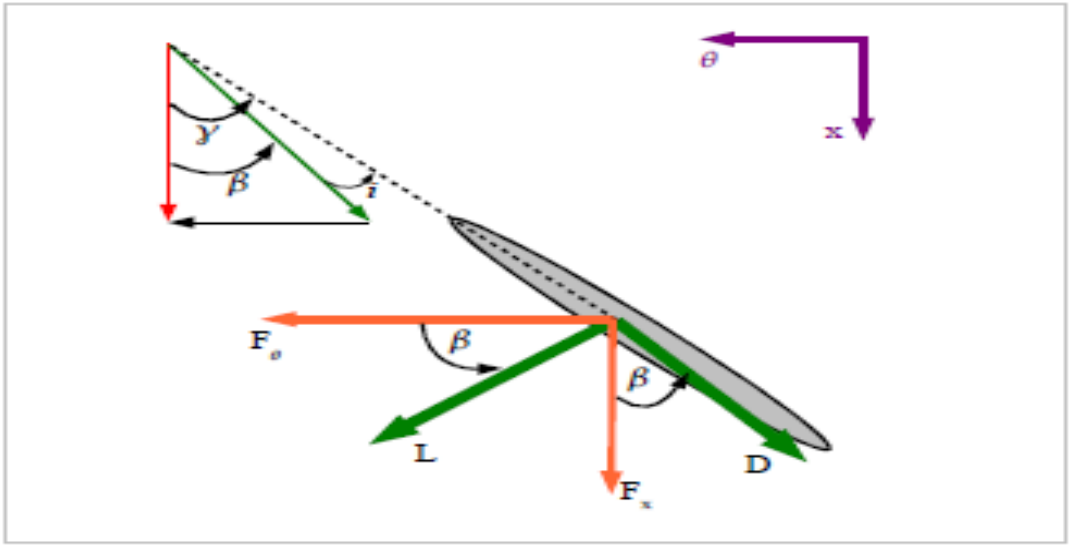

Fig. 1.5.6: The forces on the turbine blade [8].

$$dF_\theta = dL\cos\beta - dD\sin\beta \tag{1.5.23}$$

$$dF_x = dL\sin\beta + dD\cos\beta \tag{1.5.24}$$

dL and *dD* can be found from the definition of the lift and drag coefficients as follows:

$$dL = C_L\frac{1}{2}\rho W^2 cdr \tag{1.5.25}$$

$$dD = C_D\frac{1}{2}\rho W^2 cdr \tag{1.5.26}$$

where *dL* and *dD* are the lift and drag forces on the blade element respectively.

If there are *B* blades, by combining Equation (1.5.23) and Equation (1.5.25), it can be shown that:

$$dF_x = B\frac{1}{2}\rho W^2(C_L\sin\beta + C_D\cos\beta)cdr \tag{1.5.27}$$

$$dF_\theta = B\frac{1}{2}\rho W^2(C_L\cos\beta - C_D\sin\beta)cdr \tag{1.5.28}$$

The Torque on an element, dT is simply the tangential force multiplied by the radius.

$$dT = B\frac{1}{2}\rho W^2(C_L\cos\beta - C_D\sin\beta)crdr \tag{1.5.29}$$

The effect of the drag force is clearly seen in the equations, an increase in thrust force on the machine and a decrease in torque (and power output). These equations can be made more useful by noting that β and *W* can be expressed in terms of induction factors etc. i.e. Equations (1.5.21) and (1.5.22). Substituting and carrying out some algebra yields:

$$dF_x = \sigma' \pi \rho \frac{V^2(1-a)^2}{\cos^2 \beta}(C_L \sin\beta + C_D \cos\beta) r dr \tag{1.5.30}$$

$$dT = \sigma' \pi \rho \frac{V^2(1-a)^2}{\cos^2 \beta}(C_L \cos\beta - C_D \sin\beta) r^2 dr \tag{1.5.31}$$

where σ' is the local solidity:

$$\sigma' = \frac{Bc}{2\pi r} \tag{1.5.32}$$

Tip Loss Correction

Losses at the tip of the turbine blade are introduced in a similar manner to those found in wind tip vorticies on turbine blades. It can be accounted for these losses in BEM theory by means of a correction factor. This correction factor *Q* varies from 0 to 1 and simulates the reduction in forces along the blade.

$$Q = \frac{2}{\pi}\cos^{-1}\left[exp\left\{-\left(\frac{B/2[1-r/R]}{(r/R)\cos\beta}\right)\right\}\right] \tag{1.5.33}$$

The results from $\cos^{-1}$ *must be in radians*. Apply the tip loss correction factor to Eqn 1.5.7 and Eqn 1.5.17:

$$dF_x = Q\rho V_1^2[4a(1-a)]\pi r dr \tag{1.5.34}$$

$$dT = Q4a'(1-a)\rho V \Omega r^3 \pi dr \tag{1.5.35}$$

From the above, we now have four equations, two dervied from momentum theory which express the axial thrust and the torque in terms of flow parameters (Equations (1.5.35) and (1.5.34):

$$dF_x = Q\rho V_1^2[4a(1-a)]\pi r dr \tag{1.5.36}$$

$$dT = Q4a'(1-a)\rho V\Omega r^3\pi dr \tag{1.5.37}$$

Also we have two equations derived from considering the blade forces which express the axial force and torque in terms of the lift and drag coefficients of the aerofoil Eqn 1.5.30 and Eqn 1.5.31:

$$dF_x = \sigma'\pi\rho\frac{V^2(1-a)^2}{\cos^2\beta}(C_L\sin\beta + C_D\cos\beta)rdr \tag{1.5.38}$$

$$dT = \sigma'\pi\rho\frac{V^2(1-a)^2}{\cos^2\beta}(C_L\cos\beta - C_D\sin\beta)r^2dr \tag{1.5.39}$$

To calculate rotor performance Eqn 1.5.34 and Eqn 1.5.35 from a momentum balance are equated with Eqn 1.5.30 and Eqn 1.5.31:

$$\frac{a}{1-a} = \frac{\sigma'[C_L\sin\beta + C_D\cos\beta]}{4Q\cos^2\beta} \tag{1.5.40}$$

$$\frac{a'}{1-a} = \frac{\sigma'[C_L\cos\beta - C_D\sin\beta]}{4Q\lambda_r cos^2\beta} \tag{1.5.41}$$

Power Output

Eqn 1.5.40 and Eqn 1.5.41 are used in the blade design procedure. The contribution to the total power from each annulus is [8]:

$$dP = \Omega dT \tag{1.5.42}$$

The total power from the rotor is:

$$P = \int_{r_h}^{R} dPdr = \int_{r_h}^{R} \Omega dTdr \tag{1.5.43}$$

where r_h is the hub radius. The power coefficient C_p is given by:

$$C_P = \frac{P}{P_{wind}} = \frac{\int_{r_h}^{R} \Omega dT}{\frac{1}{2}\rho\pi R^2 V^3} \tag{1.5.44}$$

Using Eqn 1.5.31, it is possible to develop an integral for the power coefficient directly. After some algebra:

$$C_P = \frac{8}{\lambda^2}\int_{\lambda_h}^{\lambda} Q\lambda_r^3 a'(1-a)\left[1 - \frac{C_D}{C_L}\tan\beta\right] d\lambda_r \tag{1.5.45}$$

Blade Design Procedure

The following is a blade design procedure as explained by reference [8]:

1) Determine the rotor diameter required from site conditions and $P = 0.5C_p\rho\eta\pi R^2V^3$

where,

P: is the power output

C_p : is the expected coefficient of performance (0.4 for a modern three bladed wind turbine)

η : is the expected electrical and mechanical efficiencies (0.9 is a suitable value)

R : is the tip radius

V : is the expected wind velocity

λ	B
1	8-24
2	6-12
3	3-6
4	3-4
more than 4	1-3

Table 1.5.1: The number of blades [8].

2) Choose a tip speed ratio for the machine. For water pumping pick $1 < \lambda < 3$ (which gives a high torque) and for electrical power generation pick $4 < \lambda < 10$.

3) Choose a number of blades *B*, using Table 1.5.1, which is based on practical experience.

4) Select an airfoil. For $\lambda < 3$ curved plates can be used.

5) Obtain and examine lift and drag coefficient curves for the aerofoil in question.

6) Choose the design aerodynamic conditions for each aerofoil. Typically select 80% of the maximum lift value.

7) Divide the blade into *N* elements. Typically 10 to 20 elements would be used.

8) As a first guess for the blade twist and chord, use the blade shape derived with wake rotation, zero drag and zero tip losses. Note that these equations provide an initial guess only. The equations are given as follows:

$$\beta = 90^\circ - \frac{2}{3}\tan^{-1}\left(\frac{1}{\lambda_r}\right) \tag{1.5.46}$$

$$a = \left(1 + \frac{4\cos^2\beta}{\sigma' C_L \sin\beta}\right)^{-1} \tag{1.5.47}$$

$$a' = \frac{1-3a}{4a-1} \tag{1.5.48}$$

9) Calculate rotor performance and then modify the design as necessary. This is an iterative process. The application of BEM can be sometimes confusing as it can be used to either to design i.e. select γ and c or to analyze the performance of a blade.

It should be noted that different aerofoil profiles may be used at different spans of the blade, for example, a thick aerofoil may be selected for the hub to give greater strength.

Chapter 2

Literature Review on Blade Different Formulations & Research Plan

2.1 Introduction

The wind turbine blade can be considered as a pretwisted beam. Hence it is essential to understand how to analyze and work with beams. Beam element is a versatile line-element where in general it has six degrees of freedom at each node, which include three translational displacements along the x, y, and z directions and three rotational displacements about the x, y, and z directions as shown on the right side node of the beam of Fig. 2.1.1 shows the positive directions of these displacements.

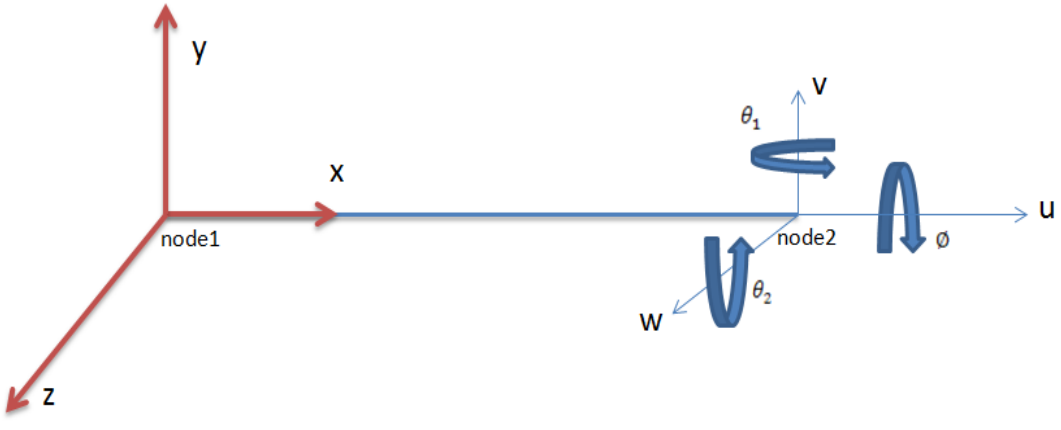

Fig. 2.1.1: Beam element with six degrees of freedom at each node.

Beam element can be used to simulate a slender structure that has a uniform cross- section. The stiffness constant of a beam element is derived by combining the stiffness constants of a beam under pure bending, a truss element, and a torsion bar. A beam element can represent a beam in bending, a truss element, and a bar in torsion. To derive the element stiffness equation for a beam element that subjected to all these loadings, we start first by deriving the

stiffness equation of a beam subjected to bending loading only, and then superimpose the stiffness of a truss subjected to axial loading only and then superimpose the stiffness of a bar subjected to torsional loading only to obtain the resultant stiffness equation for all loadings .

2.2 Aeroelasticity

Aeroelasticity is the study of the mutual interaction between the aerodynamic and elastic forces, and the influence of this interaction on blade design [9]. Wind turbine Blade is a very flexible, and this flexibility is the main factor for the various types of the aeroelastic phonemena.

The aeroelastic phonemena happen when the structural deformations induce some additional aerodynamic forces which in turn produce some additional structural deformations that again induce more aerodynamic forces. The dynamic aeroelasticity phenomena is the one involves the interactions among all the inertial, aerodynamical, and elastic forces, while the static aeroelastic phenomena is the one involves the interations between aerodynamical and elastic forces. Fig. 2.2.1 show the relationship between the all these forces.

For wind turbine blade, such interactions are tremendous because of the couplings among all the aerodynamics axial, bending and torsional loadings (forces and moments) acting on the blade. These interactions may tend to become less and less until a condition of equilibrium stability is reached, or they may tend to diverge and destroy the structure.

The static aeroelasticity includes the following:

1) Static divergence

2) Load redistribution

3) Control reversal and effectiveness

4) Aeroelastic effects on static stability

And the dynamic Aeroelasticity includes the following:

1) Flutter

2) Buffeting

3) Dynamic response

4) Aero-elastic effects on dynamic stability

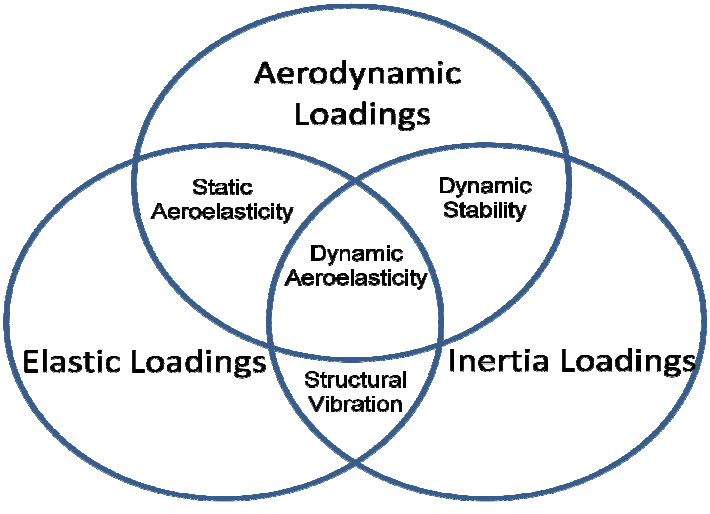

Fig. 2.2.1: The summary of loadings and their responses.

The following are explanation of some common aero-elastic terms:

- ***Flutter*** : is a dynamic instability occurring in a blade at a speed called the flutter speed, where the elasticity of the structure plays an essential part in the instability.
- ***Buffeting*** : are the transient vibrations of blade structural components due to aero-dynamic impulses produced by the wake around the blade, or other components of the wind turbine mild.
- ***Dynamic response*** : is the transient response of blade structural components produced by quick applied loads due to gusts, gun reactions, abrupt control motions, moving shock waves, or other dynamic loads.
- ***Load Distribution*** : It is due to the influence of the elastic deformations of the blade structure on the distribution of aero-dynamic pressures over that structure.

- ***Divergence*** : is the static instability of the wind turbine blade, at a speed called the divergence speed, where the elasticity of the blade surface plays an essential role in the instability.
- ***Control Effectiveness*** : It is due to the influence of elastic deformations of the blade structure on the controllability of the blade.

2.3 Large Deformation versus Small Deformation

When the deformation of the wind turbine blade is small i.e. less than 10% of the length of the blade, we can use the deformation linear is linear and this happens when the change in volume is almost negligible. However, once we have deformations that are greater than 10% of the length of the blade, we should use the appropriate stress and strain tensors to account for for this large deformation. We should also use the appropriate constitutive relations that account for that large deformation of the blade.

The above strain tensor is known as the Green-Lagrange strain tensor. It is also a second order tensor because it has two independent indices. An obvious question is how the Green-Lagrange strain tensor compares to the small deformation strain tensor that we did make assumptions to derive. We start by substituting the displacement equation for the deformation gradient tensor to obtain:

$$E_{ij} = \frac{1}{2}\left(\delta_{ij} + \frac{\partial u_i}{\partial x_j'} + \frac{\partial u_j}{\partial x_i'} + \frac{\partial u_k}{\partial x_i'}\frac{\partial u_k}{\partial x_j'} - \delta_{ij} \right) = \frac{1}{2}\left(\frac{\partial u_i}{\partial x_j'} + \frac{\partial u_j}{\partial x_i'} + \frac{\partial u_k}{\partial x_i'}\frac{\partial u_k}{\partial x_j'} \right) \tag{2.3.1}$$

We obtain the above because when a quantity is multiplied by the kronecker delta we obtain the same quantity back, with the free index from the kronecker delta being exchanged with the repeated index on the quantity it is multiplying. It should be noted that the large deformation

strain tensor includes many nonlinear higher order terms which indicate that all the large deformation analyses are *nonlinear*. Recall that the small deformation strain tensor is:

$$\varepsilon_{ij} = \frac{1}{2}\left(\frac{\partial u_i}{\partial x_j'} + \frac{\partial u_j}{\partial x_i'} \right) \tag{2.3.2}$$

Therefore by assuming that the deformation is small, we drop all the nonlinear higher order terms from the Green-Lagrange strain tensor and keep the linear terms only.

2.4 Aeroelastic Coupling Schemes

Due to changes of aerodynamics loads on the wind turbine blades, these blades twist. Due that twisting, there is a direct influence on the angle of attack, changing loads and affecting output power. This is directly exploited in classic pitch control used in not only wind turbines but in rotors of all types. When the pitch changes are rapid enough, they can affect not only average loads and power, but vibratory loads as well, influencing fatigue life throughout the system. Even quite small angles of twist can have significant impact.

Any time the wind turbine blade becomes aeroelastically “active” (i.e. when the elastic deformations play a role in the aerodynamic loading), the dynamic stability of the blade will be affected. Veers et al. [10] address two of the most common stability constraints, namely flutter and divergence.

Flutter is the condition where the phasing between the aerodynamic load fluctuations and elastic deformations are such that a resonant condition is achieved. Every wing will have a flutter boundary at some speed. For wind turbines the boundary is defined at the rotational

speed (typically determined in still air) at which the blade will flutter. The stability margin is the difference between the flutter speed and normal operating speed.

Divergence is a quasi-static condition where the blade twists in response to increasing load in a direction that further increases the load. If this condition exists on a blade there will be an operating speed at which the increase in loads caused by the deformation exceeds the ability of the blade to resist the load, called divergence.

The stability boundaries were determined with respect to the amount of twist coupling built into the blade. A coupling coefficient, α, was defined to facilitate the generic examination of stability effects.

For a blade with bending-twist coupling, the matrix equation for blade bending and twisting strains ε_b and ε_t due to bending and twisting loads M_b and M_t are:

$$\begin{bmatrix} EI & -g \\ -g & GK \end{bmatrix} \begin{Bmatrix} \varepsilon_b \\ \varepsilon_t \end{Bmatrix} = \begin{Bmatrix} M_b \\ M_t \end{Bmatrix} \tag{2.4.1}$$

where EI and GK are the beam bending and torsional stiffness, respectively. The coupling coefficient, g , is constrained to values that keep the system positive definite. The range of realizable g values is limited to:

$$g = \alpha\sqrt{EIGK}; \quad -1 < \alpha < 1. \tag{2.4.2}$$

It should noted that equation (1.6.2.1) that include the coupling between bending and twisting loads will change later when I include the couplings of all other possible aerodynamic loading acting on the blade in addition to the inclusion of the nonlinear higher order terms due the large nonlinear large deformation assumption.

2.5 Optimization of Blade Design

The aerodynamic and structural design of rotors for horizontal axis wind turbine (HAWT) involves many conflicting requirements, for example, maximum performance, minimum loads and minimum noise. The wind turbine operates in very different conditions from normal variation in wind speed to extreme wind occurrences. Optimum efficiency is not obtainable in the entire wind speed range, since power regulation is needed to prevent generator burnout at high wind speeds. Optimum efficiency is limited to a single-design wind speed for stall regulated HAWT with fixed speed of rotation.

Several optimization methods exist . They are typically based on a numerical optimization algorithm. Multipoint design methods have a larger degree of flexibility for optimization objective and the majority allows multiple constraints. The first generation of the methods involved maximum annual energy production as objective, since this includes off-design performance with no or only few constraints on loads. The reported improvements of the annual energy production are promising, but they often arrive from an increase in swept area for the same generator size.

Unfortunately, this will result in larger loads on tower and the blade roots. Actually, the increase in loads often exceeds the increase in energy yield. Optimum design should not be restricted to aerodynamic performance. In most of the cases, the key factor is the minimum cost of energy, and this should be the objective. This leads to the development of second generation design tools, where the optimization objective is the minimization of the cost of energy. Cost of energy is by definition the ratio of the total costs from manufacture and erection of the wind turbine to the annual energy production. Proper cost estimate involves calculation of fatigue loads as well as extreme loads on all main components and a cost function describing the coupling between design loads and cost. Using a multi-disciplinary design method for direct shape design of HAWT rotors.

In the present research, the author main concern is to use a numerical optimization, where the objective is to have the displacements and rotations (six degrees of freedom) at the tip of the blade under a certain maximum limit with a set of multiple constraints that are allowed i.e. extreme loads, material Young's modulus and/or material density.

The optimization of the wind turbine blade displacements and rotations is a feature that can be done in the MATLAB code and is not really the concentration of this research. The design of any blade rotor can be utilized to demonstrate the capabilities of this design method within the MATLAB code. It should be noted that:

- Loads constraints and cost estimation were important for the applicability of the optimization results.
- With traditional airfoil characteristics and blade structure, shape optimization of the rotor reduced cost of energy compared to a rotor of the same size.
- The optimum specific power can also be a constraint.
- Optimum airfoil characteristics showed that the airfoil sections should have a relative high maximum lift on the entire blade.

2.6 Finite Element Beam Formulation

Consider a cantilever beam, under pure bending (without axial loads or torsion loads) of a total of four degrees of freedom, two at each node i.e. two deflections and two rotations, V_1, θ_1, V_2, and θ_2. For example for the cantilever beam shown in Fig. 2.6.1, the right-side free end has $\theta = \theta_2$ and $V_2 = V$ while the left-side fixed end has zero values of displacement and rotation since it is a fixed end.

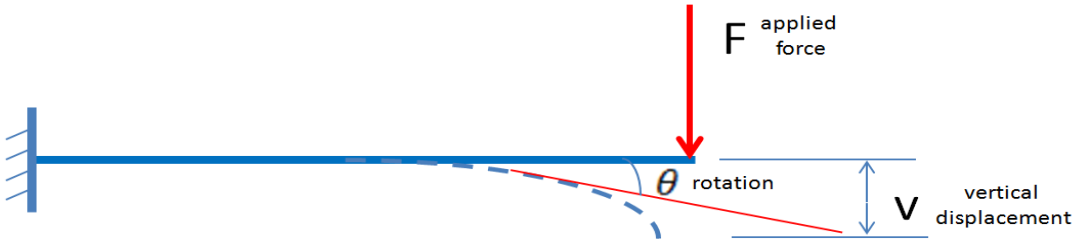

Fig. 2.6.1: Cantilever beam with two degrees of freedom at each node.

Since there are four degrees of freedom, the size of the stiffness matrix of a beam element has the size 4 x 4. Eqn 2.6.1 is the equation of a beam element, which is under pure bending load (no axial or torsion loads) that relates the force vector, displacement vector and the 4 x 4 symmetric stiffness matrix (where the stiffness matrix contain the values of Young's modulus E, moment of inertia I and the length of the element L).

$$\begin{pmatrix} F_i \\ M_i \\ F_j \\ M_j \end{pmatrix} = \begin{pmatrix} (12EI)/L^3 & (6EI)/L^2 & -(12EI)/L^3 & (6EI)/L^2 \\ (6EI)/L2 & (4EI)/L & -(6EI)/L^2 & (2EI)/L \\ -(12EI)/L^3 & -(6EI)/L^2 & (12EI)/L^3 & -(6EI)/L^2 \\ (6EI)/L^2 & (2EI)/L & -(6EI)/L^2 & (4EI)/L \end{pmatrix} \begin{pmatrix} v_i \\ \theta_i \\ v_j \\ \theta_j \end{pmatrix} \quad (2.6.1)$$

Using this equation, we can solve problems in which several beam elements are connected in an uniaxial direction. If the beam elements are oriented in more than one direction, we will have to first transform the above Eqn 2.6.1 into a global stiffness matrix equation which involves using some trigonometric relations. However, Eqn 2.6.1 can be used for solving a beam problem loaded under bending loads only.

Stiffness matrix of a beam element with bending and axial loads in local coordinates

The stiffness equation for the combined bending and axial load can be written by superimposing the axial stiffness terms over the bending stiffness. For axial loading, the structural equation is:

$$\begin{pmatrix} f_{1x} \\ f_{2x} \end{pmatrix} = AE/L \begin{pmatrix} 1 & -1 \\ -1 & 1 \end{pmatrix} \begin{pmatrix} d_{1x} \\ d_{2x} \end{pmatrix} \tag{2.6.2}$$

The combined axial and bending loading matrix equation can be obtained by superimposing Eqn 2.6.1 and Eqn 2.6.2 as follows:

$$\begin{pmatrix} f_{1x} \\ f_{1y} \\ m_1 \\ f_{2x} \\ f_{2y} \\ m_2 \end{pmatrix} = \begin{pmatrix} C_1 & 0 & 0 & -C_1 & 0 & 0 \\ 0 & 12C_2 & 6C_2L & 0 & -12C_2 & 6C_2L \\ 0 & 6C_2L & 4C_2L^2 & 0 & -6C_2L & 2C_2L^2 \\ -C_1 & 0 & 0 & C_1 & 0 & 0 \\ 0 & -12C_2 & -6C_2L & 0 & 12C_2 & -6C_2L \\ 0 & 6C_2L & 2C_2L^2 & 0 & -6C_2L & 4C_2L^2 \end{pmatrix} \begin{pmatrix} d_{1x} \\ d_{1y} \\ \varphi_1 \\ d_{2x} \\ d_{2y} \\ \varphi_2 \end{pmatrix} \tag{2.6.3}$$

Where the resultant matrix is,

$$[k] = \begin{bmatrix} C_1 & 0 & 0 & -C_1 & 0 & 0 \\ 0 & 12C_2 & 6C_2L & 0 & -12C_2 & 6C_2L \\ 0 & 6C_2L & 4C_2L^2 & 0 & -6C_2L & 2C_2L^2 \\ -C_1 & 0 & 0 & C_1 & 0 & 0 \\ 0 & -12C_2 & -6C_2L & 0 & 12C_2 & -6C_2L \\ 0 & 6C_2L & 2C_2L^2 & 0 & -6C_2L & 4C_2L^2 \end{bmatrix} \tag{2.6.4}$$

where $C_1 = \frac{AE}{L}$ and $C_2 = \frac{EI}{L^3}$

Beam Element with combined loading Bending, Axial, and Torsion

The torsional structural equation for the torsional loads m_{1x} and m_{2x} and their corresponding deflections are φ_{1x} and φ_{2x} .

$$\begin{pmatrix} m_{1x} \\ m_{1x} \end{pmatrix} = JG/L \begin{pmatrix} 1 & -1 \\ -1 & 1 \end{pmatrix} \begin{pmatrix} \varphi_{1x} \\ \varphi_{2x} \end{pmatrix} \quad (2.6.6)$$

3-D Beam Element

Consider a 3-D beam element of Fig. 2.6.5 that has 6 DOF at each node, and 12 DOF for each element.

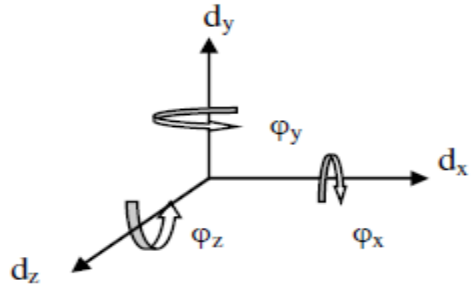

Fig. 2.6.2: Six degrees of freedom.

Eqn 2.6.6 can be superimposed on the stiffness matrix equation Eqn 2.6.3 (of the combined bending and axial loads) to obtain the stiffness matrix equation that include all the axial, bending and torsional loadings acted on a beam.

Therefore, the obtained stiffness matrix by superimposing all the axial, bending, and torsional loadings in the XY, XZ, and YZ planes is:

$$
K=\begin{bmatrix}
\hat{d}_{1x} & \hat{d}_{1y} & \hat{d}_{1z} & \hat{\phi}_{1x} & \hat{\phi}_{1y} & \hat{\phi}_{1z} & \hat{d}_{2x} & \hat{d}_{2y} & \hat{d}_{2z} & \hat{\phi}_{2x} & \hat{\phi}_{2y} & \hat{\phi}_{2z} \\
\frac{AE}{L} & 0 & 0 & 0 & 0 & 0 & -\frac{AE}{L} & 0 & 0 & 0 & 0 & 0 \\
0 & \frac{12EI_z}{L^3} & 0 & 0 & 0 & \frac{6EI_z}{L^2} & 0 & -\frac{12EI_z}{L^3} & 0 & 0 & 0 & \frac{6EI_z}{L^2} \\
0 & 0 & \frac{12EI_y}{L^3} & 0 & -\frac{6EI_y}{L^2} & 0 & 0 & 0 & -\frac{12EI_y}{L^3} & 0 & -\frac{6EI_y}{L^2} & 0 \\
0 & 0 & 0 & \frac{GJ}{L} & 0 & 0 & 0 & 0 & 0 & -\frac{GJ}{L} & 0 & 0 \\
0 & 0 & -\frac{6EI_y}{L^2} & 0 & \frac{4EI_y}{L} & 0 & 0 & 0 & \frac{6EI_y}{L^2} & 0 & \frac{2EI_y}{L} & 0 \\
0 & \frac{6EI_z}{L^2} & 0 & 0 & 0 & \frac{4EI_z}{L} & 0 & -\frac{6EI_z}{L^2} & 0 & 0 & 0 & \frac{2EI_z}{L} \\
-\frac{AE}{L} & 0 & 0 & 0 & 0 & 0 & \frac{AE}{L} & 0 & 0 & 0 & 0 & 0 \\
0 & -\frac{12EI_z}{L^3} & 0 & 0 & 0 & -\frac{6EI_z}{L^2} & 0 & \frac{12EI_z}{L^3} & 0 & 0 & 0 & -\frac{6EI_z}{L^2} \\
0 & 0 & -\frac{12EI_y}{L^3} & 0 & \frac{6EI_y}{L^2} & 0 & 0 & 0 & \frac{12EI_y}{L^3} & 0 & \frac{6EI_y}{L^2} & 0 \\
0 & 0 & 0 & -\frac{GJ}{L} & 0 & 0 & 0 & 0 & 0 & \frac{GJ}{L} & 0 & 0 \\
0 & 0 & -\frac{6EI_y}{L^2} & 0 & \frac{2EI_y}{L} & 0 & 0 & 0 & \frac{6EI_y}{L^2} & 0 & \frac{4EI_y}{L} & 0 \\
0 & \frac{6EI_z}{L^2} & 0 & 0 & 0 & \frac{2EI_z}{L} & 0 & -\frac{6EI_z}{L^2} & 0 & 0 & 0 & \frac{4EI_z}{L}
\end{bmatrix}
$$

(1.4.1.1.15)

2.7 Non-linearity due to large Deformation of the Blade

Non-linearity of any structural object can come from any the following:

1) Non-linearity due nonlinear boundary conditions.
2) Non-linearity due nonlinear materials.

3) Non-linearity due nonlinear large deformations.

In the present research, the author only considering the nonlinearity due the large deformation of the blade (displacement exceed 10% of the length of the blade) where the high order terms of the strain are kept through the derivation of the components of the total strain energy due the application of all the aerodynamic loadings and their couplings.

This lead to have two additional nonlinear stiffness matrices in the nonlinear dynamic equation of motion that can be solved for the the six degrees of freedom of displacements at any x along the length of the blade using the nonlinear Newmark scheme.

2.8 Research Tasks and Plan

2.8.1 Lagrangian Beam Formulation

Using the following Lagrangian equations of motion approach:

1) Assuming that deformation is large (where higher order terms of strain are kept through derivation) and *considering* all the extensional, torsional and flexural loadings acting on the blade with their couplings, variable airfoil cross sections with warping effects, shear deflection, rotary inertia and with blade's pretwist, the total strain energy, total kinetic energy and the partial derivatives of the external work external work due to the aerodynamic loading acting on the blade can be calculated and then substituted in the Lagrange equations of motion.
2) The "assumed modes method" is used, in which displacements are assumed to be an expansion of products of time-step dependent constants and polynomial functions of x (where x is the coordinate along the length of the blade) that satisfy the boundary

conditions at the fixed end where x=0 (hub of the blade) and at the free end where x=L (tip of the blade).

3) Then mass matrix, linear and non linear stiffness matrices and the load vector R of the dynamic equations of motion are deduced from the Lagrange equations of motion. The steps of the linear and nonlinear Newmark implicit iteration schemes used for solving the linear and nonlinear dynamic equations of motion respectively were explained in detail.
4) To modify the above formulation for the small linear deformation, all what should be done is to eleminate the higher order terms of the strain that we kept for the large deformation (or simply assume the nonlinear stiffness matrices are not exist)
5) Creating a MATLAB code that contain the mathematical formulations that mentioned above for the linear and nonlinear deformations.

2.8.2 Model Validation

2.8.2.1 Experimental Testing

There will be no experimental testing will be conducted through this present research period on any wind turbine blade prototype or on a real working wind turbine in the field due to the difficulty to do that. So to verify my MATLAB code (that contain all the mathematical formulation of the present research) displacement results after solving for all the unknown displacements u, v *and* w in the directions of x, y and z axes respectively, the bending rotations θ_1 *and* θ_2 about the y and z axes respectively and the torsional rotation ϕ about the x

axis (using the linear and nonlinear Newmark implicit iteration schemes), the author will perform the following:

- Confirming that the linear case displacement result plots are agree with the work of Younsi et al.
- And confirming that the nonlinear case displacement result plots are agree with the Ls-Dyna code.

2.8.2.2 Blade Analysis Using Hypermesh and Ls-dyna

Consider the 3D blade Fig. 2.8.2.2.1 as an infinite number of stations that each of these stations has a 'local radius', which is the distance of the station from the centre of the rotor.

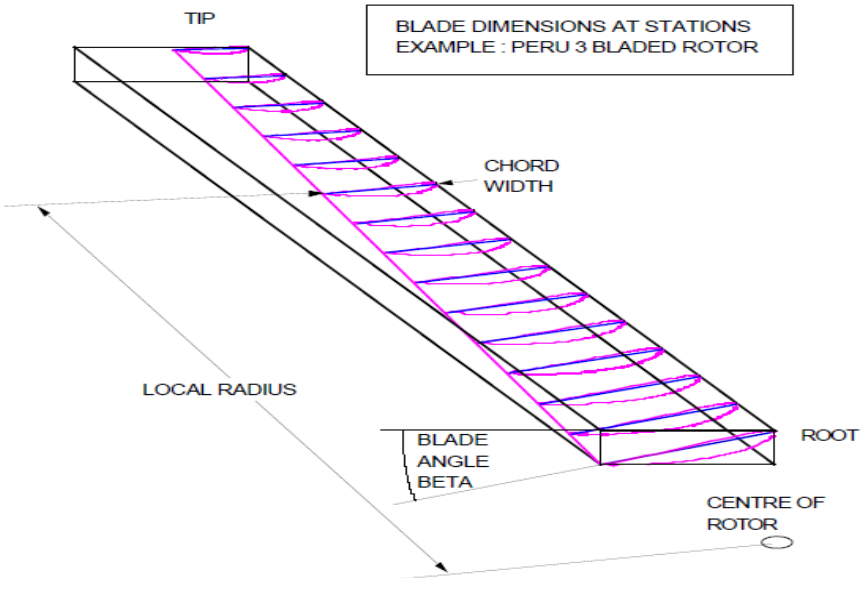

Fig. 2.8.2.2.1: The Blade stations [11]

Given the local radius, chord width and blade angle at some given number of airfoil stations, we can construct the shape of the whole blade.

where,

chord line: is the longest line within the blade section, and it joins the leading edge to the trailing edge.

blade pretwist angle (beta): is the angle between the chord line and the plane in which the rotor spins.

Essential steps to build the given blade Ls-dyna model in Hypermesh

Hypermesh, versions10 was used as the finite element preprocessor to model a pretwisted 14 m length wind turbine blade(of linearly decreasing NACA-4415 airfoil type from hub to tip) and then solve for the blade deformation using Ls-Dyna solver. The following are the essential steps that used to build the given blade Ls-dyna model in Hypermesh.

1st phase steps: creating the blade model

1) Create a Geom component.

2) Make Geom current and construct all the 1D beam elements using nodes and then lines to connect the nodes (14 1-D beams (total 15 nodes), each beam is 1 m length).

3) Solver Browser then right click ---> create ---> *MAT ---> *MAT _Elastic ---> Create *Mat_ Elastic (enter the Young's Modulus E and the poisson ratio of the material).

4) Create properties for each beam section i.e. 14 properties, by entering the associated area for each beam section as the average of the airfoil areas at the 2 nodes of that beam element section under consideration---> using a special macro---> enter the coordinates of the average airfoil as copied from an excel sheet ---> nodes of the airfoil geometry will show on the screen ---> Go to Geom ---> connect the coordinates of the airfoil geometry--->1D---> Hyperbeam to create that beam section property). Also using Hyperbeam, any airfoil beam section can be twisted as shown in the below Fig. 2.8.2.2.1.

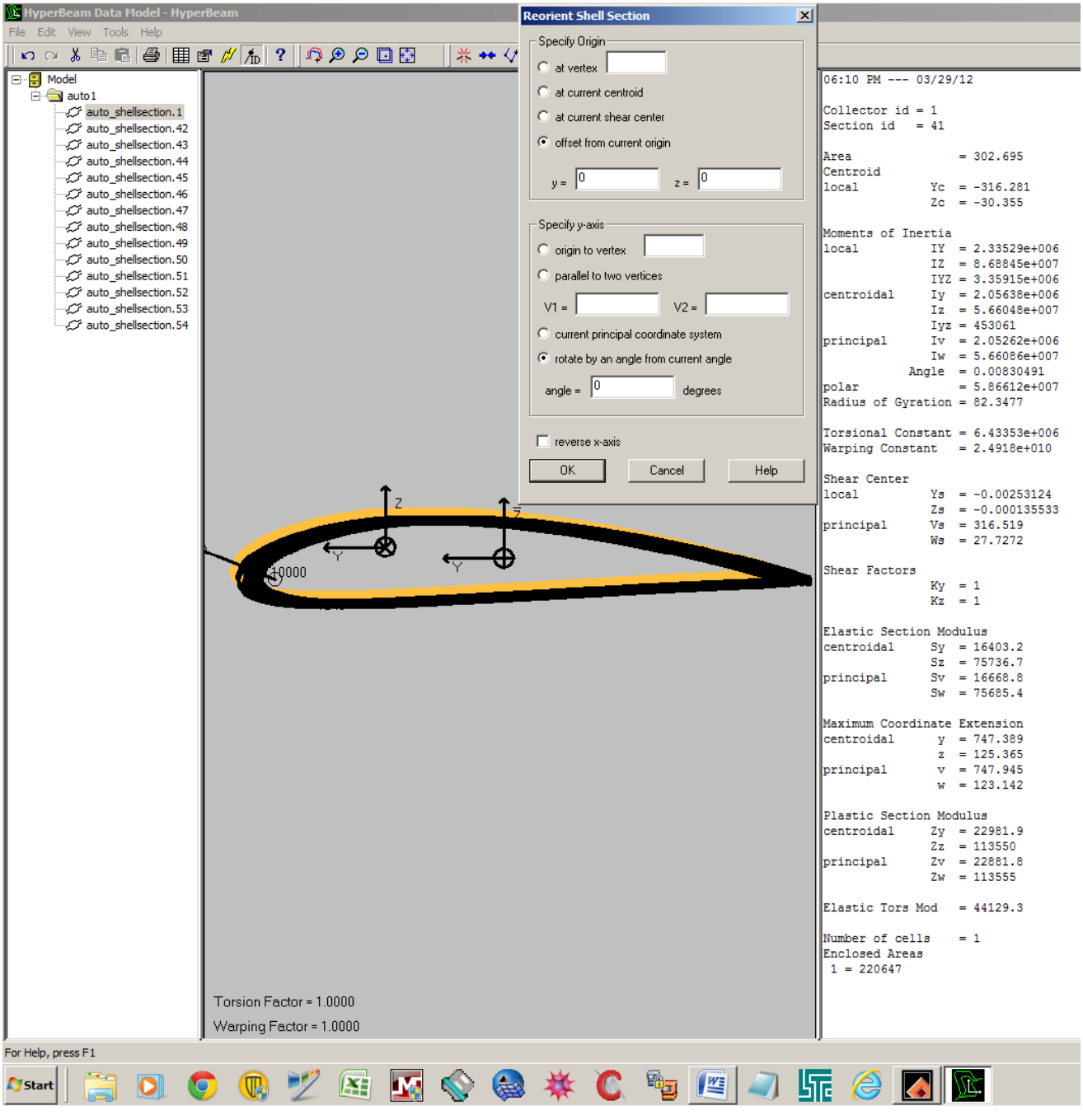

Fig. 2.8.2.2.2: Airfoil geometrical properties using Hypermesh.

5) Create 14 different 1D_beam sections that all share same material but each has its own property that created at previous step 4.

6) Meshing: Make the 1st beam element component current then 1D ---> line mesh, then select the associated property then select the the geometry of the 1st beam then Mesh.

7) Create a constraint collector.

8) Make constraint current and select left node and apply constraints at the hub of the blade (where x=o). Since each 1D_beam section (that created in step 5) has different average airfoil area, then all the 14 1-D beam elements will change to a 3-D blade as shown in Fig. 2.8.2.2.3.

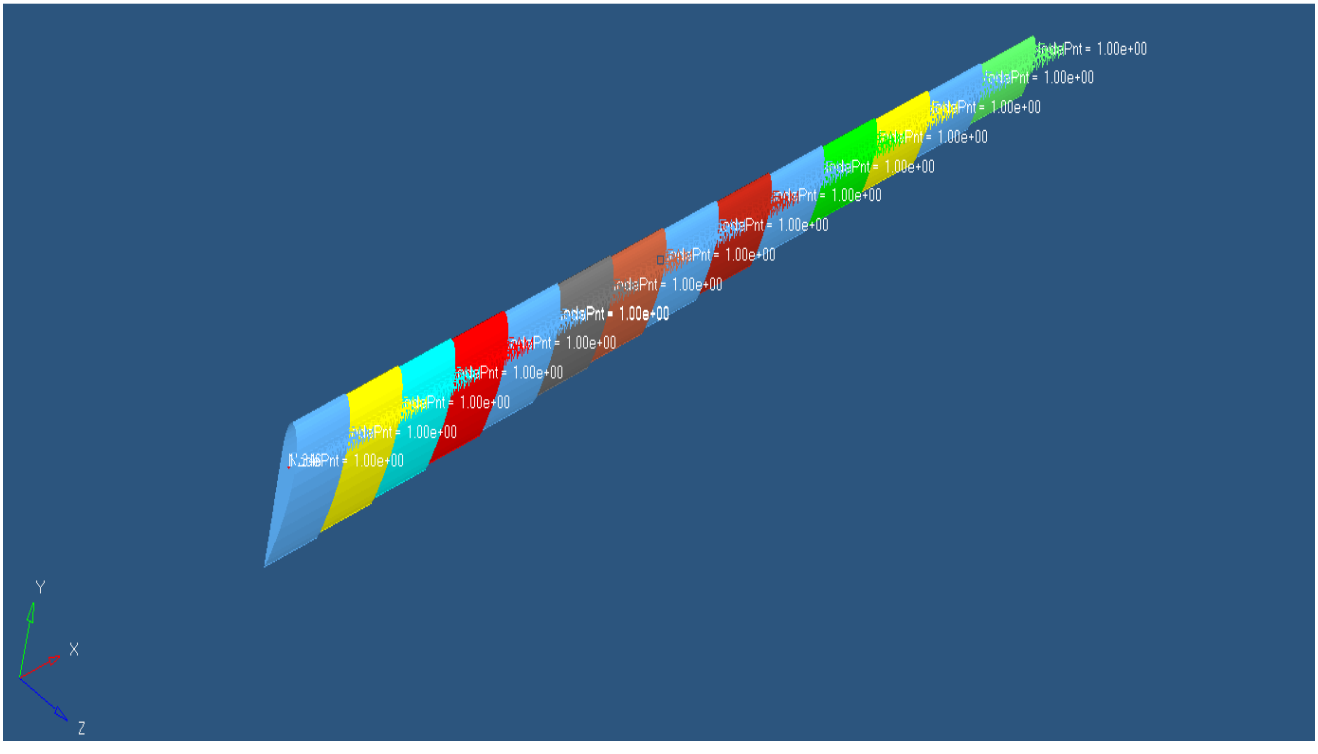

Fig. 2.8.2.2.3: Changing 1D beams to a 3D blade using Hypermesh.

2nd phase steps: creating the aerodynamic load curves

1. In the Solver Browser right click and select Create>Set>*Set_Node_List.

2. Name it Node1.

3. Select the first node to be loaded and create the set.

4. Repeat for each node to be loaded. Until you have a Node_Set for each of the nodes.

5. Create your curves for each of the loads you want, X,Y,Z and Rotational X,Y,Z (view ---> Solver Browser --> *Define ---> create ---> *Define_Curve --> New --> enter X (time) and Y (load). Then load curves data will looks like Fig. 2.8.2.2.4.

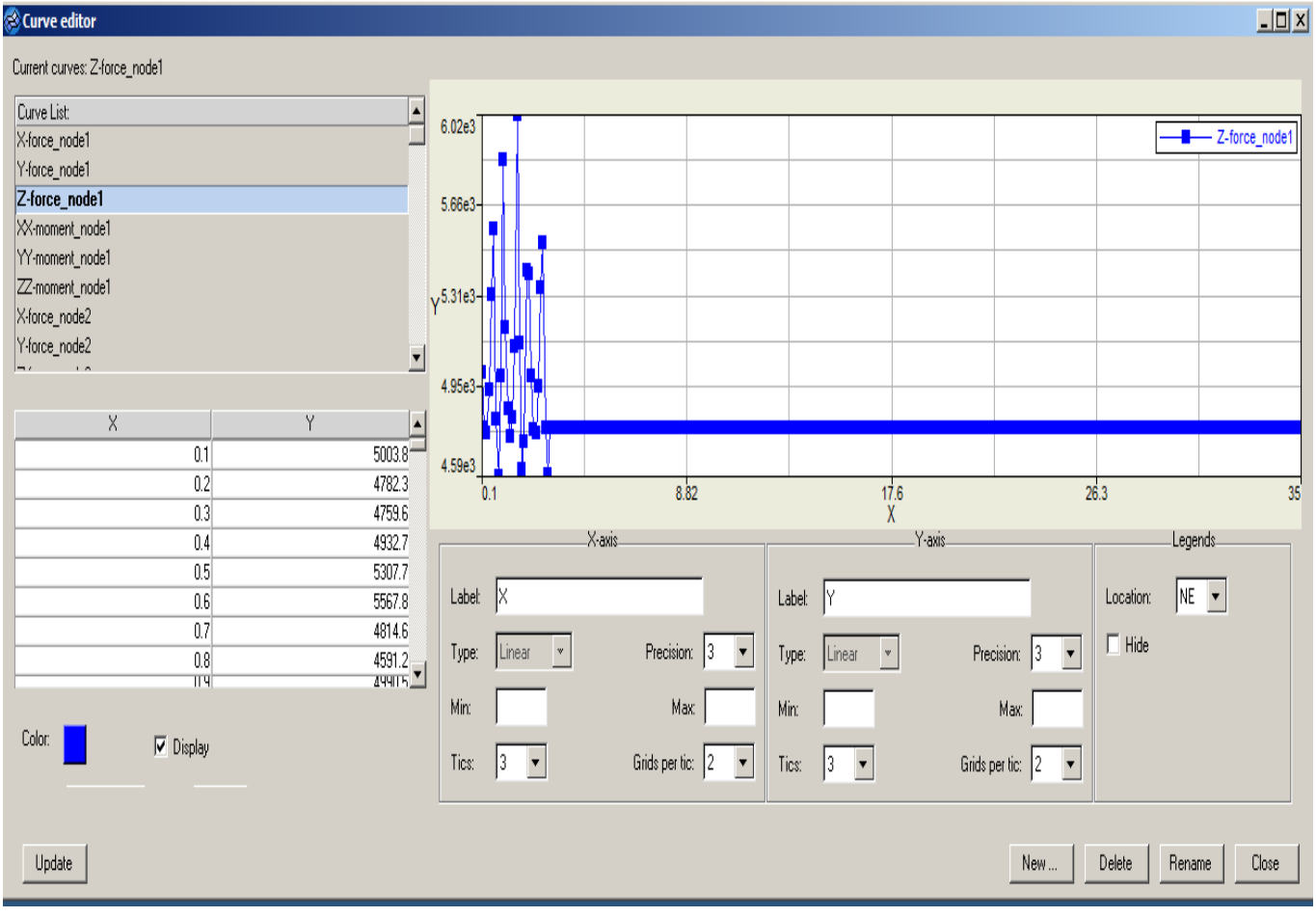

Fig. 2.8.2.2.4: The load curves data.

6. In the Solver Browser right click and select Create>Load>*Load_Node_Set.

7. Name it Load1.

8. When the card editor opens click NSID and pick the first node set.

9. Click DOFX and pick 1 (for the x component).

10. Click LCID and pick the curve for the X Load for the first node.

11. Repeat this procedure for the same node_set and pick DOFX 2 (Y Translational) and pick the LCID for the Y translational load curve.

12. Do this procedure for each node and every DOFX (1,2,3 are X,Y,Z translational and 5,6,7 are X,Y,Z rotational) so that every node has all load curves associated with it.

The final blade model cards are shown in Fig. 2.8.2.2.5.

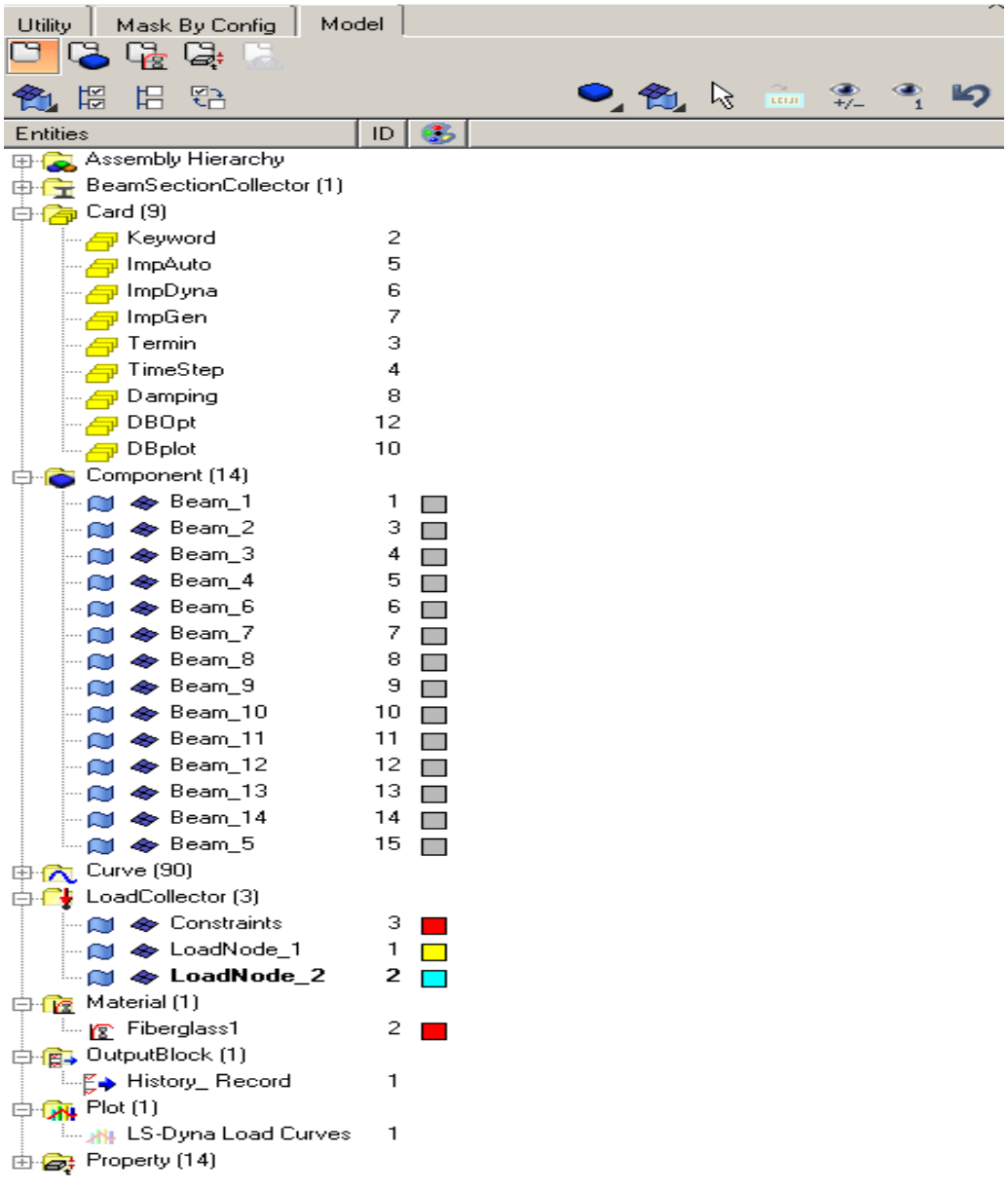

Fig. 2.8.2.2.5: The final blade Ls-Dyna model.

And the final blade model with all the added aerodynamic loadings Fx, Fy, Fz, Mx, My and Mz at each of the 15 nodes, starting at node1 (where x=0) and ending at node1 (where x=L) are shown in Fig. 2.8.2.2.6.

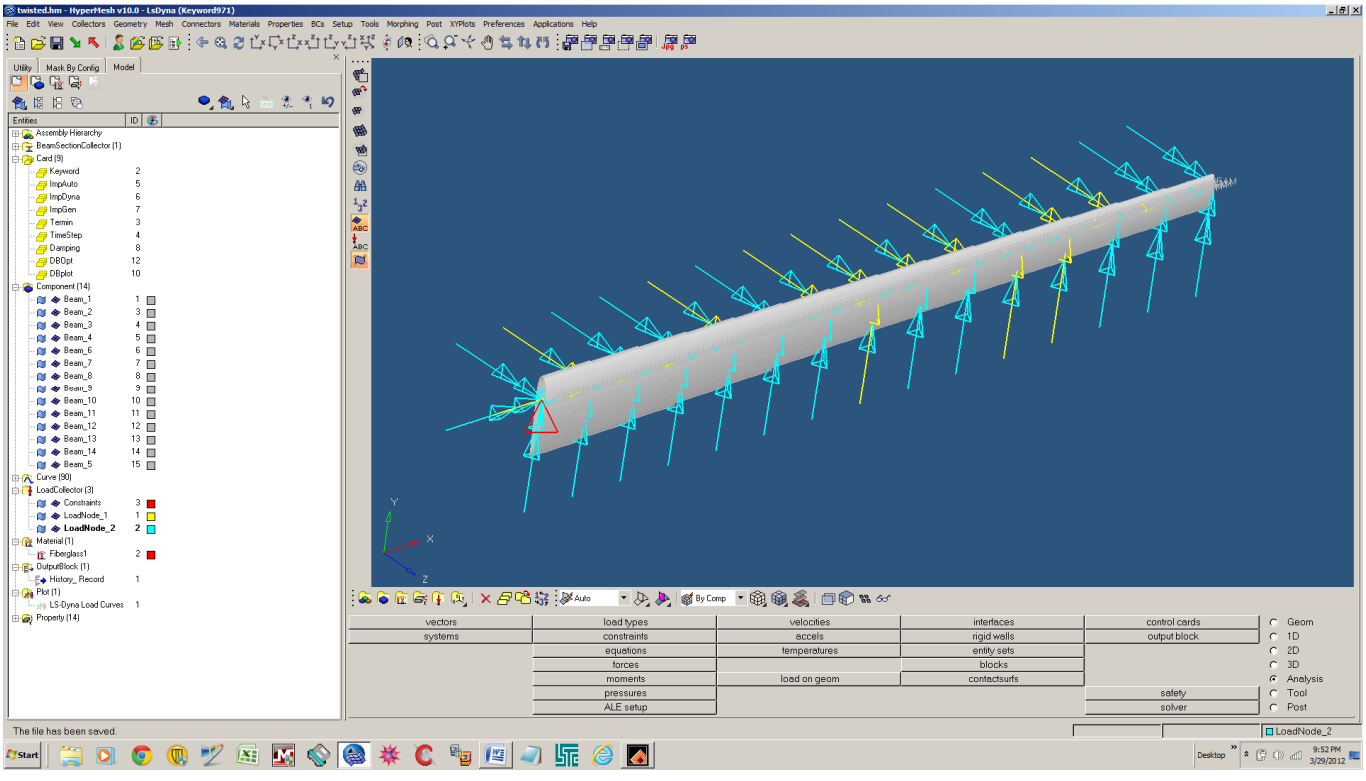

Fig. 2.8.2.2.6: All stations loadings.

The blade solution of the present research formulation for the linear small deformation case using the MATLAB code is compared with the same blade solution for the displacements and rotations plots (six degrees of freedom) at the blade tip with Younsi et al work.

While the blade solution of the present research formulation for the nonlinear large deformation case using the MATLAB code is compared with the same blade solution for the displacements and rotations plots (six degrees of freedom) at the blade tip with Ls-Dyna work.

It should be also noted that many other commercial codes have been tried throughout the present research to generate the geometrical blade properties for some given blade airfoil stations that linearly decrease from hub to tip as shown in Fig. 1.8.2.2. For example, the new commercial code VABS (Variational Asymptotical Beam Sectional Analysis) is one of the codes that can be used to model the wind turbine blade structure for which one dimension is much larger than the other even if the blade is made of composite materials and have a

complex internal structures. Another commercial code is NuMad, one of set of codes created by NREL that able to create a 3D blade structure from the 2D airfoils. NuMad is a stand-alone, GUI pre-processor for ANSYS finite element analysis software developed by Daniel Laird at Sandia National Laboratories. Some other codes like Concord and X-FOIL are used to create the 2D airfoils from their known coordinates. It should be noted that composite material work is not the concentration of the present research since that was done before.

2.9 Torsion of Arbitrary Cross-sections

2.9.1 Saint-Venant's Torsion Theory

It should be noted that for any non circular cross-sections, plane cross-sections will not remain plane after any torsional deformation and therefore warping of the cross-sections will occur. This problem of torsion and warping need to resolved in order to predict to a high accuracy the stress distribution and the deformation of a shaft of any arbitrary cross-sections. The problem of a cylindrical shaft under torsion was analyzed by Barre de Saint-Venant [12], who utilized the semi-inverse method (which rely on guessing a part of the solution, then trying to determine the rest of the solution in a rational way where all the differential equations and boundary conditions should be satisfied.

Consider a cylindrical shaft under torsion, with the x-axis along its length and with the ends at x=0 and x=L respectively.

The shear stresses in the cross-sections that perpendicular to the x-axis are:

$$\tau = \frac{Tr}{J} \qquad (2.9.1.1)$$

where r is the given radius vector measured from the central x-axis of the shaft.

The displacements in the x, y and z directions on the shaft are:

$$u = -\phi \; xz, \; \mathrm{v} = \phi \; xy \text{ and } w = \phi\psi\,(y, z) \tag{2.9.1.2}$$

where $\psi(y,z)$ is some function of y and z, called warping function, and ϕ is the angle of twist per unit of length of the shaft and is assumed to be very small (<<1).

The differential equations of equilibrium are:

$$\begin{aligned}
&\frac{\partial \sigma_{xx}}{\partial x} + \frac{\partial \sigma_{xy}}{\partial y} + \frac{\partial \sigma_{xz}}{\partial z} + \rho X = 0, \\
&\frac{\partial \sigma_{yx}}{\partial x} + \frac{\partial \sigma_{yy}}{\partial y} + \frac{\partial \sigma_{yz}}{\partial z} + \rho Y = 0, \\
&\frac{\partial \sigma_{zx}}{\partial x} + \frac{\partial \sigma_{zy}}{\partial y} + \frac{\partial \sigma_{zz}}{\partial z} + \rho Z = 0,
\end{aligned} \tag{2.9.1.3}$$

where,

ρ : is the density of the substance.

ρX, ρY, ρZ : are the body forces (*X, Y and Z* are the projections on the coordinate axes of the mass forces (i.e. gravity) acting on each part of the body, relative to the mass of that part.

Relying on the function $\psi(y,z)$ to satisfy the above differential equilibrium equations and assuming that the body forces are negligible. The B.C.s on the lateral surface of the shaft are:

$$\begin{aligned}
&\sigma_{yy} l_y + \sigma_{yz} l_z = 0 \\
&\sigma_{zy} l_y + \sigma_{zz} l_z = 0 \\
&\sigma_{xy} l_y + \sigma_{xz} l_z = 0
\end{aligned} \tag{2.9.1.4}$$

and the B.C.s at the ends x=0 and x=L :

$\sigma_{xx} = 0$ and σ_{xy} and σ_{xz} are equipollent to the torque T (2.9.1.5)

Consider l_y, l_z as the direction cosine constants for the lateral surface and ($l_x = 0$) as the direction cosine constant for the direction along the shaft length . From Eqn 2.9.1.2 , we can get the stresses values by using Hooke's law.

$$\sigma_{zx} = \phi G(\frac{\partial \psi}{\partial z} + y),\ \sigma_{xy} = \phi G(\frac{\partial \psi}{\partial z} - z) \text{ and } \sigma_{yz} = \sigma_{yy} = \sigma_{zz} = \sigma_{xx} = 0 \qquad (2.9.1.6)$$

A substitution of these values into Eqns 2.9.1.3 shows that the equilibrium equations is satisfied if $\psi(y,z)$ satisfied Eqn 2.9.1.7 within the cross-section of the cylinder :

$$\frac{\partial^2 \psi}{\partial y^2} + \frac{\partial^2 \psi}{\partial z^2} = 0 \qquad (2.9.1.7)$$

To satisfy the B.C.s, Eqn 2.9.1.4, we should maintain:

$$(\frac{\partial \psi}{\partial y} - z)\cos(l, y) + (\frac{\partial \psi}{\partial z} + y)\cos(l, z) = 0 \quad \text{on } C\,, \qquad (2.9.1.8)$$

where C is the boundary of the cross-section of the region R that shown in Fig. 2.9.1.1 .

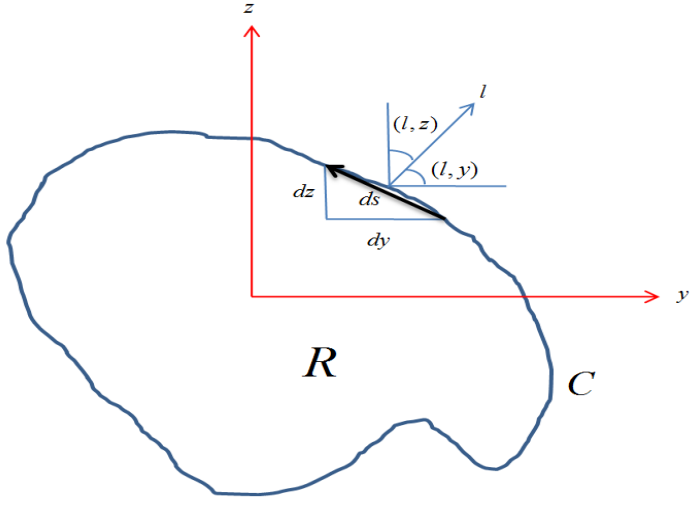

Fig. 2.9.1.1: An arbitrary cross-section under torsion (adapted from [12]).

but $\frac{\partial \psi}{\partial y}\cos(y,l) + \frac{\partial \psi}{\partial z}\cos(z,l) \equiv \frac{\partial \psi}{\partial l}$

Therefore the B.C.(s) of Eqn (2.9.1.9) can be written as:

$$\frac{\partial \psi}{\partial l} = z\cos(y,l) - y\cos(z,l) \text{ on } C. \qquad (2.9.1.9)$$

The B.C.(s) of Eqn 2.9.1.6 are satisfied if:

$$\iint_R \sigma_{xy} dydz = 0, \text{ and } \iint_R \sigma_{xz} dydz = 0, \qquad (2.9.1.10)$$

$$\iint_R (y\sigma_{xz} - z\sigma_{xy}) dydz = T \qquad (2.9.1.11)$$

We can verify that Eqns. 2.9.1.10 are satisfied if $\psi(y,z)$ satisfies Eqn 2.9.1.7 and Eqn 2.9.1.9 because: $\iint_R \sigma_{xy} dydz = \phi G \iint_R (\frac{\partial \psi}{\partial y} - z) dydz = \phi G \iint_R \left\{ \frac{\partial}{\partial y}[y(\frac{\partial \psi}{\partial y} - z)\ ] + \frac{\partial}{\partial z}[y(\frac{\partial \psi}{\partial z} + y)\ ] \right\} dydz,$

since $\psi(y,z)$ satisfies Eqn. 2.9.1.7. By applying the Gauss theorem to the final integral, it becomes as a line integral on the boundary C:

$$\phi G \int_C y\left[\frac{\partial \psi}{\partial l} - z\cos(y,l) + y\cos(z,l) \right] ds$$

which vanishes on account of Eqn 2.9.1.9. Similarly, the second Eqn of Eqns. 2.9.1.10 must be satisfied. Finally, the last condition of Eqn. 2.9.1.11 is :

$$T = \phi G \iint_R (y^2 + z^2 + y\frac{\partial \psi}{\partial z} - z\frac{\partial \psi}{\partial y}) dydz \qquad (2.9.1.12)$$

$$\text{but } J = \iint_R (y^2 + z^2 + y\frac{\partial \psi}{\partial z} - z\frac{\partial \psi}{\partial y}) dydz \qquad (2.9.1.13)$$

which implies, $$T = \phi GJ \qquad (2.9.1.14)$$

where,

ϕ : is the angle of twist at a specific location x along the shaft

GJ : is a proportionality constant or torsional rigidity of the shaft

G : is the shear modulus of the shaft

J : is the polar moment of inertia of the shaft cross-section if it is circular.

2.9.2 Prandtl Stress Function Theory

Prandtl [12] proposed an approach to calculate the warping in which he considers the stress components as the principal unknowns. Assuming that only σ_{yx} and σ_{zx} differ from zero, then all the equations of equilibrium Eqn 2.9.1.3 are satisfied if

$$\frac{\partial \sigma_{yx}}{\partial y} + \frac{\partial \sigma_{zx}}{\partial z} = 0 \qquad (2.9.2.1)$$

Also Prandtl [12] observes that this equation is identically satisfied if σ_{yx} and σ_{zx} are derived from a stress function $\varphi(y,z)$ in such a way that:

$$\sigma_{yx} = \frac{\partial \varphi}{\partial z} \text{ and } \sigma_{zx} = -\frac{\partial \varphi}{\partial y} \qquad (2.9.2.2)$$

This stress function $\varphi(y,z)$ can be an arbitrary function as long as the stress system Eqn 2.9.2.2 satisfy the boundary conditions Eqn 2.9.1.4 and Eqn 2.9.2.1 and the compatibility conditions.

From Eqn 2.9.2.1, we can figure out that the compatibility requires that (in absence of body forces) the following:

$\nabla^2 \sigma_{yx} = 0$ and $\nabla^2 \sigma_{zx} = 0$, where, ∇^2 denotes $(\frac{\partial^2}{\partial y^2} + \frac{\partial^2}{\partial z^2})$, hence,

$$\frac{\partial}{\partial y} \nabla^2 \varphi = 0 \text{ and } \frac{\partial}{\partial z} \nabla^2 \varphi = 0 \qquad (2.9.2.3)$$

$$\nabla^2 \varphi = const. \qquad (2.9.2.4)$$

Of the boundary conditions Eqn 2.9.1.4 only the last equation is not identically satisfied but from Fig. 2.9.1.1, we note that:

$$l_y = \cos(l, y) = \frac{dz}{ds} \text{ and } l_z = \cos(l, z) = -\frac{dy}{ds} \qquad (2.9.2.5)$$

We can write the last equation of Eqn 2.9.1.4 as :

$$\frac{\partial \varphi}{\partial z}\frac{\partial z}{\partial s}+\frac{\partial \varphi}{\partial y}\frac{\partial y}{\partial s}=\frac{\partial \varphi}{\partial s}=0,\ \text{on}\ C. \qquad (2.9.2.6)$$

Hence $\varphi(y,z)$ must be constant along the boundary curve C. For a simply connected region, it is general enough to set :

$$\varphi = 0,\ \text{on}\ C. \qquad (2.9.2.7)$$

It remains to examine the boundary conditions Eqn 2.9.1.5. The first, $\sigma_{xx}=0$, follows the starting assumption. The other conditions are stated in Eqns 2.9.1.10 and Eqn 2.9.1.11.

but $\iint_R \sigma_{xy}dydz=\iint_R \frac{\partial \varphi}{\partial z}dydz$, by Gauss' theorem, this is $\int_C \varphi\ l_z\ ds$, and it vanishes on account of Eqn 2.9.2.7.

Similarly, the resultant force in z-direction vanishes. Thus Eqn. 2.9.1.10 are satisfied.

Finally, Eqn 2.9.1.11 requires that: $T=-\iint_R (y\frac{\partial \varphi}{\partial y}+z\frac{\partial \varphi}{\partial z})dydz$

which can be transformed by Gauss' theorem as follows:

$$T=-\iint_R \left\{ \frac{\partial}{\partial y}(y\varphi)+\frac{\partial}{\partial z}(z\varphi)-2\varphi \right\} dydz$$

$$=-\int_C \left\{ y\varphi\cos(l,y)+z\varphi\cos(l,z) \right\} ds+\iint_R 2\varphi dydz \qquad (2.9.2.8)$$

If R is simply connected region, the line integral vanishes by the boundary conditions Eqn 2.9.2.7, implies:

$$T=2\iint_R \varphi\ dydz \qquad (2.9.2.9)$$

Thus, all differential equations and boundary conditions concerning stresses are satisfied if φ obeys Eqn 2.9.2.6, Eqn 2.9.2.7 and Eqn 2.9.2.8. But there remains an indeterminante constant in Eqn 2.9.2.6. This constant has to be determined by boundary conditions on displacements. From Eqn 2.9.1.2 and Eqn 2.9.1.6, we get:

$$\frac{\partial w}{\partial y} = \frac{\sigma_{xy}}{G} + \alpha z \text{ and } \frac{\partial w}{\partial z} = \frac{\sigma_{xz}}{G} - \alpha y \qquad (2.9.2.10)$$

Differentiating with respect to z and y, respectively, and subtracting we get:

$$\frac{1}{G}\left(\frac{\partial \sigma_{xy}}{\partial z} - \frac{\partial \sigma_{xz}}{\partial y}\right) = -2\alpha \qquad (2.9.2.11)$$

Hence, a substitution from (2.9.2.7) gives

$$\frac{\partial^2 \varphi}{\partial y^2} + \frac{\partial^2 \varphi}{\partial z^2} = -2G\alpha \qquad (2.9.2.12)$$

In this way, the problem of torsion is to the solution of the poisson Eqn 2.9.2.12 with boundary condition Eqn 2.9.2.7.

Elliptical Cross-section

Let us apply the Prandtl approach [12] to calculate the warping of an elliptical cross section

$$\text{where } \frac{y^2}{a^2} + \frac{z^2}{b^2} - 1 = 0 \qquad (2.9.2.13)$$

Then Eqn 2.9.2.12 and Eqn 2.9.2.7 are satisfied by having the stress function:

$$\varphi = -\frac{a^2 b^2 G\alpha}{(a^2 + b^2)}\left(\frac{y^2}{a^2} + \frac{z^2}{b^2} - 1\right) \qquad (2.9.2.14)$$

Eqn 2.9.2.8 gives the relation between the torque and the rate of twist $\theta = \frac{d\phi}{dx}$

$$T = \frac{\pi a^3 b^3}{(a^2 + b^2)} G \frac{d\phi}{dx} \qquad (2.9.2.15)$$

The stresses are given by Eqn 2.9.2.2. Note the following curves have an interesting meaning:

$$\varphi(y, z) = const$$

The slope dz/dy of the tangent to such a curve is determined by the formula:

$$\frac{\partial \varphi}{\partial y} + \frac{\partial \varphi}{\partial z}\frac{\partial z}{\partial y} = 0 \qquad (2.9.2.16)$$

Hence, according to Eqn 2.9.2.2, we have

$\sigma_{yx} = \frac{\partial \varphi}{\partial z}$ and $\sigma_{zx} = -\frac{\partial \varphi}{\partial y}$, which implies: $\frac{\partial z}{\partial y} = \frac{\sigma_{xz}}{\sigma_{xy}}$.

The magnitude of shearing stress is:

$$\tau = (\sigma_{xy}{}^2 + \sigma_{xz}{}^2)^{\frac{1}{2}} = [(\frac{\partial \varphi}{\partial y})^2 + (\frac{\partial \varphi}{\partial z})^2]^{\frac{1}{2}} \qquad (2.9.2.17)$$

The maximum shearing stress is :

$$\tau = 2G\frac{a^2 b}{a^2 + b^2}\theta \qquad (2.9.2.18)$$

Now the warping (out of plane displacements) function $\psi(y,z)$ for a constant elliptic cross-section can easily be shown to be :

$$\psi = -\frac{a^2 - b^2}{a^2 + b^2} y z = Kyz \qquad (2.9.2.19)$$

where $K = \frac{a^2 - b^2}{a^2 + b^2}$ is a constant depends on the two diameters a and b of the ellipse.

So as mentioned earlier in section 2.9.1, shafts or cylinders of a non-circular cross-section undergo warping when subjected to pure torsion. An example is the warping that occurs in the shafts with elliptical cross sections i.e. Eqn 2.9.2.19.

For the present research, warping will be calculated at many selected given stations from hub to tip of the given wind turbine blade (that has different airfoil dimentions at different cross sections) where at each selected station there is only a one calculated value of warping that is different from the next station. Therefore, warping in the present research is considered to be dependent on x coordinate only and is independent of the y and z coordinates which is different from the above mentioned constant elliptic cross-section case.

2.9.3 Cross-section Geometrical Properties

2.9.3.1 Torsional Rigidity Calculation

The analytical calculation of the exact values of the “torsional rigidity” for cylindrical bars is limited to a few number of cross-sections. Exact solutions for the ellipse, circle and equilateral triangle are listed in [13] while the approximations for rectangular cross-sections are available in [14]. The approximated solution for many cross-sections such as trapezoids, triangle, semicircles, are listed in handbooks such Roark [15]. A good approach to approximate the torsional rigidity of any cylindrical solid cross-section is detailed in [15, 16]. Some cross sections can be considered as a combination of an ellipse, rectangle and triangle, etc.

There are many softwares that can be used to calculate the geometrical properties for any cross section including warping, moment of inertias and torsional rigidity [16] but for my work I used the Hypermesh version 10 to calculate such properties that needed for my analysis.

2.9.3.2 Second Moment of Inertia

There are three types of moment of inertia: The second moment of inertia, the product moment of inertia and the polar moment of inertia. Consider a beam with a cross-sectional area A (that has a plane region of a particular shape which is perpendicular to the beam's axis). And consider *λ* to be a straight line in the plane (which is by definition, perpendicular to the axis of the beam). The “second moment of area” of the region A about the line *λ* is:

$$I_\lambda = \int_A n^2 \, \mathrm{d}A \qquad (2.9.3.2.1)$$

where d*A* is the elemental area; and *n* is the perpendicular distance from the element d*A* to the line *λ*

If the line *λ* is the *x* axis and the bending force is parallel to the y axis, the second moment of area can be computed as:

$$I_x = \iint_A y^2 \, \mathrm{d}x \, \mathrm{d}y \qquad (2.9.3.2.2)$$

To calculate the bending stresses, the above equation can only be used when cross-sections are symmetrical about the *x*-axis. But if cross-sections are not symmetrical, the second moment of area about both the *x*-axis and *y*-axis and the product moment of area, I_{xy}, (explained in the next section) are required.

2.9.3.3 Product Moment of Inertia

The scalar of the "second moment of area" for a beam about a certain axis, describes the beam's resistance to bending along that axis. Some beams will deflect in a direction other than the direction they are loaded. Consider, for example, a leaf spring running along the *x* axis and directed such that its surface normal is in the (0,1,1) vector direction. If we push downward on it in the (0, 0, −1) vector direction, we get a bending moment in the (0,1,0) vector direction. However, even that the spring is moving downward, it is primarily deflecting in the (0, −1, −1) vector direction. This behavior should be captured by the "product moment of area".

The product moment of area is:

$$I_{xy} = \int_A xy \, \mathrm{d}A \qquad (2.9.3.3.1)$$

where,

x: is the perpendicular distance from *y* axis to the element d*A.*

y: is the perpendicular distance from *x* axis to the element d*A*.

2.9.3.4 Polar Moment of Inertia

Polar moment of inertia is defined as the quantity that used to predict an object's ability to resist torsion, in objects with an invariant circular cross-section and insignificant warping. It is used to calculate the angular displacement of an object when it is subjected to a torque. It is analogous to the area moment of inertia that predicts an object's ability to resist bending. The larger the polar moment of inertia, means the less the beam can twist, when subjected to a given torque. It should be noted that “polar moment of inertia” should not be confused with “moment of inertia”, which characterizes an object's angular acceleration due to a torque.

Limitations

The “polar moment of inertia” can not be utilized to analyze any non-circular cross-section shaft. For non-circular cross-sections shafts, the “torsional constant” should be calculated instead of the “polar moment of inertia”. In objects with significant cross-sectional variation (along the axis of the applied torque), which cannot be analyzed in segments, a more careful approach should be used. However the “polar moment of inertia” can be utilized to compute the “moment of inertia” of an object with arbitrary cross-section.

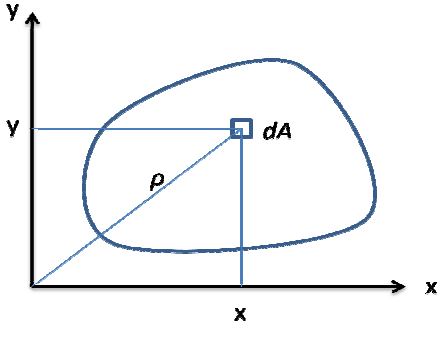

Fig. 2.9.3.4.1: The polar moment of inertia.

A schematic of Fig. 2.9.3.4.1 show how the “polar moment of inertia” is calculated for an arbitrary shape about an axis *o*.

$$J_z = \int_A \rho^2 \, dA \qquad (2.9.3.4.1)$$

where J_z is the "polar moment of inertia" about the axis *z*; and ρ is the radial distance to the element *dA* from the axis *z.*

For a circular section with radius r:

$$J_z = \int_0^{2\pi} \int_0^r \rho^2 \rho \, d\rho \, d\phi = \frac{\pi r^4}{2} \qquad (2.9.3.4.2)$$

For a rectangular section with sides b and h:

$$J_z = \int_{-b/2}^{b/2} \int_{-h/2}^{h/2} (x^2 + y^2) \, dx \, dy = \frac{bh}{12}(b^2 + h^2) \qquad (2.9.3.4.3)$$

The SI unit for the "polar moment of inertia" is the same as the "*area moment of inertia"* i.e. m^4.

Conversion from Area Moment of Inertia

Using the perpendicular axis theorem, the polar moment of inertia J_z is related to the area moments of inertia about the other two mutually perpendicular axes: $J_z = I_x + I_y$. The "polar moment of inertia" J_z appears in the formulae describes torsional stress and angular displacement.

Torsional stress

$$\tau = \frac{Tr}{J_z} \qquad (2.9.3.4.4)$$

where T is the torque; r is the distance from the center; and J_z is the polar moment of inertia.

In a circular shaft, the shear stress is maximum at the surface of the shaft where the torque is maximum:

$$T_{\max} = \frac{\tau_{\max} J_z}{r} \qquad (2.9.3.4.5)$$

Chapter 3

Total Strain Energy, Total Kinetic Energy, Aerodynamic loadings & External Work

3.1 Introduction

Wind turbine blades similar to helicopter rotor blades [17] have the structure of pre-twisted beams that react due to extension, torsion, flexure and the coupling interactions among all these loads. A number of approximate theories used for the pre-twisted beam have been developed by different researchers to analyze its complex geometry.

For example, the potential and kinetic energy relationships were given by Carnegie [18] for a pre-twisted cantilever blade using the standard variational approach to deduce the equations of motion and allowing for torsion, bending, rotary inertia and deflections due to shear without any warping effect. Yardimoglu and Yildirim [19] derived the strain energy and kinetic energy for pretwisted Timoshenko beam undergoing bending-bending load coupling. More recently, Ozgumus and Kaya derived [20, 21] the strain energy and kinetic energy to obtain the equations of motion for a rotating beam considering bending-torsional coupling considering the effect of the centrifugal force and the effect of shear as in a Timoshenku beam. And Liu, Friend and Yeo [22], derived the strain energy and kinetic energy considering axial-torsional coupling vibration for a pretwisted beam that has an elliptic cross section. Then they obtained the equations of motion using Hamilton's principle assuming an elliptical cross section warping. The calculation of warping for an eliplitical cross section is elementary and is easy to calculate.

In this chapter, the total strain and total kinetic energy were derived for both the linear small deformation case and the nonlinear large deformation case.

Also the pitch moment, thrust, centrifugal forces (that allow us to obtain the external work acting on the blade), boundary conditions and damping on the blade will be discussed. It should be noted that the six unknown displacements at any x along the blade's length direction were assumed to be expanded a series of products of time dependent constants and polynomials expansion and then computed by solving the dynamic equations of motion.

3.2 Dynamic Equations of Motion

Consider the blade shown in Fig. 3.2.1 as a Timoshenko beam with a pretwisted angle β.

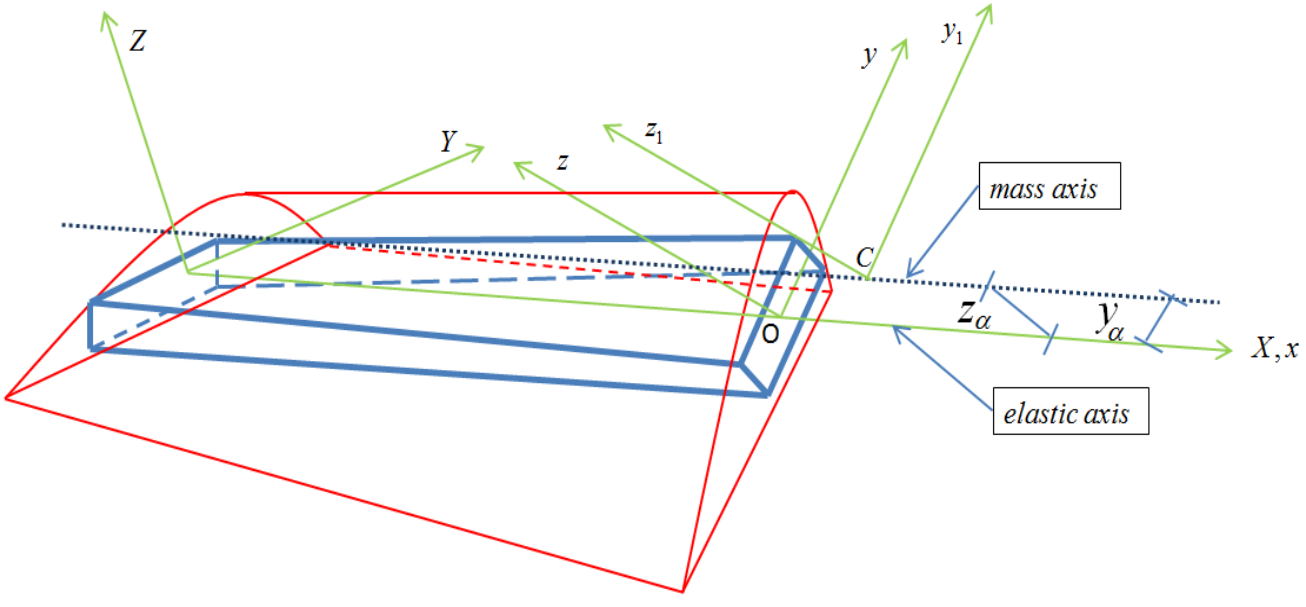

Fig. 3.2.1: Pre-twisted asymmetrical blade structure coordinate systems.

The blade has at any x along the lengthwise three displacements u, v and w in the directions of x, y and z axes respectively, bending rotations θ_1 and θ_2 about the y and z axes respectively and torsional rotation ϕ about the x axis. Also we are considering ψ as the airfoil cross sectional warping.

By applying the following Lagrange equations [23] to the blade of Fig. 3.2.1, we will obtain all the equations of motion:

$$\frac{d}{dt}\left(\frac{\partial T}{\partial \dot{q}_m}\right)-\frac{\partial T}{\partial q_m}+\frac{\partial U_{Total}}{\partial q_m}+\frac{\partial U_{B.C.s}}{\partial q_m}+\frac{\partial F}{\partial \dot{q}_m}-\frac{\partial W_{ext}}{\partial q_m}=0 \qquad (3.2.1)$$

where,

q_m: is equal to $a_m,\ b_m,\ c_m,\ d_m,\ e_m\ or\ f_m$

T: is the total Kinetic energy

U_{Total}: is the total strain energy

W_{ext}: is the external work on the blade due to the applied aerodynamic pressure

F: is the applied nonconservative damping force if blade assumed to be of viscous type [61].

$$F=\frac{1}{2}c\int_0^a\int_0^b(\dot{u}^2+\dot{v}^2+\dot{w}^2)\,\mathrm{d}x\,\mathrm{d}y$$

where c has a different value for each term of the mode expansion. Simple calculation give:

$$F=\frac{1}{2}\frac{ab}{4}\sum_{n=1}^{N}\sum_{m=1}^{M}c_{m,n}(\dot{u}_{m,n}^2+\dot{v}_{m,n}^2+\dot{w}_{m,n}^2)$$

The damping coefficient $c_{m,n}$ is related to modal damping ratio, that can be evaluated from experiments, by $\varsigma_{m,n}=c_{m,n}/(2\mu_{m,n}\omega_{m,n})$, where $\omega_{m,n}$ is the natural circular frequency of mode (m,n) and $\mu_{m,n}$ is the modal mass of this mode, given by:

$$\mu_{m,n}=\rho_S h(ab/4)$$

In the present research, the author considers only the material damping and neglects the viscous damping i.e. neglecting the term $\frac{\partial F}{\partial \dot{q}_m}=0$, which results in reducing one term of the equations 3.2.1 to become:

$$\frac{d}{dt}\left(\frac{\partial T}{\partial \dot{q}_m}\right) - \frac{\partial T}{\partial q_m} + \frac{\partial U_{Total}}{\partial q_m} + \frac{\partial U_{B.C.s}}{\partial q_m} - \frac{\partial W_{ext}}{\partial q_m} = 0 \qquad (3.2.2)$$

3.3 Computation of the Total Strain Energy

By adding all the different derived strain energies from Appendix A i.e. equations (A.1), (A.2) and (A.3), we get the total strain energy [9, 13, 18, 20-22, 24-26]:

$$U_{Total} = \frac{1}{2}\int_0^L \{ E(I_{yy}\theta_1'^2 + 2I_{yz}\theta_1'\theta_2' + I_{zz}\theta_2'^2) + kGA((w'-\theta_1)^2 + (v'-\theta_2)^2 \}dx + \frac{1}{2}\int_0^L P[v'^2 - 2y_\alpha v'\phi' + (I_p/A(x))\phi'^2]dx + \frac{1}{2}\int_0^L P[w'^2 - 2z_\alpha w'\phi' + (I_p/A(x))\phi'^2]dx + \frac{1}{2}E\int_0^L \frac{1}{4}Aw'^4 dx + \frac{1}{2}E\int_0^L \frac{1}{2}I_p w'^2\phi'^2 dx + \int_0^L [K_1\theta_1'\phi' + K_2\theta_2'\phi']dx + \int_0^L \iint_A dydz\{\frac{1}{2}E\varepsilon_{xx}^2 + 2G(\varepsilon_{xy}^2 + \varepsilon_{xz}^2)\}dx + \int_0^L \frac{1}{2}EI_p\phi''^2 dx \qquad (3.3)$$

where,

$$\varepsilon_{xx} = \left[\frac{\partial \bar{u}}{\partial x} + \theta\frac{\partial \psi}{\partial x} + \frac{\partial \theta}{\partial x}\psi + \frac{1}{2}\left(\frac{\partial \bar{u}}{\partial x}\right)^2 + \frac{1}{2}\left(\theta\frac{\partial \psi}{\partial x}\right)^2 + \frac{\partial \bar{u}}{\partial x}\theta\frac{\partial \psi}{\partial x} + \frac{1}{2}\left(\frac{\partial \theta}{\partial x}\psi\right)^2 + \theta\frac{\partial \psi}{\partial x}\frac{\partial \theta}{\partial x}\psi + \frac{\partial \bar{u}}{\partial x}\frac{\partial \theta}{\partial x}\psi + \frac{1}{2}r^2\theta^2\right] \text{ where, } r^2 = y_1^2 + z_1^2 \qquad (3.3\text{-a})$$

$$\varepsilon_{xy} = \frac{1}{2}\theta[-z_1] \text{ and } \varepsilon_{xz} = \frac{1}{2}\theta[y_1] \qquad (3.3\text{-b})$$

3.4 Computation of the Total Kinetic Energy

By adding all the different derived kinetic energies [9, 13, 18, 20, 22, 24-26] from Appendix B i.e. equations (B.1.2), (B.2) and (B.3), we got the total strain energy as:

$$T = \frac{1}{2}\int_0^L \rho(x)\Big[\ \dot{\bar{u}}^2 A(x) + 2\dot{\bar{u}}\,(\frac{\partial\dot{\phi}}{\partial x})\,\psi\,A(x) + (\frac{\partial\dot{\phi}}{\partial x})^2\,\psi^2\,A(x) + I_p(x)\dot{\phi}^2\ \Big]dx$$

$$+\frac{1}{2}\int_0^L \rho(x)\Big\{\ \bar{\Omega}^2 z^2 A(x)\theta_2^2 - \bar{\Omega}^2 y^2 A(x)\phi^2 - \bar{\Omega}^2 z^2 A(x)\theta_2^2\phi^2 + \frac{1}{4}\bar{\Omega}^2 y^2 A(x)\phi^4 + \bar{\Omega}^2 A(x)\bar{u}^2 + 2\bar{\Omega}^2 y^2 A(x)\phi\dot{\theta}_2 - 2\bar{\Omega} z^2 A(x)\phi\dot{\theta}_2$$

$$+\bar{\Omega} z^2 A(x)\phi^3\dot{\theta}_2 + z^2 A(x)\,\dot{\theta}_2^2 - z^2 A(x)\phi^2\,\dot{\theta}_2^2 + 2\bar{\Omega} y^2 A(x)\theta_2\dot{\phi} + 2\bar{\Omega} z^2 A(x)\,\theta_2\dot{\phi} - \bar{\Omega} y^2 A(x)\theta_2\phi^2\dot{\phi} - \bar{\Omega} z^2$$

$$A(x)\,\theta_2\phi^2\dot{\phi} + 2y^2 A(x)\theta_2\phi\dot{\theta}_2\dot{\phi} - 2z^2 A(x)\theta_2\phi\dot{\theta}_2\dot{\phi} + y^2 A(x)\,\dot{\phi}^2 + z^2 A(x)\dot{\phi}^2 + y^2 A(x)\theta_2^2\dot{\phi}^2\ \Big\}dx$$

$$+\frac{1}{2}\int_0^L m(x)\Big[\ (\dot{v} + z_\alpha\dot{\phi})^2 + (\dot{w} + y_\alpha\dot{\phi})^2\ \Big]dx + \frac{1}{2}\int_0^L \Big\{\ \rho(x)I_{zz}\,(\dot{\theta}_2 + z_\alpha\dot{\phi}')^2 + \rho(x)I_{yy}\,(\dot{\theta}_1 + y_\alpha\dot{\phi}')^2\cdot\ \Big\}dx$$

$$-\frac{\Omega^2}{2}\int_0^L m(x)\Big[\ (v' + z_\alpha\phi')^2 + (w' + y_\alpha\phi')^2\ \Big]xdx + \frac{1}{2}\int_0^L \Big[\ \frac{I_{zz}\rho(x)(\theta_2 + z_\alpha\dot{\phi}' + z_\alpha'\dot{\phi})^2}{g}$$

$$+\frac{I_{yy}\rho(x)(\theta_1 + y_\alpha\dot{\phi}' + y_\alpha'\dot{\phi})^2}{g}\ \Big]\ dx \qquad (3.4)$$

3.5 Displacement Expansion

The author assumed a summation of a product of time dependent constants and polynomials expansion for the three displacements $\bar{u}, v, w$ and the three rotations θ_1, θ_2, ϕ at any x along the blade length as shown below in order to solve for them using the Assumed Modes Method:

$$\bar{u} = \sum_{n=1}^{N} a_n(t)\phi_n(x),$$

similarly, $v = \sum_{n=1}^{N} b_n(t)\phi_n(x)$, $w = \sum_{n=1}^{N} c_n(t)\phi_n(x)$, $\theta_1 = \sum_{n=1}^{N} d_n(t)\phi_n(x)$, $\theta_2 = \sum_{n=1}^{N} e_n(t)\phi_n(x)$, and

$$\phi = \sum_{n=1}^{N} f_n(t)\phi_n(x) \qquad (3.5)$$

where the polynomial functions $\phi_n(x) = (x/L)^{n+1}$ and $a_n(t), b_n(t), c_n(t), d_n(t), e_n(t)$ and $f_n(t)$ are the time dependent constants that need to be solved using the equations of motion and Newmark non-linear iteration scheme.

3.6 Thrusts, torques, centrifugal forces and pitch moments

True distributions of the aerodynamic loadings that needed for the structural analysis of the wind turbine blades, are difficult to predict and usually require some flow codes such as CFD to determine their accurate magnitude. In this section I am providing a simple model for the estimate of blade forces suitable for use in structural analysis. Thrust forces are directed in the axial direction (i.e., following the blade shaft axis). Torque forces are tangent to the radius arc. Centrifugal forces are normal to the axis. As noted earlier that according to the BEM theory [27], air loads on a section airfoil of the blade are proportional to the dynamic pressure at only that section.

The premise of the simplified model is that a) the forces can be modeled by a set of point loads rather than distributed pressures, and b) the magnitudes of these point loads can be estimated using the below load formulaes, c) An interpolation scheme needed to have all computed forces and moments as a function of the blade lengthwise x. Fig. 3.6.1 below, illustrates how the three principal forces - thrust, torque and centrifugal- are applied as point loads acting on a radial span of the blade.

The aerodynamic forces (lift, drag and pitching moment) as shown in Fig. 3.6.1 are directly linked to the type of flow, relative wind velocities and the wind attack angles to the airfoil sections.

$$\textbf{Lift:} \qquad L = \frac{1}{2}\rho \; V_{rel}^2 \; c \; C_l$$

$$\textbf{Drag:} \qquad D = \frac{1}{2}\rho \; V_{rel}^2 \, c \; C_d$$

$$\textbf{Pitch Moment:} \qquad PM = \frac{1}{2}\rho \; V_{rel}^2 \; c^2 \; C_m \qquad (3.6.1)$$

The simplified model is stating that (a) the forces can be modeled by a set of station loads rather than distributed loads, and (b) then the magnitudes of these station loads can be

predicted using the below listed load formulas, (c) then an interpolation scheme will interpolate all computed station loads (forces and moments) as a function of the blade lengthwise x.

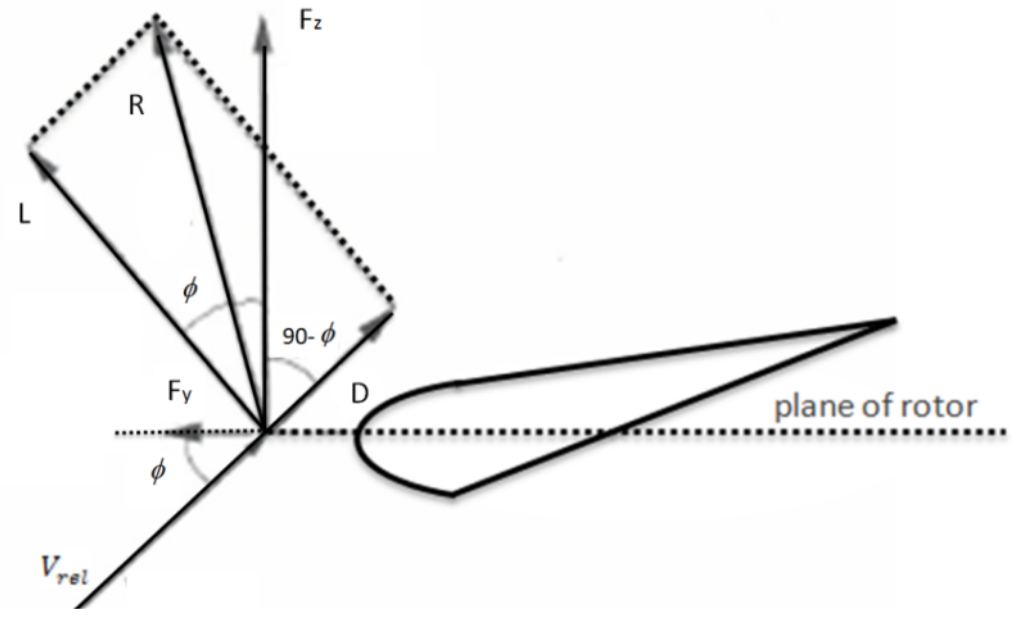

Fig. 3.6.1: The lift and drag forces.

Fig. 3.6.2 below, illustrates how the three principal forces - thrust, torque and centrifugal- are applied as point loads acting on a radial span of the blade. Thrust forces are always axial in their direction (i.e., following the blade shaft axis). Torque forces will be tangent to the radius arc and centrifugal forces are normal to the axis.

Then all the forces and moments acting at the selected airfoil stations along the blade can be calculated from the following formulaes [28-30]:

$$\textbf{Centrifugal force:} \quad Fx = m\, r\, \Omega^2$$

$$\textbf{Torque force:} \quad Fy = L \sin\phi - D \cos\phi$$

$$\textbf{Thrust force:} \quad Fz = L \cos\phi + D \sin\phi$$

$$\textbf{Moment in x-direction:} \quad Mx = PM + Fy\, z_\alpha + Fz\, y_\alpha \qquad (3.6.2)$$

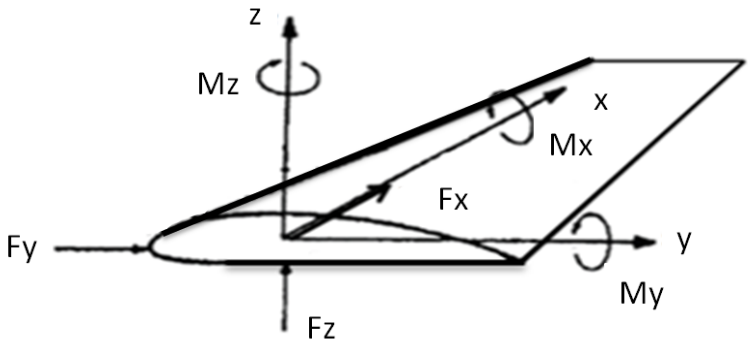

Fig. 3.6.2: The aerodynamic loads (adapted from [27]).

where,

C_l , C_d and C_m : are the lift, drag and pitch moment coefficients respectively

ϕ : is flow angle of the airfoil section

ρ : is the density of the air

c : is the chord length of the airfoil section

m : is the mass of the airfoil section

V_{rel} (or W) : is the wind relative speed

Ω : is angular speed of rotor

r : is the distance from root of the blade to the airfoil section

y_α and z_α: are the distance between centre-of-flexure and centroid in y and z direction respectively for a specific airfoil section

3.7 External Work

The work done by external forces [23, 27, 31] on the blade is:

$$W_{ext} = \int_0^L [F_x(x)\bar{u} + F_y(x)v + F_z(x)w + M_x(x)\phi + M_y(x)\theta_1 + M_z(x)\theta_2]dx \qquad (3.7.1)$$

where,

$F_x(x)$, $F_y(x)$ and $F_z(x)$: are the interpolated functions at all stations of the forces at each time step acting in the direction of x, y and z axes respectively.

$M_x(x)$, $M_y(x)$ and $M_z(x)$ are the interpolated functions at all stations of the moments at each time step acting in the direction of x, y and z axes respectively.

$$\frac{\partial W_{ext}}{\partial a_m} = \frac{\partial}{\partial a_m}\int_0^L F_x(x)\sum_{n=1}^{N} a_n(t)\phi_n(x)\,dx = \int_0^L F_x(x)\phi_m(x)\,dx$$

similarly,

$$\frac{\partial W_{ext}}{\partial b_m} = \int_0^L F_y(x)\phi_m(x)\,dx \tag{3.7.2}$$

$$\frac{\partial W_{ext}}{\partial c_m} = \int_0^L F_z(x)\phi_m(x)\,dx \tag{3.7.3}$$

$$\frac{\partial W_{ext}}{\partial d_m} = \int_0^L M_y(x)\phi_m(x)\,dx \tag{3.7.4}$$

$$\frac{\partial W_{ext}}{\partial e_m} = \int_0^L M_z(x)\phi_m(x)\,dx \tag{3.7.5}$$

$$\frac{\partial W_{ext}}{\partial f_m} = \int_0^L M_x(x)\phi_m(x)\,dx \tag{3.7.6}$$

3.8 Boundary Conditions

The blade strain energy due to the boundary conditions at x=0 and x=L:

$$U_{B.C.s} = U_{B.C.1} + U_{B.C.2}$$

$$= \frac{1}{2}k_{0\bar{u}}\bar{u}^2(0) + \frac{1}{2}k_{0v}v^2(0) + \frac{1}{2}k_{0w}w^2(0) + \frac{1}{2}K_{0\phi}\phi^2(0) + \frac{1}{2}K_{0\theta_1}{\theta_1}^2(0) + \frac{1}{2}K_{0\theta_2}{\theta_2}^2(0)$$
$$+ \frac{1}{2}k_{l\bar{u}}\bar{u}^2(L) + \frac{1}{2}k_{lv}v^2(L) + \frac{1}{2}k_{lw}w^2(L) + \frac{1}{2}K_{l\phi}\phi^2(L) + \frac{1}{2}K_{l\theta_1}{\theta_1}^2(L) + \frac{1}{2}K_{l\theta_2}{\theta_2}^2(L)$$

where ($k_{0\bar{u}}$, k_{0v}, k_{0w}, $k_{l\bar{u}}$, k_{lv}, k_{lw}) and ($K_{0\phi}$, $K_{0\theta_1}$, $K_{0\theta 2}$, $K_{l\phi}$, , $K_{l\theta_1}$, $K_{l\theta 2}$) are the linear and rotational spring stiffnesses at $x = 0$ and $x = L$ respectively.

$$\frac{\partial U_{B.C.s}}{\partial a_m} = \frac{\partial}{\partial a_m}\left(\frac{1}{2}k_{0\bar{u}}\bar{u}^2(0) + \frac{1}{2}k_{l\bar{u}}\bar{u}^2(L)\right) = k_{0\bar{u}}\bar{u}(0)\frac{\partial}{\partial a_m}\bar{u}(0) + k_{l\bar{u}}\bar{u}(L)\frac{\partial}{\partial a_m}\bar{u}(L)$$

Considering the polynomials $\phi_n(x) = (x/L)^{n+1}$ as mentioned in section 3.5, implies:

$\bar{u}(0) = 0$ and $\bar{u}(L) = \sum_{n=1}^{N} a_n$, implies:

$$\frac{\partial U_{B.C.s}}{\partial a_m} = k_{l\bar{u}} \sum_{n=1}^{N} a_n \tag{3.8}$$

Similarly, for $\frac{\partial U_{B.C.s}}{\partial b_m}$, $\frac{\partial U_{B.C.s}}{\partial c_m}$, $\frac{\partial U_{B.C.s}}{\partial d_m}$, $\frac{\partial U_{B.C.s}}{\partial e_m}$ and $\frac{\partial U_{B.C.s}}{\partial f_m}$

Since the blade has a fixed end at x=0 and a free end at x=L, we can set up the following:

$k_{0\bar{u}}$, k_{0v}, k_{0w} and $K_{0\phi}$, $K_{0\theta_1}$, $K_{0\theta 2}$ to large number and $k_{l\bar{u}}$, k_{lv}, k_{lw} and $K_{l\phi}$, $K_{l\theta_1}$, $K_{l\theta 2}$ to zero or very small number.

Chapter 4

Obtaining the Lagrange Equations of Motion

4.1 Introduction

A carefully selected sample of the pretwisted beam or wind turbine blade literature is analyzed, such as the exact solutions of Timoshenko's equation for simply supported uniform beams as given by Anderson [32], and the general equations of motion of a pre-twisted cantilever blade derived by Carnegie [33]. Carnegie [18] extended the study of the general equations of motion of a pre-twisted cantilever blade allowing for torsion, bending, rotary inertia and deflections due to shear but he did not include the warping effect. Dawson et al. [34] found the natural frequencies of pre-twisted cantilever beams of uniform rectangular cross-section allowing for shear deformation and rotary inertia by the numerical integration of a set of first-order simultaneous differential equations. Carnegie and Thomas [35] investigated the effects of shear deformation and rotary inertia on the frequencies of flexural vibration of pre-twisted uniform and tapered cantilever beams by using the finite-difference method. The semi-inverse method was proposed by Saint Venant for solving the elastic deformation of prismatic rods under resultant end loadings. This was referenced and utilized by Dawson, Ghosh, and Carnegie [34], Xu, Zhong and Zhang [12], and Sokolnikoff [13]. The strain energy of bending-torsional and their coupling were investigated by Kima, Fub and Kimc [36] and was modified to include the shear effect of a Timoshenku beam by Kaya and Ozgumus [20]. Banerjee [37, 38] had an approach for the Bernoulli and another one for the Timoshenko symmetric beam where bending was uncoupled from torsion and/or axial loading. Banerjee and Williams [39] published some work about coupled torsional–bending for asymmetrical Timoshenko beam where the elastic mass axis is different from the centroid axis. Subrahmanyam, Kulkarni and Rao worked on coupled bending-bending vibrations of pretwisted cantilever blade [40, 41], and

also they worked on coupled bending-torsion vibrations of rotating blades of asymmetric aerofoil cross section with allowance for shear deflection and rotary inertia by use of the Reissner method [24].

The equations of motion for thin-walled beam with non-symmetric cross-section subjected to linearly variable axial force were derived by Kim, Fub and Kim [36]. Also one of these early approximate approaches was Chu's helical fiber assumption [42], where stresses are initially determined along and perpendicular to helical fibers of the beam's pretwist. Even though Chu's predictions matched experimental results for thin-walled beams, it was nevertheless a flawed theory that predicted axial–torsional coupling where warping wasn't present i.e. for the case of beams with circular cross-sections. Similar approahes include the works of Rosen [43, 44], Hodges [45], Krenk [46] on static axial–torsional coupling and Tsuiji [47] on the dynamic response. In recent years, warping function-based beam theories that based on semi inverse and variational methods appear to have become widely accepted. The semi-inverse method was proposed by Saint Venant for solving the elastic deformation of prismatic rods under resultant force and moment end loads [12, 13, 34].

More recently, Liu, James and Yeo [22], investigated the coupled axial–torsional vibration of pretwisted beams of elliptic cross section. The equations of motion governing the extension, torsion, and cross-sectional warping of pretwisted beams were derived from Hamilton's principle.

The calculation of warping for an eliplitical cross section is elementary and is easy to calculate.

Younsi et al. [28] used a finite element approach based on a variational formulation of the theory of beams to calculate the blade tip vertical displacement for a 14m untwisted blade of a variable NACA 4415 type airfoil. Younsi et al. interpolated the forces and moments for a given wind velocity and attack angle, for all points of the lift line along the blade using a parametric method based on Bézier surfaces.

In the present research, the author study the linear deformation of a wind turbine blade of the same characteristics of the blade that was considered by Younsi et al. [28] (i.e. 14m untwisted blade of a variable NACA 4415 type airfoil) assuming the effect of all the extensional, torsional and flexural loadings with all their couplings, shear deflection, rotary inertia, warping of the airfoil cross-section that varies linearly from hub to tip. The strain and kinetic energies were derived to obtain the dynamic equations of motion that were solved to compute the displacemts and rotations at many stations along the blade length using the linear Newmark iteration scheme that will be discussed in more detail in section 6.4 .

Then the author extend his work to include the nonlinear large deformation case which creates two additional nonlinear stiffness matrices. Also the blade's pretwist is included. Then the nonlinear dynamic equations of motion are solved for the three unknown displacements in the directions of x, y and z axes and the three unknown rotations about the x, y and z axes at the required stations along the lengthwise of the given blade using the nonlinear Newmark iteration scheme that will be discussed in more detail in section 6.6 .

4.2 Derivation of the Lagrange Equations of Motion

Using Eq. (3.2.2) for $q_m = a_m$:

$$\frac{d}{dt}\left(\frac{\partial T}{\partial \dot{a}_m}\right) - \frac{\partial T}{\partial a_m} + \frac{\partial U_{Total}}{\partial a_m} + \frac{\partial U_{B.C.s}}{\partial a_m} - \frac{\partial W_{ext}}{\partial a_m} = 0$$

Substituting for $\frac{\partial W_{ext}}{\partial a_m} = \int_0^L F_x(x)\phi_m(x)dx$, $\frac{\partial U_{B.C.s}}{\partial a_m} = 0$ (since given polynomial functions $\phi_n(x) = (x/L)^{n+1}$ that discussed in section 2.3 satisfy the B.C.s), $\frac{\partial U_{Total}}{\partial a_m}$, $\frac{d}{dt}\left(\frac{\partial T}{\partial \dot{a}_m}\right)$ and $\frac{\partial T}{\partial a_m}$ (that was derived in Appendix C and D), implies,

$$\frac{d}{dt}\left(\frac{\partial T}{\partial \dot{a}_m}\right)-\frac{\partial T}{\partial a_m}+\frac{\partial U_{Total}}{\partial a_m}+\frac{\partial U_{B.C.s}}{\partial a_m}-\frac{\partial W_{ext}}{\partial a_m}=\rho\sum_{n=1}^{N} s_{Amn}\,\ddot{a}_n+\rho\sum_{n=1}^{N} s'_{D_1mn}\,\ddot{f}_n-\overline{\Omega}^2\rho\sum_{n=1}^{N} s_{Amn}a_n+E$$

$$\sum_{n=1}^{N} S_{Amn}\,a_n+E\sum_{n=1}^{N} S_{D_5mn}\,f_n+E\sum_{n=1}^{N} S'_{D_1mn}\,f_n+\frac{1}{2}E\sum_{n=1}^{N}\sum_{k=1}^{K} S_{Amnk}\,a_na_k+\frac{1}{2}E\sum_{n=1}^{N}\sum_{k=1}^{K} S_{D_6mnk}$$

$$f_nf_k+E\sum_{n=1}^{N}\sum_{k=1}^{K} S_{D_5mnk}\,f_na_k+\frac{1}{2}E\sum_{n=1}^{N}\sum_{k=1}^{K} S''_{D_2mnk}\,f_nf_k+E\sum_{n=1}^{N}\sum_{k=1}^{K} S'_{D_9mnk}\,f_nf_k+E$$

$$\sum_{n=1}^{N}\sum_{k=1}^{K} S'_{D_1mnk}\,f_na_k+\frac{1}{2}E\sum_{n=1}^{N}\sum_{k=1}^{K} S_{I_pmnk}\,f_nf_k+E\sum_{n=1}^{N}\sum_{k=1}^{K} S_{Amnk}\,a_na_k+E\sum_{n=1}^{N}\sum_{k=1}^{K} S_{D_5mnk}\,f_na_k+E$$

$$\sum_{n=1}^{N}\sum_{k=1}^{K} S'_{D_1mnk}\,f_na_k+\frac{1}{2}E\sum_{n=1}^{N}\sum_{k,l=1}^{K,L} S_{Amnkl}\,a_na_ka_l+\frac{1}{2}E\sum_{n=1}^{N}\sum_{k,l=1}^{K,L} S_{D_6mnkl}\,f_nf_ka_l+E\sum_{n=1}^{N}\sum_{k,l=1}^{K,L}$$

$$S_{D_5mnkl}\,f_na_ka_l+\frac{1}{2}E\sum_{n=1}^{N}\sum_{k,l=1}^{K,L} S''_{D_2mnkl}\,f_nf_ka_l+E\sum_{n=1}^{N}\sum_{k,l=1}^{K,L} S'_{D_9mnkl}\,f_nf_ka_l+E\sum_{n=1}^{N}\sum_{k,l=1}^{K,L} S'_{D_1mnkl}$$

$$f_na_ka_l+\frac{1}{2}E\sum_{n=1}^{N}\sum_{k,l=1}^{K,L} S_{I_pmnkl}\,f_nf_ka_l+E\sum_{n=1}^{N}\sum_{k=1}^{K} S_{D_5mnk}\,f_na_k+E\sum_{n=1}^{N}\sum_{k=1}^{K} S_{D_6mnk}\,f_nf_k+E$$

$$\sum_{n=1}^{N}\sum_{k=1}^{K} S'_{D_9mnk}\,f_nf_k+\frac{1}{2}E\sum_{n=1}^{N}\sum_{k,l=1}^{K,L} S_{D_5mnkl}\,f_na_ka_l+\frac{1}{2}E\sum_{n=1}^{N}\sum_{k,l=1}^{K,L} S_{D_7mnkl}\,f_nf_kf_l+E\sum_{n=1}^{N}\sum_{k,l=1}^{K,L}$$

$$S_{D_6mnkl}\,f_nf_ka_l+\frac{1}{2}E\sum_{n=1}^{N}\sum_{k,l=1}^{K,L} S''_{D_{10}mnkl}\,f_nf_kf_l+E\sum_{n=1}^{N}\sum_{k,l=1}^{K,L} S'_{D_{22}mnkl}\,f_nf_kf_l+E\sum_{n=1}^{N}\sum_{k,l=1}^{K,L} S'_{D_9mnkl}$$

$$f_nf_ka_l+\frac{1}{2}E\sum_{n=1}^{N}\sum_{k,l=1}^{K,L} S_{D_{12}mnkl}\,f_nf_kf_l+E\sum_{n=1}^{N}\sum_{k=1}^{K} S'_{D_1mnk}\,f_na_k+E\sum_{n=1}^{N}\sum_{k=1}^{K} S'_{D_9mnk}\,f_nf_k+E$$

$$\sum_{n=1}^{N}\sum_{k=1}^{K} S''_{D_2mnk}\,f_nf_k+\frac{1}{2}E\sum_{n=1}^{N}\sum_{k,l=1}^{K,L} S'_{D_1mnkl}\,f_na_ka_l+\frac{1}{2}E\sum_{n=1}^{N}\sum_{k,l=1}^{K,L} S'_{D_{22}mnkl}\,f_nf_kf_l+E\sum_{n=1}^{N}\sum_{k,l=1}^{K,L}$$

$$S'_{D_9mnkl}\,f_nf_ka_l+\frac{1}{2}E\sum_{n=1}^{N}\sum_{k,l=1}^{K,L} S'''_{D_3mnkl}\,f_nf_kf_l+E\sum_{n=1}^{N}\sum_{k,l=1}^{K,L} S''_{D_{10}mnkl}\,f_nf_kf_l+E\sum_{n=1}^{N}\sum_{k,l=1}^{K,L} S''_{D_2mnkl}$$

$$f_nf_ka_l+\frac{1}{2}E\sum_{n=1}^{N}\sum_{k,l=1}^{K,L} S'_{D_{28}mnkl}\,f_nf_kf_l-\int_0^L F_x(x)\phi_m(x)\,dx=0 \qquad \text{(4.2-a)}$$

Similarly, by using Eqn (3.2.2) for $q_m = b_m, c_m, d_m, e_m,$ and $f_m,$ we obtain the following equations (4.2-b), (4.2-c), (4.2-d), (4.2-e) and (4.2-f) respectively:

$$\frac{d}{dt}\left(\frac{\partial T}{\partial \dot{b}_m}\right) - \frac{\partial T}{\partial b_m} + \frac{\partial U_{Total}}{\partial b_m} + \frac{\partial U_{B.C.s}}{\partial b_m} - \frac{\partial W_{ext}}{\partial b_m} = \rho\sum_{n=1}^{N} s_{Amn}\ddot{b}_n + \rho\sum_{n=1}^{N} s_{z_\alpha Amn}\ddot{f}_n + \Omega^2\rho\sum_{n=1}^{N} S_{xAmn}b_n + \Omega^2\rho\sum_{n=1}^{N} S_{xz_\alpha Amn}f_n + kG\sum_{n=1}^{N} S_{Amn}b_n - kG\sum_{n=1}^{N} {}'s_{Amn}e_n + \sum_{n=1}^{N} S_{Pmn}b_n - \sum_{n=1}^{N} S_{Py_\alpha mn}f_n - \int_0^L F_y(x)\phi_m(x)dx = 0 \qquad (4.2\text{-b})$$

$$\frac{d}{dt}\left(\frac{\partial T}{\partial \dot{c}_m}\right) - \frac{\partial T}{\partial c_m} + \frac{\partial U_{Total}}{\partial c_m} + \frac{\partial U_{B.C.s}}{\partial c_m} - \frac{\partial W_{ext}}{\partial c_m} = \rho\sum_{n=1}^{N} s_{Amn}\ddot{c}_n + \rho\sum_{n=1}^{N} s_{y_\alpha Amn}\ddot{f}_n + \Omega^2\rho\sum_{n=1}^{N} S_{xAmn}c_n + \Omega^2\rho\sum_{n=1}^{N} S_{xy_\alpha Amn}f_n + kG\sum_{n=1}^{N} S_{Amn}c_n - kG\sum_{n=1}^{N} {}'s_{Amn}d_n + \sum_{n=1}^{N} S_{Pmn}c_n - \sum_{n=1}^{N} S_{Pz_\alpha mn}f_n + \frac{1}{2}E\sum_{n=1}^{N}\sum_{k,l=1}^{K,L} S_{Amnkl}c_n c_k c_l + \frac{1}{2}E\sum_{n=1}^{N}\sum_{k,l=1}^{K,L} S_{I_p mnkl}c_n f_k f_l - \int_0^L F_z(x)\phi_m(x)dx = 0 \qquad (4.2\text{-c})$$

$$\frac{d}{dt}\left(\frac{\partial T}{\partial \dot{d}_m}\right) - \frac{\partial T}{\partial d_m} + \frac{\partial U_{Total}}{\partial d_m} + \frac{\partial U_{B.C.s}}{\partial d_m} - \frac{\partial W_{ext}}{\partial d_m} = \rho\sum_{n=1}^{N} s_{I_y mn}\ddot{d}_n + \rho\sum_{n=1}^{N} s'_{I_y y_\alpha mn}\ddot{f}_n - \frac{\rho}{g}\sum_{n=1}^{N} s_{I_y mn}d_n - \frac{\rho}{g}\sum_{n=1}^{N} s'_{y_\alpha I_y mn}\dot{f}_n - \frac{\rho}{g}\sum_{n=1}^{N} s_{y_\alpha {}'I_y mn}\dot{f}_n + E\sum_{n=1}^{N} S_{I_y mn}d_n + E\sum_{n=1}^{N} S_{I_{yz}mn}e_n - kG\sum_{n=1}^{N} s'_{Amn}c_n + kG\sum_{n=1}^{N} s_{Amn}d_n + \sum_{n=1}^{N} S_{K_1 mn}f_n - \int_0^L M_y(x)\phi_m(x)\,dx = 0 \qquad (4.2\text{-d})$$

$$\frac{d}{dt}\left(\frac{\partial T}{\partial \dot{e}_m}\right) - \frac{\partial T}{\partial e_m} + \frac{\partial U_{Total}}{\partial e_m} + \frac{\partial U_{B.C.s}}{\partial e_m} - \frac{\partial W_{ext}}{\partial e_m} = -\overline{\Omega}\rho\sum_{n=1}^{N} s_{I_z mn}\dot{f}_n - \overline{\Omega}\rho\sum_{n=1}^{N} s_{I_y mn}\dot{f}_n + \overline{\Omega}\rho\sum_{n=1}^{N}\sum_{k,l=1}^{K,L} s_{I_y mnkl}\dot{f}_n f_k f_l + \overline{\Omega}\rho\sum_{n=1}^{N}\sum_{k,l=1}^{K,L} s_{I_y mnkl}f_n\dot{f}_k f_l + \overline{\Omega}\rho\sum_{n=1}^{N}\sum_{k,l=1}^{K,L} s_{I_y mnkl}f_n f_k\dot{f}_l + \rho\sum_{n=1}^{N} s_{I_y mn}\ddot{e}_n - \rho\sum_{n=1}^{N}\sum_{k,l=1}^{K,L} s_{I_y mnkl}$$

$$\dot{f}_n\, f_k\, \dot{e}_l \;-\rho\sum_{n=1}^{N}\sum_{k,l=1}^{K,L} s_{I_y mnkl}\, f_n\, \dot{f}_k\, \dot{e}_l \;-\rho\sum_{n=1}^{N}\sum_{k,l=1}^{K,L} s_{I_y mnkl}\, f_n\, f_k\, \ddot{e}_l \;+\rho\sum_{n=1}^{N}\sum_{k,l=1}^{K,L} s_{I_z mnkl}\, \dot{e}_n\, f_k\, \dot{f}_l \;+\rho\sum_{n=1}^{N}\sum_{k,l=1}^{K,L}$$

$$s_{I_z mnkl}\, e_n\, \dot{f}_k\, \dot{f}_l \;+\rho\sum_{n=1}^{N}\sum_{k,l=1}^{K,L} s_{I_z mnkl}\, e_n\, f_k\, \ddot{f}_l \;-\rho\sum_{n=1}^{N}\sum_{k,l=1}^{K,L} s_{I_y mnkl}\, \dot{e}_n\, f_k\, \dot{f}_l \;-\rho\sum_{n=1}^{N}\sum_{k,l=1}^{K,L} s_{I_y mnkl}\; e_n\, \dot{f}_k\, \dot{f}_l \;-\rho\sum_{n=1}^{N}\sum_{k,l=1}^{K,L}$$

$$s_{I_y mnkl}\, e_n\, f_k\, \ddot{f}_l \;+\rho\sum_{n=1}^{N} s_{I_z mn}\, \ddot{e}_n \;+\rho\sum_{n=1}^{N} s'_{I_z z_\alpha mn}\, \ddot{f}_n \;-\; \overline{\Omega}^2\rho\sum_{n=1}^{N} s_{I_y mn} e_n \;+\; \overline{\Omega}^2\rho\sum_{n=1}^{N}\sum_{k,l=1}^{K,L} s_{I_y mnkl}\, f_n\, f_k\, e_l \;-\cdot\overline{\Omega}\rho\sum_{n=1}^{N}$$

$$s_{I_z mn}\; \dot{f}_n \;-\overline{\Omega}\rho\sum_{n=1}^{N} s_{I_y mn}\, \dot{f}_n \;+\frac{1}{2}\overline{\Omega}\rho\sum_{n=1}^{N}\sum_{k,l=1}^{K,L} s_{I_z mnkl}\, f_n\, f_k\, \dot{f}_l \;+\frac{1}{2}\overline{\Omega}\rho\sum_{n=1}^{N}\sum_{k,l=1}^{K,L} s_{I_y mnkl}\, f_n\, f_k\, \dot{f}_l \;-\rho\sum_{n=1}^{N}\sum_{k,l=1}^{K,L}$$

$$s_{I_z mnkl}\, f_n \dot{e}_k\, \dot{f}_l \;+\; \rho\sum_{n=1}^{N}\sum_{k,l=1}^{K,L} s_{I_y mnkl}\, f_n \dot{e}_k\, \dot{f}_l \;-\; \rho\sum_{n=1}^{N}\sum_{k,l=1}^{K,L} s_{I_z mnkl}\; e_n\; \dot{f}_k\; \dot{f}_l \;-\; \frac{\rho}{g}\sum_{n=1}^{N} s_{I_z mn}\; e_n \;-\; \frac{\rho}{g}$$

$$\sum_{n=1}^{N}\sum_{k=1}^{K} s'_{I_z z_\alpha z'_\alpha mnk}\, \dot{f}_n\, \dot{f}_k \;+\; E\sum_{n=1}^{N} S_{I_z mn}\; e_n + E\sum_{n=1}^{N} S_{I_{yz} mn}\; d_n \;-kG\sum_{n=1}^{N} s'_{Amn}\; b_n \;+kG\sum_{n=1}^{N} s_{Amn}\; e_n \;+\sum_{n=1}^{N}$$

$$S_{K_2 mn}\; f_n - \int_0^L M_z(x)\phi_m(x)\; dx \;=0 \qquad \text{(4.2-e)}$$

$$\frac{d}{dt}\left(\frac{\partial T}{\partial \dot{f}_m}\right) - \frac{\partial T}{\partial f_m} + \frac{\partial U_{Total}}{\partial f_m} + \frac{\partial U_{B.C.s}}{\partial f_m} - \frac{\partial W_{ext}}{\partial f_m} = \rho\sum_{n=1}^{N} {}'s_{D_1 mn}\, \ddot{a}_n \;+\rho\sum_{n=1}^{N} S_{D_2 mn}\, \ddot{f}_n \;+\rho\sum_{n=1}^{N} s_{I_p mn}\; \ddot{f}_n \;+\overline{\Omega}\rho\sum_{n=1}^{N}$$

$$s_{I_z mn}\, \dot{e}_n \;+\overline{\Omega}\rho\sum_{n=1}^{N} s_{I_y mn}\, \dot{e}_n \;-\overline{\Omega}\sum_{n=1}^{N}\sum_{k,l=1}^{K,L} s_{I_z mnkl}\, \dot{e}_n\; f_k\; f_l \;-\overline{\Omega}\sum_{n=1}^{N}\sum_{k,l=1}^{K,L} s_{I_z mnkl}\, e_n\, \dot{f}_k\; f_l \;-\overline{\Omega}\sum_{n=1}^{N}\sum_{k,l=1}^{K,L} s_{I_z mnkl}\, e_n\, f_k\, \dot{f}_l$$

$$-\frac{1}{2}\overline{\Omega}\rho\sum_{n=1}^{N}\sum_{k,l=1}^{K,L} s_{I_y mnkl}\, \dot{e}_n\; f_k\; f_l \;-\frac{1}{2}\overline{\Omega}\rho\sum_{n=1}^{N}\sum_{k,l=1}^{K,L} s_{I_y mnkl}\, e_n\; \dot{f}_k\; f_l \;-\frac{1}{2}\overline{\Omega}\rho\sum_{n=1}^{N}\sum_{k,l=1}^{K,L} s_{I_y mnkl}\, e_n\; f_k\; \dot{f}_l \;+\rho\sum_{n=1}^{N}\sum_{k,l=1}^{K,L}$$

$$s_{I_z mnkl}\, \dot{e}_n\; f_k\, \dot{e}_l \;+\rho\sum_{n=1}^{N}\sum_{k,l=1}^{K,L} s_{I_z mnkl}\, e_n\, \dot{f}_k\, \dot{e}_l \;+\rho\sum_{n=1}^{N}\sum_{k,l=1}^{K,L} s_{I_z mnkl}\, e_n\, f_k\, \ddot{e}_l \;-\rho\sum_{n=1}^{N}\sum_{k,l=1}^{K,L} s_{I_y mnkl}\; \dot{e}_n\; f_k\, \dot{e}_l \;-\rho\sum_{n=1}^{N}\sum_{k,l=1}^{K,L}$$

$$s_{I_y mnkl}\, e_n\; \dot{f}_k\, \dot{e}_l \;-\rho\sum_{n=1}^{N}\sum_{k,l=1}^{K,L} s_{I_y mnkl}\, e_n\; f_k\, \ddot{e}_l \;+\rho\sum_{n=1}^{N} s_{I_z mn}\; \ddot{f}_n \;+\rho\sum_{n=1}^{N} s_{I_y mn}\; \ddot{f}_n \;+\rho\sum_{n=1}^{N}\sum_{k,l=1}^{K,L} s_{I_z mnkl}\; \dot{e}_n\, e_k\, \dot{f}_l$$

$$+\rho\sum_{n=1}^{N}\sum_{k,l=1}^{K,L} s_{I_z mnkl}\; e_n\, \dot{e}_k\, \dot{f}_l \;+\rho\sum_{n=1}^{N}\sum_{k,l=1}^{K,L} s_{I_z mnkl}\, e_n\, e_k\, \ddot{f}_l \;+\sum_{n=1}^{N} s_{Mz_\alpha mn}\, \ddot{b}_n \;+\sum_{n=1}^{N} s_{Mz_\alpha{}^2 mn}\, \ddot{f}_n \;+\sum_{n=1}^{N} s_{My_\alpha mn}\; \ddot{c}_n$$

$$+\sum_{n=1}^{N} s_{My_\alpha{}^2 mn}\ddot{f}_n + \rho\sum_{n=1}^{N} {}'s_{I_z z_\alpha mn}\ddot{e}_n + \rho\sum_{n=1}^{N} S_{I_z z_\alpha{}^2 mn}\ddot{f}_n + \rho\sum_{n=1}^{N} {}'s_{I_y y_\alpha mn}\ddot{d}_n + \rho\sum_{n=1}^{N} S_{I_y y_\alpha{}^2 mn}\ddot{f}_n + \frac{\rho}{g}\sum_{n=1}^{N}$$

$${}'s_{I_z z_\alpha mn}\dot{e}_n + \frac{\rho}{g}\sum_{n=1}^{N} s_{I_z z_\alpha{}' mn}\dot{e}_n + \frac{\rho}{g}\sum_{n=1}^{N} S_{I_z z_\alpha{}^2 mn}\ddot{f}_n + \frac{\rho}{g}\sum_{n=1}^{N} s_{I_z z_\alpha{}'^2 mn}\ddot{f}_n + \frac{\rho}{g}\sum_{n=1}^{N} {}'s_{I_y y_\alpha mn}\dot{d}_n + \frac{\rho}{g}\sum_{n=1}^{N} s_{I_y y_\alpha{}' mn}\dot{d}_n$$

$$+\frac{\rho}{g}\sum_{n=1}^{N} S_{I_y y_\alpha{}^2 mn}\ddot{f}_n + \frac{\rho}{g}\sum_{n=1}^{N} s_{I_y y_\alpha{}'^2 mn}\ddot{f}_n + \overline{\Omega}^2\rho\sum_{n=1}^{N} s_{I_z mn} f_n + \overline{\Omega}^2\rho\sum_{n=1}^{N}\sum_{k,l=1}^{K,L} s_{I_y mnkl} e_n e_k f_l - \frac{1}{2}\overline{\Omega}^2\rho\sum_{n=1}^{N}\sum_{k,l=1}^{K,L}$$

$$s_{I_z mnkl} f_n f_k f_l - \overline{\Omega}\rho\sum_{n=1}^{N} s_{I_z mn}\dot{e}_n + \overline{\Omega}\rho\sum_{n=1}^{N} s_{I_y mn}\dot{e}_n - \frac{3}{2}\overline{\Omega}\rho\sum_{n=1}^{N}\sum_{k,l=1}^{K,L} s_{I_y mnkl} f_n f_k \dot{e}_l + \rho\sum_{n=1}^{N}\sum_{k,l=1}^{K,L} s_{I_y mnkl} f_n \dot{e}_k \dot{e}_l +$$

$$\overline{\Omega}\rho\sum_{n=1}^{N}\sum_{k,l=1}^{K,L} s_{I_z mnkl} e_n \dot{f}_k f_l + \overline{\Omega}\rho\sum_{n=1}^{N}\sum_{k,l=1}^{K,L} s_{I_y mnkl} e_n \dot{f}_k f_l - \rho\sum_{n=1}^{N}\sum_{k,l=1}^{K,L} s_{I_z mnkl} e_n \dot{e}_k \dot{f}_l + \rho\sum_{n=1}^{N}\sum_{k,l=1}^{K,L} s_{I_y mnkl} e_n \dot{e}_k \dot{f}_l$$

$$+\Omega^2\sum_{n=1}^{N} S_{xMz_\alpha mn} b_n + \Omega^2\sum_{n=1}^{N} S_{xMz_\alpha{}^2 mn} f_n + \Omega^2\sum_{n=1}^{N} S_{xMy_\alpha mn} c_n + \Omega^2\sum_{n=1}^{N} S_{xMy_\alpha{}^2 mn} f_n - \sum_{n=1}^{N} S_{Py_\alpha mn} b_n + 2\sum_{n=1}^{N}$$

$$S_{(PI_p/A)mn} f_n - \sum_{n=1}^{N} S_{Pz_\alpha mn} c_n + \frac{1}{2}E\sum_{n=1}^{N}\sum_{k,l=1}^{K,L} S_{I_p mnkl} c_n c_k f_l + \sum_{n=1}^{N} S_{K_1 mn} d_n + \sum_{n=1}^{N} S_{K_2 mn} e_n + E\sum_{n=1}^{N} S_{D_5 mn}$$

$$a_n + E\sum_{n=1}^{N} S_{D_6 mn} f_n + E\sum_{n=1}^{N} S'_{D_9 mn} f_n + \frac{1}{2}E\sum_{n=1}^{N}\sum_{k=1}^{K} S_{D_5 mnk} a_n a_k + \frac{1}{2}E\sum_{n=1}^{N}\sum_{k=1}^{K} S_{D_7 mnk} f_n f_k +$$

$$E\sum_{n=1}^{N}\sum_{k=1}^{K} S_{D_6 mnk} a_n f_k + \frac{1}{2}E\sum_{n=1}^{N}\sum_{k=1}^{K} S''_{D_{10} mnk} f_n f_k + E\sum_{n=1}^{N}\sum_{k=1}^{K} S'_{D_{22} mnk} f_n f_k + E\sum_{n=1}^{N}\sum_{k=1}^{K} S'_{D_9 mnk}$$

$$a_n f_k + \frac{1}{2}E\sum_{n=-4}^{N}\sum_{k=-4}^{K} S_{D_{12} mnk} f_n f_k + E\sum_{n=1}^{N} {}'S_{D_1 mn} a_n + E\sum_{n=1}^{N} {}'S_{D_9 mn} f_n + E\sum_{n=1}^{N} S''_{D_2 mn} f_n + \frac{1}{2}$$

$$E\sum_{n=1}^{N}\sum_{k=1}^{K} {}'S_{D_1 mnk} a_n a_k + \frac{1}{2}E\sum_{n=1}^{N}\sum_{k=1}^{K} {}'S_{D_{22} mnk} f_n f_k + E\sum_{n=1}^{N}\sum_{k=1}^{K} {}'S_{D_9 mnk} a_n f_k + \frac{1}{2}E\sum_{n=1}^{N}\sum_{k=1}^{K}$$

$$S'''_{D_3 mnk} f_n f_k + E\sum_{n=1}^{N}\sum_{k=1}^{K} {}''S_{D_{10} mnk} f_n f_k + E\sum_{n=1}^{N}\sum_{k=1}^{K} {}''S_{D_2 mnk} a_n f_k + \frac{1}{2}E\sum_{n=1}^{N}\sum_{k=1}^{K} {}'S_{D_{28} mnk} f_n f_k$$

$$+ E\sum_{n=1}^{N}\sum_{k=1}^{K} S_{D_6 mnk} a_n f_k + E\sum_{n=1}^{N}\sum_{k=1}^{K} S_{D_7 mnk} f_n f_k + E\sum_{n=1}^{N}\sum_{k=1}^{K} S'_{D_{22} mnk} f_n f_k + \frac{1}{2}E\sum_{n=1}^{N}\sum_{k,l=1}^{K,L}$$

$$S_{D_6 mnkl} a_n a_k f_l + \frac{1}{2}E\sum_{n=1}^{N}\sum_{k,l=1}^{K,L} S_{D_8 mnkl} f_n f_k f_l + E\sum_{n=1}^{N}\sum_{k,l=1}^{K,L} S_{D_7 mnkl} a_n f_k f_l + \frac{1}{2}E\sum_{n=1}^{N}\sum_{k,l=1}^{K,L} S''_{D_{23} mnkl}$$

$$f_n f_k f_l + E \sum_{n=1}^{N} \sum_{k,l=1}^{K,L} S'_{D_{24}mnkl} f_n f_k f_l + E \sum_{n=1}^{N} \sum_{k,l=1}^{K,L} S'_{D_{22}mnkl} a_n f_k f_l + \frac{1}{2} E \sum_{n=1}^{N} \sum_{k,l=1}^{K,L} S_{D_{30}mnkl} f_n f_k f_l$$

$$+ E \sum_{n=1}^{N} \sum_{k=1}^{K} S_{D_5mnk} a_n a_k + E \sum_{n=1}^{N} \sum_{k=1}^{K} S_{D_6mnk} a_n f_k + E \sum_{n=1}^{N} \sum_{k=1}^{K} S'_{D_9mnk} a_n f_k + \frac{1}{2} E \sum_{n=1}^{N} \sum_{k,l=1}^{K,L}$$

$$S_{D_5mnkl} a_n a_k a_l + \frac{1}{2} E \sum_{n=1}^{N} \sum_{k,l=1}^{K,L} S_{D_7mnkl} a_n f_k f_l + E \sum_{n=1}^{N} \sum_{k,l=1}^{K,L} S_{D_6mnkl} a_n a_k f_l + \frac{1}{2} E \sum_{n=1}^{N} \sum_{k,l=1}^{K,L} S''_{D_{10}mnkl}$$

$$a_n f_k f_l + E \sum_{n=1}^{N} \sum_{k,l=1}^{K,L} S'_{D_{22}mnkl} a_n f_k f_l + E \sum_{n=1}^{N} \sum_{k,l=1}^{K,L} S'_{D_9mnkl} a_n a_k f_l + \frac{1}{2} E \sum_{n=1}^{N} \sum_{k,l=1}^{K,L} S_{D_{12}mnkl} a_n f_k f_l +$$

$$E \sum_{n=1}^{N} \sum_{k=1}^{K} S_{D_2mnk} a_n f_k + E \sum_{n=1}^{N} \sum_{k=1}^{K} ''S_{D_{10}mnk} f_n f_k + E \sum_{n=1}^{N} \sum_{k=1}^{K} S'''_{D_3mnk} f_n f_k + \frac{1}{2} E \sum_{n=1}^{N} \sum_{k,l=1}^{K,L} ''S_{D_2mnkl}$$

$$a_n a_k f_l + \frac{1}{2} E \sum_{n=1}^{N} \sum_{k,l=1}^{K,L} ''S_{D_{23}mnkl} f_n f_k f_l + E \sum_{n=1}^{N} \sum_{k,l=1}^{K,L} ''S_{D_{10}mnkl} a_n f_k f_l + \frac{1}{2} E \sum_{n=1}^{N} \sum_{k,l=1}^{K,L} S''''_{D_4mnkl}$$

$$f_n f_k f_l + E \sum_{n=1}^{N} \sum_{k,l=1}^{K,L} '''S_{D_{25}mnkl} f_n f_k f_l + E \sum_{n=1}^{N} \sum_{k,l=1}^{K,L} '''S_{D_3mnkl} a_n f_k f_l + \frac{1}{2} E \sum_{n=1}^{N} \sum_{k,l=1}^{K,L} ''S_{D_{29}mnkl} f_n f_k f_l$$

$$+ E \sum_{n=1}^{N} \sum_{k=1}^{K} S'_{D_9mnk} a_n f_k + E \sum_{n=1}^{N} \sum_{k=1}^{K} S'_{D_{22}mnk} f_n f_k + E \sum_{n=1}^{N} \sum_{k=1}^{K} S''_{D_{10}mnk} f_n f_k + \frac{1}{2} E \sum_{n=1}^{N} \sum_{k,l=1}^{K,L} S'_{D_9mnkl}$$

$$a_n a_k f_l + \frac{1}{2} E \sum_{n=1}^{N} \sum_{k,l=1}^{K,L} S'_{D_{24}mnkl} f_n f_k f_l + E \sum_{n=1}^{N} \sum_{k,l=1}^{K,L} S'_{D_{22}mnkl} a_n f_k f_l + \frac{1}{2} E \sum_{n=1}^{N} \sum_{k,l=1}^{K,L} S'''_{D_{25}mnkl}$$

$$f_n f_k f_l + E \sum_{n=1}^{N} \sum_{k,l=1}^{K,L} S''_{D_{23}mnkl} f_n f_k f_l + E \sum_{n=1}^{N} \sum_{k,l=1}^{K,L} S''_{D_{10}mnkl} a_n f_k f_l + \frac{1}{2} E \sum_{n=1}^{N} \sum_{k,l=1}^{K,L} S'_{D_{11}mnkl} f_n f_k f_l$$

$$+ E \sum_{n=1}^{N} \sum_{k=1}^{K} 'S_{D_9mnk} a_n f_k + E \sum_{n=1}^{N} \sum_{k=1}^{K} 'S_{D_{22}mnk} f_n f_k + E \sum_{n=1}^{N} \sum_{k=1}^{K} ''S_{D_{10}mnk} f_n f_k + \frac{1}{2} E \sum_{n=1}^{N} \sum_{k,l=1}^{K,L} 'S_{D_9mnkl}$$

$$a_n a_k f_l + \frac{1}{2} E \sum_{n=1}^{N} \sum_{k,l=1}^{K,L} 'S_{D_{24}mnkl} f_n f_k f_l + E \sum_{n=1}^{N} \sum_{k,l=1}^{K,L} 'S_{D_{22}mnkl} a_n f_k f_l + \frac{1}{2} E \sum_{n=1}^{N} \sum_{k,l=1}^{K,L} '''S_{D_{25}mnkl}$$

$$f_n f_k f_l + E \sum_{n=1}^{N} \sum_{k,l=1}^{K,L} ''S_{D_{23}mnkl} f_n f_k f_l + E \sum_{n=1}^{N} \sum_{k,l=1}^{K,L} ''S_{D_{10}mnkl} a_n f_k f_l + \frac{1}{2} E \sum_{n=1}^{N} \sum_{k,l=1}^{K,L} 'S_{D_{11}mnkl} f_n f_k f_l$$

$$+ E \sum_{n=1}^{N} \sum_{k=1}^{K} 'S_{D_1mnk} a_n a_k + E \sum_{n=1}^{N} \sum_{k=1}^{K} 'S_{D_9mnk} a_n f_k + E \sum_{n=1}^{N} \sum_{k=1}^{K} ''S_{D_2mnk} a_n f_k + \frac{1}{2} E \sum_{n=1}^{N} \sum_{k,l=1}^{K,L} 'S_{D_1mnkl}$$

$$a_n a_k a_l + \frac{1}{2} E \sum_{n=1}^{N} \sum_{k,l=1}^{K,L} {}'S_{D_{22}mnkl}\, a_n f_k f_l + E \sum_{n=1}^{N} \sum_{k,l=1}^{K,L} {}'S_{D_9mnkl}\, a_n a_k f_l + \frac{1}{2} E \sum_{n=1}^{N} \sum_{k,l=1}^{K,L} {}'''S_{D_3mnkl}\, a_n f_k f_l$$

$$+ E \sum_{n=1}^{N} \sum_{k,l=1}^{K,L} {}''S_{D_{10}mnkl}\, a_n f_k f_l + E \sum_{n=1}^{N} \sum_{k,l=1}^{K,L} {}''S_{D_2mnkl}\, a_n a_k f_l + \frac{1}{2} E \sum_{n=1}^{N} \sum_{k,l=1}^{K,L} {}'S_{D_{28}mnkl}\, a_n f_k f_l + E$$

$$\sum_{n=1}^{N} \sum_{k=1}^{K} S_{I_p mnk}\, a_n f_k + E \sum_{n=1}^{N} \sum_{k=1}^{K} S_{D_{12}mnk}\, f_n f_k + E \sum_{n=1}^{N} \sum_{k=1}^{K} S'_{D_{28}mnk}\, f_n f_k + \frac{1}{2} E \sum_{n=1}^{N} \sum_{k,l=1}^{K,L} S_{I_p mnkl}\, a_n a_k f_l$$

$$+ \frac{1}{2} E \sum_{n=1}^{N} \sum_{k,l=1}^{K,L} S_{D_{30}mnkl}\, f_n f_k f_l + E \sum_{n=1}^{N} \sum_{k,l=1}^{K,L} S_{D_{12}mnkl}\, a_n f_k f_l + \frac{1}{2} E \sum_{n=1}^{N} \sum_{k,l=1}^{K,L} S''_{D_{29}mnkl}\, f_n f_k f_l + E$$

$$\sum_{n=1}^{N} \sum_{k,l=1}^{K,L} S'_{D_{11}mnkl}\, f_n f_k f_l + E \sum_{n=1}^{N} \sum_{k,l=1}^{K,L} S'_{D_{28}mnkl}\, a_n f_k f_l + \frac{1}{2} E \sum_{n=1}^{N} \sum_{k,l=1}^{K,L} S_{D_{27}mnkl}\, f_n f_k f_l + G \sum_{n=1}^{N} S_{I_p mn}$$

$$f_n + E \sum_{n=1}^{N} S''_{I_p mn}\, f_n - \int_0^L M_x(x)\phi_m(x)dx = 0 \qquad \text{(4.2-f)}$$

Chapter 5

Arranging the Mass, Linear & Non-linear Stiffness Matrices

5.1 Introduction

In next section 5.2, all the linear matrices (mass and stiffness matrices) are deduced from the previous section derived lagrangian equations (4.2-a) to (4.2-f). These linear matrices can be used to solve the linear dynamic equations of motion (Eqn 6.1.1a) for the six degrees of freedom of displacement at any x along the blade length(three displacements in the directions of x, y and z axes and the three rotations about the x, y and z axes).

In section 5.3, all the nonlinear stiffness matrices in addition to the linear matrices (mass and stiffness matrices) are also deduced from the previous section derived lagrangian equations (4.2-a) to (4.2-f). These linear and nonlinear matrices can be used to solve the nonlinear dynamic equations of motion (Eqn 6.1.1b) again for the six degrees of freedom of displacement at any x along the blade length. The solution procedure for both linear and nonlinear cases will explained in detail in next chapter.

5.2 Arranging the Linear Mass and Stiffness Matrices

These are the terms from Eq. (4.2-a) to Eq. (4.2-f) from section 4.2 that contribute to $[K]_L$:

$$-\overline{\Omega}^2\rho\sum_{n=1}^{N} s_{Amn}a_n + E\sum_{n=1}^{N} S_{Amn}\,a_n + E\sum_{n=1}^{N} S_{D_5mn}\,f_n + E\sum_{n=1}^{N} S'_{D_1mn}\,f_n \qquad \text{from Eq. (4.2-a)}$$

$$\Omega^2\rho\sum_{n=1}^{N} S_{xAmn}b_n + \Omega^2\rho\sum_{n=1}^{N} S_{xz_\alpha Amn}f_n + kG\sum_{n=1}^{N} S_{Amn}\,b_n - kG\sum_{n=1}^{N} 's_{Amn}\,e_n + \sum_{n=1}^{N} S_{Pmn}\,b_n - \sum_{n=1}^{N} S_{Py_\alpha mn}\,f_n$$

from Eq. (4.2-b)

$$\Omega^2\rho\sum_{n=1}^{N} S_{xAmn}c_n + \Omega^2\rho\sum_{n=1}^{N} S_{xy_\alpha Amn}f_n + kG\sum_{n=1}^{N} S_{Amn}\,c_n - kG\sum_{n=1}^{N} {}'s_{Amn}\,d_n + \sum_{n=1}^{N} S_{Pmn}\,c_n - \sum_{n=1}^{N} S_{Pz_\alpha mn}\,f_n$$

from Eq. (4.2-c)

$$-\frac{\rho}{g}\sum_{n=1}^{N} s_{I_y mn}\,d_n + E\sum_{n=1}^{N} S_{I_y mn}\,d_n + E\sum_{n=1}^{N} S_{I_{yz}mn}\,e_n - kG\sum_{n=1}^{N} s'_{Amn}\,c_n + kG\sum_{n=1}^{N} s_{Amn}\,d_n + \sum_{n=1}^{N} S_{K_1 mn}\,f_n$$

from Eq. (4.2-d)

$$-\overline{\Omega}^2\rho\sum_{n=1}^{N} s_{I_y mn}e_n - \frac{\rho}{g}\sum_{n=1}^{N} s_{I_z mn}\,e_n + E\sum_{n=1}^{N} S_{I_z mn}\,e_n + E\sum_{n=1}^{N} S_{I_{yz}mn}\,d_n - kG\sum_{n=1}^{N} s'_{Amn}\,b_n + kG\sum_{n=1}^{N} s_{Amn}\,e_n + \sum_{n=1}^{N} S_{K_2 mn}\,f_n$$

from Eq. (4.2-e)

$$\overline{\Omega}^2\rho\sum_{n=1}^{N} s_{I_z mn}f_n + \Omega^2\sum_{n=1}^{N} S_{xMz_\alpha mn}b_n + \Omega^2\sum_{n=1}^{N} S_{xMz_\alpha{}^2 mn}f_n + \Omega^2\sum_{n=1}^{N} S_{xMy_\alpha mn}c_n + \Omega^2\sum_{n=1}^{N} S_{xMy_\alpha{}^2 mn}f_n$$

$$-\sum_{n=1}^{N} S_{Py_\alpha mn}\,b_n + 2\sum_{n=1}^{N} S_{(PI_p/A)mn}\,f_n - \sum_{n=1}^{N} S_{Pz_\alpha mn}\,c_n + \sum_{n=1}^{N} S_{K_1 mn}\,d_n + \sum_{n=1}^{N} S_{K_2 mn}\,e_n + E\sum_{n=1}^{N} S_{D_5 mn}\,a_n +$$

$$E\sum_{n=1}^{N} S_{D_6 mn}\,f_n + E\sum_{n=1}^{N} S'_{D_9 mn}\,f_n + E\sum_{n=1}^{N} {}'S_{D_1 mn}\,a_n + E\sum_{n=1}^{N} {}'S_{D_9 mn}\,f_n + E\sum_{n=1}^{N} S''_{D_2 mn}\,f_n + G\sum_{n=1}^{N} S_{I_p mn}\,f_n + E\sum_{n=1}^{N} S''_{I_p mn}\,f_n$$

from Eq. (4.2-f)

And the blocks of the linear stiffness matrix $[K]_L$ are obtained as follows:

$$[K]_L = \begin{bmatrix} K_{11} & K_{12} & K_{13} & K_{14} & K_{15} & K_{16} \\ K_{21} & K_{22} & K_{23} & K_{24} & K_{25} & K_{26} \\ K_{31} & K_{32} & K_{33} & K_{34} & K_{35} & K_{36} \\ K_{41} & K_{42} & K_{43} & K_{44} & K_{45} & K_{46} \\ K_{51} & K_{52} & K_{53} & K_{54} & K_{55} & K_{56} \\ K_{61} & K_{62} & K_{63} & K_{64} & K_{65} & K_{66} \end{bmatrix} \qquad (5.2.1)$$

where,

$K_{11} = E\ [\ S_{Amn}\ ] - \overline{\Omega}^2 \rho\ [\ s_{Amn}\ ]$, $K_{12} = 0$, $K_{13} = 0$, $K_{14} = 0$, $K_{15} = 0$, $K_{16} = E\ \big[\ [\ S_{D_5 mn}\ ] + [\ S'_{D_1 mn}\ ]$

$\big]$, $K_{21} = 0$, $K_{22} = kG\ [\ S_{Amn}\ ] + [\ S_{Pmn}\ ] + \Omega^2 \rho [S_{xAmn}]$, $K_{23} = 0$, $K_{24} = 0$, $K_{25} = -kG\ [\ 's_{Amn}\ ]$,

$K_{26} = -[\ S_{Py_\alpha mn}\ ] + \Omega^2 \rho [S_{xz_\alpha Amn}]$, $K_{31} = 0$, $K_{32} = 0$, $K_{33} = kG\ [\ S_{Amn}\ ] + [\ S_{Pmn}\ ] + \Omega^2 \rho [S_{xAmn}]$,

$K_{34} = -kG\ [\ 's_{Amn}\ ]$, $K_{35} = 0$, $K_{36} = -[\ S_{Pz_\alpha mn}\ ] + \Omega^2 \rho [S_{xy_\alpha Amn}]$, $K_{41} = 0$, $K_{42} = 0$, $K_{43} = -kG$

$[\ s'_{Amn}\ ]$, $K_{44} = E\ [\ S_{I_y mn}\ ] + kG\ [\ s_{Amn}\ ] - \dfrac{\rho}{g}\ [\ s_{I_y mn}\ ]$, $K_{45} = E\ [\ S_{I_{yz} mn}\ ]$, $K_{46} = [\ S_{K_1 mn}\ ]$, $K_{51} = 0$,

$K_{52} = -kG\ [\ s'_{Amn}\ ]$, $K_{53} = 0$, $K_{54} = E\ [\ S_{I_{yz} mn}\ ]$, $K_{55} = -\rho \overline{\Omega}^2 [s_{I_y mn}] + E\ [\ S_{I_z mn}\ ] + kG\ [\ s_{Amn}\ ]$

$- \dfrac{\rho}{g}\ [\ s_{I_z mn}\ ]$, $K_{56} = [\ S_{K_2 mn}\ ]$, $K_{61} = E\ \big[\ [\ S_{D_5 mn}\ ] + [\ 'S_{D_1 mn}\ ]\ \big]$, $K_{62} = -[\ S_{Py_\alpha mn}\ ] + \Omega^2 [S_{xMz_\alpha mn}]$

, $K_{63} = -[\ S_{Pz_\alpha mn}\ ] + \Omega^2 [S_{xMy_\alpha mn}]$, $K_{64} = [\ S_{K_1 mn}\ ]$, $K_{65} = [\ S_{K_2 mn}\ ]$, $K_{66} = 2[\ S_{(PI_p / A) mn}\ ]$

$+ \rho \overline{\Omega}^2 [s_{I_z mn}] + E\ \big[\ [\ S_{D_6 mn}\ ] + [\ S'_{D_9 mn}\ ] + [\ 'S_{D_9 mn}\ ] + [\ S''_{D_2 mn}\ ] + [\ S''_{I_p mn}\ ]\ \big] + \Omega^2 [S_{xMz_\alpha{}^2 mn}]$

$+ \Omega^2 [S_{xMy_\alpha{}^2 mn}] + G\ [\ S_{I_p mn}\ ]$

These are the terms from Eq. (4.2-a) to Eq. (4.2-f) from section 4.2 that contribute to $[M]_L$:

$\rho \sum_{n=1}^{N} s_{Amn} \ddot{a}_n + \rho \sum_{n=1}^{N} s'_{D_1 mn} \ddot{f}_n$ from Eq. (4.2-a)

$\rho \sum_{n=1}^{N} s_{Amn} \ddot{b}_n + \rho \sum_{n=1}^{N} s_{z_\alpha Amn} \ddot{f}_n$ from Eq. (4.2-b)

$\rho \sum_{n=1}^{N} s_{Amn} \ddot{c}_n + \rho \sum_{n=1}^{N} s_{y_\alpha Amn} \ddot{f}_n$ from Eq. (4.2-c)

$\rho \sum_{n=1}^{N} s_{I_y mn} \ddot{d}_n + \rho \sum_{n=1}^{N} s'_{I_y y_\alpha mn} \ddot{f}_n$ from Eq. (4.2-d)

$\rho \sum_{n=1}^{N} s_{I_y mn} \ddot{e}_n + \rho \sum_{n=1}^{N} s_{I_z mn} \ddot{e}_n + \rho \sum_{n=1}^{N} s'_{I_z z_\alpha mn} \ddot{f}_n$ from Eq. (4.2-e)

$$\rho\sum_{n=1}^{N} {}'s_{D_1mn}\ddot{a}_n + \rho\sum_{n=1}^{N} S_{D_2mn}\ddot{f}_n + \rho\sum_{n=1}^{N} s_{I_pmn}\ddot{f}_n + \rho\sum_{n=1}^{N} s_{I_zmn}\ddot{f}_n + \rho\sum_{n=1}^{N} s_{I_ymn}\ddot{f}_n + \sum_{n=1}^{N} s_{Mz_\alpha mn}\ddot{b}_n +$$

$$\sum_{n=1}^{N} s_{Mz_\alpha{}^2mn}\ddot{f}_n + \sum_{n=1}^{N} s_{My_\alpha mn}\ddot{c}_n + \sum_{n=1}^{N} s_{My_\alpha{}^2mn}\ddot{f}_n + \rho\sum_{n=1}^{N} {}'s_{I_zz_\alpha mn}\ddot{e}_n + \rho\sum_{n=1}^{N} S_{I_zz_\alpha{}^2mn}\ddot{f}_n + \rho\sum_{n=1}^{N} {}'s_{I_yy_\alpha mn}\ddot{d}_n$$

$$+\rho\sum_{n=1}^{N} S_{I_yy_\alpha{}^2mn}\ddot{f}_n + \frac{\rho}{g}\left(\sum_{n=1}^{N} S_{I_zz_\alpha{}^2mn}\ddot{f}_n + \sum_{n=1}^{N} s_{I_zz_\alpha{}'^2mn}\ddot{f}_n + \sum_{n=1}^{N} S_{I_yy_\alpha{}^2mn}\ddot{f}_n + \sum_{n=1}^{N} s_{I_yy_\alpha{}'^2mn}\ddot{f}_n\right)$$

from Eq. (4.2-f)

And the blocks of the mass matrix $[M]_L$ are obtained as follows:

$$[M]_L = \begin{bmatrix} M_{11} & M_{12} & M_{13} & M_{14} & M_{15} & M_{16} \\ M_{21} & M_{22} & M_{23} & M_{24} & M_{25} & M_{26} \\ M_{31} & M_{32} & M_{33} & M_{34} & M_{35} & M_{36} \\ M_{41} & M_{42} & M_{43} & M_{44} & M_{45} & M_{46} \\ M_{51} & M_{52} & M_{53} & M_{54} & M_{55} & M_{56} \\ M_{61} & M_{62} & M_{63} & M_{64} & M_{65} & M_{66} \end{bmatrix} \qquad (5.2.2)$$

where,

$M_{11} = \rho[s_{Amn}]$, $M_{12} = 0$, $M_{13} = 0$, $M_{14} = 0$, $M_{15} = 0$, $M_{16} = \rho\ [\ s'_{D_1mn}\ ]$, $M_{21} = 0$, $M_{22} = \rho[s_{Amn}]$,

$M_{23} = 0$, $M_{24} = 0$, $M_{25} = 0$, $M_{26} = \rho[s_{z_\alpha Amn}]$, $M_{31} = 0$, $M_{32} = 0$, $M_{33} = \rho[s_{Amn}]$, $M_{34} = 0$,

$M_{35} = 0$, $M_{36} = \rho[s_{y_\alpha Amn}]$, $M_{41} = 0$, $M_{42} = 0$, $M_{43} = 0$, $M_{44} = \rho[s_{I_ymn}]$, $M_{45} = 0$, $M_{46} = \rho\ [s'_{I_yy_\alpha}]$,

$M_{51} = 0$, $M_{52} = 0$, $M_{53} = 0$, $M_{54} = 0$, $M_{55} = \rho\,[s_{I_zmn}] + \rho[s_{I_ymn}]$, $M_{56} = \rho\ [s'_{I_zz_\alpha}]$, $M_{61} = \rho\ [\ 's_{D_1mn}\ ]$

, $M_{62} = [s_{Mz_\alpha mn}]$, $M_{63} = [s_{My_\alpha mn}]$, $M_{64} = \rho['s_{I_yy_\alpha mn}]$, $M_{65} = \rho['s_{I_zz_\alpha mn}]$, $M_{66} = \rho\big[\ [\ S_{D_2mn}\ ] + [\ s_{I_pmn}\ ]$

$+\ [S_{I_yy_\alpha^2}] + [s_{I_zmn}] + [s_{I_ymn}] + [S_{I_zz_\alpha^2}]\ \big] + \frac{\rho}{g}\big[\ [\ S_{I_zz_\alpha^2mn}\ ] + [\ s_{I_zz'^2_\alpha mn}\ ] + [\ S_{I_yy_\alpha^2mn}\ ] + [\ s_{I_yy'^2_\alpha mn}\ ]\ \big]$

$+[s_{My_\alpha{}^2mn}] + [s_{Mz_\alpha{}^2mn}]$

The damping matrix was computed as was done by Younsi et al. [28] :

$[C]_L = \alpha[M]_L + \beta[K]_L$, where the constants are given as [48] :

$\alpha = 0.01498$ and $\beta = 0.10405$.

5.3 Arranging the Non-linear Stiffness Matrices

These are the terms from Eq. (4.2-a) to Eq. (4.2-f) from section 4.2 that contribute to the first nonlinear stiffness matrix $[K]_{NL1}$:

$$\frac{1}{2} E \sum_{n=1}^{N}\sum_{k=1}^{K} S_{Amnk}\, a_n a_k + \frac{1}{2} E \sum_{n=1}^{N}\sum_{k=1}^{K} S_{D_6 mnk}\, f_n f_k \; E \sum_{n=1}^{N}\sum_{k=1}^{K} S_{D_5 mnk}\, f_n a_k + \frac{1}{2} E \sum_{n=1}^{N}\sum_{k=1}^{K} S''_{D_2 mnk}\, f_n f_k$$

$$+ E \sum_{n=1}^{N}\sum_{k=1}^{K} S'_{D_9 mnk}\, f_n f_k + E \sum_{n=1}^{N}\sum_{k=1}^{K} S'_{D_1 mnk}\, f_n a_k + \frac{1}{2} E \sum_{n=1}^{N}\sum_{k=1}^{K} S_{I_p mnk}\, f_n f_k + E \sum_{n=1}^{N}\sum_{k=1}^{K} S_{Amnk}\, a_n a_k$$

$$+ E \sum_{n=1}^{N}\sum_{k=1}^{K} S_{D_5 mnk}\, f_n a_k + E \sum_{n=1}^{N}\sum_{k=1}^{K} S'_{D_1 mnk}\, f_n a_k + E \sum_{n=1}^{N}\sum_{k=1}^{K} S_{D_5 mnk}\, f_n a_k + E \sum_{n=1}^{N}\sum_{k=1}^{K} S_{D_6 mnk}\, f_n f_k +$$

$$E \sum_{n=1}^{N}\sum_{k=1}^{K} S'_{D_9 mnk}\, f_n f_k + E \sum_{n=1}^{N}\sum_{k=1}^{K} S'_{D_1 mnk}\, f_n a_k + E \sum_{n=1}^{N}\sum_{k=1}^{K} S'_{D_9 mnk}\, f_n f_k + E \sum_{n=1}^{N}\sum_{k=1}^{K} S''_{D_2 mnk}\, f_n f_k$$

from Eq. (4.2-a)

$$- \frac{\rho}{g} \sum_{n=1}^{N}\sum_{k=1}^{K} s'_{I_z z_\alpha z'_\alpha mnk}\, \dot{f}_n\, \dot{f}_k$$

from Eq. (4.2-e)

$$+ \frac{1}{2} E \sum_{n=1}^{N}\sum_{k=1}^{K} S_{D_5 mnk}\, a_n a_k + \frac{1}{2} E \sum_{n=1}^{N}\sum_{k=1}^{K} S_{D_7 mnk}\, f_n f_k + E \sum_{n=1}^{N}\sum_{k=1}^{K} S_{D_6 mnk}\, a_n f_k + \frac{1}{2} E \sum_{n=1}^{N}\sum_{k=1}^{K} S''_{D_{10} mnk}$$

$$f_n f_k + E \sum_{n=1}^{N}\sum_{k=1}^{K} S'_{D_{22} mnk}\, f_n f_k + E \sum_{n=1}^{N}\sum_{k=1}^{K} S'_{D_9 mnk}\, a_n f_k + \frac{1}{2} E \sum_{n=1}^{N}\sum_{k=1}^{K} S_{D_{12} mnk}\, f_n f_k + \frac{1}{2} E \sum_{n=1}^{N}\sum_{k=1}^{K}$$

$$'S_{D_1 mnk}\, a_n a_k + \frac{1}{2} E \sum_{n=1}^{N}\sum_{k=1}^{K} 'S_{D_{22} mnk}\, f_n f_k + E \sum_{n=1}^{N}\sum_{k=1}^{K} 'S_{D_9 mnk}\, a_n f_k + \frac{1}{2} E \sum_{n=1}^{N}\sum_{k=1}^{K} S'''_{D_3 mnk}\, f_n f_k + E$$

$$\sum_{n=1}^{N}\sum_{k=1}^{K} ''S_{D_{10}mnk}\ f_n f_k + E\sum_{n=1}^{N}\sum_{k=1}^{K} ''S_{D_2mnk}\ a_n f_k + \frac{1}{2}E\sum_{n=1}^{N}\sum_{k=1}^{K} 'S_{D_{28}mnk}\ f_n f_k + E\sum_{n=1}^{N}\sum_{k=1}^{K} S_{D_6mnk}\ a_n f_k$$

$$+ E\sum_{n=1}^{N}\sum_{k=1}^{K} S_{D_7mnk}\ f_n f_k + E\sum_{n=1}^{N}\sum_{k=1}^{K} S'_{D_{22}mnk}\ f_n f_k + E\sum_{n=1}^{N}\sum_{k=1}^{K} S_{D_5mnk}\ a_n a_k + E\sum_{n=1}^{N}\sum_{k=1}^{K} S_{D_6mnk}\ a_n f_k$$

$$+ E\sum_{n=1}^{N}\sum_{k=1}^{K} S'_{D_9mnk}\ a_n f_k + E\sum_{n=1}^{N}\sum_{k=1}^{K} S_{D_2mnk}\ a_n f_k + E\sum_{n=1}^{N}\sum_{k=1}^{K} ''S_{D_{10}mnk}\ f_n f_k + E\sum_{n=1}^{N}\sum_{k=1}^{K} S'''_{D_3mnk}$$

$$f_n f_k + E\sum_{n=1}^{N}\sum_{k=1}^{K} S'_{D_9mnk}\ a_n f_k + E\sum_{n=1}^{N}\sum_{k=1}^{K} S'_{D_{22}mnk}\ f_n f_k + E\sum_{n=1}^{N}\sum_{k=1}^{K} S''_{D_{10}mnk}\ f_n f_k + E\sum_{n=1}^{N}\sum_{k=1}^{K}$$

$$'S_{D_9mnk}\ a_n f_k + E\sum_{n=1}^{N}\sum_{k=1}^{K} 'S_{D_{22}mnk}\ f_n f_k + E\sum_{n=1}^{N}\sum_{k=1}^{K} ''S_{D_{10}mnk}\ f_n f_k + E\sum_{n=1}^{N}\sum_{k=1}^{K} 'S_{D_1mnk}\ a_n a_k + E$$

$$\sum_{n=1}^{N}\sum_{k=1}^{K} 'S_{D_9mnk}\ a_n f_k + E\sum_{n=1}^{N}\sum_{k=1}^{K} ''S_{D_2mnk}\ a_n f_k + E\sum_{n=1}^{N}\sum_{k=1}^{K} S_{I_pmnk}\ a_n f_k + E\sum_{n=1}^{N}\sum_{k=1}^{K} S_{D_{12}mnk}\ f_n f_k$$

$$+ E\sum_{n=1}^{N}\sum_{k=1}^{K} S'_{D_{28}mnk}\ f_n f_k \qquad \text{from Eq. (4.2-f)}$$

And the blocks of the nonlinear stiffness matrix $[K]_{NL1}$ are obtained as follows:

$$[K]_{NL1} = \begin{bmatrix} K_{11}^{NL1} & K_{12}^{NL1} & K_{13}^{NL1} & K_{14}^{NL1} & K_{15}^{NL1} & K_{16}^{NL1} \\ K_{21}^{NL1} & K_{22}^{NL1} & K_{23}^{NL1} & K_{24}^{NL1} & K_{25}^{NL1} & K_{26}^{NL1} \\ K_{31}^{NL1} & K_{32}^{NL1} & K_{33}^{NL1} & K_{34}^{NL1} & K_{35}^{NL1} & K_{36}^{NL1} \\ K_{41}^{NL1} & K_{42}^{NL1} & K_{43}^{NL1} & K_{44}^{NL1} & K_{45}^{NL1} & K_{46}^{NL1} \\ K_{51}^{NL1} & K_{52}^{NL1} & K_{53}^{NL1} & K_{54}^{NL1} & K_{55}^{NL1} & K_{56}^{NL1} \\ K_{61}^{NL1} & K_{62}^{NL1} & K_{63}^{NL1} & K_{64}^{NL1} & K_{65}^{NL1} & K_{66}^{NL1} \end{bmatrix} \qquad (5.2.3)$$

where,

$$K_{11}^{NL1} = \frac{3}{2}E\sum_{k=1}^{K}\ [\ S_{Amnk}\ ]\ a_k\ ,\quad K_{12}^{NL1} = 0,\ K_{13}^{NL1} = 0,\ K_{14}^{NL1} = 0,\ K_{15}^{NL1} = 0,\ K_{16}^{NL1} = \frac{1}{2}E\ [\ 3\sum_{k=1}^{K}[\ S_{D_6mnk}\ ]$$

$$f_k\ + 6\sum_{k=1}^{K}[\ S_{D_5mnk}\ ]\ a_k\ + 6\sum_{k=1}^{K}[\ S'_{D_9mnk}\ ]\ f_k\ + 6\sum_{k=1}^{K}[\ S'_{D_1mnk}\ ]\ a_k\ + \sum_{k=1}^{K}[\ S_{I_pmnk}\ ]\ f_k\ + \ 3\sum_{k=1}^{K}$$

$$\left[S''_{D_2 mnk} \right] f_k \Big], \quad K_{21}^{NL1} = 0, \quad K_{22}^{NL1} = 0, \quad K_{23}^{NL1} = 0, \quad K_{24}^{NL1} = 0, \quad K_{25}^{NL1} = 0, \quad K_{26}^{NL1} = 0, \quad K_{31}^{NL1} = 0,$$

$$K_{32}^{NL1} = 0, \; K_{33}^{NL1} = 0, \; K_{34}^{NL1} = 0, \; K_{35}^{NL1} = 0, \; K_{36}^{NL1} = 0, \quad K_{41}^{NL1} = 0, \; K_{42}^{NL1} = 0, \; K_{43}^{NL1} = 0, \; K_{44}^{NL1} = 0, \; K_{45}^{NL1} = 0,$$

$$K_{46}^{NL1} = 0, \quad K_{51}^{NL1} = 0, \; K_{52}^{NL1} = 0, \; K_{53}^{NL1} = 0, \; K_{54}^{NL1} = 0, \; K_{55}^{NL1} = 0, \; K_{56}^{NL1} = 0, \; K_{61}^{NL1} = E \Big[\frac{3}{2} \sum_{k=1}^{K} \left[S_{D_5 mnk} \right]$$

$$a_k + 3 \sum_{k=1}^{K} \left[S_{D_6 mnk} \right] f_k + 3 \sum_{k=1}^{K} \left[S'_{D_9 mnk} \right] f_k + \frac{3}{2} \sum_{k=1}^{K} \left['S_{D_1 mnk} \right] a_k + 3 \sum_{k=1}^{K} \left['S_{D_9 mnk} \right] f_k + 2$$

$$\sum_{k=1}^{K} \left[''S_{D_2 mnk} \right] f_k + \sum_{k=1}^{K} \left[S_{D_2 mnk} \right] f_k + \sum_{k=1}^{K} \left[S_{I_p mnk} \right] f_k \Big], \; K_{62}^{NL1} = 0, \; K_{63}^{NL1} = 0, \; K_{64}^{NL1} = 0,$$

$$K_{65}^{NL1} = 0, \; K_{66}^{NL1} = E \Big[\frac{3}{2} \sum_{k=1}^{K} \left[S_{D_7 mnk} \right] f_k + \frac{3}{2} \sum_{k=1}^{K} \left[S''_{D_{10} mnk} \right] f_k + 3 \sum_{k=1}^{K} \left[S'_{D_{22} mnk} \right] f_k + \frac{3}{2} \sum_{k=1}^{K} \Big[$$

$$S_{D_{12} mnk} \Big] f_k + \frac{3}{2} \sum_{k=1}^{K} \left['S_{D_{22} mnk} \right] f_k + \frac{3}{2} \sum_{k=1}^{K} \left[S'''_{D_3 mnk} \right] f_k + 3 \sum_{k=1}^{K} \left[''S_{D_{10} mnk} \right] f_k + \frac{1}{2} \sum_{k=1}^{K} \left['S_{D_{28} mnk} \right.$$

$$\Big] f_k + \sum_{k=1}^{K} \left[S'_{D_{28} mnk} \right] f_k \Big]$$

These are the terms from Eq. (4.2-a) to Eq. (4.2-f) from section 4.2 that contribute to the second nonlinear stiffness matrix $[K]_{NL2}$:

$$\frac{1}{2} E \sum_{n=1}^{N} \sum_{k,l=1}^{K,L} S_{Amnkl} a_n a_k a_l + \frac{1}{2} E \sum_{n=1}^{N} \sum_{k,l=1}^{K,L} S_{D_6 mnkl} f_n f_k a_l + E \sum_{n=1}^{N} \sum_{k,l=1}^{K,L} S_{D_5 mnkl} f_n a_k a_l + \frac{1}{2} E$$

$$\sum_{n=1}^{N} \sum_{k,l=1}^{K,L} S''_{D_2 mnkl} f_n f_k a_l + E \sum_{n=1}^{N} \sum_{k,l=1}^{K,L} S'_{D_9 mnkl} f_n f_k a_l + E \sum_{n=1}^{N} \sum_{k,l=1}^{K,L} S'_{D_1 mnkl} f_n a_k a_l + \frac{1}{2} E \sum_{n=1}^{N} \sum_{k,l=1}^{K,L}$$

$$S_{I_p mnkl} f_n f_k a_l + \frac{1}{2} E \sum_{n=1}^{N} \sum_{k,l=1}^{K,L} S_{D_5 mnkl} f_n a_k a_l + \frac{1}{2} E \sum_{n=1}^{N} \sum_{k,l=1}^{K,L} S_{D_7 mnkl} f_n f_k f_l + E \sum_{n=1}^{N} \sum_{k,l=1}^{K,L} S_{D_6 mnkl}$$

$$f_n f_k a_l + \frac{1}{2} E \sum_{n=1}^{N} \sum_{k,l=1}^{K,L} S''_{D_{10} mnkl} f_n f_k f_l + E \sum_{n=1}^{N} \sum_{k,l=1}^{K,L} S'_{D_{22} mnkl} f_n f_k f_l + E \sum_{n=1}^{N} \sum_{k,l=1}^{K,L} S'_{D_9 mnkl} f_n f_k a_l$$

$$+ \frac{1}{2} E \sum_{n=1}^{N} \sum_{k,l=1}^{K,L} S_{D_{12} mnkl} f_n f_k f_l + \frac{1}{2} E \sum_{n=1}^{N} \sum_{k,l=1}^{K,L} S'_{D_1 mnkl} f_n a_k a_l + \frac{1}{2} E \sum_{n=1}^{N} \sum_{k,l=1}^{K,L} S'_{D_{22} mnkl} f_n f_k f_l +$$

$$E\sum_{n=1}^{N}\sum_{k,l=1}^{K,L} S'_{D_9 mnkl}\, f_n f_k a_l + \frac{1}{2} E\sum_{n=1}^{N}\sum_{k,l=1}^{K,L} S'''_{D_3 mnkl}\, f_n f_k f_l + E\sum_{n=1}^{N}\sum_{k,l=1}^{K,L} S''_{D_{10} mnkl}\, f_n f_k f_l + E$$

$$\sum_{n=1}^{N}\sum_{k,l=1}^{K,L} S''_{D_2 mnkl}\, f_n f_k a_l + \frac{1}{2} E\sum_{n=1}^{N}\sum_{k,l=1}^{K,L} S'_{D_{28} mnkl}\, f_n f_k f_l \qquad \text{from Eq. (4.2-a)}$$

$$\frac{1}{2} E\sum_{n=1}^{N}\sum_{k,l=1}^{K,L} S_{Amnkl} c_n c_k c_l + \frac{1}{2} E\sum_{n=1}^{N}\sum_{k,l=1}^{K,L} S_{I_p mnkl} c_n f_k f_l \qquad \text{from Eq. (4.2-c)}$$

$$+\overline{\Omega}\rho\sum_{n=1}^{N}\sum_{k,l=1}^{K,L} s_{I_y mnkl}\dot{f}_n f_k f_l + \overline{\Omega}\rho\sum_{n=1}^{N}\sum_{k,l=1}^{K,L} s_{I_y mnkl} f_n \dot{f}_k f_l + \overline{\Omega}\rho\sum_{n=1}^{N}\sum_{k,l=1}^{K,L} s_{I_y mnkl} f_n f_k \dot{f}_l - \rho\sum_{n=1}^{N}\sum_{k,l=1}^{K,L}$$

$$s_{I_y mnkl}\dot{f}_n f_k \dot{e}_l - \rho\sum_{n=1}^{N}\sum_{k,l=1}^{K,L} s_{I_y mnkl} f_n \dot{f}_k \dot{e}_l - \rho\sum_{n=1}^{N}\sum_{k,l=1}^{K,L} s_{I_y mnkl} f_n f_k \ddot{e}_l + \rho\sum_{n=1}^{N}\sum_{k,l=1}^{K,L} s_{I_z mnkl}\dot{e}_n f_k \dot{f}_l + \rho$$

$$\sum_{n=1}^{N}\sum_{k,l=1}^{K,L} s_{I_z mnkl} e_n \dot{f}_k \dot{f}_l + \rho\sum_{n=1}^{N}\sum_{k,l=1}^{K,L} s_{I_z mnkl} e_n f_k \ddot{f}_l - \rho\sum_{n=1}^{N}\sum_{k,l=1}^{K,L} s_{I_y mnkl}\dot{e}_n f_k \dot{f}_l - \rho\sum_{n=1}^{N}\sum_{k,l=1}^{K,L} s_{I_y mnkl} e_n \dot{f}_k \dot{f}_l$$

$$-\rho\sum_{n=1}^{N}\sum_{k,l=1}^{K,L} s_{I_y mnkl} e_n f_k \ddot{f}_l + \overline{\Omega}^2\rho\sum_{n=1}^{N}\sum_{k,l=1}^{K,L} s_{I_y mnkl} f_n f_k e_l + \frac{1}{2}\overline{\Omega}\rho\sum_{n=1}^{N}\sum_{k,l=1}^{K,L} s_{I_z mnkl} f_n f_k \dot{f}_l + \frac{1}{2}\overline{\Omega}\rho\sum_{n=1}^{N}\sum_{k,l=1}^{K,L}$$

$$s_{I_y mnkl} f_n f_k \dot{f}_l - \rho\sum_{n=1}^{N}\sum_{k,l=1}^{K,L} s_{I_z mnkl} f_n \dot{e}_k \dot{f}_l + \rho\sum_{n=1}^{N}\sum_{k,l=1}^{K,L} s_{I_y mnkl} f_n \dot{e}_k \dot{f}_l - \rho\sum_{n=1}^{N}\sum_{k,l=1}^{K,L} s_{I_z mnkl} e_n \dot{f}_k \dot{f}_l$$

$$\text{from Eq. (4.2-e)}$$

$$-\overline{\Omega}\sum_{n=1}^{N}\sum_{k,l=1}^{K,L} s_{I_z mnkl}\dot{e}_n f_k f_l - \overline{\Omega}\sum_{n=1}^{N}\sum_{k,l=1}^{K,L} s_{I_z mnkl} e_n \dot{f}_k f_l - \overline{\Omega}\sum_{n=1}^{N}\sum_{k,l=1}^{K,L} s_{I_z mnkl} e_n f_k \dot{f}_l - \frac{1}{2}\overline{\Omega}\rho\sum_{n=1}^{N}\sum_{k,l=1}^{K,L}$$

$$s_{I_y mnkl}\dot{e}_n f_k f_l - \frac{1}{2}\overline{\Omega}\rho\sum_{n=1}^{N}\sum_{k,l=1}^{K,L} s_{I_y mnkl} e_n \dot{f}_k f_l - \frac{1}{2}\overline{\Omega}\rho\sum_{n=1}^{N}\sum_{k,l=1}^{K,L} s_{I_y mnkl} e_n f_k \dot{f}_l + \rho\sum_{n=1}^{N}\sum_{k,l=1}^{K,L} s_{I_z mnkl}\dot{e}_n f_k \dot{e}_l$$

$$+\rho\sum_{n=1}^{N}\sum_{k,l=1}^{K,L} s_{I_z mnkl} e_n \dot{f}_k \dot{e}_l + \rho\sum_{n=1}^{N}\sum_{k,l=1}^{K,L} s_{I_z mnkl} e_n f_k \ddot{e}_l - \rho\sum_{n=1}^{N}\sum_{k,l=1}^{K,L} s_{I_y mnkl}\dot{e}_n f_k \dot{e}_l - \rho\sum_{n=1}^{N}\sum_{k,l=1}^{K,L}$$

$$s_{I_y mnkl} e_n \dot{f}_k \dot{e}_l - \rho\sum_{n=1}^{N}\sum_{k,l=1}^{K,L} s_{I_y mnkl} e_n f_k \ddot{e}_l + \rho\sum_{n=1}^{N}\sum_{k,l=1}^{K,L} s_{I_z mnkl}\dot{e}_n e_k \dot{f}_l + \rho\sum_{n=1}^{N}\sum_{k,l=1}^{K,L} s_{I_z mnkl} e_n \dot{e}_k \dot{f}_l$$

$$+\rho\sum_{n=1}^{N}\sum_{k,l=1}^{K,L} s_{I_z mnkl} e_n e_k \ddot{f}_l + \overline{\Omega}^2\rho\sum_{n=1}^{N}\sum_{k,l=1}^{K,L} s_{I_y mnkl} e_n e_k f_l - \frac{1}{2}\overline{\Omega}^2\rho\sum_{n=1}^{N}\sum_{k,l=1}^{K,L} s_{I_z mnkl} f_n f_k f_l - \frac{3}{2}\overline{\Omega}\rho\sum_{n=1}^{N}\sum_{k,l=1}^{K,L}$$

$$s_{I_y mnkl} f_n f_k \dot{e}_l + \rho \sum_{n=1}^{N} \sum_{k,l=1}^{K,L} s_{I_y mnkl} f_n \dot{e}_k \dot{e}_l + \overline{\Omega}\rho \sum_{n=1}^{N} \sum_{k,l=1}^{K,L} s_{I_z mnkl} e_n \dot{f}_k f_l + \overline{\Omega}\rho \sum_{n=1}^{N} \sum_{k,l=1}^{K,L} s_{I_y mnkl} e_n \dot{f}_k f_l$$

$$- \rho \sum_{n=1}^{N} \sum_{k,l=1}^{K,L} s_{I_z mnkl} e_n \dot{e}_k \dot{f}_l + \rho \sum_{n=1}^{N} \sum_{k,l=1}^{K,L} s_{I_y mnkl} e_n \dot{e}_k \dot{f}_l + \frac{1}{2} E \sum_{n=1}^{N} \sum_{k,l=1}^{K,L} S_{I_p mnkl} c_n c_k f_l + \frac{1}{2} E \sum_{n=1}^{N} \sum_{k,l=1}^{K,L} S_{D_6 mnkl}$$

$$a_n a_k f_l + \frac{1}{2} E \sum_{n=1}^{N} \sum_{k,l=1}^{K,L} S_{D_8 mnkl} f_n f_k f_l + E \sum_{n=1}^{N} \sum_{k,l=1}^{K,L} S_{D_7 mnkl} a_n f_k f_l + \frac{1}{2} E \sum_{n=1}^{N} \sum_{k,l=1}^{K,L} S''_{D_{23} mnkl} f_n f_k f_l +$$

$$E \sum_{n=1}^{N} \sum_{k,l=1}^{K,L} S'_{D_{24} mnkl} f_n f_k f_l + E \sum_{n=1}^{N} \sum_{k,l=1}^{K,L} S'_{D_{22} mnkl} a_n f_k f_l + \frac{1}{2} E \sum_{n=1}^{N} \sum_{k,l=1}^{K,L} S_{D_{30} mnkl} f_n f_k f_l + \frac{1}{2} E$$

$$\sum_{n=1}^{N} \sum_{k,l=1}^{K,L} S_{D_5 mnkl} a_n a_k a_l + \frac{1}{2} E \sum_{n=1}^{N} \sum_{k,l=1}^{K,L} S_{D_7 mnkl} a_n f_k f_l + E \sum_{n=1}^{N} \sum_{k,l=1}^{K,L} S_{D_6 mnkl} a_n a_k f_l + \frac{1}{2} E \sum_{n=1}^{N} \sum_{k,l=1}^{K,L}$$

$$S''_{D_{10} mnkl} a_n f_k f_l + E \sum_{n=1}^{N} \sum_{k,l=1}^{K,L} S'_{D_{22} mnkl} a_n f_k f_l + E \sum_{n=1}^{N} \sum_{k,l=1}^{K,L} S'_{D_9 mnkl} a_n a_k f_l + \frac{1}{2} E \sum_{n=1}^{N} \sum_{k,l=1}^{K,L} S_{D_{12} mnkl}$$

$$a_n f_k f_l + \frac{1}{2} E \sum_{n=1}^{N} \sum_{k,l=1}^{K,L} {}''S_{D_2 mnkl} a_n a_k f_l + \frac{1}{2} E \sum_{n=1}^{N} \sum_{k,l=1}^{K,L} {}''S_{D_{23} mnkl} f_n f_k f_l + E \sum_{n=1}^{N} \sum_{k,l=1}^{K,L} {}''S_{D_{10} mnkl} a_n f_k f_l$$

$$+ \frac{1}{2} E \sum_{n=1}^{N} \sum_{k,l=1}^{K,L} S''''_{D_4 mnkl} f_n f_k f_l + E \sum_{n=1}^{N} \sum_{k,l=1}^{K,L} {}'''S_{D_{25} mnkl} f_n f_k f_l + E \sum_{n=1}^{N} \sum_{k,l=1}^{K,L} {}'''S_{D_3 mnkl} a_n f_k f_l + \frac{1}{2} E$$

$$\sum_{n=1}^{N} \sum_{k,l=1}^{K,L} {}''S_{D_{29} mnkl} f_n f_k f_l + \frac{1}{2} E \sum_{n=1}^{N} \sum_{k,l=1}^{K,L} S'_{D_9 mnkl} a_n a_k f_l + \frac{1}{2} E \sum_{n=1}^{N} \sum_{k,l=1}^{K,L} S'_{D_{24} mnkl} f_n f_k f_l + E \sum_{n=1}^{N} \sum_{k,l=1}^{K,L}$$

$$S'_{D_{22} mnkl} a_n f_k f_l + \frac{1}{2} E \sum_{n=1}^{N} \sum_{k,l=1}^{K,L} S'''_{D_{25} mnkl} f_n f_k f_l + E \sum_{n=1}^{N} \sum_{k,l=1}^{K,L} S''_{D_{23} mnkl} f_n f_k f_l + E \sum_{n=1}^{N} \sum_{k,l=1}^{K,L} S''_{D_{10} mnkl}$$

$$a_n f_k f_l + \frac{1}{2} E \sum_{n=1}^{N} \sum_{k,l=1}^{K,L} S'_{D_{11} mnkl} f_n f_k f_l + \frac{1}{2} E \sum_{n=1}^{N} \sum_{k,l=1}^{K,L} {}'S_{D_9 mnkl} a_n a_k f_l + \frac{1}{2} E \sum_{n=1}^{N} \sum_{k,l=1}^{K,L} {}'S_{D_{24} mnkl} f_n f_k f_l +$$

$$E \sum_{n=1}^{N} \sum_{k,l=1}^{K,L} {}'S_{D_{22} mnkl} a_n f_k f_l + \frac{1}{2} E \sum_{n=1}^{N} \sum_{k,l=1}^{K,L} {}'''S_{D_{25} mnkl} f_n f_k f_l + E \sum_{n=1}^{N} \sum_{k,l=1}^{K,L} {}''S_{D_{23} mnkl} f_n f_k f_l + E \sum_{n=1}^{N}$$

$$\sum_{k,l=1}^{K,L} {}''S_{D_{10} mnkl} a_n f_k f_l + \frac{1}{2} E \sum_{n=1}^{N} \sum_{k,l=1}^{K,L} {}'S_{D_{11} mnkl} f_n f_k f_l + \frac{1}{2} E \sum_{n=1}^{N} \sum_{k,l=1}^{K,L} {}'S_{D_1 mnkl} a_n a_k a_l + \frac{1}{2} E \sum_{n=1}^{N} \sum_{k,l=1}^{K,L}$$

$${}'S_{D_{22} mnkl} a_n f_k f_l + E \sum_{n=1}^{N} \sum_{k,l=1}^{K,L} {}'S_{D_9 mnkl} a_n a_k f_l + \frac{1}{2} E \sum_{n=1}^{N} \sum_{k,l=1}^{K,L} {}'''S_{D_3 mnkl} a_n f_k f_l + E \sum_{n=1}^{N} \sum_{k,l=1}^{K,L} {}''S_{D_{10} mnkl}$$

$$a_n f_k f_l + E \sum_{n=1}^{N} \sum_{k,l=1}^{K,L} {}''S_{D_2 mnkl}\ a_n a_k f_l + \frac{1}{2} E \sum_{n=1}^{N} \sum_{k,l=1}^{K,L} {}'S_{D_{28} mnkl}\ a_n f_k f_l + \frac{1}{2} E \sum_{n=1}^{N} \sum_{k,l=1}^{K,L} S_{I_p mnkl}\ a_n a_k f_l + \frac{1}{2}$$

$$E \sum_{n=1}^{N} \sum_{k,l=1}^{K,L} S_{D_{30} mnkl}\ f_n f_k f_l + E \sum_{n=1}^{N} \sum_{k,l=1}^{K,L} S_{D_{12} mnkl}\ a_n f_k f_l + \frac{1}{2} E \sum_{n=1}^{N} \sum_{k,l=1}^{K,L} S''_{D_{29} mnkl}\ f_n f_k f_l + E \sum_{n=1}^{N} \sum_{k,l=1}^{K,L}$$

$$S'_{D_{11} mnkl}\ f_n f_k f_l + E \sum_{n=1}^{N} \sum_{k,l=1}^{K,L} S'_{D_{28} mnkl}\ a_n f_k f_l + \frac{1}{2} E \sum_{n=1}^{N} \sum_{k,l=1}^{K,L} S_{D_{27} mnkl}\ f_n f_k f_l \qquad \text{from Eq. (4.2-f)}$$

And the blocks of the nonlinear stiffness matrix $[K]_{NL2}$ are obtained as follows:

$$[K]_{NL2} = \begin{bmatrix} K_{11}^{NL2} & K_{12}^{NL2} & K_{13}^{NL2} & K_{14}^{NL2} & K_{15}^{NL2} & K_{16}^{NL2} \\ K_{21}^{NL2} & K_{22}^{NL2} & K_{23}^{NL2} & K_{24}^{NL2} & K_{25}^{NL2} & K_{26}^{NL2} \\ K_{31}^{NL2} & K_{32}^{NL2} & K_{33}^{NL2} & K_{34}^{NL2} & K_{35}^{NL2} & K_{36}^{NL2} \\ K_{41}^{NL2} & K_{42}^{NL2} & K_{43}^{NL2} & K_{44}^{NL2} & K_{45}^{NL2} & K_{46}^{NL2} \\ K_{51}^{NL2} & K_{52}^{NL2} & K_{53}^{NL2} & K_{54}^{NL2} & K_{55}^{NL2} & K_{56}^{NL2} \\ K_{61}^{NL2} & K_{62}^{NL2} & K_{63}^{NL2} & K_{64}^{NL2} & K_{65}^{NL2} & K_{66}^{NL2} \end{bmatrix} \qquad (5.2.4)$$

where,

$$K_{11}^{NL2} = \frac{1}{2} E \sum_{k,l=1}^{K,L} [\ S_{Amnkl}\ ]\ a_k a_l\ ,\ K_{12}^{NL2} = 0,\ \ K_{13}^{NL2} = 0,\ K_{14}^{NL2} = 0,\ \ K_{15}^{NL2} = 0,\ K_{16}^{NL2} = E\ [\ \frac{3}{2} \sum_{k,l=1}^{K,L} [$$

$$S_{D_6 mnkl}\ ]\ f_k a_l + \frac{3}{2} \sum_{k,l=1}^{K,L} [\ S_{D_5 mnkl}\ ]\ a_k a_l + \frac{3}{2} \sum_{k,l=1}^{K,L} [\ S''_{D_2 mnkl}\ ]\ f_k a_l + 3 \sum_{k,l=1}^{K,L} [\ S'_{D_9 mnkl}\ ]\ f_k a_l + \frac{3}{2} \sum_{k,l=1}^{K,L} [$$

$$S'_{D_1 mnkl}\ ]\ a_k a_l + \frac{1}{2} \sum_{k,l=1}^{K,L} [\ S_{I_p mnkl}\ ]\ f_k a_l + \frac{1}{2} \sum_{k,l=1}^{K,L} [\ S_{D_7 mnkl}\ ]\ f_k f_l + \frac{3}{2} \sum_{k,l=1}^{K,L} [\ S''_{D_{10} mnkl}\ ]\ f_k f_l + \frac{3}{2}$$

$$\sum_{k,l=1}^{K,L} [\ S'_{D_{22} mnkl}\ ]\ f_k f_l + \frac{1}{2} \sum_{k,l=1}^{K,L} [\ S_{D_{12} mnkl}\ ]\ f_k f_l + \frac{1}{2} \sum_{k,l=1}^{K,L} [\ S'''_{D_3 mnkl}\ ]\ f_k f_l + \frac{1}{2} \sum_{k,l=1}^{K,L} [\ S'_{D_{28} mnkl}\ ]$$

$$f_k f_l\ ]\ ,\ K_{21}^{NL2} = 0,\ K_{22}^{NL2} = 0,\ K_{23}^{NL2} = 0,\ \ K_{24}^{NL2} = 0,\ K_{25}^{NL2} = 0,\ \ K_{26}^{NL2} = 0,\ \ K_{31}^{NL2} = 0,\ \ K_{32}^{NL2} = 0,\ K_{33}^{NL2} =$$

$$\frac{1}{2} E \sum_{k,l=1}^{K,L} [\ S_{Amnkl}\ ]\ c_k c_l + \frac{1}{2} E \sum_{k,l=1}^{K,L} [\ S_{I_p mnkl}\ ]\ f_k f_l\ ,\ K_{34}^{NL2} = 0,\ \ K_{35}^{NL2} = 0,\ \ K_{36}^{NL2} = 0,\ \ K_{41}^{NL2} = 0,$$

$$K_{42}^{NL2}=0,\ K_{43}^{NL2}=0,\ K_{44}^{NL2}=0,\ K_{45}^{NL2}=0,\ K_{46}^{NL2}=0,\ K_{51}^{NL2}=0,\ K_{52}^{NL2}=0,\ K_{53}^{NL2}=0,\ K_{54}^{NL2}=0,$$

$$K_{55}^{NL2}=\ \rho\Big[\sum_{k,l=1}^{K,L}[s_{I_z mnkl}]\,\dot{f}_k\,\dot{f}_l\ +\sum_{k,l=1}^{K,L}[s_{I_z mnkl}]\,f_k\,\ddot{f}_l\ -\sum_{k,l=1}^{K,L}[s_{I_y mnkl}]\,\dot{f}_k\,\dot{f}_l\ -\sum_{k,l=1}^{K,L}[s_{I_y mnkl}]\,f_k\,\ddot{f}_l\ -\sum_{k,l=1}^{K,L}$$

$$[s_{I_z mnkl}]\,\dot{f}_k\,\dot{f}_l\ \Big],\quad K_{56}^{NL2}=3\overline{\Omega}\rho\sum_{k,l=1}^{K,L}[s_{I_y mnkl}]\,f_k\,\dot{f}_l\ -2\rho\sum_{k,l=1}^{K,L}[s_{I_y mnkl}]\,\dot{e}_k\,\dot{f}_l-\rho\sum_{k,l=1}^{K,L}[s_{I_y mnkl}]\,\ddot{e}_k\,f_l+\overline{\Omega}^2\rho$$

$$\sum_{k,l=1}^{K,L}[s_{I_y mnkl}]\,e_k\,f_l+\frac{1}{2}\overline{\Omega}\rho\sum_{k,l=1}^{K,L}[s_{I_y mnkl}]\,f_k\,\dot{f}_l+\frac{1}{2}\overline{\Omega}\rho\sum_{k,l=1}^{K,L}[s_{I_z mnkl}]\,f_k\,\dot{f}_l\ ,\ K_{61}^{NL2}=\ E\ [\ \frac{3}{2}\sum_{k,l=1}^{K,L}[\ S_{D_6 mnkl}\ ]$$

$$a_k f_l\ +\frac{3}{2}\sum_{k,l=1}^{K,L}[\ S_{D_7 mnkl}\ ]\ f_k f_l\ +\ 3\ \sum_{k,l=1}^{K,L}[\ S'_{D_{22}mnkl}\ ]\ f_k f_l\ +\frac{1}{2}\sum_{k,l=1}^{K,L}[\ S_{D_5 mnkl}\ ]\ a_k a_l\ +\frac{3}{2}\ \sum_{k,l=1}^{K,L}[\ S''_{D_{10}mnkl}\ ]$$

$$f_k f_l\ +\frac{3}{2}\sum_{k,l=1}^{K,L}[\ S'_{D_9 mnkl}\ ]\ \ a_k f_l\ \ +\frac{3}{2}\ \sum_{k,l=1}^{K,L}[\ S_{D_{12}mnkl}\ ]\ \ f_k f_l+\frac{3}{2}\sum_{k,l=1}^{K,L}[\ ''S_{D_2 mnkl}\ ]\ a_k f_l\ +3\sum_{k,l=1}^{K,L}[\ ''S_{D_{10}mnkl}\ ]$$

$$f_k f_l\ +\frac{3}{2}\ \sum_{k,l=1}^{K,L}[\ '''S_{D_3 mnkl}\ ]\ f_k f_l\ \ +\frac{3}{2}\sum_{k,l=1}^{K,L}[\ 'S_{D_9 mnkl}\ ]\ a_k f_l\ \ +\frac{3}{2}\sum_{k,l=1}^{K,L}[\ 'S_{D_{22}mnkl}\ ]\ \ f_k f_l+\frac{1}{2}\sum_{k,l=1}^{K,L}[\ 'S_{D_1 mnkl}\ ]$$

$$a_k a_l\ \ \ +\frac{1}{2}\sum_{k,l=1}^{K,L}[\ 'S_{D_{28}mnkl}\ ]\ \ f_k f_l\ \ \ +\frac{1}{2}\sum_{k,l=1}^{K,L}[\ S_{I_p mnkl}\ ]\ \ a_k f_l\ \ +\sum_{k,l=1}^{K,L}[\ S'_{D_{28}mnkl}\ ]\ \ f_k f_l\ \ \ ]\ ,\ \ K_{62}^{NL2}=0,$$

$$K_{63}^{NL2}=\ \ \frac{1}{2}E\sum_{k,l=1}^{K,L}[S_{I_p mnkl}]\,c_k\,f_l\ ,\ \ K_{64}^{NL2}=0,\ \ K_{65}^{NL2}=-2\overline{\Omega}\sum_{k,l=1}^{K,L}[s_{I_z mnkl}]\,f_k\,\dot{f}_l-\overline{\Omega}\,\rho\sum_{k,l=1}^{K,L}[s_{I_y mnkl}]\,f_k\,\dot{f}_l$$

$$+\rho\sum_{k,l=1}^{K,L}[s_{I_z mnkl}]\,\dot{e}_k\,\dot{f}_l\ \ \ +\rho\sum_{k,l=1}^{K,L}[s_{I_z mnkl}]\,\ddot{e}_k\,f_l\ \ +2\rho\sum_{k,l=1}^{K,L}[s_{I_z mnkl}]\,\dot{e}_k\,\dot{f}_l\ \ +\rho\sum_{k,l=1}^{K,L}[s_{I_z mnkl}]\,e_k\,\ddot{f}_l+\overline{\Omega}^2\rho\sum_{k,l=1}^{K,L}$$

$$[s_{I_y mnkl}]\,e_k\,f_l-\rho\sum_{k,l=1}^{K,L}[s_{I_y mnkl}]\,\ddot{e}_k\,f_l\ +\overline{\Omega}\rho\sum_{k,l=1}^{K,L}[s_{I_z mnkl}]\,f_k\,\dot{f}_l\ +\overline{\Omega}\rho\sum_{k,l=1}^{K,L}[s_{I_y mnkl}]\,f_k\,\dot{f}_l\ -\rho\sum_{k,l=1}^{K,L}[s_{I_z mnkl}]\,\dot{e}_k\,\dot{f}_l$$

$$,\ K_{66}^{NL2}=-\overline{\Omega}\sum_{k,l=1}^{K,L}[s_{I_z mnkl}]\,\dot{e}_k\,f_l\ -\frac{1}{2}\overline{\Omega}\rho\sum_{k,l=1}^{K,L}[s_{I_y mnkl}]\,\dot{e}_k\,f_l\ +\rho\ \sum_{k,l=1}^{K,L}[s_{I_z mnkl}]\,\dot{e}_k\,\dot{e}_l-\frac{1}{2}\overline{\Omega}^2\rho\sum_{k,l=1}^{K,L}[s_{I_z mnkl}]\,f_k\,f_l$$

$$-\frac{3}{2}\overline{\Omega}\rho\sum_{k,l=1}^{K,L}[\ s_{I_y mnkl}]\,\dot{e}_k\,f_l\ +E\ [\ \frac{1}{2}\ \sum_{k,l=1}^{K,L}[\ S_{D_8 mnkl}\ ]\ \ f_k f_l+\frac{3}{2}\sum_{k,l=1}^{K,L}[\ S''_{D_{23}mnkl}\ ]\ \ f_k f_l\ +\frac{3}{2}\sum_{k,l=1}^{K,L}[\ S'_{D_{24}mnkl}\ ]$$

$$f_k f_l\ +\sum_{k,l=1}^{K,L}[\ S_{D_{30}mnkl}\ ]\ \ f_k f_l\ \ +\frac{3}{2}\sum_{k,l=1}^{K,L}[\ ''S_{D_{23}mnkl}\ ]\ f_k f_l+\frac{1}{2}\sum_{k,l=1}^{K,L}[\ S''''_{D_4 mnkl}\ ]\ f_k f_l\ \ +\frac{3}{2}\sum_{k,l=1}^{K,L}[\ '''S_{D_{25}mnkl}\ ]$$

$$f_k f_l + \frac{1}{2}\sum_{k,l=1}^{K,L}\left[\ ''S_{D_{29}mnkl}\ \right]\ f_k f_l + \frac{1}{2}\sum_{k,l=1}^{K,L}\left[\ S'''_{D_{25}mnkl}\ \right]\ f_k f_l + \frac{3}{2}\sum_{k,l=1}^{K,L}\left[\ S'_{D_{11}mnkl}\ \right]\ f_k f_l + \frac{1}{2}\sum_{k,l=1}^{K,L}\left[\ 'S_{D_{24}mnkl}\ \right]$$

$$f_k f_l + \frac{1}{2}\sum_{k,l=1}^{K,L}\left[\ 'S_{D_{11}mnkl}\ \right]\ f_k f_l + \frac{1}{2}\sum_{k,l=1}^{K,L}\left[\ S''_{D_{29}mnkl}\ \right]\ f_k f_l + \frac{1}{2}\sum_{k,l=1}^{K,L}\left[\ S_{D_{27}mnkl}\ \right]\ f_k f_l\ \ ]$$

Chapter 6

Displacements Solution Using the Newmark Implicit Procedure

6.1 Introduction

Considering the expansion of the six unknown displacements as discussed in section 3.5:

$\bar{u} = \sum_{n=1}^{N} a_n(t)\phi_n(x), \quad v = \sum_{n=1}^{N} b_n(t)\phi_n(x), \; w = \sum_{n=1}^{N} c_n(t)\phi_n(x), \; \theta_1 = \sum_{n=1}^{N} d_n(t)\phi_n(x), \; \theta_2 = \sum_{n=1}^{N} e_n(t)\phi_n(x),$ and

$\phi = \sum_{n=1}^{N} f_n(t)\phi_n(x)$

where,

$\phi_n(x) = (x/L)^{n+1}$ are the polynomials (function of x)

$a_n(t), b_n(t), c_n(t), d_n(t), e_n(t)$ and $f_n(t)$ are the time dependent constants

In order to solve for the six unknown displacements [48-53], we need to solve first one of the below dynamic equations of motion (6.1.1a) or (6.1.1b) for :

$\delta_i^t = [a_n(t), b_n(t), c_n(t), d_n(t), e_n(t), f_n(t)]^T$ using the linear or the non-linear Newmark procedure

respectively (depeding if whether small or large deformation is considered).

$$[K]_L \delta_i^t + [C]_L \dot{\delta}_i^t + [M]_L \ddot{\delta}_i^t = R^t \qquad (6.1.1a)$$

$$\left[[K]_L + [K]_{NL1}(\delta_{i-1}^t) + [K]_{NL2}(\delta_{i-1}^t) \right] \delta_i^t + [C]_L \dot{\delta}_i^t + [M]_L \ddot{\delta}_i^t = R^t \qquad (6.1.1b)$$

where,

$[K]_L$, $[C]_L$ and $[M]_L$ are the linear matrices

$[K]_{NL1}$, $[K]_{NL2}$ are the non-linear matrices

R^t is the aerodynamic load vector that can be obtained as follows:

$$R^t = \begin{bmatrix} \int_0^L F_x(x)\phi_m(x)dx \\ \int_0^L F_y(x)\phi_m(x)dx \\ \int_0^L F_z(x)\phi_m(x)dx \\ \int_0^L M_y(x)\phi_m(x)dx \\ \int_0^L M_z(x)\phi_m(x)dx \\ \int_0^L M_x(x)\phi_m(x)dx \end{bmatrix} \qquad (6.1.2)$$

It should be noted that for the small deformation problems, the nonlinear matrices $[K]_{NL1}$, $[K]_{NL2}$ are neglected from our calculations and they are only taken into consideration if we have the large deformation case.

6.2 Implicit Dynamics versus Explicit Dynamics Schemes

In general, there are two types of schemes (or algorithms) that used to solve dynamics problems: 1) implicit and 2) explicit. In explicit schemes the solution may be advanced without storing a matrix to solve a system of equations, while in implicit scheme, a matrix is solved one or more times per step to advance the solution. Implicit schemes are tend to be numerically stable, permitting large time steps, but the cost per time step is high and storage requirements tend to increase dramatically with the size of the finite element mesh, particularly in large three-dimensional problems. On the other hand, explicit schemes tend to be inexpensive per time step and require less storage than implicit schemes, but numerical stability requires that small time steps be used. A survey of explicit methods, the step-by-step computational

procedure for the widely used central difference method and some developments of the method are given in Part I [54]. Generally, implicit algorithms are most effective for structural dynamics problems (in which the response is controlled by a relatively low frequency modes, while explicit algorithms are very efficient for wave propagation problems (in which intermediate and high frequency structural modes are exist.

The method is implicit if the solution at time $t + \Delta t$ requires consideration of the equilibrium condition at at time $t + \Delta t$ and the method requires the solution of a set of simultaneous equations at each time step wherein the coefficient matrix is a combination of the mass, damping and stiffness matrices. In large scale problems the solution to these equations may be computationally expensive.

The three most commonly used implicit time integration methods for solving linear problems are: Newmark, Houbolt and Wilson-θ methods. Additional development in implicit methods are given in [55] and more reviews of mixed implicit-explicit finite element procedures are found in [56] . Zienkiewicz et al. have given a set of single-step algorithms to solve dynamic problems [57-62] . It should be noted that these available implicit algorithms are unconditional stabile (for linear problems) which is a big advandage over the explicit algorithms.

6.3 The Linear Implicit Newmark Methods

As mentioned in section 6.2, the most important implicit time integration methods for linear problems are: Newmark, Houbolt and Wilson-θ methods. The procedures (step by step) of these methods for solving linear structural dynamics problems are little bit different from those procedures required for solving nonlinear problems, even that both procedures share the same basic techniques.

The most widely used family of implicit methods of direct time integration for solving semi-discrete equations of motion is the Newmark's family of methods [48, 63, 64].

The Newmark integration scheme can also be understood to be an extension of the linear acceleration method.

The Newmark method is based on the following assumptions:

$$\dot{X}_{t+\Delta t} = \dot{X}_t + \Delta t[(1-\gamma)\ddot{X}_t + \gamma\ddot{X}_{t+\Delta t}] \qquad (6.3.1)$$

and

$$X_{t+\Delta t} = X_t + \Delta t\dot{X}_t + (\Delta t)^2\,[(\tfrac{1}{2}-\beta)\ddot{X}_t + \beta\ddot{X}_{t+\Delta t}] \qquad (6.3.2)$$

Where the parameters β and γ determine the stability and accuracy of the algorithm. For $\gamma = \frac{1}{2}$ and $= \frac{1}{6}$, the relations (6.3.1) and (6.3.2) correspond to the linear acceleration method (which is also obtained using $\theta = 1$ in the Wilson- θ method). Newmark [64] originally proposed as an unconditionally stable scheme the constant-average-aceleration method (also called trapezoidal rule), in which case $\gamma = \frac{1}{2}$ and $\beta = \frac{1}{4}$ as shown in Fig. 6.3.1.

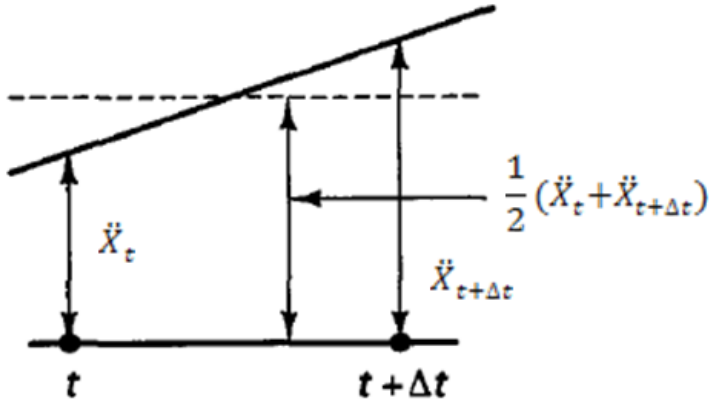

Fig. 6.3.1: Newmark's constant-average-acceleration scheme (adapted from [48]).

In addition to eqns (6.3.1) and (6.3.2), for solution of displacements, velocities and accelerations at time $t + \Delta t$, the equilibrium equations of motion are also considered at time $t + \Delta t$:

$$M\ddot{X}_{t+\Delta t} + C\dot{X}_{t+\Delta t} + KX_{t+\Delta t} = R_{t+\Delta t} \tag{6.3.3}$$

Solving Eqn 6.3.2 for $\ddot{X}_{t+\Delta t}$ in terms of $X_{t+\Delta t}$ and then substituting for $\ddot{X}_{t+\Delta t}$ in Eqn 6.3.1, we obtain equations for $\ddot{X}_{t+\Delta t}$ and $\dot{X}_{t+\Delta t}$ each in terms of the unknown displacements $X_{t+\Delta t}$ only. These two relations for $\ddot{X}_{t+\Delta t}$ and $\dot{X}_{t+\Delta t}$ into eqn (6.3.3) to solve for $X_{t+\Delta t}$ as shown in Eqn 6.3.4.

$$[K + \frac{\gamma}{\beta\Delta t}C + \frac{1}{\beta(\Delta t)^2}M]X_{t+\Delta t} = R_{t+\Delta t} + C\left\{\frac{\gamma}{\beta\Delta t}X_t + \left(\frac{\gamma}{\beta} - 1\right)\dot{X}_t + \Delta t\left(\frac{\gamma}{2\beta} - 1\right)\ddot{X}_t\right\}$$

$$-M\left\{\frac{1}{\beta(\Delta t)^2}X_t + \frac{1}{\beta\Delta t}\dot{X}_t + \left(\frac{\gamma}{2\beta} - 1\right)\ddot{X}_t\right\} \tag{6.3.4}$$

Then using (6.3.1) and (6.3.2), we can solve for $\ddot{X}_{t+\Delta t}$ and $\dot{X}_{t+\Delta t}$.

The matrix $K + \frac{\gamma}{\beta\Delta t}C + \frac{1}{\beta(\Delta t)^2}M$ in Eq. (6.3.4) is usually referred to as the 'effective stiffness matrix' and is denoted by $\widehat{K}$. Some assumption on the form of C is necessary for damped structural systems. If Rayleigh damping is assumed, then as given by [48]:

$$C = aM + bK \tag{6.3.5}$$

where a and b are given Rayleigh constants.

The algorithm operates as follows: we start at t=0; initial conditions prescribe X_0 and $\dot{X}_0$ (from these and the equations of equilibrium at t=0 we find $\ddot{X}_0$, if $\ddot{X}_0$ is not prescribed); then eqn (6.3.4) is solved for $X_{\Delta t}$; eqn (6.3.2) is solved for $\ddot{X}_{\Delta t}$ and eqn (6.3.1) is solved for $\dot{X}_{\Delta t}$; then eqn (6.3.4) yields $X_{2\Delta t}$ and so on.

Warburton [65] has suggested a direct approach in which the effective load vector depends only on the displacements at t and $t - \Delta t$, thus eliminating the necessity of additional computation of velocity and acceleration components, $\dot{X}$ and $\ddot{X}$, at time t. The recurrence

relation can be obtained as follows: use the equilibrium equations at times $t-\Delta t$, t and $t+\Delta t$ and Newmark's basic assumptions, eqn (6.3.1) and eqn (6.3.2), at times t and $t-\Delta t$. We have seven equations with six unknowns $\ddot{X}_{t+\Delta t}$, $\ddot{X}_t$, $\ddot{X}_{t-\Delta t}$, $\dot{X}_{t+\Delta t}$, $\dot{X}_t$ and $\dot{X}_{t-\Delta t}$ which can be eliminated. For $\gamma=\frac{1}{2}$, it is given by the following set of simultaneous equations:

$$(M+\tfrac{\Delta t}{2}C+\beta(\Delta t)^2K)X_{t+\Delta t}=(\Delta t)^2(\beta R_{t+\Delta t}+(1-2\beta)R_t+\beta R_{t-\Delta t})$$

$$+(2M-(\Delta t)^2(1-2\beta)K)X_t-(M-\tfrac{\Delta t}{2}C+\beta(\Delta t)^2K)X_{t-\Delta t} \qquad (6.3.6)$$

The solution for $X_{t+\Delta t}$ requires knowledge of X_t and $X_{t-\Delta t}$ and therefore, a special starting procedure is necessary. It is more common and more accurate to calculate $X_{\Delta t/2}$ by use of the central difference scheme. The same relation in the form of a three point finite difference formula has been given earlier by Chan et al. [66] in 1962, for $\gamma=\frac{1}{2}$ and $\beta=\frac{1}{4}$.

Zienkiewicz [67], Chaix and Leteux [68] derived the following general recurrence relation between three successive displacements similar to eqn (6.3.6) involving parameters γ and β:

$$(M+\gamma\,\Delta tC+\beta(\Delta t)^2K)X_{t+\Delta t}=(\Delta t)^2\left(\beta R_{t+\Delta t}+\left(\tfrac{1}{2}+\gamma-2\beta\right)R_t+\left(\tfrac{1}{2}-\gamma+\beta\right)R_{t-\Delta t}\right)+(2M-$$

$$(1-2\gamma)\Delta tC-\left(\tfrac{1}{2}+\gamma-2\beta\right)(\Delta t)^2K)\,X_t-(M+(-1+\gamma)\Delta tC+\left(\tfrac{1}{2}-\gamma+\beta\right)(\Delta t)^2K)\,X_{t-\Delta t}$$

(6.3.7)

The Newmark method is unconditionally stable if $\gamma\geq 0.5$ and $\beta\geq\frac{(2\gamma+1)^2}{16}$ [69]. Positive algorithms damping is introduced if $\gamma>0.5$ and negative algorithmic damping leading eventually to an unbounded response if <0.5. Thus in most applications $\gamma=0.5$ is used.

If $\gamma=0.5$ and $\beta=0$, the Newmark fotmulae (6.3.1) and (6.3.2) reduce to the central difference method, provided $\dot{X}_{t+\Delta t/2}=\dot{X}_t+(\frac{1}{2})\Delta t\ddot{X}_t$. Many stability issues of the method were discussed by Gladwell and Thomas [70] and Hughes [71]. The discretization errors of the method for numerical integration were analysed by Brown [72]. Stability and other properties of well known members of the Newmark family of methods are summarized in Table 6.5.1.

6.4 The Linear Implicit Newmark Iteration Procedure Steps

The steps for the linear Newmark implicit iteration procedure [48, 52, 63] as shown in Chart 6.4.1 are detailed as follows:

A. Initial calculations

1. Set initial conditions at $t = 0$ for δ_t, $\dot{\delta}_t$ and $\ddot{\delta}_t$

   where, $\delta_t = [a_n(t), b_n(t), c_n(t), d_n(t), e_n(t), f_n(t)]^T$

2. Select the time step size Δt and the parameters β and γ and calculate integration constants:

   $\gamma \geq 0.50$; $\beta \geq 0.25(0.5 + \gamma)^2$ (=0.5 and β =0.25 is a good choice)

   $$a_0 = \frac{1}{\beta \Delta t^2},\ a_1 = \frac{\gamma}{\beta \Delta t},\ a_2 = \frac{1}{\beta \Delta t},\ a_3 = \frac{1}{2\beta} - 1,\ a_4 = \frac{\gamma}{\beta} - 1,$$

   $$a_5 = \frac{\Delta t}{2}\left(\frac{\gamma}{\beta} - 2\right),\ a_6 = \Delta t\,(1 - \gamma),\ \text{and } a_7 = \Delta t\,\gamma$$

3. Form the global stiffness and mass matrices, K and M, and then the damping matrix C.

   $C = aM + bK$; if Rayleigh or ratio damping is assumed

   where, a and b are Rayleigh constants.

4. Form global effective stiffness matrix $\hat{K}$: $\hat{K} = K + a_0 M + a_1 C$ Triangularize $\hat{K}$: $\hat{K} = LDL^T$.

5. Steps 3-5 may vary depending on the matrix solution method employed.

B. For each time step

1. Calculate effective load vector at $t + \Delta t$:

   $$\hat{R}_{t+\Delta t} = R_{t+\Delta t} + [ML](a_0 \delta_t + a_2 \dot{\delta}_t + a_3 \ddot{\delta}_t) + [CL](a_1 \delta_t + a_4 \dot{\delta}_t + a_5 \ddot{\delta}_t)$$

2. Solve for the displacements at time $+\Delta t$:

   $$LDL^T \delta_{t+\Delta t} = \hat{R}_{t+\Delta t}$$

3. Calculate accelerations and velocities at time $+\Delta t$:

   $$\ddot{\delta}_{t+\Delta t} = a_0(\delta_{t+\Delta t} - \delta_t) - a_2 \dot{\delta}_t - a_3 \ddot{\delta}_t$$

   $$\dot{\delta}_{t+\Delta t} = \dot{\delta}_t + a_6 \ddot{\delta}_t + a_7 \ddot{\delta}_{t+\Delta t}$$

4. Iterate for next time step $t + \Delta t$ by going to step 1 of B.

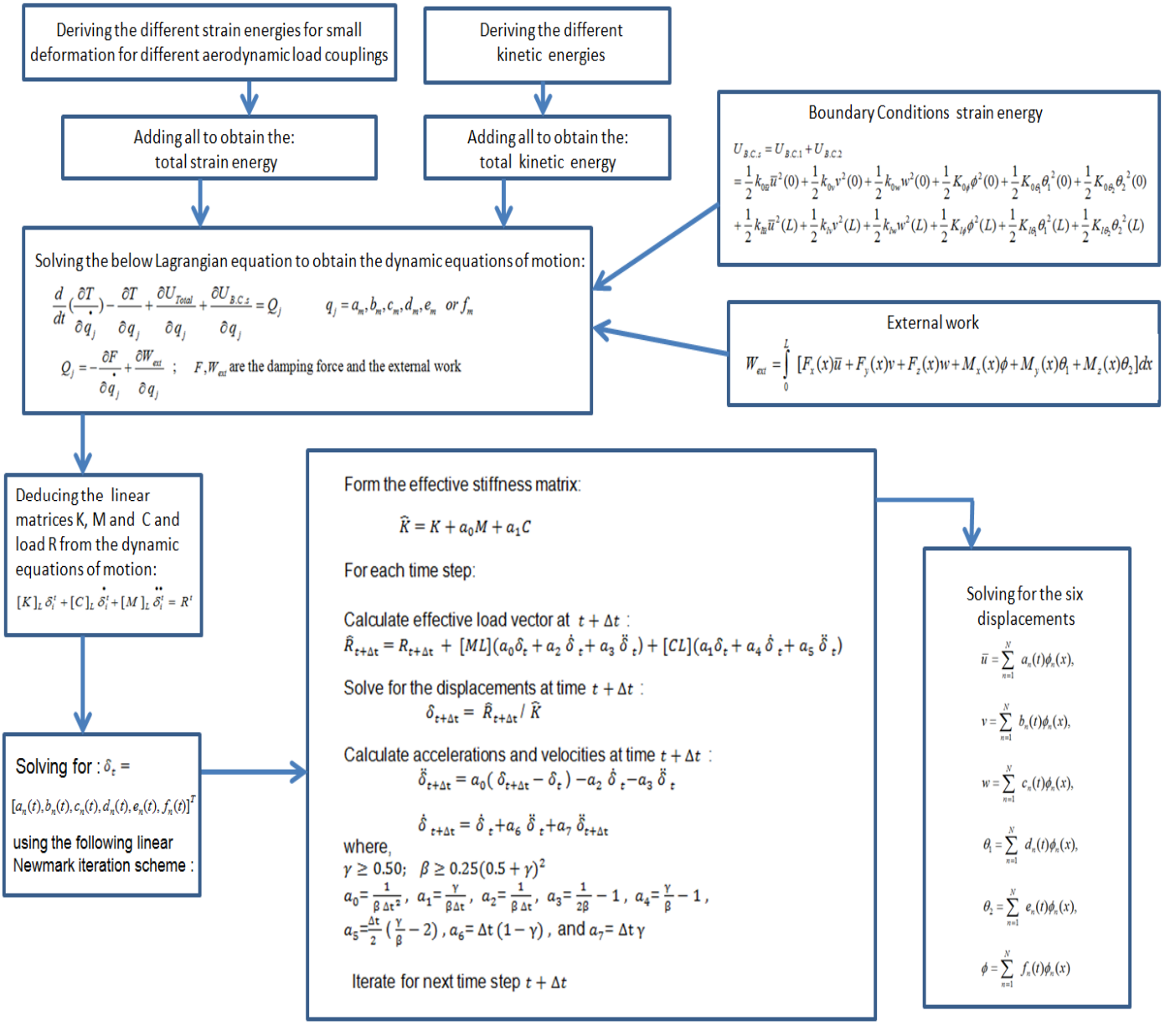

Chart 6.4.1: Linear Newmark procedure flow chart.

6.5 Stability Conditions for the Newmark Methods

A summary of the stability conditions for the Newmark method [69-71, 73-75] are given as

follows:

Unconditional :

$$2\beta \geq \gamma \geq 0.50 \tag{6.5.1}$$

Conditional :

$$\gamma \geq 0.50 \tag{6.5.2}$$

$$\beta < \gamma/2 \tag{6.5.3}$$

$$\omega\, \Delta t \geq \Omega_{crit} \tag{6.5.4}$$

$$\Omega_{crit} = \frac{\xi\left(\gamma - \frac{1}{2}\right) + \left[\frac{\gamma}{2} - \beta + \xi^2\left(\gamma - \frac{1}{2}\right)^2\right]^{0.5}}{\left(\frac{\gamma}{2} - \beta\right)} \tag{6.5.5}$$

Where ω is the undamped frequency of vibration and $\xi = (\frac{a}{\omega} + \frac{b}{\omega})$ is the damping ratio. Note that if $\gamma = \frac{1}{2}$ viscous damping has no effect on stability.

It should be noted that when $\gamma > \frac{1}{2}$ the effect of viscous damping is to increase the critical time step of conditionally stable Newmark methods. In the case of Rayleigh damping ξ is determined by ω. The explicit central difference mehod generally results in considerable savings in computing cost when compared with the linear acceleration and Fox-Goodwin methods. The average acceleration method is one of he most effective and popular implicit techniques used for structural dynamics problems.

Because the higher modes of semi-discrete structural dynamic equations are artefacts of the (finite element) discretization process and not representative of the behavior of the governing partial differential equations of motion, it is generally viewed as desirable. And often is considered absolutely necessary, to have some form of algorithmic damping present to remove the participation of the high-frequency modal components. At the same time it is

required to maintain good accuracy in the important lower modes.

In the Newmark method, $\gamma > \frac{1}{2}$ is necessary to introduce high frequency dissipation.

Unfortunately this adversely affects accuracy in the lower modes.

Method	Type	β	γ	Stability Condition **	Order of Accuracy
Average acceleration (trapezoidal rule)	Implicit	1/4	1/2	unconditional	2
Linear acceleration	Implicit	1/6	1/2	$\Omega_{crit} = 2\sqrt{3}$	2
Fox-Goodwin formula	Implicit	1/12	1/2	$\Omega_{crit} = \sqrt{6}$	2 ***
Central difference	Explicit *	0	1/2	$\Omega_{crit} = 2$	2 ****

Table 6.5.1: Properties of the members of the Newmark family of methods [63].

* Strictly speaking, M and C tobe diagonal for the central difference method to be explicit.
** Stability is based on the undamped case in which the damping ratio $\xi = 0$.
*** Fourth order accuracy is achieved for the Fox-Goodwin method if $C = 0$.
**** Second order accuracy is achieved if and only if $= 1/2$.

6.6 The Non-linear Implicit Newmark Iteration Procedure Steps

The steps for the non-linear Newmark implicit iteration procedure [48, 52, 63] as shown in Chart 6.6.1 are as follows:

1. Set initial conditions at $t = 0$ for δ_t, $\dot{\delta}_t$ and $\ddot{\delta}_t$

   where $\delta_t = [a_n(t), b_n(t), c_n(t), d_n(t), e_n(t), f_n(t)]^T$

2. Select time step size Δt, the Newmark parameters $\beta=0.25$ and $\gamma=0.5$ and calculate the following constants: $a_0 = \frac{1}{\beta \Delta t^2}$, $a_1 = \frac{\gamma}{\beta \Delta t}$, $a_2 = \frac{1}{\beta \Delta t}$, $a_3 = \frac{1}{2\beta} - 1$, $a_4 = \frac{\gamma}{\beta} - 1$, $a_5 = \frac{\Delta t}{2}\left(\frac{\gamma}{\beta} - 2\right)$, $a_6 = \Delta t\, \gamma$, and $a_7 = \Delta t\,(1 - \gamma)$

3. Form the linear matrices $[K]_L$, $[M]_L$ and $[C]_L$ and the non-linear matrices $[K]_{NL1t}$ and $[K]_{NL2t}$.

4. Form the effective stiffness matrix:

   $\widehat{K} = [KT]_t + a_0[M]_L + a_1[C]_L$, where $[KT]_t = [KL] + [K]_{NL1t} + [K]_{NL2t}$, and $[K]_{NL1}$ and $[K]_{NL2}$ are the non-linear stifness matrices. Note that initially $[K]_{NL1t} = [K]_{NL2t} = 0$.

5. Form the effective load vector:

   $\hat{R}_{t+\Delta t} = R_{t+\Delta t} + [ML](a_2\,\dot{\delta}_t + a_3\,\ddot{\delta}_t) + [CL](a_4\,\dot{\delta}_t + a_5\,\ddot{\delta}_t) - [KT]_t\,\delta_t$

6. Solve for the displacement increments

   delta$\delta = \widehat{K}^{-1}\hat{R}_{t+\Delta t}$

7. Iterate for dynamic equilibrium:

   a) For i=i+1

   b) Evaluate the (i-1)th approximation to the acceleration, velocities and displacements:

   $\ddot{\delta}_{t+\Delta t}^{i-1} = a_0 \text{delta}\delta^{i-1} - a_2\,\dot{\delta}_t - a_3\,\ddot{\delta}_t$

   $\dot{\delta}_{t+\Delta t}^{i-1} = a_1 \text{delta}\delta^{i-1} - a_4\,\dot{\delta}_t - a_5\,\ddot{\delta}_t$

   $\delta_{t+\Delta t}^{i-1} = \text{delta}\delta^{i-1} + \delta_t$

   c) Evaluate the updated (i-1)th residual force

   $\psi_{t+\Delta t}^{i-1} = R_{t+\Delta t} - ([ML]\ddot{\delta}_{t+\Delta t}^{i-1} + [CL]_t\,\dot{\delta}_{t+\Delta t}^{i-1} + [KT]_t\,\delta_{t+\Delta t}^{i-1})$

   d) Solve for the ith corrected displacement increments

   $\widehat{K}_t\,\Delta\delta^{\text{i}} = \psi_{t+\Delta t}^{i-1}$

   e) Evaluate the corrected displacement increments

   $\text{delta}\delta^{i} = \text{delta}\delta^{i-1} + \Delta\delta^{\text{i}}$

   f) Check for convergence of the iteration process: $\frac{abs(\Delta\delta^{\text{i}})}{\text{abs}(\delta_t + \text{delta}\delta^{i})} \leq$ **tolerance factor**

   If 'No' , return to step 7a, otherwise continue

8. Return to step 4 to process the next time step.

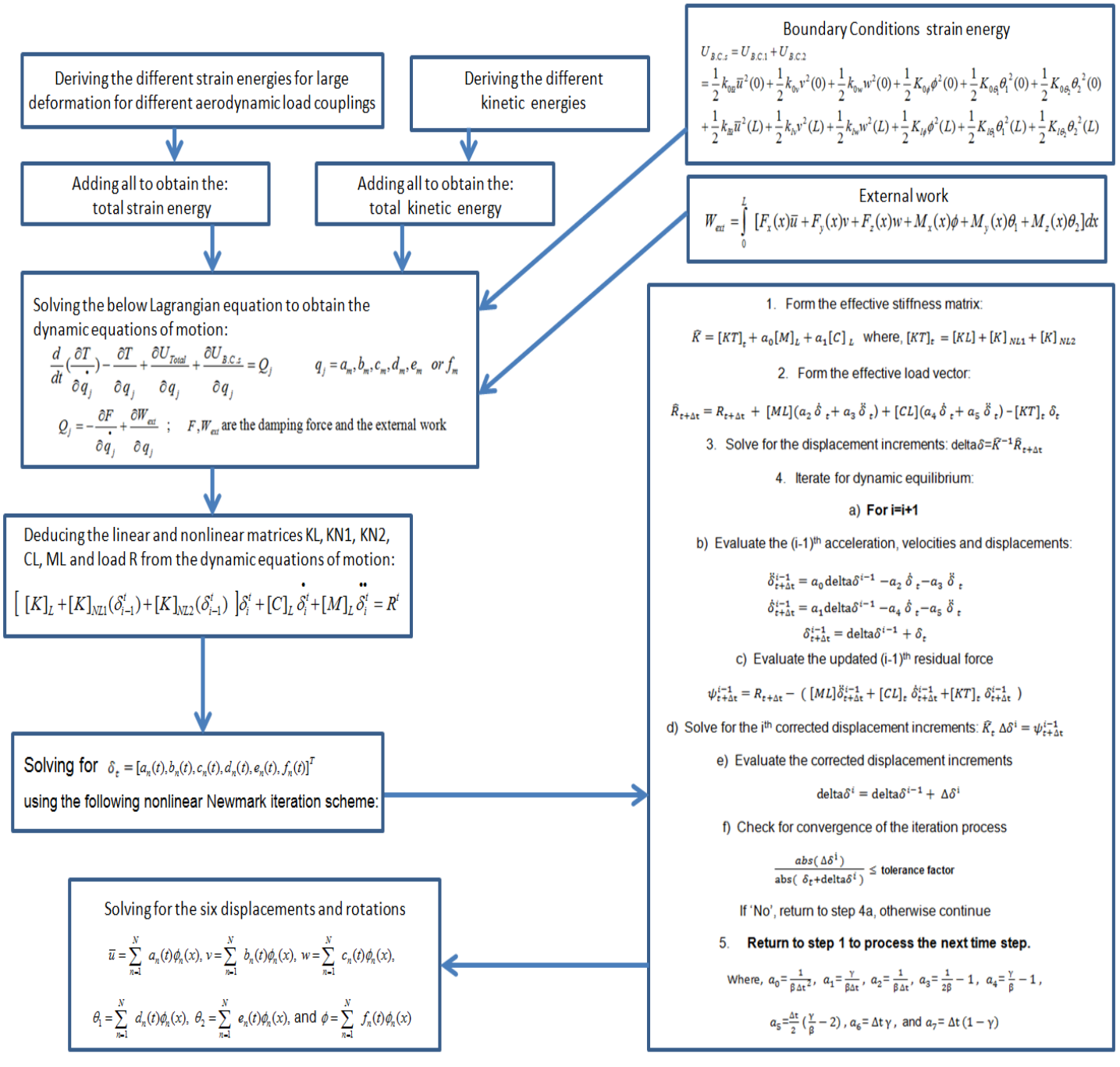

Chart 6.6.1: Non-linear Newmark procedure flow chart.

Chapter7

The Selected Blade Design

7.1 Introduction

The design of wind turbine blades requires a set of input data that describing the geometrical and structural characteristics of the blade, such as blade length, thickness distribution, chord length distribution, blade twist, root connection, etc. The radius of the rotor, i.e. the length of the rotor's blade, can be determined from the rotor's area which depends in it's value on the rated power of the wind turbine.

The rated power can be calculated from the equation:

$$P_{rat} = 0.5\rho V_{rat}^3 A C_{p,rat} \qquad (7.1.1)$$

For example if we have a rated power $P_{rat} = 150$ KW that defined at one value of wind speed and power coefficient. These two values can be chosen by experience and will directly influence the size of the wind turbine rotor, i.e. the diameter. However, experience has shown that most machines have a rated speed V_{rat} around 10m/s and for small fast running machines lower values can be realized. Hence, for this design, V_{rat} = 9.5 m/s is selected.

The maximum power coefficient attained for an ideal wind turbine is $C_{p,\max}$=16/27 =59%, but from manufacturer data and test results of Ta'ani et al. [76], most machines of this size operate at C_p = 40%., which is chosen for this design. Also for this design, the air density is selected as ρ =1.25 kg/m.

7.2 Rotor Specifications and Dimensions

With the parameters selection of previous section 7.1, the only remaining unknown is the rotor's area that can be calculated from Eqn 5.1 as: $A = P_{rat}/(0.5\rho V_{rat}^3 C_{p,rat}) = 699.75$ m^2, and the diameter of the rotor will be $d = (4A/\pi)^{0.5} =$ 29.86 m. The wind turbine rotor consists of two main components, hub and blade, as shown in Fig.4.5.1.1. The hub can be rigid in the case of fixed pitch, or can have rotating flanges for variable pitch machines. The hub and flange, including axle assembly, is assigned a radius of 0.93 m, where the blade length is taken to be 14m as shown in Fig. 7.2.1.

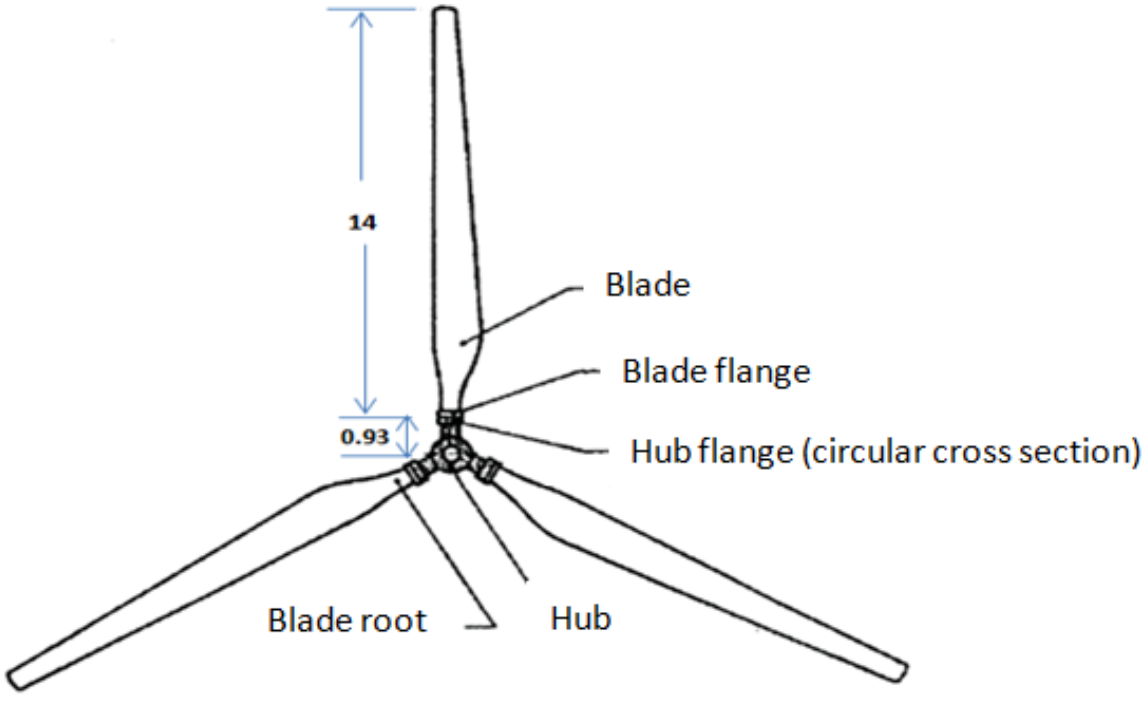

Fig. 7.2.1: Three blade rotor assembly (adapted from [27]).

If we zoom in on Fig. 7.2.1, each of the the three blades will look like the blade shown in Fig. 7.2.2. The blade construction looks like that was given by Habalia and Saleh [27] but our present blade is bigger and longer.

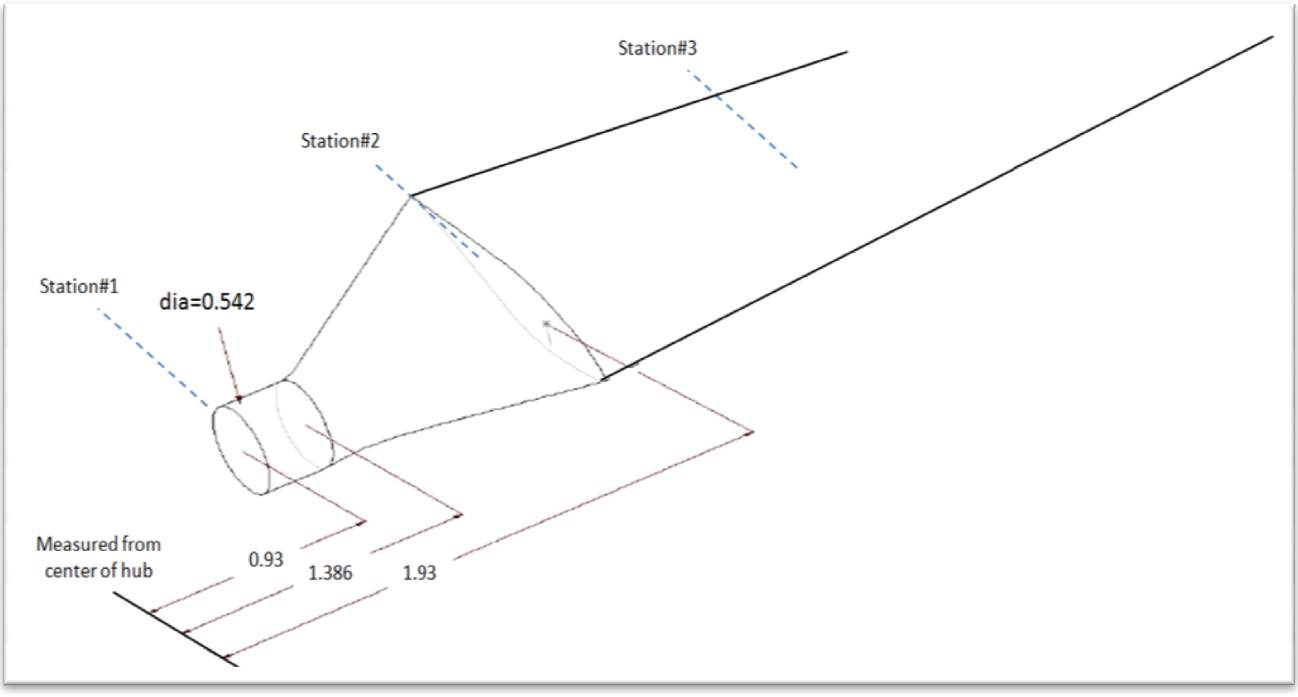

Fig. 7.2.2: Blade shape and dimensions.

7.3 Angle of Attack

The angle of attack (α) for wind turbine blade station (or airfoil) is the angle between the profile's chord line and direction of the airflow wind (i.e. relative velocity) is calculated by this expression which is completely different from that related to the helicopter [77, 78]:

$$\alpha = \phi - (\beta + \theta_p)$$

where,

ϕ (flow angle) is the angle between the relative velocity and the rotor plane

β (twist angle) is the angle measured relative to the tip chord of the blade

θ_p (pitch angle) is the angle between the tip chord and the rotor plane

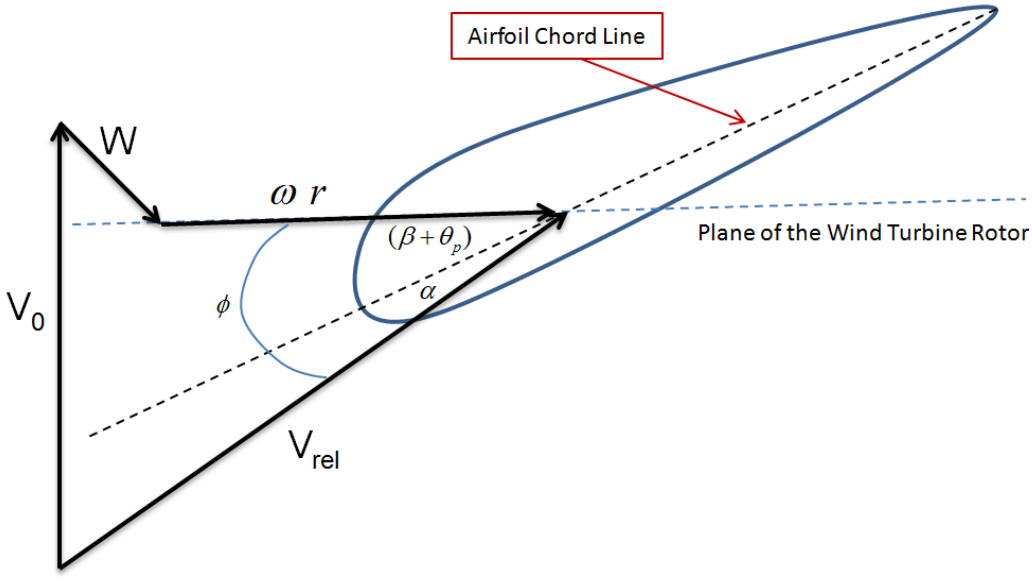

Fig. 7.3.1: Flow around an airfoil section.

The angle of attack (α) for a wind turbine may be determined by the coefficient of lift and drag. The design angle should be the angle where the lift is the biggest, and the drag is the smallest. A rotor blade will stop providing enough lift once the wind hits at a steeper α. The rotor blades must therefore be twisted to achieve an optimal α throughout the length of the blade. Assume that the tip pitch angle θ_p is zero, then α will be equal to $\phi - \beta$. Note that the Lift diminishes and drag increases at α over 15 degrees [79]. Therefore the twisting angle should be chosen in a way to optimize α in such a way to be high but not exceeding the stall angle. Considering W, the induced velocity constant we can easily find from Fig. 7.3.1 that if the rotational speed grow, ωr will reduce the flow angle ϕ where the blade needs to be twisted to keep α optimized.

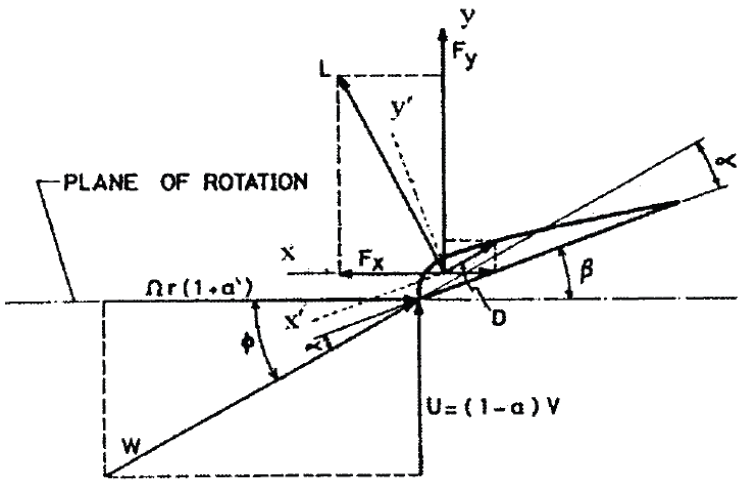

Fig. 7.3.2: Velocity and forces at a blade element at radius r [27]

From the velocity triangle in Fig. 7.3.2 and as explained by [27, 80], the twist angle β is large near near the root, where the rotational speed(is $V_t = r\Omega$) low and small at the tip where the rotational speed is high. This situation suggests a match between the twist and rotational speed, since the relative wind velocity W is

$$W = U + \Omega r$$

The procedure is to either:

1) fixing Ω and searching for the optimum twist β or

2) fixing β and searching for the optimum Ω

The choice number one is better because it is easier for designing the gear and the generator. Blade rotational speed was chosen to be 75 rpm. As a first estimate of the twist, we use the equation for twist of the zero lift line:

$$\beta = ((R\alpha_t/r) - \alpha_t) - k(1 - r/R) \tag{7.3.1}$$

where α_t is the angle of attack at the blade's tip and k is a constant such that k > 0.

α_t can be calculated from the velocity triangle shown in Fig. 7.3.2 as follows:

Knowing that the angular velocity $\Omega = 2\pi * 75/60s = 7.8575$ rad/sec we obtain for example the rotational tip speed $V_t = R\Omega = 39.27\, m/s.$ Just for an example, taking a mean free stream wind speed of $U = 7m/s,$ which is usually taken as a design wind speed [27], then from Fig. 7.3.2, we get $\phi = \tan^{-1}(U/V_t) = \tan^{-1}(7/39.2) = 10.1^0.$

Implies, $\alpha = 10.1 - \beta$ that is applicable at tip blade station only.

Consequently, we may have different blade's twist angle and different blade's flow angle value at each station of the blade since the value of r (the distance to the station under consideration) is different. This means that α will be different for each station of the blade under consideration.

7.4 Airfoil Profile Properties

The rotor blade aerodynamical design is a key element in determining the efficiency of the wind turbine. It is crucial sometimes in a optimum rotor blade design to select one or more 2D airfoil sections to form a smooth blade profile. A typical blade cross-sectional airfoil geometry is shown in Fig. 7.4.1.

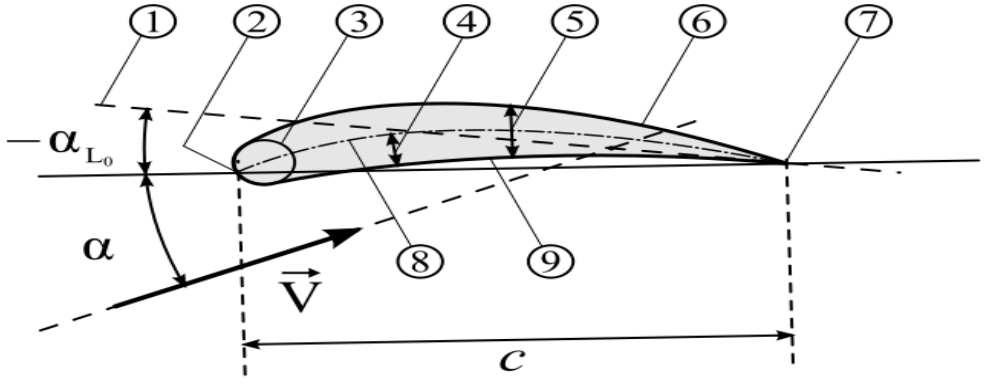

Fig. 7.4.1: Airfoil geometry [81].

where,

- **1**: zero lift line
- **2**: leading edge
- **3**: nose circle
- **4**: camber
- **5**: thickness
- **6**: upper surface
- **7**: trailing edge
- **8**: main camber line
- **9**: lower surface

7.4.1 NACA4415 Airfoil Profile Properties

Below Table 7.4.1.1 show the NACA-4415 airfoil coordinates [82-84] where the size of the airfoil shape depends directly on the size of its chord.

Upper Surface		Lower Surface	
x/c	y/c	x/c	y/c
0	0	0	0
1.25	3.07	1.25	-1.79
2.5	4.17	2.5	-2.48
5	5.74	5	-3.27
7.5	6.91	7.5	-3.71
10	7.84	10	-3.98
15	9.27	15	-4.18
20	10.25	20	-4.15
25	10.92	25	-3.98
30	11.25	30	-3.75
40	11.25	40	-3.25

50	10.53	50	-2.72
60	9.3	60	-2.14
70	7.63	70	-1.55
80	5.55	80	-1.03
90	3.08	90	-0.57
95	1.67	95	-0.36
100	0	100	0

Table 7.4.1.1: NACA-4415 airfoil coordinates [82-84].

By plotting these coordinates, we can obtain the geometrical shape of the NACA4415 airfoil as shown in Fig. 7.4.1.1

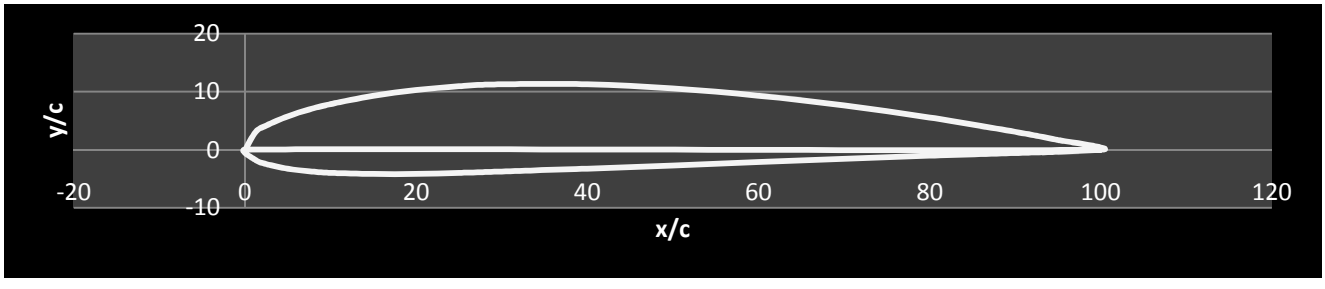

Fig. 7.4.1.1: Geometrical shape of NACA-4415 airfoil (plotted using Table 7.4.1.1 data).

The NACA4415 Wind Tunnel Profile Coefficients Cl, Cd and Cm w.r.t. the angle of attack at a Reynolds number of around 1,000,000 [83] are shown in Table 7.4.1.2.

AOA	C_l	C_{dp}	$C_{m/4}$
-20.1	-0.38	0.2555	0.0118
-18.0	-0.32	0.2181	0.0047
-16.1	-0.27	0.1854	-0.0002
-14.1	-0.24	0.1613	0.0021
-12.1	-0.47	0.1541	0.0058
-10.2	-0.60	-0.0141	-0.1014
-8.1	-0.40	-0.0139	-0.0990
-6.1	-0.19	-0.0123	-0.0981
-4.1	0.02	-0.0088	-0.0967
-2.1	0.23	-0.0061	-0.0954
0.0	0.42	-0.0005	-0.0939
2.1	0.63	0.0049	-0.0931
4.1	0.86	0.0126	-0.0947
6.2	1.02	0.0197	-0.0846
8.1	1.17	0.0257	-0.0745
10.2	1.26	0.0360	-0.0598
11.2	1.29	0.0432	-0.0519
12.2	1.30	0.0554	-0.0477
13.3	1.33	0.0682	-0.0467
14.3	1.35	0.0886	-0.0526
15.3	1.19	0.0750	-0.0378
16.2	1.15	0.0925	-0.0447
17.2	1.12	0.1095	-0.0497
18.2	1.10	0.1264	-0.0568
19.2	1.09	0.1469	-0.0634
20.3	1.08	0.1675	-0.0695
22.1	1.04	0.2161	-0.0877
24.1	1.03	0.2705	-0.1050

Table 7.4.1.2: Cl, Cd and Cm w.r.t. angle of attack for NACA-4415 airfoil (adapted from [83]).

Chart 7.4.1.1, Chart 7.4.1.2 and Chart 7.4.1.3 show Cl, Cd and Cm versus angle of attack respectively for the NACA4415 airfoil.

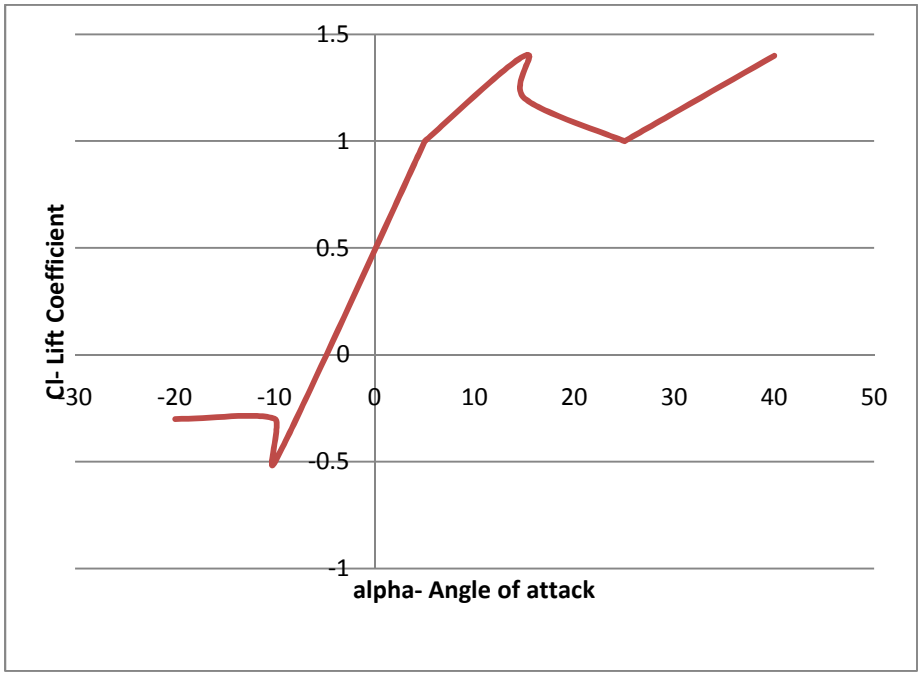

Chart 7.4.1.1: Cl versus alpha for NACA4415 (plotted using Table 7.4.1.2 data).

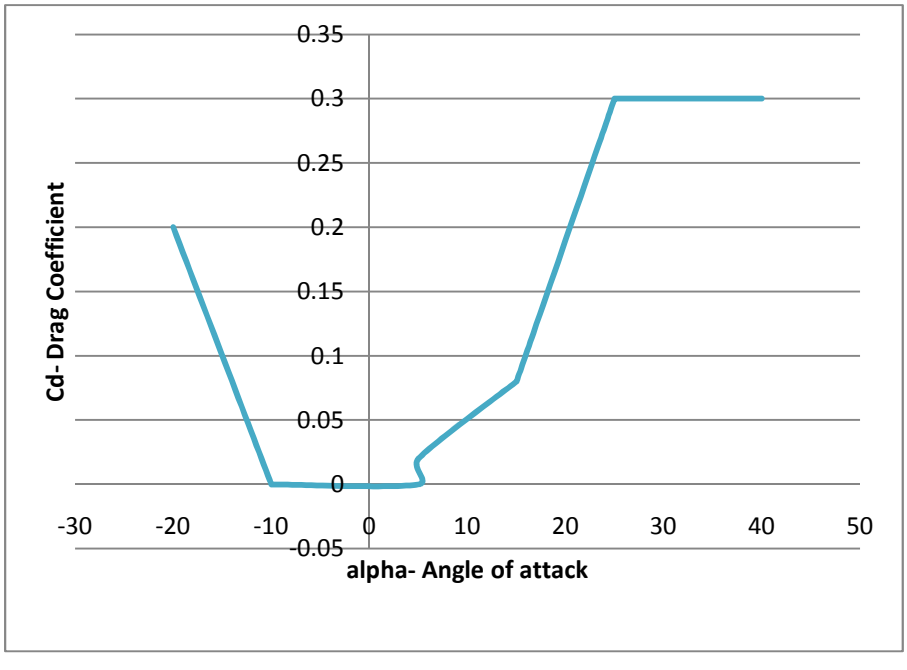

Chart 7.4.1.2: Cd versus alpha for NACA4415 (plotted using Table 7.4.1.2 data).

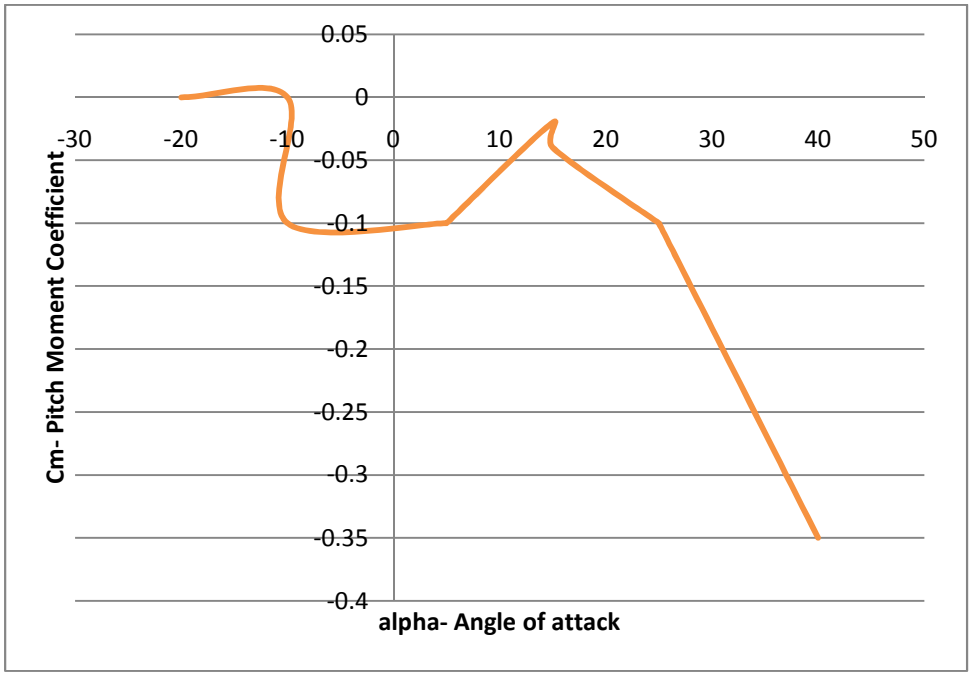

Chart 7.4.1.3: Cm versus alpha for NACA4415 (plotted using Table 7.4.1.2 data).

7.4.2 S809 Airfoil Profile Properties

Below Table 7.4.2.1 show the S809 airfoil coordinates [33, 85] where the size of the airfoil shape depends directly on the size of its chord.

Upper Surface		Lower Surface	
x/c	y/c	x/c	y/c
0.00037	0.00275	0.0014	-0.00498
0.00575	0.01166	0.00933	-0.01272
0.01626	0.02133	0.02321	-0.02162
0.03158	0.03136	0.04223	-0.03144
0.05147	0.04143	0.06579	-0.04199
0.07568	0.05132	0.09325	-0.05301
0.1039	0.06082	0.12397	-0.06408
0.1358	0.06972	0.15752	-0.07467
0.17103	0.07786	0.19362	-0.08447
0.2092	0.08505	0.23175	-0.09326
0.24987	0.09113	0.27129	-0.1006

0.29259	0.09594	0.31188	-0.10589
0.33689	0.09933	0.35328	-0.10866
0.38223	0.10109	0.39541	-0.10842
0.42809	0.10101	0.43832	-0.10484
0.47384	0.09843	0.48234	-0.09756
0.52005	0.09237	0.52837	-0.08697
0.56801	0.08356	0.57663	-0.07442
0.61747	0.07379	0.62649	-0.06112
0.66718	0.06403	0.6771	-0.04792
0.71606	0.05462	0.72752	-0.03558
0.76314	0.04578	0.77668	-0.02466
0.80756	0.03761	0.82348	-0.01559
0.84854	0.03017	0.86677	-0.00859
0.88537	0.02335	0.90545	-0.0037
0.91763	0.01694	0.93852	-0.00075
0.94523	0.01101	0.96509	0.00054
0.96799	0.006	0.98446	0.00065
0.98528	0.00245	0.99612	0.00024
0.99623	0.00054	1	0
1	0	0	0

Table 7.4.2.1: Coordinates of S809 airfoil profile [33, 35, 85].

By plotting these coordinates, we can obtain the geometrical shape of the S809 airfoil as shown in Fig. 7.4.2.1

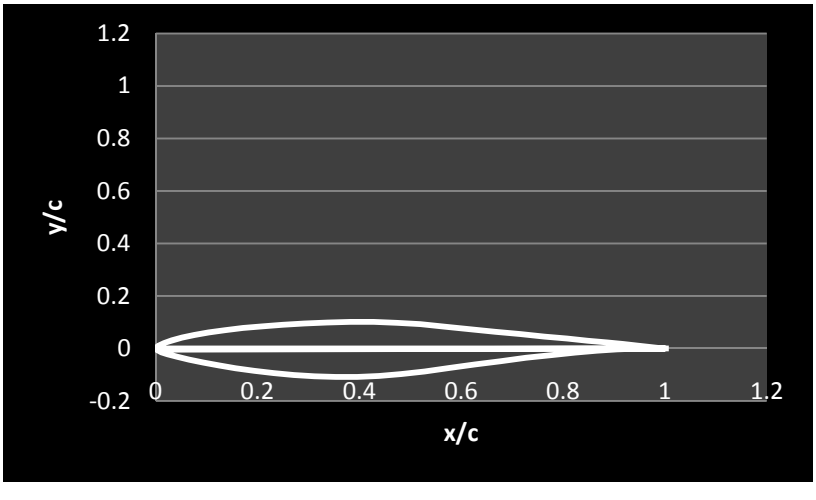

Fig. 7.4.2.1: Geometrical shape of S809 airfoil (plotted using Table 7.4.2.1data).

The S809 Wind Tunnel Profile Coefficients Cl, Cd and Cm w.r.t. the angle of attack shown in Table 7.4.2.2. This relations were obtained at the Delft University of Technology Low Speed Laboratory low-turbulence wind tunnel with a Reynolds number of 1,000,000 ,Somers [85, 86].

Angle of Attack	Cl	Cd	Cm
-1.04	0.019	0.0095	-0.0408
-0.01	0.139	0.0094	-0.0435
1.02	0.258	0.0096	-0.0462
2.05	0.378	0.0099	-0.0487
3.07	0.497	0.01	-0.0514
4.1	0.617	0.01	-0.0538
5.13	0.736	0.0097	-0.056
6.16	0.851	0.0095	-0.0571
7.18	0.913	0.0127	-0.0506
8.2	0.952	0.0169	-0.0439
9.21	0.973	0.0247	-0.0374
10.2	0.952	0.0375	-0.0397
11.21	0.947	0.0725	-0.0345
12.23	1.007	0.0636	-0.042
13.22	1.031	0.0703	-0.042
14.23	1.055	0.0828	-0.0419
15.23	1.062	0.1081	-0.0418
16.22	1.043	0.1425	-0.0452
17.21	0.969	0.1853	-0.0458
18.19	0.938	0.1853	-0.0544
19.18	0.929	0.1853	-0.0658
20.16	0.923	0.1853	-0.0783

Table 7.4.2.2: Cl, Cd and Cm w.r.t. angle of attack for S809 airfoil [33, 35, 85].

Using the linear interpolation and extrapolation techniques, we can extend the values of coefficients Cl, Cd and Cm w.r.t. alpha of Table 7.4.2.2 to include all the required coefficients for other required angle of attack values as shown.

Linear interpolation

Generally, linear interpolation takes two data points, say (x_a,y_a) and (x_b,y_b), and the interpolant is given by:

$$y = y_a + (y_b - y_a)\frac{(x - x_a)}{(x_b - x_a)} \text{ at the point } (x,y) \qquad (7.4.2.1)$$

`

Linear extrapolation

If the two data points nearest the point x_* to be extrapolated are (x_{k-1},y_{k-1}) and (x_k,y_k), linear extrapolation gives the function:

$$y(x_*) = y_{k-1} + \frac{x_* - x_{k-1}}{x_k - x_{k-1}}(y_k - y_{k-1}). \qquad (7.4.2.2)$$

Plotting the corresponding Cl w.r.t alpha, Cd w.r.t. alpha and Cm w.r.t. alpha, for the S809, we obtain chart 7.4.2.1, chart 7.4.2.2 and chart 7.4.2.3 respectively.

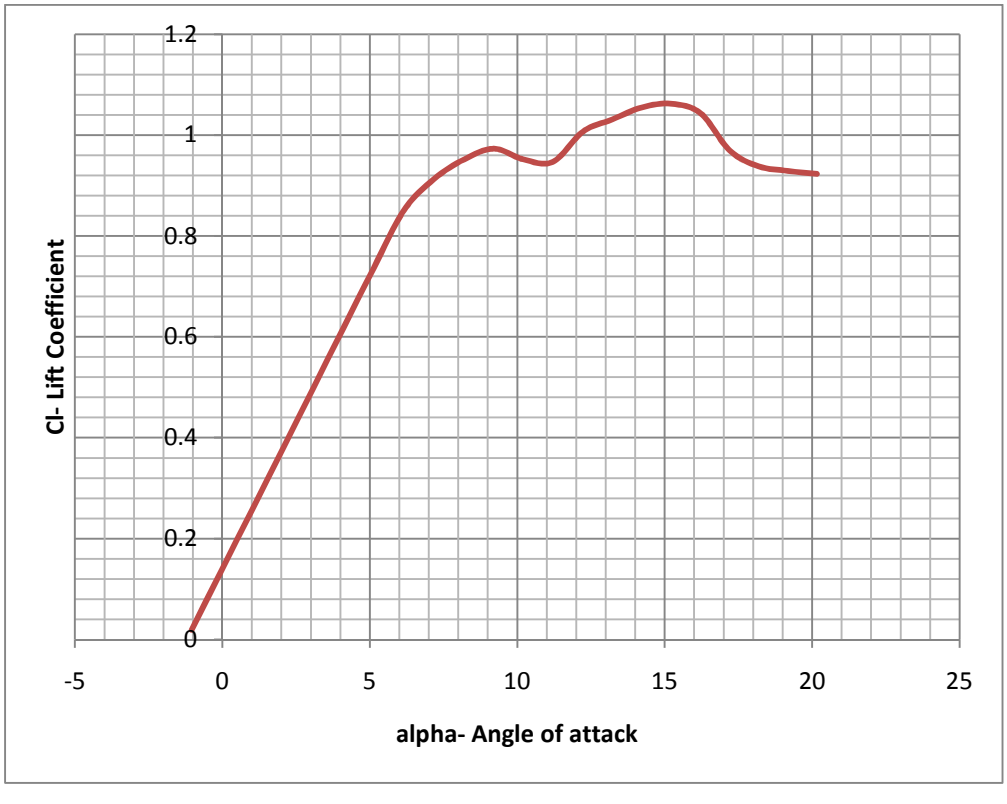

Chart 7.4.2.1: Cl versus alpha for S809 (plotted using Table 7.4.2.2 data).

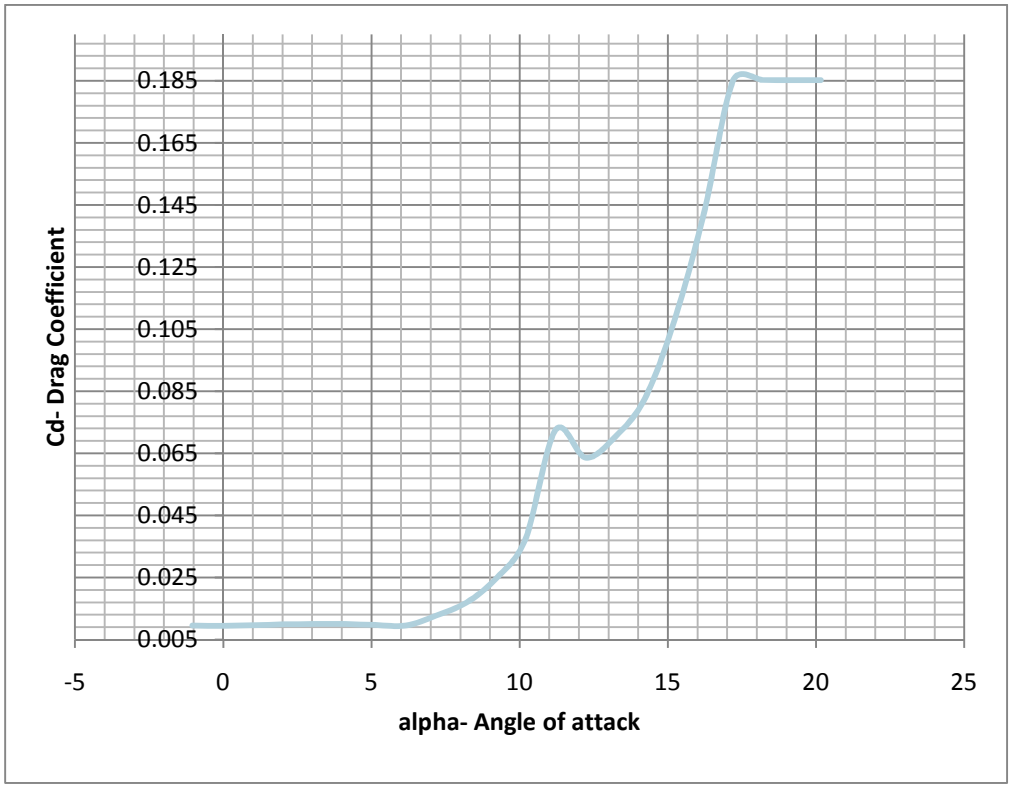

Chart 7.4.2.2: Cd versus alpha for S809 (plotted using Table 7.4.2.2 data).

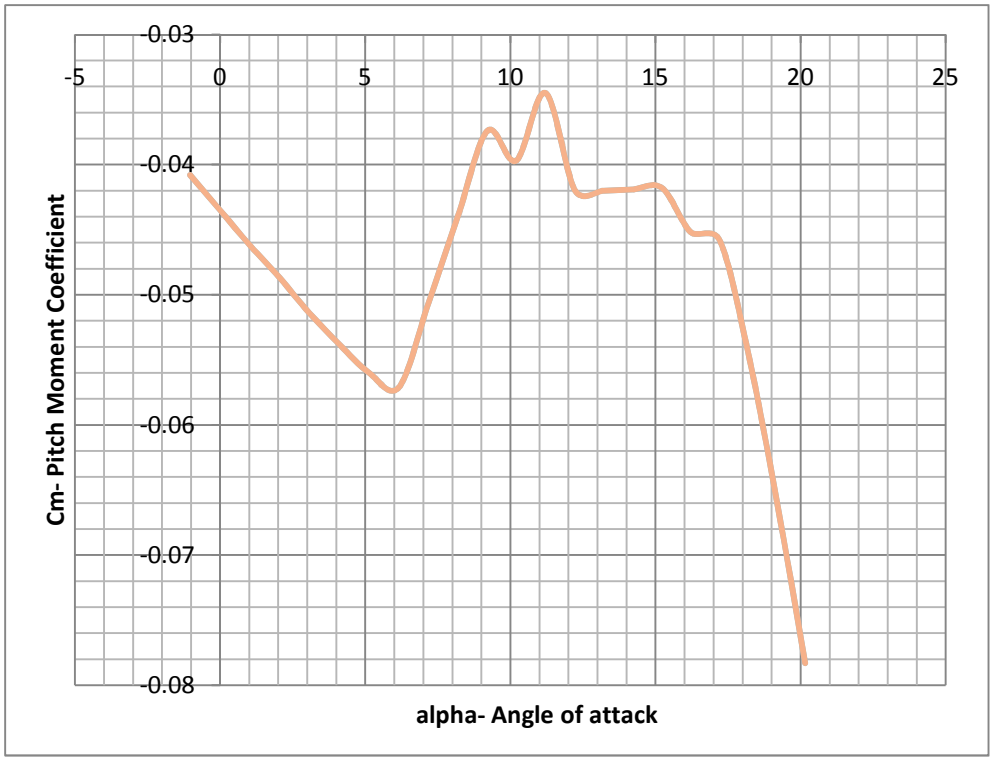

Chart 7.4.2.3: Cm versus alpha for S809 (plotted using Table 7.4.2.2 data).

By interpolating or by looking precisely at these charts we can easily obtain the associated values of Cl, Cd and Cm at each station of the our blade by only knowing the angle of attack. And by knowing the values of Cl, Cd and Cm, and some other necessary blade properties, I will able obtain the aerodynamic loading as Fx, Fy, Fz, Mx, My and Mz.

The angle of attack definition and its relation to other important angles will be discussed in next section because understanding this is so important for the blade aerodynamic loading calculation.

7.5 Blade Different Airfoil Geometrical Properties

Considering the present blade of 14m length, as shown in Fig 7.5.1, where the blade is divided into 15 stations. Each of two consecutive stations is separated by 1m.

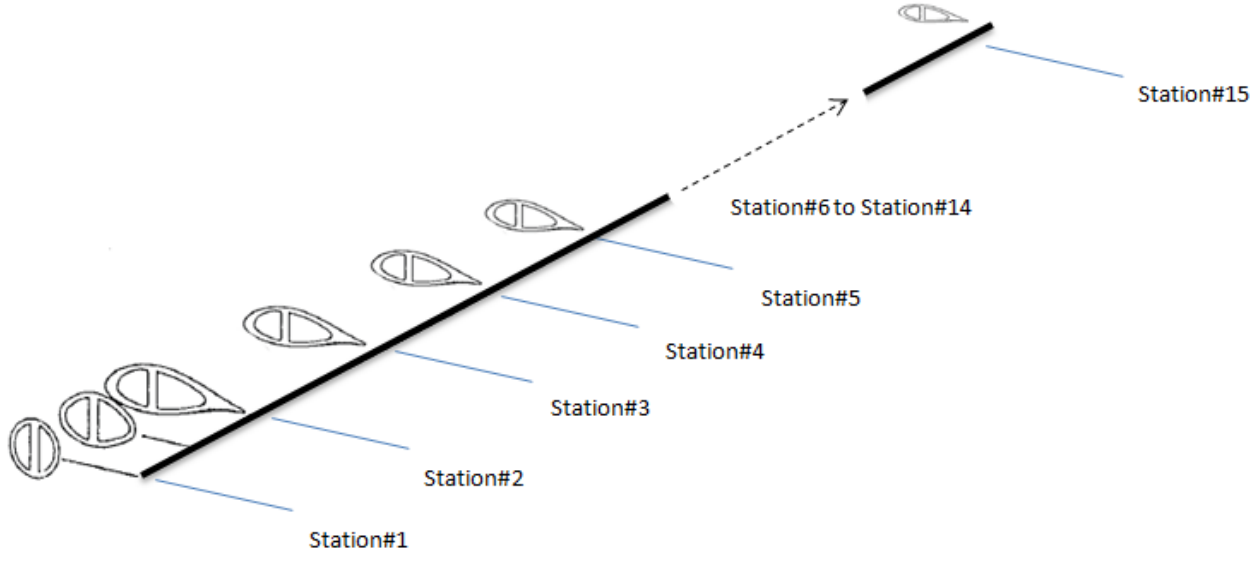

Fig. 7.5.1: Blade different airfoil profiles.

The blade profile at each of these stations is shown in Table 7.5.1, where the NACA4415 airfoil profile was considered for all stations that linearly increasing in cross section from station

1 to station 2 and linearly decreasing in cross section from station 2 to station15 (at tip of the blade).

Station(m)	Airfoil station x-location(m)	Chord(m)	Thickness(m)	Twist angle (degree)	Profile
1	0	0.542	0.11382	14	NACA4415
2	1	1.467035	0.30807735	13	NACA4415
3	2	1.401105	0.29423205	12	NACA4415
4	3	1.35518	0.2845878	11	NACA4415
5	4	1.269245	0.26654145	10	NACA4415
6	5	1.2033	0.252693	9	NACA4415
7	6	1.137385	0.23885085	8	NACA4415
8	7	1.071455	0.22500555	7	NACA4415
9	8	1.005525	0.21116025	6	NACA4415
10	9	0.939595	0.19731495	5	NACA4415
11	10	0.873665	0.18346965	4	NACA4415
12	11	0.807735	0.16962435	3	NACA4415
13	12	0.741805	0.15577905	2	NACA4415
14	13	0.675875	0.14193375	1	NACA4415
15	14	0.675875	0.14193375	0	NACA4415

Table 7.5.1: Blade stations airfoil profile properties.

By knowing or by computing the angle of attack (α) at each station by using $\alpha = \phi - \beta$, as was discussed in section 7.3, then we can select the associated Cl, Cd and Cm coefficients at each station of the blade by using the charts 7.4.1.1, 7.4.1.2 and 7.4.1.3. Some authors assume that α change in relation with the blade azimuth angle as shown in Fig. 7.5.2 [87] where inboard alpha is higher than the outboard alpha and alpha incrementaly decreases from azimuth angle zero to azimuth angle 180 and then incrementaly increases from azimuth angle 180 degrees to azimuth angle 360 degrees to go back to the same value that it was at zero degree .

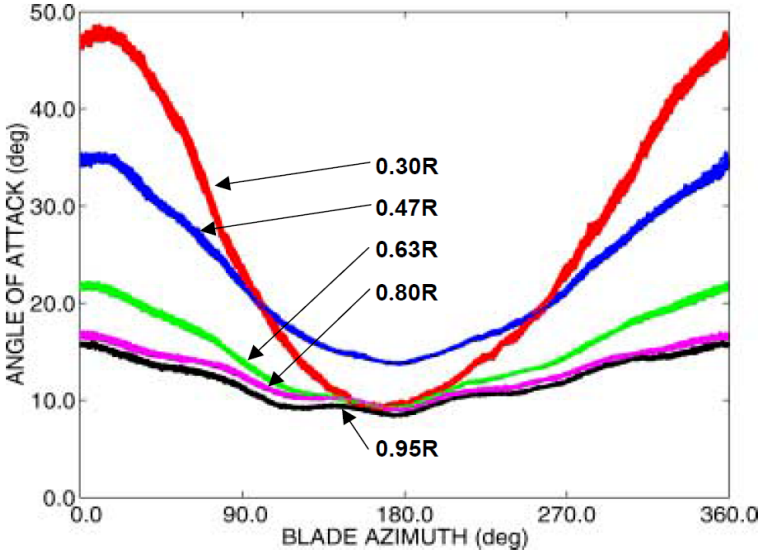

Fig. 7.5.2: Angle of attack versus Azimuth angle [87].

Other authors might model the wind gust as a sinusoidal change of the angle of attack (α) where it changes as a function of time, for example, α = 15 + 10 sin 6t as was given by references [28, 88] which is in agreement of the present author's assumption.

Consider the blade rotational speed V_{ti}, wind flow angle ϕ, blade relative speed V_{reli} as given in Eqns 7.5.1, 7.5.2 and 7.5.3 respectively.

$$V_{ti} = \Omega X_i \tag{7.5.1}$$

$$\phi = \text{atan}\,(\text{U}/V_{ti}) \tag{7.5.2}$$

$$V_{reli} = \left(U^2 + {V_{ti}}^2\right)^{0.5} \tag{7.5.3}$$

where ρ, Ω and U are defined as given in Table 7.5.2.

Air density ρ (rho) kg/m^3	1.25
rpm	43
Angular speed Ω (omega) = 2 π rpm/60	4.5029
Mean free stream wind speed U- m/s	25

Table 7.5.2: Wind properties.

By taking the values of β (twist angle) as given in Table 7.5.1, the given wind parameters as listed in Table 7.5.2, we can calculate the values V_{ti}, ϕ and V_{reli} using Eqns 7.5.1 , 7.5.2 and 7.5.3 and then we can calculate the angle of attack using, $\alpha = \phi - \beta$, at each of the given stations as shown in Table 7.5.3.

Station (m)	x-location (m)	Angular velocity omega 2*pi*rpm	Rotational speed Vti (m/s)	Flow angle (radian)	Wind relative velocity Vreli (m/s)	Angle of Attack (degree)
1	0	4.5029	0	1.5708	25	40
2	1	4.5029	4.5029	1.3926	25.4023	30.7895
3	2	4.5029	9.0059	1.225	26.5727	22.1892
4	3	4.5029	13.5088	1.0754	28.4164	14.6153
5	4	4.5029	18.0118	0.9465	30.8127	8.2283
6	5	4.5029	22.5147	0.8377	33.6439	2.9941
7	6	4.5029	27.0177	0.7466	36.8097	-1.2213
8	7	4.5029	31.5206	0.6705	40.2312	-4.581
9	8	4.5029	36.0236	0.6067	43.8486	-7.2398
10	9	4.5029	40.5265	0.5527	47.6172	-9.3304
11	10	4.5029	45.0295	0.5068	51.5039	-10.9613
12	11	4.5029	49.5324	0.4674	55.4839	-12.219
13	12	4.5029	54.0354	0.4333	59.5384	-13.1719
14	13	4.5029	58.5383	0.4036	63.6533	-13.8741
15	14	4.5029	63.0413	0.3775	67.8174	-14.3684

Table 7.5.3: Angle of Attack Values at All Considered Stations.

7.6 Calculation Procedure of the R -Load vector at Each Airfoil Station for every time step

At each airfoil station and due to the applied aerodynamic pressure, the following four components of loading can be calculated as shown in Fig. 3.6.1 and Fig. 7.6.1.1:

- ***Fx*** : centrifugal force acting on the x-direction or along the length of the blade.
- ***Fy*** : force acting on the y-direction of the blade.

- ***Fz*** : force acting on the z-direction of the blade.
- ***Mx*** : torsion around the x-axis, mainly due to the pitch moment plus moments due to ***Fy*** *and* ***Fz***

The moments My and Mz are found as a result of applying the above four components of loadings i.e. we don't have to calculate My and Mz.

- ***My*** is the bending moment acting in y-direction due to force ***Fz.***
- ***Mz*** is the bending moment acting in z-direction due to force ***Fy.***

Table 7.6.1.1 show the forces and moments calculated at each of the 15 stations using Eqns of section 3.6 for the given values of the angle of attacks that were computed earlier and listed in Table 7.5.3.

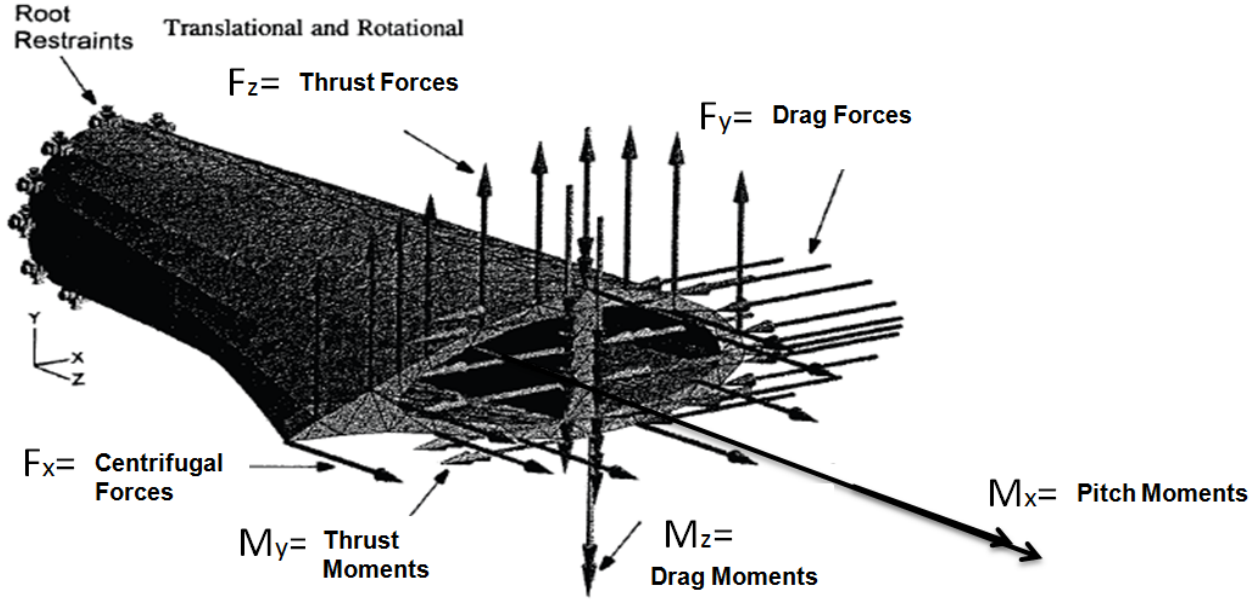

Fig. 7.6.1.1: Aerodynamic Forces and Moments [27].

Station # or location	Angle of Attack (degree)	Cl	Cd	Cm	L	D	Pitch Moment (Nm)	Fx (N)	Fy (N)	Fz (N)	Mx (Nm)
1 (at x=0)	40.0385	2.66	0.57	-0.665	563.2	120.6797	-76.3098	0	517.2	253.3	21.6703
2	30.8234	2.3376	0.5009	-0.5844	1383.1	296.371	-507.2511	2.1376	1154	817.5	-220.2619
3	22.2187	2.0366	0.4364	-0.5092	1259.3	269.851	-441.1045	3.8911	927.9	893.1	-602.671

4	14.6409	1.7715	0.3796	-0.4429	1193.7	255.7982	-398.4579	5.2877	760.3	955.2	-109.8173
5	8.2507	1.548	0.3317	-0.387	1165.9	249.8318	-369.9474	6.3544	634.2	1009.7	-84.6115
6	3.0139	1.3732	0.3	-0.3332	1169	255.3842	-341.3525	7.1184	537.1	1069.2	-58.5652
7	-1.2037	1.2608	0.3	-0.263	1214.4	288.9575	-288.0977	7.6067	455.3	1162.3	-0.9592
8	-4.565	1.1712	0.3	-0.207	1269.4	325.1634	-240.3757	7.8466	384.2	1252.8	48.3634
9	-7.2252	1.1003	0.3	-0.1627	1329.5	362.4979	-197.6454	7.8651	321.9	1339.9	89.7716
10	-9.3169	1.0445	0.3	-0.1278	1390.8	399.4572	-159.9229	7.6892	267.3	1422.1	123.0573
11	-10.949	1.001	0.3	-0.1006	1450	434.5373	-127.3623	7.3462	220	1497.6	147.8931
12	-12.207	1.0244	0.2732	-0.0927	1592	424.5552	-116.3497	6.8631	253.5	1628	159.6402
13	-13.16	1.0434	0.2522	-0.087	1714.9	414.5148	-106.0269	6.267	283.3	1741.4	164.2314
14	-13.863	1.0575	0.2368	-0.0828	1809.9	405.2416	-95.7305	5.585	306.3	1829.3	161.8792
15 (at x=L)	-14.358	1.0674	0.2259	-0.0798	1871.4	396.0582	-85.3276	4.8443	321.7	1885.6	153.0529

Table 7.6.1.1: Aerodynamic forces and moments at different stations in and about x,y and z directions.

This will enable us to calculate all the interpolated force functions that represent all the station forces $F_x(x)$, $F_y(x)$ and $F_z(x)$ and to calculate all the interpolated moment function of all the station moments $M_x(x)$ as a function of x (the coordinate along the blade length) using the MATLAB code of the present research.

The aerodynamic load vector R^t (i.e. the right side of the dynamic equations of motion) can be computed using the following Eqn 7.6.1.

$$R\_load\ (time) = R^t = \begin{bmatrix} \int_0^L F_x(x)\phi_m(x)dx \\ \int_0^L F_y(x)\phi_m(x)dx \\ \int_0^L F_z(x)\phi_m(x)dx \\ \int_0^L M_y(x)\phi_m(x)dx \\ \int_0^L M_z(x)\phi_m(x)dx \\ \int_0^L M_x(x)\phi_m(x)dx \end{bmatrix} = \begin{bmatrix} \int_0^L F_x(x)\phi_1(x)dx \\ \int_0^L F_x(x)\phi_2(x)dx \\ \int_0^L F_y(x)\phi_1(x)dx \\ \int_0^L F_y(x)\phi_2(x)dx \\ \int_0^L F_z(x)\phi_1(x)dx \\ \int_0^L F_z(x)\phi_2(x)dx \\ \int_0^L M_y(x)\phi_1(x)dx \\ \int_0^L M_y(x)\phi_2(x)dx \\ \int_0^L M_z(x)\phi_1(x)dx \\ \int_0^L M_z(x)\phi_2(x)dx \\ \int_0^L M_x(x)\phi_1(x)dx \\ \int_0^L M_x(x)\phi_2(x)dx \end{bmatrix} \qquad (7.6.1)$$

Specifying , for example, that m= 1 to M=2, implies that $\phi_1(x) = (x/L)^2$ and $\phi_2(x) = (x/L)^3$ since the given polynomial expansion is $\phi_m(x) = (x/L)^{m+1}$ as was discussed in section 3.5.

It should be noted that all the above steps of the calculation of the load vector R^t have to be repeated for each of the given time steps since R^t is a function of the angle of attack (which is function of the given time steps) at the given blade stations.

Chapter 8
Implementation and Numerical Results

8.1 Introduction

Consider that the present blade for both examples of the next two sections 8.2.1 and 8.2.2 share the following assumptions:

- The blade has a 14 m length and a Young's modulus of 17 GPa.
- The blade is clamped at one end (cantilever) and submitted to non-uniformly distributed aerodynamic forces (described above), to centrifugal forces and gravitational forces moving with an angular velocity Ω of 4.5029 rad/s.
- Wind turbine rotor is in upwind configuration.
- The blade airfoil section is of NACA4415 type and is wise-piece variable along the radius.
- The nacelle is adjustable with a yaw angle that varies so as to always align the wind velocity normal to the rotation plan of the blade, so that the yaw error can be neglected.
- The connection between the blade and the hub is rigid.
- The deformation is large.
- The analysis of the blade's response concerns the study of the behavior of the blade submitted to a gust of wind of 25 m/s speed during 3 s. The direction of the gust is considered parallel to the axis of the hub (rotor).
- The wind's attack angle to the blade varies as a function of time, according to $\alpha = 15 + 10 \sin 6t$. This assumption means that the variation of the gust excitation is modeled by the variation of the attack angle.

It should be noted that the blade share the same geometry of NACA4415 as the blade for the linear case example (section 8.2.1) that was studied by Younsi et al. [28].

But for the nonlinear example case (section 8.2.2), the blade is different from that given by Younsi et al. [28] by the following differences:

- The nonlinear blade example has a pretwisted geometry as mentioned above.
- The nonlinear blade example has a lower material density.
- The nonlinear blade example considers the large deformation case while Younsi et al. [28] considered only the small deformation case.

8.2 Numerical Application and Results

8.2.1 Linear Small Deformation Case Example

Consider an untwisted 14 m length blade of a Young's modulus of 17 GPa and a material density of 600 Kg/m^3, as listed in the below Table 8.2.1.1, that behave in a linear small deformation.

Blade Length	Air Density	Young's Modulus	Blade Density	Blade Airfoil Type	Wind Speed	Rated Power & Rated Speed
14 m untwisted	1.25 Kg/m^3	17 GPa	500 Kg/m^3	NACA-4415	25 m/s	150 KW & 9.5m/s

Table 8.2.1.1: Blade properties for the linear example.

It should be noted again that we are considering the same problem that was solved by Younsi et al. [28] so that we can compare our solution by their solution. The application concerns the study of the behavior of the blade submitted to a gust of wind of 25 m/s speed during 3 seconds. Fig. 8.2.1.1 shows the main dimensions of the blade, the line of the centers of gravity as well as the line of aerodynamic centers.

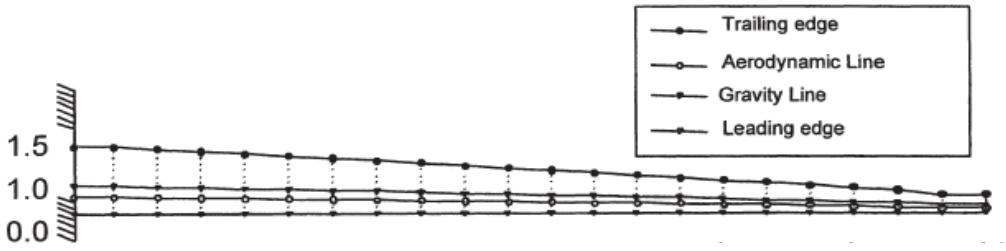

Fig. 8.2.1.1: Blade geometry and neutral axis line as given by Younsi et al. [28]

The aerodynamic forces Fx, Fy and Fz and the aerodynamic moments Mx, My and Mz were calculated at all the given 15 stations (or nodes) using the formulas listed in section 3.6 and section 7.6 and input to the Ls-Dyna model using Hypermesh as shown in Fig. 8.2.1.2.

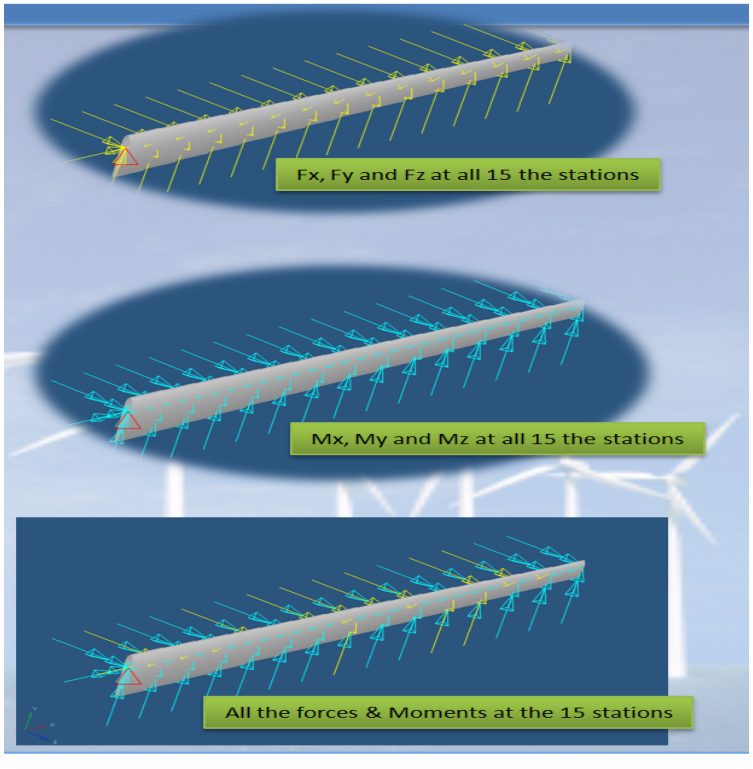

Fig. 8.2.1.2: Forces and Moments at all the given 15 Stations.

While for the MATLAB code (present research code), all these aerodynamic forces and moments were interpolated to have them as function of x (the coordinate along the length of the blade) and this process have to be repeated for each of the given time steps in order to obtain the R-load vector per Eqn 7.6.1 (as was explained in section 7.6). By having all the derived linear mass, dynamic and stiffness matrices (that derived in section 5.2) and the

calculated R-load vector at each time step, the author was able to solve the dynamic equation of motion(Eqn 6.1.1a) using the MATLAB code and the linear Newmark iteration scheme (that was explained in section 6.4) for the vibration response at all the given blade stations. Below in Fig. 8.2.1.2, the displacements and rotations at the blade's tip are shown:

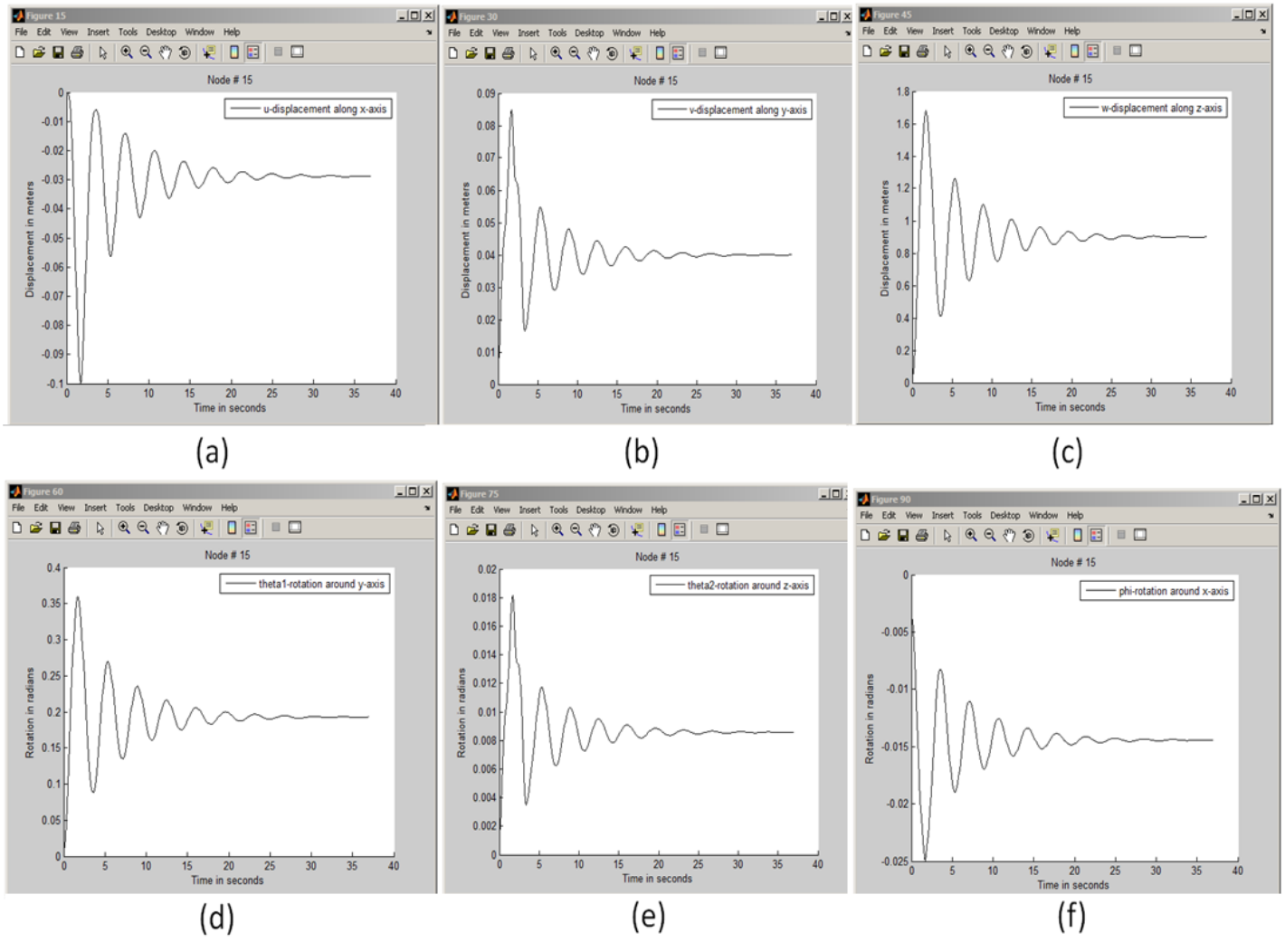

Fig. 8.2.1.2: Blade tip linear displacements and rotations.
(a) Displacement in x-direction; (b) Displacement in y-direction;
(c) Displacement in z-direction; (d) Rotation about y-direction;
(e) Rotation about z-direction; and (f) Rotation about x-direction

Fig. 8.2.1.3 shows a two-plot comparison of the blade's tip displacement in the vertical flapwise direction between the present work and that of Younsi et al. [28] for the same blade problem. In Fig. 8.2.1.3 (a), the peak and stabilized displacements are 1.75m and 1.021 m

respectively while the peak and stabilized displacements values in Fig. 8.2.1.3 (b) are 1.68 m and 0.92 m. We observe that both plots have the same kind of trend but the current study has lower peak and steady state displacements. Current work not only shows an agreement with the hypothesis of the linearity of the solution introduced by Younsi et al. but also has lower displacement values. This is due to the fact of the inclusion of all the loadings and their couplings and the blade's cross-sectional warping. Note that the vertical direction is along the z-axis in this work while it is along the y-axis in the work of Younsi et al. [28] .

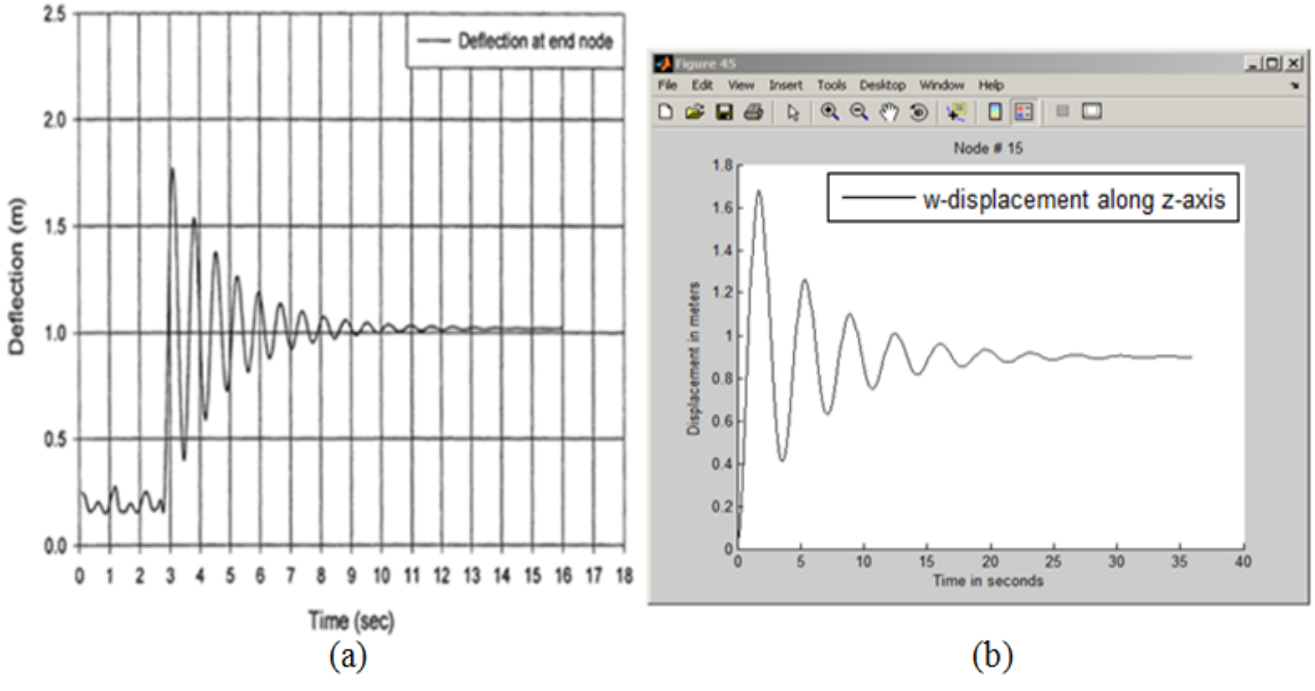

Fig. 8.2.1.3: Comparison of (a) Younsi et el. published work [28].
(b) present work.

8.2.2 Non-linear Large Deformation Case Example

Consider a pretwisted 14 m length blade of a Young's modulus of 17 GPa and a material density of 500 Kg/m^3, as listed in the below Table 8.2.2.1, that behave in a nonlinear large deformation.

Blade Length	Air Density	Young's Modulus	Blade Density	Blade Airfoil Type	Wind Speed	Rated Power & Rated Speed
14 m pretwisted	1.25 Kg/m^3	17 GPa	500 Kg/m^3	NACA-4415	25 m/s	150 KW & 9.5m/s

Table 8.2.2.1: Blade properties for the non-linear example.

The present blade is modeled as a combination of 14 beams (each of 1m length) separated by 15 main nodes or stations. The pre-twist angles for these 15 stations as going from the hub to the tip of the blade are respectively equal to 14,13,12,11,10,9,8,7,6,5,4,3,2,1 and 0.

It should be noted that the pretwist of the present blade change the values of the geometrical properties at each of the given blade stations from those calculated by Younsi et al. [28].

The aerodynamic forces and moments were calculated and then interpolated as a function of the lengthwise x of the blade using the same method of the linear example of previous section 8.2.1. By having all the linear mass, dynamic and stiffness matrices (that derived in section 5.2) and the nonlinear stiffness matrices (that derived in section 5.3) and the calculated R-load vector at each time step, the author was able to solve the nonlinear dynamic equation of motion (6.1.1b) using the MATLAB code and the nonlinear Newmark iteration scheme (that was explained in section 6.6) for the vibration response at all the given blade stations. The displacements and rotations were computed at all the 15 blade stations. (where node# 15 as mentioned earlier is the location of the blade's tip).

The obtained solution was compared by the the same blade's response solution using the ls-Dyna code that was built using the same blade's material and geometrical properties with the same applied loading across the blade that considered for the Matlab code.

Fig. 8.2.2.1, Fig. 8.2.2.2 and Fig. 8.2.2.3 show the displacements at the blade's in x, y and z-directions respectively, using the current study Matlab code and the ls-dyna code. And Fig. 8.2.2.4, Fig. 8.2.2.5 and Fig. 8.2.2.6 show the rotational displacement at the blade's tip about the x, y and z directions respectively, using the Matlab code and the ls-Dyna code.

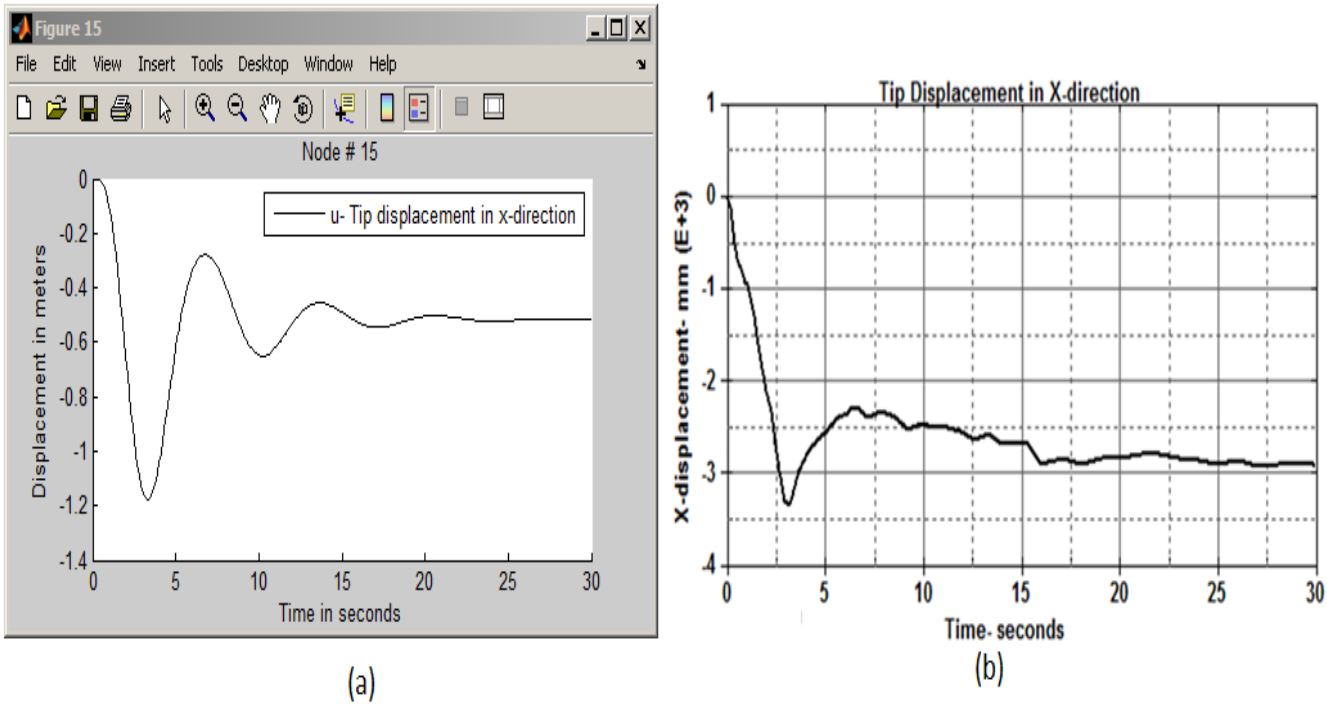

Fig. 8.2.2.1: Nonlinear plots comparison for tip displacement in x-direction.
(a) Displacement in x-direction using present work;
(b) Displacement in x-direction using Ls-Dyna.

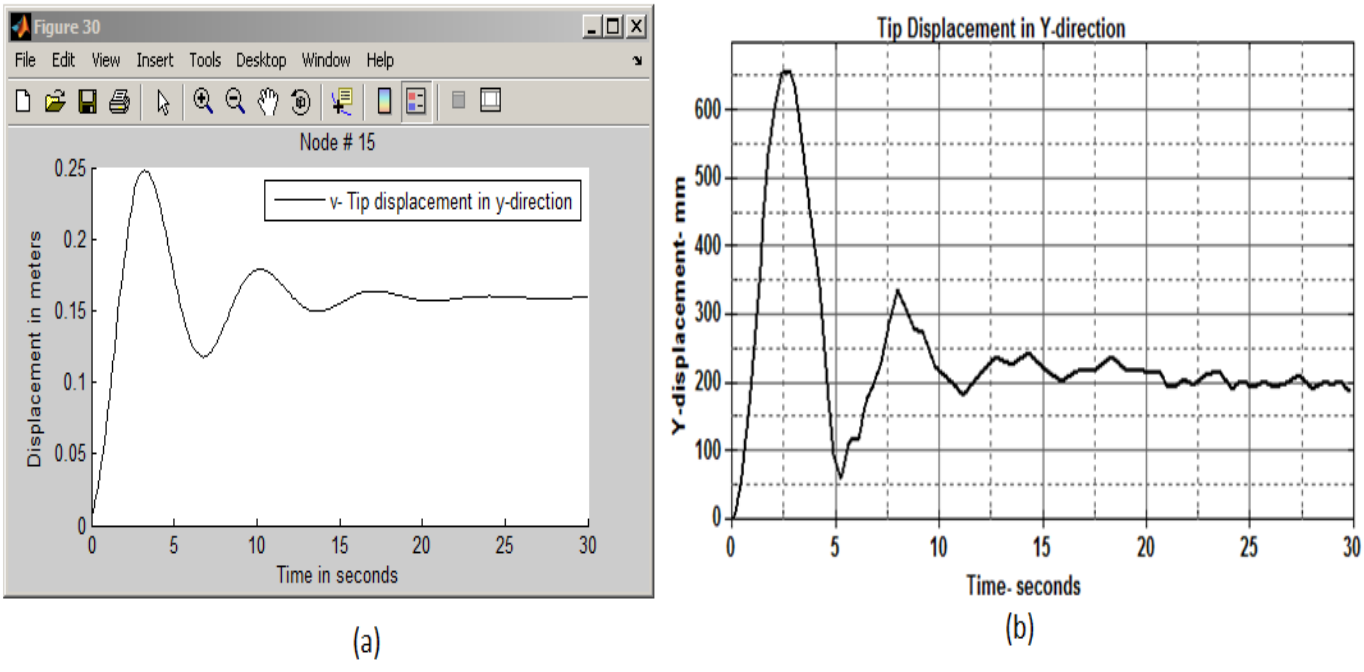

Fig. 8.2.2.2: Nonlinear plots comparison for tip displacement in y-direction.
(a) Displacement in y-direction using present work;
(b) Displacement in y-direction using Ls-Dyna.

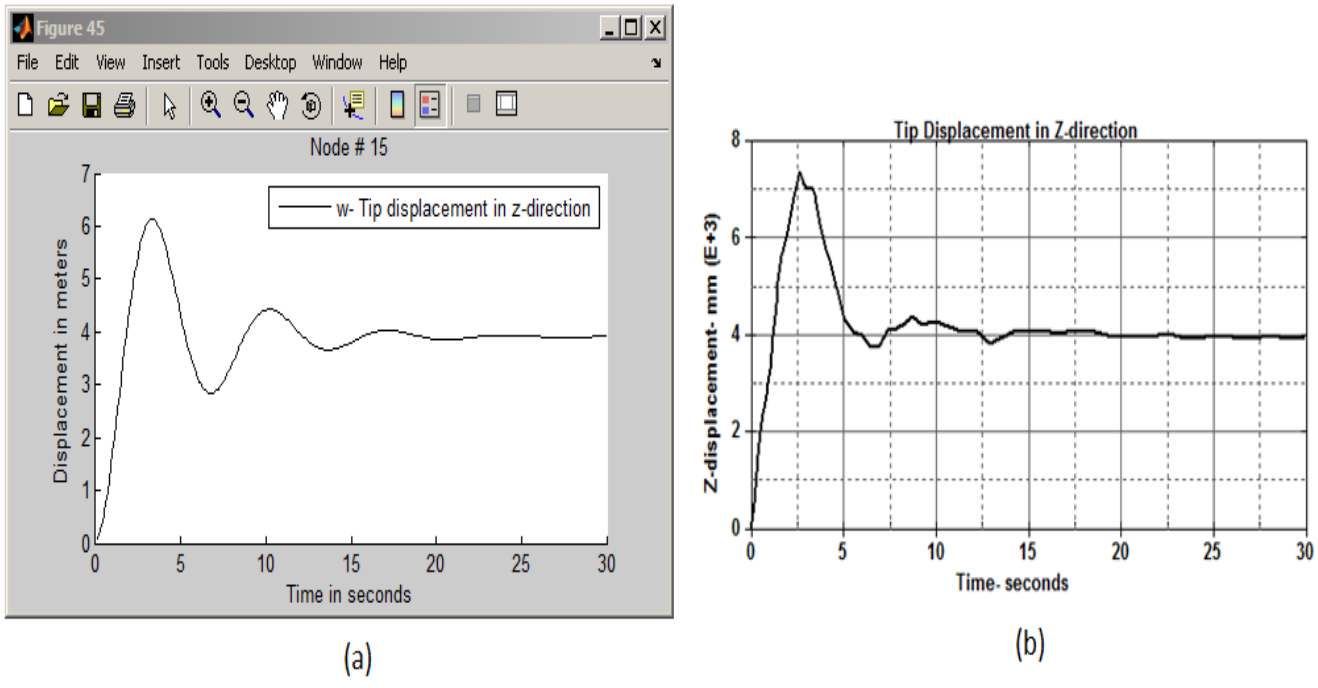

Fig. 8.2.2.3: Nonlinear plots comparison for tip displacement in z-direction.
(a) Displacement in z-direction using present work;
(b) Displacement in z-direction using Ls-Dyna.

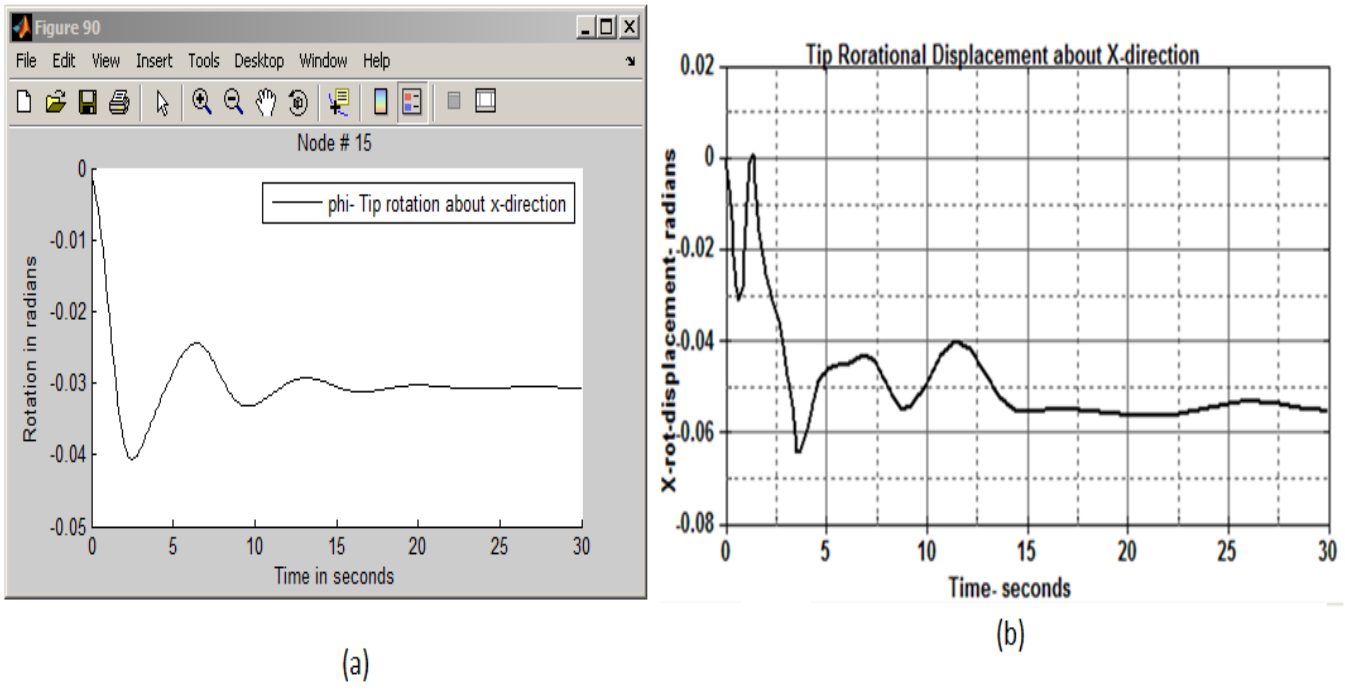

Fig. 8.2.2.4: Nonlinear plots comparison for tip rot. displ. about x-direction.
(a) Rotational displacement about x-direction using present work;
(b) Rotational displacement about x-direction using Ls-Dyna.

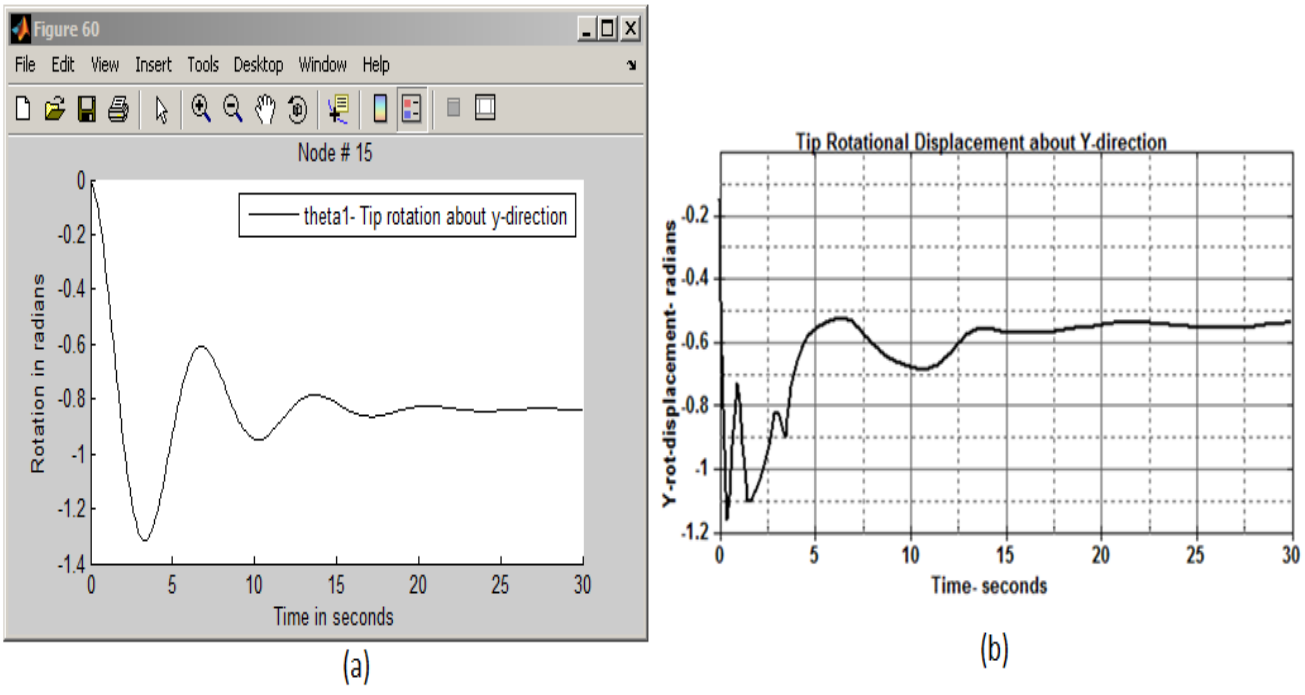

Fig. 8.2.2.5: Nonlinear plots comparison for tip rot. displ. about y-direction.
(a) Rotational displacement about y-direction using present work;
(b) Rotational displacement about y-direction using Ls-Dyna.

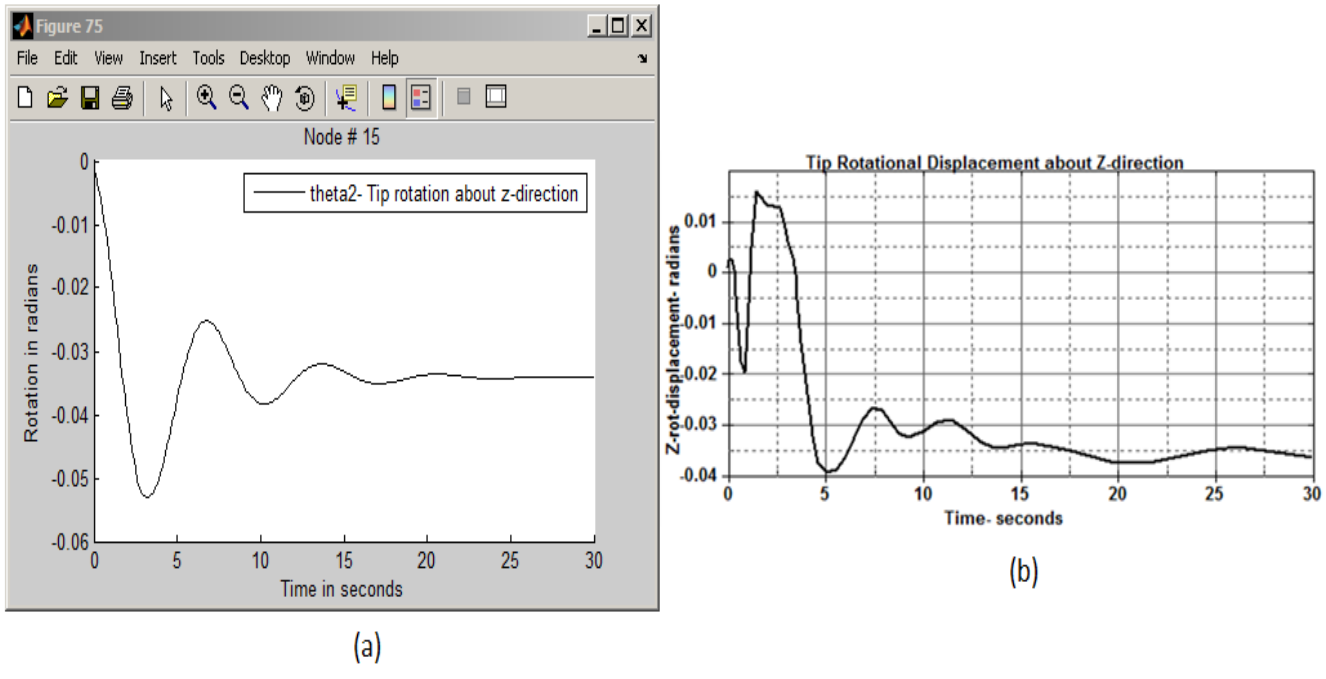

Fig. 8.2.2.6: Nonlinear plots comparison for tip rot. displ. about z-direction.
(a) Rotational displacement about z-direction using present work;
(b) Rotational displacement about z-direction using Ls-Dyna.

Chapter 9
Conclusion and Related Future Work

9.1 Conclusion

For the linear example case, the present study plot of the displacement in the vertical direction at the blade's tip agrees agrees as far as trend with the plot of the same displacement that were given by Younsi et al. study [28] even that both plots has different peak values. The advantage of the present study method on Younsi et al. study [28] is the accuracy of the obtained displacements and rotations solution due to the inclusion of the cross-sectional warping of the blade and the consideration of all the aerodynamic loads and all the possible load couplings that acting on the blade. The other advantage is the capability of the present research method of solving the displacements and rotations for any pretwisted blade while Younsi et al. [28] study was limited to the untwisted blade case. It is observed that there is a delay of about 3 seconds before the rapid increase in deflection in Fig. 8.2.1.3 (a) compared to Fig. 8.2.1.3 (b). This delay is due to the additional aerodynamic interactions that caused by the CFD code by which Younsi et al. study [28] performed the aerodynamic load prediction.

For the nonlinear example case, the nonlinear large deformation mathematical model for the present 14 m pretwisted wind turbine blade lead to have a set of higher order terms that contribute to the formation of two additional non-linear stiffness matrices.

We observe in Fig. 8.2.2.3 (a) and Fig. 8.2.2.3 (b) that the steady state blade's tip nonlinear displacement in the vertical z-direction for both codes (the present study Matlab code and the Ls-Dyna code), is about 4m which is about 28% of the 14 m (length of the blade). This is in agreement with the hypothesis introduced by Younsi et al. [28] that displacement is considered to be nonlinear if exceeds 10% of the length of the blade.

We also observe that even we have a similar trend of all the displacement and rotation plots for both codes solutions as shown in Fig. 8.2.2.1 to Fig. 8.2.2.6, the peak and/or the steady state values are vary in many of these plots. For example, in Fig. 8.2.2.3 (a), the peak displacement using the present study Matlab code is 6.2 m while in Fig. 8.2.2.3 (b), the peak displacement using the ls-dyna is 7.3 m. This variation is normal and it is due to the inclusion of the following additional factors in the author's present research mathematical model (Matlab code) that are not included in the Ls-Dyna code:

- The additional aerodynamic load couplings.
- The two additional nonlinear stiffness matrices of the dynamic equations of motion due to the nonlinear large deformation assumption.

The following are number of contributions for the present research:

- A new simple method that based on the airfoil wind tunnel aerodynamic parameters collected data (not based on CFD or the Bezier interpolation scheme) to calculate the R load vector.
- The mathematical formulation of this present research is capable of generating the displacements, velocities and acceleration at any point on the blade for small or large displacement for any duration of the aerodynamic loadings (for example, it can run for days) while Ls-dyna and similar current commercial softwares has a limited input data storage and the aerodynamic load data has to be entered manually.
- The present research MATLAB code is the only current code the is able to update the angle of attack by the value of the twisting rotation phi about the x-axis (along the length of the blade).
- calculation of the geometrical properties of any given blade airfoil profiles using a new created macro to be used within Hypermesh.

- The inclusion of warping and all the possible aerodynamic loadings and their couplings beside the rotary inertia, shear deflection.
- No need to send my files to the Grid or to Gigastar in order to solve as happening in case of current dynamic codes.

9.2 Related Future Work

My plan is to extend the present wind turbine blade research to include the following improvement to my present research MATLAB code:

- Add the capability to solve blades with plastic and composite materials.
- Improve the code to be able to compute the natural frequencies and plot the mode shapes for any given blade inputs.
- To be able to identify the rpm(s) of the blade that the blade designer need to avoid in order to avoid any possible excitation of the blade natural frequency.

APPENDIX A: DERIVATION OF THE DIFFERENT STRAIN ENERGIES

A. 1. Axial-Torsional Strain Energy Including Warping Effect

Two common assumptions are made for the coupled extension-torsion problem: first, that deformation parallel to the cross-sections is negligible, and second, that axial deformation consists of bulk displacement $\bar{u}$ and cross sectional warping.

Airfoil warping in wind turbine blade application is assumed to be constant throughout the cross section (or station) and vary in value between the different stations i.e. $\psi(x,y,z) = \psi(x)$ only.

To derive the axial-torsional strain energy for the pre-twisted Timoshenko beam of Fig. 3, we have to start with the Green's strain-displacement relation in order to express the strain energy in terms of large displacement fields [22]:

$$\varepsilon_{ij} = \left(\frac{\partial u_j}{\partial x_i} + \frac{\partial u_i}{\partial x_j} + \frac{\partial u_\alpha}{\partial x_i}\frac{\partial u_\alpha}{\partial x_j} \right)$$

This implies that the resulting strain components are:

$$\varepsilon_{xx} = \frac{\partial u}{\partial x} + \frac{1}{2}\left[\left(\frac{\partial u}{\partial x}\right)^2 + r^2\theta^2 \right] \quad \text{where}$$

$$\text{but } \frac{\partial u}{\partial x} = \overline{\varepsilon_{xx}} + \theta\frac{\partial \psi}{\partial x} + \frac{\partial \theta}{\partial x}\psi \quad \text{where } \overline{\varepsilon_{xx}} = \frac{\partial \bar{u}}{\partial x}, \quad \theta = \frac{\partial \phi}{\partial x} \text{ and } r^2 = y_1^2 + z_1^2$$

where ϕ, as stated earlier, is the angle of elastic rotation additional to the pre-twist angle β.

This implies that:

$$\frac{\partial u}{\partial x} = \frac{\partial \bar{u}}{\partial x} + \theta\frac{\partial \psi}{\partial x} + \frac{\partial \theta}{\partial x}\psi$$

Substituting for $\frac{\partial u}{\partial x}$ in $\varepsilon_{xx}, \varepsilon_{xy}$ and ε_{xz}

$$\varepsilon_{xx} = \frac{\partial \bar{u}}{\partial x} + \theta\frac{\partial \psi}{\partial x} + \frac{\partial \theta}{\partial x}\psi + \frac{1}{2}\left[\left(\frac{\partial \bar{u}}{\partial x}\right)^2 + r^2\theta^2 \right]$$

It should be noted that keeping the following high order terms:

$$\frac{1}{2}[(\frac{\partial \bar{u}}{\partial x})^2 + r^2\theta^2]$$

in the below derivation is an important contribution of the present work.

Expanding, implies:

$$\varepsilon_{xx} = \frac{\partial \bar{u}}{\partial x} + \theta\frac{\partial \psi}{\partial x} + \frac{\partial \theta}{\partial x}\psi + \frac{1}{2}(\frac{\partial \bar{u}}{\partial x})^2 + \frac{1}{2}(\theta\frac{\partial \psi}{\partial x})^2 + \frac{\partial \bar{u}}{\partial x}\theta\frac{\partial \psi}{\partial x} + \frac{1}{2}(\frac{\partial \theta}{\partial x}\psi)^2 + \frac{\partial \bar{u}}{\partial x}\frac{\partial \theta}{\partial x}\psi$$

$$+ \theta\frac{\partial \psi}{\partial x}\frac{\partial \theta}{\partial x}\psi + \frac{1}{2}r^2\theta^2$$

Since warping is a function of x only implies: $\frac{\partial \psi}{\partial y} = \frac{\partial \psi}{\partial z} = 0$, which implies,

$$\varepsilon_{xy} = \frac{1}{2}\theta[\frac{\partial \psi}{\partial y}(1 + \frac{\partial u}{\partial x}) - z_1] = \frac{1}{2}\theta[-z_1]$$

$$\varepsilon_{xz} = \frac{1}{2}\theta[\frac{\partial \psi}{\partial z}(1 + \frac{\partial u}{\partial x}) + y_1] = \frac{1}{2}\theta[y_1]$$

$$\varepsilon_{yy} = \frac{1}{2}\theta^2[\frac{\partial \psi}{\partial y}]^2 = 0,\ \varepsilon_{yz} = \frac{1}{2}\theta^2[\frac{\partial \psi}{\partial y}\frac{\partial \psi}{\partial z}] = 0 \text{ and } \varepsilon_{zz} = \frac{1}{2}\theta^2[\frac{\partial \psi}{\partial z}]^2 = 0$$

The result is the axial-torsional strain energy which is in agreement with [22, 36]:

$$U_{axial-torsional} = \int_0^L \iint_A dydz\{\frac{1}{2}E\varepsilon_{xx}^2 + 2G(\varepsilon_{xy}^2 + \varepsilon_{xz}^2)\}dx + \int_0^L \frac{1}{2}EI_p\phi''^2 dx \qquad \text{(A.1)}$$

A. 2. Bending-Bending-Shear Coupling Strain Energy

The strain energy due the blade's bending about the y and z directions and their couplings

including the effect of deflection due to transverse shear in two planes i.e. the case of Timoshenko beam [18, 21, 40] is:

$$U_{bending-shear} = \frac{1}{2}\int_0^L \left\{ E\left(I_{yy}\,\theta_1'^2 + 2\,I_{yz}\,\theta_1'\,\theta_2' + I_{zz}\,\theta_2'^2\right) + kGA\left((w'-\theta_1)^2 + (v'-\theta_2)^2\right) \right\} dx \qquad \text{(A.2)}$$

where,

$(')$: means derivative w.r.t. x

k : is the shear correction factor

kGA : is the shear rigidity

I_{yy}, I_{zz} : are the second moment of area of the cross-section through the centroid about the y_1 y_1 and z_1 z_1 axes respectively as shown in Fig. 3.2.1.

I_{yz} : is the product moment of area of the cross-section about the y_1 y_1 and z_1 z_1 axes as shown in Fig. 3.2.1.

A. 3. Bending-Torsional Coupling Strain Energy

The blade structure will undergo torsional deformation as it flexes because of its asymmetrical airfoil cross-section where the shear centres axis and the centroid centres axis are not coincident [21, 39] :

$$U_{bending-torsion} = \frac{1}{2}\int_0^L P\,\left[\,v'^2 - 2\,y_\alpha\,v'\,\phi' + (I_p/A)\,\phi'^2\,\right] dx + \frac{1}{2}\int_0^L P\,\left[\,w'^2 - 2\,z_\alpha\,w'\,\phi' + (I_p/A)\,\phi'^2\,\right] dx$$
$$+ \frac{1}{2}E\int_0^L \frac{1}{4}Aw'^4\,dx + \frac{1}{2}E\int_0^L \frac{1}{2}I_p w'^2\,\phi'^2\,dx + \int_0^L \left[\,K_1\,\theta_1'\,\phi' + K_2\,\theta_2'\,\phi'\,\right] dx \qquad \text{(A.3)}$$

where P is the axial force.

Appendix B: DERIVATION OF THE DIFFERENT KINETIC ENERGIES

B. 1. Kinetic Energy due to Axial-Torsional Effect

To express the axial-torsional kinetic energy in terms of the displacement field, the velocity vector $\dot{R}$ of each point in the beam is given by:

$$\dot{R} = \dot{u} = (\dot{u})\hat{e}_x + (\dot{v})\hat{e}_y + (\dot{w})\hat{e}_z$$

$$= (\dot{\bar{u}} + \dot{\theta}\psi)\hat{e}_x + \dot{\phi}(-y\sin\phi - z\cos\phi)\hat{e}_y + \dot{\phi}(y\cos\phi - z\sin\phi)\hat{e}_z$$

$$= (\dot{\bar{u}} + \dot{\theta}\psi)\hat{e}_x + r\dot{\phi}\left[-(\sin\phi)\hat{e}_r + (\cos\phi)\hat{e}_\phi \right] \qquad \text{(B.1)}$$

where $\theta = \dfrac{\partial\phi}{\partial x}$ and dot means derivative w.r.t. time.

The cartesian unit vectors ($\hat{e}_y$, $\hat{e}_z$) are transformed to cylindrical unit vectors ($\hat{e}_r$, $\hat{e}_\phi$) ,

where $\hat{e}_r = \dfrac{1}{r}(y\hat{e}_y + z\hat{e}_z)$ and $\hat{e}_\phi = \dfrac{1}{r}(-z\hat{e}_y + y\hat{e}_z)$.

The kinetic energy due to axial torsional coupling effects is given by

$$T_1 = \iiint_V \frac{1}{2}\rho\left|\dot{R}\right|^2 dV \qquad \text{(B. 1.1)}$$

Substituting of $\dot{R}$ from Eq. (B. 1) into Eq. (B.1.1) results in the following equation [22] :

$$T_1 = \iiint_V \frac{1}{2}\rho(x)\left[\dot{\bar{u}}^2 + 2\dot{\bar{u}}\,\dot{\theta}\psi + \dot{\theta}^2\psi^2 + r^2\dot{\phi}^2 \right] dV$$

where, $r^2 = y_1^2 + z_1^2$, which implies,

$$T_1 = \frac{1}{2}\int_0^L \rho(x)\left[\dot{\bar{u}}^2 A(x) + 2\dot{\bar{u}}\left(\frac{\partial\dot{\phi}}{\partial x}\right)\psi A(x) + \left(\frac{\partial\dot{\phi}}{\partial x}\right)^2\psi^2 A(x) + I_p(x)\dot{\phi}^2 \right]dx \qquad \text{(B.1.2)}$$

B. 2. Kinetic Energy due to Bending-Torsion including Centrifugal Effect

The kinetic energy due to bending-bending-torsional coupling including centrifugal effect by keeping the important higher order terms up to 4th order is [18, 21, 24, 89] :

$$T_2 = \frac{1}{2}\int_0^L \rho(x)\{\ \overline{\Omega}^2 z^2 A(x)\theta_2^{\ 2} - \overline{\Omega}^2 y^2 A(x)\phi^2 - \overline{\Omega}^2 z^2 A(x)\theta_2^{\ 2}\phi^2 + \frac{1}{4}\overline{\Omega}^2 y^2 A(x)\phi^4 + \overline{\Omega}^2 A(x)\overline{u}^2$$

$$+ 2\overline{\Omega}^2 y^2 A(x)\phi\dot{\theta}_2 - 2\overline{\Omega} z^2 A(x)\phi\dot{\theta}_2 + \overline{\Omega} z^2 A(x)\phi^3\dot{\theta}_2 + z^2 A(x)\dot{\theta}_2^{\ 2} - z^2 A(x)\phi^2\dot{\theta}_2^{\ 2} + 2\overline{\Omega} y^2 A(x)\theta_2\dot{\phi}$$

$$+ 2\overline{\Omega} z^2 A(x)\theta_2\dot{\phi} - \overline{\Omega} y^2 A(x)\theta_2\phi^2\dot{\phi} - \overline{\Omega} z^2 A(x)\theta_2\phi^2\dot{\phi} + 2y^2 A(x)\theta_2\phi\dot{\theta}_2\dot{\phi} - 2z^2 A(x)\theta_2\phi\dot{\theta}_2\dot{\phi} + y^2 A(x)$$

$$\dot{\phi}^2 + z^2 A(x)\dot{\phi}^2 + y^2 A(x)\theta_2^{\ 2}\dot{\phi}^2\ \}dx + \frac{1}{2}\int_0^L m(x)[\ (\dot{v} + z_\alpha\dot{\phi})^2 + (\dot{w} + y_\alpha\dot{\phi})^2\ ]dx + \frac{1}{2}\int_0^L \{\ \rho(x)I_{zz}$$

$$(\dot{\theta}_2 + z_\alpha\dot{\phi}')^2 + \rho(x)I_{yy}(\dot{\theta}_1 + y_\alpha\dot{\phi}')^2\ \}dx - \frac{\Omega^2}{2}\int_0^L m(x)[\ (v' + z_\alpha\phi')^2 + (w' + y_\alpha\phi')^2\ ]xdx \qquad \text{(B.2)}$$

where $\overline{\Omega}$ and Ω is the rotational speed and the angular velocity of the blade respectively.

B. 3. Kinetic Energy due to Rotary Inertia Effect

The kinetic energy due to rotary inertia effect as given by Carnegie [18] is:

$$T_3 = \frac{1}{2}\int_0^L \left[\ \frac{I_{zz}\rho(x)(\theta_2 + z_\alpha\dot{\phi}' + z_\alpha'\dot{\phi})^2}{g} + \frac{I_{yy}\rho(x)(\theta_1 + y_\alpha\dot{\phi}' + y_\alpha'\dot{\phi})^2}{g}\ \right] dx \qquad \text{(B.3)}$$

APPENDIX C: DERIVATION OF $\frac{\partial U_{Total}}{\partial q_m}$

Considering the total strain energy Eq. (2) shown in section 2.1, implies:

$$\frac{\partial U_{Total}}{\partial a_m} = E\int_0^L \iint_A \varepsilon_{xx}\frac{\partial \varepsilon_{xx}}{\partial a_m}dydzdx + 4G\int_0^L \iint_A \varepsilon_{xy}\frac{\partial \varepsilon_{xy}}{\partial a_m}dydzdx + 4G\int_0^L \iint_A \varepsilon_{xz}\frac{\partial \varepsilon_{xz}}{\partial a_m}dydzdx$$

Substituting for,

$$\frac{\partial \varepsilon_{xx}}{\partial a_m} = (\phi_{mx} + \frac{\partial \bar{u}}{\partial x}\phi_{mx} + \theta\frac{\partial \psi}{\partial x}\phi_{mx} + \frac{\partial \theta}{\partial x}\psi\,\phi_{mx}),\ \frac{\partial \varepsilon_{xy}}{\partial a_m} = \frac{1}{2}\theta\frac{\partial \psi}{\partial y}\phi_{mx} = 0 \text{ and } \frac{\partial \varepsilon_{xz}}{\partial a_m} = \frac{1}{2}\theta\frac{\partial \psi}{\partial z}\phi_{mx} = 0,$$

implies,

$$\frac{\partial U_{Total}}{\partial a_m} = E\int_0^L \iint_A [\ \frac{\partial \bar{u}}{\partial x} + \theta\frac{\partial \psi}{\partial x} + \frac{\partial \theta}{\partial x}\psi + \frac{1}{2}(\frac{\partial \bar{u}}{\partial x})^2 + \frac{1}{2}(\theta\frac{\partial \psi}{\partial x})^2 + \frac{\partial \bar{u}}{\partial x}\theta\frac{\partial \psi}{\partial x} + \frac{1}{2}$$

$$(\frac{\partial \theta}{\partial x}\psi)^2 + \theta\frac{\partial \psi}{\partial x}\frac{\partial \theta}{\partial x}\psi + \frac{\partial \bar{u}}{\partial x}\frac{\partial \theta}{\partial x}\psi + \frac{1}{2}r^2\theta^2\ ](\phi_{mx} + \frac{\partial \bar{u}}{\partial x}\phi_{mx} + \theta\frac{\partial \psi}{\partial x}\phi_{mx} + \frac{\partial \theta}{\partial x}\psi$$

$$\phi_{mx})\ dydzdx + 4G\int_0^L \iint_A \frac{1}{2}\theta\,[\frac{\partial \psi}{\partial y}(1 + (\frac{\partial \bar{u}}{\partial x} + \theta\frac{\partial \psi}{\partial x} + \frac{\partial \theta}{\partial x}\psi)) - z_1]\ 0dydzdx$$

$$+ 4G\int_0^L \iint_A \frac{1}{2}\theta\,[\frac{\partial \psi}{\partial z}(1 + (\frac{\partial \bar{u}}{\partial x} + \theta\frac{\partial \psi}{\partial x} + \frac{\partial \theta}{\partial x}\psi)) + y_1]\ 0dydzdx$$

Expanding and substituting the associated values of D's that listed in TABLE A, results in:

$$\frac{\partial U_{Total}}{\partial a_m} = E\ [\ \int_0^L \frac{\partial \bar{u}}{\partial x}\phi_{mx}\,A(x)\,dx + \int_0^L \theta\phi_{mx}\,D_5(x)\,dx + \int_0^L \frac{\partial \theta}{\partial x}\phi_{mx}\,D_1(x)\,dx + \frac{1}{2}\int_0^L (\frac{\partial \bar{u}}{\partial x})^2\phi_{mx}$$

$$A(x)\,dx + \frac{1}{2}\int_0^L \theta^2\phi_{mx}\,D_6(x)\,dx + \int_0^L \frac{\partial \bar{u}}{\partial x}\theta\phi_{mx}\,D_5(x)\,dx + \frac{1}{2}\int_0^L (\frac{\partial \theta}{\partial x})^2\phi_{mx}\,D_2(x)\,dx + \int_0^L \theta\frac{\partial \theta}{\partial x}\phi_{mx}$$

$$D_9(x)\,dx + \int_0^L \frac{\partial \bar{u}}{\partial x}\frac{\partial \theta}{\partial x}\phi_{mx}\,D_1(x)\,dx + \frac{1}{2}\int_0^L \theta^2\phi_{mx}\,I_p(x)\,dx + \int_0^L (\frac{\partial \bar{u}}{\partial x})^2\phi_{mx}\,A(x)\,dx + \int_0^L \frac{\partial \bar{u}}{\partial x}$$

$$\theta\phi_{mx}\,D_5(x)\,dx + \int_0^L \frac{\partial \bar{u}}{\partial x}\frac{\partial \theta}{\partial x}\phi_{mx}\,D_1(x)\,dx + \frac{1}{2}\int_0^L (\frac{\partial \bar{u}}{\partial x})^3\phi_{mx}\,A(x)\,dx + \frac{1}{2}\int_0^L \frac{\partial \bar{u}}{\partial x}\theta^2\phi_{mx}\,D_6(x)\,dx$$

$$+\int_0^L \left(\frac{\partial \bar{u}}{\partial x}\right)^2 \theta\phi_{mx}\ D_5(x)\ dx + \frac{1}{2}\int_0^L \frac{\partial \bar{u}}{\partial x}\left(\frac{\partial \theta}{\partial x}\right)^2 \phi_{mx}\ D_2(x)\ dx + \int_0^L \frac{\partial \bar{u}}{\partial x}\,\theta\frac{\partial \theta}{\partial x}\phi_{mx}\ D_9(x)\ dx + \int_0^L \left(\frac{\partial \bar{u}}{\partial x}\right)^2 \frac{\partial \theta}{\partial x}\phi_{mx}\ D_1(x)\ dx + \frac{1}{2}\int_0^L \theta^2 \frac{\partial \bar{u}}{\partial x}\phi_{mx}\ I_p(x)\ dx + \int_0^L \frac{\partial \bar{u}}{\partial x}\theta\phi_{mx}\ D_5(x)\ dx + \int_0^L \theta^2\phi_{mx}\ D_6(x)\ dx + \int_0^L \theta\frac{\partial \theta}{\partial x}\phi_{mx}\ D_9(x)\ dx + \frac{1}{2}\int_0^L \left(\frac{\partial \bar{u}}{\partial x}\right)^2 \theta\phi_{mx}\ D_5(x)\ dx + \frac{1}{2}\int_0^L \theta^3\phi_{mx}\ D_7(x)\ dx + \int_0^L \frac{\partial \bar{u}}{\partial x}\,\theta^2\phi_{mx}\ D_6(x)\ dx + \frac{1}{2}\int_0^L \theta\left(\frac{\partial \theta}{\partial x}\right)^2 \phi_{mx}\ D_{10}(x)\ dx + \int_0^L \theta^2\frac{\partial \theta}{\partial x}\phi_{mx}\ D_{22}(x)\ dx + \int_0^L \frac{\partial \bar{u}}{\partial x}\,\theta\frac{\partial \theta}{\partial x}\phi_{mx}\ D_9(x)\ dx + \frac{1}{2}\int_0^L \theta^3\phi_{mx}\ D_{12}(x)\ dx + \int_0^L \frac{\partial \bar{u}}{\partial x}\frac{\partial \theta}{\partial x}\phi_{mx}\ D_1(x)\ dx + \int_0^L \theta\frac{\partial \theta}{\partial x}\phi_{mx}\ D_9(x)\ dx + \int_0^L \left(\frac{\partial \theta}{\partial x}\right)^2 \phi_{mx}\ D_2(x)\ dx + \frac{1}{2}\int_0^L \left(\frac{\partial \bar{u}}{\partial x}\right)^2 \frac{\partial \theta}{\partial x}\phi_{mx}\ D_1(x)\ dx + \frac{1}{2}\int_0^L \theta^2\frac{\partial \theta}{\partial x}\phi_{mx}\ D_{22}(x)\ dx + \int_0^L \frac{\partial \bar{u}}{\partial x}\,\theta\frac{\partial \theta}{\partial x}\phi_{mx}\ D_9(x)\ dx + \frac{1}{2}\int_0^L \left(\frac{\partial \theta}{\partial x}\right)^3 \phi_{mx}\ D_3(x)\ dx + \int_0^L \theta\left(\frac{\partial \theta}{\partial x}\right)^2 \phi_{mx}\ D_{10}(x)\ dx + \int_0^L \frac{\partial \bar{u}}{\partial x}\left(\frac{\partial \theta}{\partial x}\right)^2 \phi_{mx}\ D_2(x)\ dx + \frac{1}{2}\int_0^L \theta^2\frac{\partial \theta}{\partial x}\phi_{mx}\ D_{28}(x)\ dx\ \Big]$$

Substituting for the displacements and their derivative expressions, implies,

$$\frac{\partial U_{Total}}{\partial a_m} = E\sum_{n=1}^{N}\int_0^L A(x)\,\phi_{nx}(x)\,\phi_{mx}(x)dx\ a_n + E\sum_{n=1}^{N}\int_0^L D_5(x)\,\phi_{nx}(x)\,\phi_{mx}(x)dx\ f_n + E\sum_{n=1}^{N}\int_0^L D_1(x)\,\phi_{nxx}(x)\,\phi_{mx}(x)dx\ f_n + \frac{1}{2}E\sum_{n=1}^{N}\sum_{k=1}^{K}\int_0^L A(x)\,\phi_{nx}(x)\,\phi_{kx}(x)\,\phi_{mx}(x)dx\ a_n a_k + \frac{1}{2}E\sum_{n=1}^{N}\sum_{k=1}^{K}\int_0^L D_6(x)\,\phi_{nx}(x)\,\phi_{kx}(x)\,\phi_{mx}(x)dx\ f_n f_k + E\sum_{n=1}^{N}\sum_{k=1}^{K}\int_0^L D_5(x)\,\phi_{nx}(x)\,\phi_{kx}(x)\,\phi_{mx}(x)dx\ f_n a_k + \frac{1}{2}E\sum_{n=1}^{N}\sum_{k=1}^{K}\int_0^L D_2(x)\,\phi_{nxx}(x)\,\phi_{kxx}(x)\,\phi_{mx}(x)dx\ f_n f_k + E\sum_{n=1}^{N}\sum_{k=1}^{K}\int_0^L D_9(x)\,\phi_{nx}(x)\,\phi_{kxx}(x)\,\phi_{mx}(x)dx\ f_n f_k + E\sum_{n=1}^{N}\sum_{k=1}^{K}\int_0^L D_1(x)\,\phi_{nxx}(x)\,\phi_{kx}(x)\,\phi_{mx}(x)dx\ f_n a_k + \frac{1}{2}E\sum_{n=1}^{N}\sum_{k=1}^{K}\int_0^L I_p(x)\,\phi_{nx}(x)\,\phi_{kx}(x)\,\phi_{mx}(x)dx\ f_n f_k + E\sum_{n=1}^{N}\sum_{k=1}^{K}$$

$$\int_0^L A(x)\,\phi_{nx}(x)\,\phi_{kx}(x)\,\phi_{mx}(x)dx\;a_n a_k \;+E\sum_{n=1}^{N}\sum_{k=1}^{K}\int_0^L D_5(x)\,\phi_{nx}(x)\,\phi_{kx}(x)\,\phi_{mx}(x)dx\;f_n a_k \;+\;E\sum_{n=1}^{N}\sum_{k=1}^{K}$$

$$\int_0^L D_1(x)\,\phi_{nxx}(x)\,\phi_{kx}(x)\,\phi_{mx}(x)dx\;f_n a_k \;+\frac{1}{2}\;E\sum_{n=1}^{N}\sum_{k,l=1}^{K,L}\int_0^L A(x)\,\phi_{nx}(x)\,\phi_{kx}(x)\,\phi_{lx}(x)\,\phi_{mx}(x)dx\;a_n a_k a_l$$

$$+\frac{1}{2}\;E\sum_{n=1}^{N}\sum_{k,l=1}^{K,L}\int_0^L D_6(x)\,\phi_{nx}(x)\,\phi_{kx}(x)\,\phi_{lx}(x)\,\phi_{mx}(x)dx\;f_n f_k a_l + E\sum_{n=1}^{N}\sum_{k,l=1}^{K,L}\int_0^L D_5(x)\,\phi_{nx}(x)\,\phi_{kx}(x)$$

$$\phi_{lx}(x)\,\phi_{mx}(x)dx\;f_n a_k a_l \;+\frac{1}{2}\;E\sum_{n=1}^{N}\sum_{k,l=1}^{K,L}\int_0^L D_2(x)\,\phi_{nxx}(x)\,\phi_{kxx}(x)\,\phi_{lx}(x)\,\phi_{mx}(x)dx\;f_n f_k a_l + E\sum_{n=1}^{N}\sum_{k,l=1}^{K,L}\int_0^L$$

$$D_9(x)\,\phi_{nxx}(x)\,\phi_{kx}(x)\,\phi_{lx}(x)\,\phi_{mx}(x)dx\;f_n f_k a_l + E\sum_{n=1}^{N}\sum_{k,l=1}^{K,L}\int_0^L D_1(x)\,\phi_{nxx}(x)\,\phi_{kx}(x)\,\phi_{lx}(x)\,\phi_{mx}(x)dx\;f_n a_k a_l$$

$$+\;\frac{1}{2}\;E\sum_{n=1}^{N}\sum_{k,l=1}^{K,L}\int_0^L I_p(x)\,\phi_{nx}(x)\,\phi_{kx}(x)\,\phi_{lx}(x)\,\phi_{mx}(x)dx\;f_n f_k a_l \;+E\sum_{n=1}^{N}\sum_{k=1}^{K}\int_0^L D_5(x)\,\phi_{nx}(x)\,\phi_{kx}(x)$$

$$\phi_{mx}(x)dx\;f_n a_k + E\sum_{n=1}^{N}\sum_{k=1}^{K}\int_0^L D_6(x)\,\phi_{nx}(x)\,\phi_{kx}(x)\,\phi_{mx}(x)dx\;f_n f_k + E\sum_{n=1}^{N}\sum_{k=1}^{K}\int_0^L D_9(x)\,\phi_{nx}(x)\,\phi_{kxx}(x)$$

$$\phi_{mx}(x)dx\;f_n f_k \;+\frac{1}{2}\;E\sum_{n=1}^{N}\sum_{k,l=1}^{K,L}\int_0^L D_5(x)\,\phi_{nx}(x)\,\phi_{kx}(x)\,\phi_{lx}(x)\,\phi_{mx}(x)dx\;f_n a_k a_l \;+\frac{1}{2}\;E\sum_{n=1}^{N}\sum_{k,l=1}^{K,L}\int_0^L D_7(x)\,\phi_{nx}(x)$$

$$\phi_{kx}(x)\,\phi_{lx}(x)\,\phi_{mx}(x)dx\;f_n f_k f_l \;+\;E\sum_{n=1}^{N}\sum_{k,l=1}^{K,L}\int_0^L D_6(x)\,\phi_{nx}(x)\,\phi_{kx}(x)\,\phi_{lx}(x)\,\phi_{mx}(x)dx\;f_n f_k a_l \;+\frac{1}{2}\;E\sum_{n=1}^{N}$$

$$\sum_{k,l=1}^{K,L}\int_0^L D_{10}(x)\,\phi_{nx}(x)\,\phi_{kxx}(x)\,\phi_{lxx}(x)\,\phi_{mx}(x)dx\;f_n f_k f_l + E\sum_{n=1}^{N}\sum_{k,l=1}^{K,L}\int_0^L D_{22}(x)\,\phi_{nx}(x)\,\phi_{kx}(x)\,\phi_{lxx}(x)\,\phi_{mx}(x)dx$$

$$f_n f_k f_l \;+\;E\sum_{n=1}^{N}\sum_{k,l=1}^{K,L}\int_0^L D_9(x)\,\phi_{nxx}(x)\,\phi_{kx}(x)\,\phi_{lx}(x)\,\phi_{mx}(x)dx\;f_n f_k a_l \;+\frac{1}{2}\;E\sum_{n=1}^{N}\sum_{k,l=1}^{K,L}\int_0^L D_{12}(x)\,\phi_{nx}(x)$$

$$\phi_{kx}(x)\,\phi_{lx}(x)\,\phi_{mx}(x)dx\;f_n f_k f_l + E\sum_{n=1}^{N}\sum_{k=1}^{K}\int_0^L D_1(x)\,\phi_{nxx}(x)\,\phi_{kx}(x)\,\phi_{mx}(x)dx\;f_n a_k + E\sum_{n=1}^{N}\sum_{k=1}^{K}\int_0^L$$

$$D_9(x)\,\phi_{nx}(x)\,\phi_{kxx}(x)\,\phi_{mx}(x)dx\;f_n f_k + E\sum_{n=1}^{N}\sum_{k=1}^{K}\int_0^L D_2(x)\,\phi_{nxx}(x)\,\phi_{kxx}(x)\,\phi_{mx}(x)dx\;f_n f_k \;+\frac{1}{2}\;E\sum_{n=1}^{N}\sum_{k,l=1}^{K,L}$$

$$\int_0^L D_1(x)\,\phi_{nxx}(x)\,\phi_{kx}(x)\,\phi_{lx}(x)\,\phi_{mx}(x)dx \quad f_n a_k a_l \; + \frac{1}{2}\; E \sum_{n=1}^{N} \sum_{k,l=1}^{K,L} \int_0^L D_{22}(x)\,\phi_{nx}(x)\,\phi_{kx}(x)\,\phi_{lxx}(x)\,\phi_{mx}(x)dx$$

$$f_n f_k f_l + E \sum_{n=1}^{N} \sum_{k,l=1}^{K,L} \int_0^L D_9(x)\,\phi_{nxx}(x)\,\phi_{kx}(x)\,\phi_{lx}(x)\,\phi_{mx}(x)dx \quad f_n f_k a_l \; + \frac{1}{2}\; E \sum_{n=1}^{N} \sum_{k,l=1}^{K,L} \int_0^L D_3(x)\,\phi_{nxx}(x)$$

$$\phi_{kxx}(x)\,\phi_{lxx}(x)\,\phi_{mx}(x)dx \quad f_n f_k f_l + E \sum_{n=1}^{N} \sum_{k,l=1}^{K,L} \int_0^L D_{10}(x)\,\phi_{nx}(x)\,\phi_{kxx}(x)\,\phi_{lxx}(x)\,\phi_{mx}(x)dx \quad f_n f_k f_l + E \sum_{n=1}^{N} \sum_{k,l=1}^{K,L}$$

$$\int_0^L D_2(x)\,\phi_{nxx}(x)\,\phi_{kxx}(x)\,\phi_{lx}(x)\,\phi_{mx}(x)dx \quad f_n f_k a_l \; + \frac{1}{2}\; E \sum_{n=1}^{N} \sum_{k,l=1}^{K,L} \int_0^L D_{28}(x)\,\phi_{nx}(x)\,\phi_{kx}(x)\,\phi_{lxx}(x)\,\phi_{mx}(x)dx$$

$$f_n f_k f_l$$

Further substituting for the associated S integral definitions as listed in Table B, results in:

$$\frac{\partial U_{Total}}{\partial a_m} = \; E \sum_{n=1}^{N} \; S_{Amn}\; a_n \; + E \sum_{n=1}^{N} \; S_{D_5 mn}\; f_n \; + E \sum_{n=1}^{N} \; S'_{D_1 mn}\; f_n \; + \frac{1}{2}\; E \sum_{n=1}^{N} \sum_{k=1}^{K} \; S_{Amnk}\; a_n a_k \; + \frac{1}{2}\; E \sum_{n=1}^{N} \sum_{k=1}^{K}$$

$$S_{D_6 mnk}\; f_n f_k \; + E \sum_{n=1}^{N} \sum_{k=1}^{K} \; S_{D_5 mnk}\; f_n a_k \; + \frac{1}{2}\; E \sum_{n=1}^{N} \sum_{k=1}^{K} \; S''_{D_2 mnk}\; f_n f_k \; + \; E \sum_{n=1}^{N} \sum_{k=1}^{K} \; S'_{D_9 mnk}\; f_n f_k \; + \; E$$

$$\sum_{n=1}^{N} \sum_{k=1}^{K} \; S'_{D_1 mnk}\; f_n a_k \; + \frac{1}{2}\; E \sum_{n=1}^{N} \sum_{k=1}^{K} \; S_{I_p mnk}\; f_n f_k \; + \; E \sum_{n=1}^{N} \sum_{k=1}^{K} \; S_{Amnk}\; a_n a_k \; + E \sum_{n=1}^{N} \sum_{k=1}^{K} \; S_{D_5 mnk}\; f_n a_k \; +$$

$$E \sum_{n=1}^{N} \sum_{k=1}^{K} \; S'_{D_1 mnk}\; f_n a_k \; + \frac{1}{2}\; E \sum_{n=1}^{N} \sum_{k,l=1}^{K,L} \; S_{Amnkl}\; a_n a_k a_l \; + \frac{1}{2}\; E \sum_{n=1}^{N} \sum_{k,l=1}^{K,L} \; S_{D_6 mnkl}\; f_n f_k a_l \; + \; E \sum_{n=1}^{N} \sum_{k,l=1}^{K,L}$$

$$S_{D_5 mnkl}\; f_n a_k a_l \; + \frac{1}{2}\; E \sum_{n=1}^{N} \sum_{k,l=1}^{K,L} \; S''_{D_2 mnkl}\; f_n f_k a_l \; + \; E \sum_{n=1}^{N} \sum_{k,l=1}^{K,L} \; S'_{D_9 mnkl}\; f_n f_k a_l \; + \; E \sum_{n=1}^{N} \sum_{k,l=1}^{K,L} \; S'_{D_1 mnkl}$$

$$f_n a_k a_l \; + \frac{1}{2}\; E \sum_{n=1}^{N} \sum_{k,l=1}^{K,L} \; S_{I_p mnkl}\; f_n f_k a_l \; + \; E \sum_{n=1}^{N} \sum_{k=1}^{K} \; S_{D_5 mnk}\; f_n a_k \; + E \sum_{n=1}^{N} \sum_{k=1}^{K} \; S_{D_6 mnk}\; f_n f_k \; + E \sum_{n=1}^{N} \sum_{k=1}^{K}$$

$$S'_{D_9 mnk}\; f_n f_k \; + \frac{1}{2}\; E \sum_{n=1}^{N} \sum_{k,l=1}^{K,L} \; S_{D_5 mnkl}\; f_n a_k a_l \; + \frac{1}{2}\; E \sum_{n=1}^{N} \sum_{k,l=1}^{K,L} \; S_{D_7 mnkl}\; f_n f_k f_l \; + \; E \sum_{n=1}^{N} \sum_{k,l=1}^{K,L} \; S_{D_6 mnkl}\; f_n f_k a_l$$

$$+ \frac{1}{2}\; E \sum_{n=1}^{N} \sum_{k,l=1}^{K,L} \; S''_{D_{10} mnkl}\; f_n f_k f_l \; + \; E \sum_{n=1}^{N} \sum_{k,l=1}^{K,L} \; S'_{D_{22} mnkl}\; f_n f_k f_l \; + E \sum_{n=1}^{N} \sum_{k,l=1}^{K,L} \; S'_{D_9 mnkl}\; f_n f_k a_l \; + \frac{1}{2}\; E$$

$$\sum_{n=1}^{N}\sum_{k,l=1}^{K,L} S_{D_{12}mnkl}\ f_n f_k f_l + E\sum_{n=1}^{N}\sum_{k=1}^{K} S'_{D_1mnk}\ f_n a_k + E\sum_{n=1}^{N}\sum_{k=1}^{K} S'_{D_9mnk}\ f_n f_k + E\sum_{n=1}^{N}\sum_{k=1}^{K} S''_{D_2mnk}$$

$$f_n f_k + \frac{1}{2} E\sum_{n=1}^{N}\sum_{k,l=1}^{K,L} S'_{D_1mnkl}\ f_n a_k a_l + \frac{1}{2} E\sum_{n=1}^{N}\sum_{k,l=1}^{K,L} S'_{D_{22}mnkl}\ f_n f_k f_l + E\sum_{n=1}^{N}\sum_{k,l=1}^{K,L} S'_{D_9mnkl}\ f_n f_k a_l + \frac{1}{2}$$

$$E\sum_{n=1}^{N}\sum_{k,l=1}^{K,L} S'''_{D_3mnkl}\ f_n f_k f_l + E\sum_{n=1}^{N}\sum_{k,l=1}^{K,L} S''_{D_{10}mnkl}\ f_n f_k f_l + E\sum_{n=1}^{N}\sum_{k,l=1}^{K,L} S''_{D_2mnkl}\ f_n f_k a_l + \frac{1}{2} E$$

$$\sum_{n=1}^{N}\sum_{k,l=1}^{K,L} S'_{D_{28}mnkl}\ f_n f_k f_l$$

Similarly we can derive $\frac{\partial U_{Total}}{\partial b_m}$, $\frac{\partial U_{Total}}{\partial c_m}$, $\frac{\partial U_{Total}}{\partial d_m}$, $\frac{\partial U_{Total}}{\partial e_m}$ and $\frac{\partial U_{Total}}{\partial f_m}$ as:

$$\frac{\partial U_{Total}}{\partial b_m} = kG\sum_{n=1}^{N} S_{Amn}\ b_n - kG\sum_{n=1}^{N} 's_{Amn}\ e_n + \sum_{n=1}^{N} S_{Pmn}\ b_n - \sum_{n=1}^{N} S_{Py_\alpha mn}\ f_n$$

$$\frac{\partial U_{Total}}{\partial c_m} = kG\sum_{n=1}^{N} S_{Amn}\ c_n - kG\sum_{n=1}^{N} 's_{Amn}\ d_n + \sum_{n=1}^{N} S_{Pmn}\ c_n - \sum_{n=1}^{N} S_{Pz_\alpha mn}\ f_n + \frac{1}{2} E\sum_{n=1}^{N}\sum_{k,l=1}^{K,L} S_{Amnkl}$$

$$c_n c_k c_l + \frac{1}{2} E\sum_{n=1}^{N}\sum_{k,l=1}^{K,L} S_{I_p mnkl} c_n f_k f_l$$

$$\frac{\partial U_{Total}}{\partial d_m} = E\left(\sum_{n=1}^{N} S_{I_y mn}\ d_n + \sum_{n=1}^{N} S_{I_{yz} mn}\ e_n\right) - kG\sum_{n=1}^{N} s'_{Amn}\ c_n + kG\sum_{n=1}^{N} s_{Amn}\ d_n + \sum_{n=1}^{N} S_{K_1 mn}\ f_n$$

$$\frac{\partial U_{Total}}{\partial e_m} = E\left(\sum_{n=1}^{N} S_{I_z mn}\ e_n + \sum_{n=1}^{N} S_{I_{yz} mn}\ d_n\right) - kG\sum_{n=1}^{N} s'_{Amn}\ b_n + kG\sum_{n=1}^{N} s_{Amn}\ e_n + \sum_{n=1}^{N} S_{K_2 mn}\ f_n$$

$$\frac{\partial U_{Total}}{\partial f_m} = -\sum_{n=1}^{N} S_{Py_\alpha mn}\ b_n + 2\sum_{n=1}^{N} S_{(PI_p/A)mn}\ f_n - \sum_{n=1}^{N} S_{Pz_\alpha mn}\ c_n + \frac{1}{2} E\sum_{n=1}^{N}\sum_{k,l=1}^{K,L} S_{I_p mnkl}\ c_n c_k f_l + \sum_{n=1}^{N} S_{K_1 mn}$$

$$d_n + \sum_{n=1}^{N} S_{K_2 mn}\ e_n + E\sum_{n=1}^{N} S_{D_5 mn}\ a_n + E\sum_{n=1}^{N} S_{D_6 mn}\ f_n + E\sum_{n=1}^{N} S'_{D_9 mn}\ f_n + \frac{1}{2} E\sum_{n=1}^{N}\sum_{k=1}^{K} S_{D_5 mnk}$$

$$a_n a_k + \frac{1}{2} E\sum_{n=1}^{N}\sum_{k=1}^{K} S_{D_7 mnk}\ f_n f_k + E\sum_{n=1}^{N}\sum_{k=1}^{K} S_{D_6 mnk}\ a_n f_k + \frac{1}{2} E\sum_{n=1}^{N}\sum_{k=1}^{K} S''_{D_{10} mnk}\ f_n f_k + E$$

$$\sum_{n=1}^{N}\sum_{k=1}^{K} S'_{D_{22} mnk}\ f_n f_k + E\sum_{n=1}^{N}\sum_{k=1}^{K} S'_{D_9 mnk}\ a_n f_k + \frac{1}{2} E\sum_{n=-4}^{N}\sum_{k=-4}^{K} S_{D_{12} mnk}\ f_n f_k + E\sum_{n=1}^{N} 'S_{D_1 mn}\ a_n$$

$$+ E \sum_{n=1}^{N} {}'S_{D_9 mn} f_n + E \sum_{n=1}^{N} S''_{D_2 mn} f_n + \frac{1}{2} E \sum_{n=1}^{N} \sum_{k=1}^{K} {}'S_{D_1 mnk} a_n a_k + \frac{1}{2} E \sum_{n=1}^{N} \sum_{k=1}^{K} {}'S_{D_{22} mnk} f_n f_k$$

$$+ E \sum_{n=1}^{N} \sum_{k=1}^{K} {}'S_{D_9 mnk} a_n f_k + \frac{1}{2} E \sum_{n=1}^{N} \sum_{k=1}^{K} S'''_{D_3 mnk} f_n f_k + E \sum_{n=1}^{N} \sum_{k=1}^{K} {}''S_{D_{10} mnk} f_n f_k + E \sum_{n=1}^{N} \sum_{k=1}^{K}$$

$$''S_{D_2 mnk} a_n f_k + \frac{1}{2} E \sum_{n=1}^{N} \sum_{k=1}^{K} {}'S_{D_{28} mnk} f_n f_k + E \sum_{n=1}^{N} \sum_{k=1}^{K} S_{D_6 mnk} a_n f_k + E \sum_{n=1}^{N} \sum_{k=1}^{K} S_{D_7 mnk} f_n f_k + E$$

$$\sum_{n=1}^{N} \sum_{k=1}^{K} S'_{D_{22} mnk} f_n f_k + \frac{1}{2} E \sum_{n=1}^{N} \sum_{k,l=1}^{K,L} S_{D_6 mnkl} a_n a_k f_l + \frac{1}{2} E \sum_{n=1}^{N} \sum_{k,l=1}^{K,L} S_{D_8 mnkl} f_n f_k f_l + E \sum_{n=1}^{N} \sum_{k,l=1}^{K,L}$$

$$S_{D_7 mnkl} a_n f_k f_l + \frac{1}{2} E \sum_{n=1}^{N} \sum_{k,l=1}^{K,L} S''_{D_{23} mnkl} f_n f_k f_l + E \sum_{n=1}^{N} \sum_{k,l=1}^{K,L} S'_{D_{24} mnkl} f_n f_k f_l + E \sum_{n=1}^{N} \sum_{k,l=1}^{K,L}$$

$$S'_{D_{22} mnkl} a_n f_k f_l + \frac{1}{2} E \sum_{n=1}^{N} \sum_{k,l=1}^{K,L} S_{D_{30} mnkl} f_n f_k f_l + E \sum_{n=1}^{N} \sum_{k=1}^{K} S_{D_5 mnk} a_n a_k + E \sum_{n=1}^{N} \sum_{k=1}^{K} S_{D_6 mnk} a_n f_k +$$

$$E \sum_{n=1}^{N} \sum_{k=1}^{K} S'_{D_9 mnk} a_n f_k + \frac{1}{2} E \sum_{n=1}^{N} \sum_{k,l=1}^{K,L} S_{D_5 mnkl} a_n a_k a_l + \frac{1}{2} E \sum_{n=1}^{N} \sum_{k,l=1}^{K,L} S_{D_7 mnkl} a_n f_k f_l + E \sum_{n=1}^{N} \sum_{k,l=1}^{K,L}$$

$$S_{D_6 mnkl} a_n a_k f_l + \frac{1}{2} E \sum_{n=1}^{N} \sum_{k,l=1}^{K,L} S''_{D_{10} mnkl} a_n f_k f_l + E \sum_{n=1}^{N} \sum_{k,l=1}^{K,L} S'_{D_{22} mnkl} a_n f_k f_l + E \sum_{n=1}^{N} \sum_{k,l=1}^{K,L} S'_{D_9 mnkl} a_n a_k f_l$$

$$+ \frac{1}{2} E \sum_{n=1}^{N} \sum_{k,l=1}^{K,L} S_{D_{12} mnkl} a_n f_k f_l + E \sum_{n=1}^{N} \sum_{k=1}^{K} S_{D_2 mnk} a_n f_k + E \sum_{n=1}^{N} \sum_{k=1}^{K} {}''S_{D_{10} mnk} f_n f_k + E \sum_{n=1}^{N} \sum_{k=1}^{K} S'''_{D_3 mnk}$$

$$f_n f_k + \frac{1}{2} E \sum_{n=1}^{N} \sum_{k,l=1}^{K,L} {}''S_{D_2 mnkl} a_n a_k f_l + \frac{1}{2} E \sum_{n=1}^{N} \sum_{k,l=1}^{K,L} {}''S_{D_{23} mnkl} f_n f_k f_l + E \sum_{n=1}^{N} \sum_{k,l=1}^{K,L} {}''S_{D_{10} mnkl} a_n f_k f_l$$

$$+ \frac{1}{2} E \sum_{n=1}^{N} \sum_{k,l=1}^{K,L} S''''_{D_4 mnkl} f_n f_k f_l + E \sum_{n=1}^{N} \sum_{k,l=1}^{K,L} {}'''S_{D_{25} mnkl} f_n f_k f_l + E \sum_{n=1}^{N} \sum_{k,l=1}^{K,L} {}'''S_{D_3 mnkl} a_n f_k f_l + \frac{1}{2} E$$

$$\sum_{n=1}^{N} \sum_{k,l=1}^{K,L} {}''S_{D_{29} mnkl} f_n f_k f_l + E \sum_{n=1}^{N} \sum_{k=1}^{K} S'_{D_9 mnk} a_n f_k + E \sum_{n=1}^{N} \sum_{k=1}^{K} S'_{D_{22} mnk} f_n f_k + E \sum_{n=1}^{N} \sum_{k=1}^{K} S''_{D_{10} mnk}$$

$$f_n f_k + \frac{1}{2} E \sum_{n=1}^{N} \sum_{k,l=1}^{K,L} S'_{D_9 mnkl} a_n a_k f_l + \frac{1}{2} E \sum_{n=1}^{N} \sum_{k,l=1}^{K,L} S'_{D_{24} mnkl} f_n f_k f_l + E \sum_{n=1}^{N} \sum_{k,l=1}^{K,L} S'_{D_{22} mnkl} a_n f_k f_l$$

$$+ \frac{1}{2} E \sum_{n=1}^{N} \sum_{k,l=1}^{K,L} S'''_{D_{25} mnkl} f_n f_k f_l + E \sum_{n=1}^{N} \sum_{k,l=1}^{K,L} S''_{D_{23} mnkl} f_n f_k f_l + E \sum_{n=1}^{N} \sum_{k,l=1}^{K,L} S''_{D_{10} mnkl} a_n f_k f_l + \frac{1}{2}$$

$$E\sum_{n=1}^{N}\sum_{k,l=1}^{K,L} S'_{D_{11}mnkl}\, f_n f_k f_l + E\sum_{n=1}^{N}\sum_{k=1}^{K} 'S_{D_9mnk}\, a_n f_k + E\sum_{n=1}^{N}\sum_{k=1}^{K} 'S_{D_{22}mnk}\, f_n f_k + E\sum_{n=1}^{N}\sum_{k=1}^{K} ''S_{D_{10}mnk}$$

$$f_n f_k + \frac{1}{2} E\sum_{n=1}^{N}\sum_{k,l=1}^{K,L} 'S_{D_9mnkl}\, a_n a_k f_l + \frac{1}{2} E\sum_{n=1}^{N}\sum_{k,l=1}^{K,L} 'S_{D_{24}mnkl}\, f_n f_k f_l + E\sum_{n=1}^{N}\sum_{k,l=1}^{K,L} 'S_{D_{22}mnkl}\, a_n f_k f_l$$

$$+\frac{1}{2} E\sum_{n=1}^{N}\sum_{k,l=1}^{K,L} '''S_{D_{25}mnkl}\, f_n f_k f_l + E\sum_{n=1}^{N}\sum_{k,l=1}^{K,L} ''S_{D_{23}mnkl}\, f_n f_k f_l + E\sum_{n=1}^{N}\sum_{k,l=1}^{K,L} ''S_{D_{10}mnkl}\, a_n f_k f_l + \frac{1}{2}$$

$$E\sum_{n=1}^{N}\sum_{k,l=1}^{K,L} 'S_{D_{11}mnkl}\, f_n f_k f_l + E\sum_{n=1}^{N}\sum_{k=1}^{K} 'S_{D_1mnk}\, a_n a_k + E\sum_{n=1}^{N}\sum_{k=1}^{K} 'S_{D_9mnk}\, a_n f_k + E\sum_{n=1}^{N}\sum_{k=1}^{K} ''S_{D_2mnk}$$

$$a_n f_k + \frac{1}{2} E\sum_{n=1}^{N}\sum_{k,l=1}^{K,L} 'S_{D_1mnkl}\, a_n a_k a_l + \frac{1}{2} E\sum_{n=1}^{N}\sum_{k,l=1}^{K,L} 'S_{D_{22}mnkl}\, a_n f_k f_l + E\sum_{n=1}^{N}\sum_{k,l=1}^{K,L} 'S_{D_9mnkl}\, a_n a_k f_l$$

$$+\frac{1}{2} E\sum_{n=1}^{N}\sum_{k,l=1}^{K,L} '''S_{D_3mnkl}\, a_n f_k f_l + E\sum_{n=1}^{N}\sum_{k,l=1}^{K,L} ''S_{D_{10}mnkl}\, a_n f_k f_l + E\sum_{n=1}^{N}\sum_{k,l=1}^{K,L} ''S_{D_2mnkl}\, a_n a_k f_l + \frac{1}{2} E$$

$$\sum_{n=1}^{N}\sum_{k,l=1}^{K,L} 'S_{D_{28}mnkl}\, a_n f_k f_l + E\sum_{n=1}^{N}\sum_{k=1}^{K} S_{I_p mnk}\, a_n f_k + E\sum_{n=1}^{N}\sum_{k=1}^{K} S_{D_{12}mnk}\, f_n f_k + E\sum_{n=1}^{N}\sum_{k=1}^{K} S'_{D_{28}mnk}$$

$$f_n f_k + \frac{1}{2} E\sum_{n=1}^{N}\sum_{k,l=1}^{K,L} S_{I_p mnkl}\, a_n a_k f_l + \frac{1}{2} E\sum_{n=1}^{N}\sum_{k,l=1}^{K,L} S_{D_{30}mnkl}\, f_n f_k f_l + E\sum_{n=1}^{N}\sum_{k,l=1}^{K,L} S_{D_{12}mnkl}\, a_n f_k f_l + \frac{1}{2} E$$

$$\sum_{n=1}^{N}\sum_{k,l=1}^{K,L} S''_{D_{29}mnkl}\, f_n f_k f_l + E\sum_{n=1}^{N}\sum_{k,l=1}^{K,L} S'_{D_{11}mnkl}\, f_n f_k f_l + E\sum_{n=1}^{N}\sum_{k,l=1}^{K,L} S'_{D_{28}mnkl}\, a_n f_k f_l + \frac{1}{2} E\sum_{n=1}^{N}\sum_{k,l=1}^{K,L}$$

$$S_{D_{27}mnkl}\, f_n f_k f_l + G\sum_{n=1}^{N} S_{I_p mn}\, f_n + E\sum_{n=1}^{N} S''_{I_p mn}\, f_n$$

APPENDIX D: DERIVATION OF $\frac{\partial T}{\partial q_m}$ AND $\frac{d}{dt}(\frac{\partial T}{\partial \dot{q}_m})$

Considering the total kinetic energy Eq. (3) in section 2.2 and a constant material density along the blade length, implies,

$$\frac{\partial T}{\partial a_m} = \overline{\Omega}^2 \rho \int_0^L A(x)\bar{u}\frac{\partial}{\partial a_m}\bar{u}dx = \overline{\Omega}^2 \rho \sum_{n=1}^{N} \int_0^L A(x)\phi_n(x)\phi_m(x)dx a_n = \overline{\Omega}^2 \rho \sum_{n=1}^{N} s_{Amn} a_n$$

$$\frac{d}{dt}(\frac{\partial T}{\partial \dot{a}_m}) = \frac{d}{dt}\Big[\frac{1}{2}\int_0^L \rho(x)\Big[2A(x)\dot{\bar{u}}\frac{\partial}{\partial a_m}\dot{\bar{u}} + 2A(x)\ \psi\ (\frac{\partial \dot{\phi}}{\partial x})\frac{\partial}{\partial a_m}\dot{\bar{u}} \Big]dx$$

$$= \rho \int_0^L A(x) \sum_{n=1}^{N} \ddot{a}_n \phi_n(x)\ \phi_m(x)\ dx + \rho \int_0^L D_1(x) \sum_{n=1}^{N} \ddot{f}_n \phi_{nx}(x)\ \phi_m(x)\ dx$$

$$= \rho \sum_{n=1}^{N} s_{Amn}\ \ddot{a}_n + \rho \sum_{n=1}^{N} s'_{D_1 mn}\ \ddot{f}_n$$

$$\frac{\partial T}{\partial b_m} = -\Omega^2 \rho \sum_{n=1}^{N} S_{xAmn} b_n - \Omega^2 \rho \sum_{n=1}^{N} S_{xz_\alpha Amn} f_n \ ;\ \frac{d}{dt}(\frac{\partial T}{\partial \dot{b}_m}) = \rho \sum_{n=1}^{N} s_{Amn}\ddot{b}_n + \rho \sum_{n=1}^{N} s_{z_\alpha Amn}\ \ddot{f}_n$$

$$\frac{\partial T}{\partial c_m} = -\Omega^2 \rho \sum_{n=1}^{N} S_{xAmn} c_n - \Omega^2 \rho \sum_{n=1}^{N} S_{xy_\alpha Amn} f_n \ ;\ \frac{d}{dt}(\frac{\partial T}{\partial \dot{c}_m}) = \rho \sum_{n=1}^{N} s_{Amn}\ddot{c}_n + \rho \sum_{n=1}^{N} s_{y_\alpha Amn}\ \ddot{f}_n$$

$$\frac{\partial T}{\partial d_m} = \frac{\rho}{g} \sum_{n=1}^{N} s_{I_y mn}\ d_n + \frac{\rho}{g} \sum_{n=1}^{N} \int_0^L s'_{I_y y_\alpha mn}\ \dot{f}_n + \frac{\rho}{g} \sum_{n=1}^{N} s_{I_y y'_\alpha mn}\ \dot{f}_n$$

$$\frac{d}{dt}(\frac{\partial T}{\partial \dot{d}_m}) = \rho \sum_{n=1}^{N} s_{I_y mn}\ddot{d}_n + \rho \sum_{n=1}^{N} s'_{I_y y_\alpha mn}\ \ddot{f}_n$$

$$\frac{\partial T}{\partial e_m} = \overline{\Omega}^2 \rho \sum_{n=1}^{N} s_{I_y mn} e_n - \overline{\Omega}^2 \rho \sum_{n=1}^{N} \sum_{k,l=1}^{K,L} s_{I_y mnkl}\ f_n\ f_k\ e_l + \overline{\Omega}\rho \sum_{n=1}^{N} s_{I_z mn}\ \dot{f}_n - \frac{1}{2}\overline{\Omega}\rho \sum_{n=1}^{N} \sum_{k,l=1}^{K,L} s_{I_z mnkl}\ f_n\ f_k\ \dot{f}_l$$

$$+ \overline{\Omega}\rho \sum_{n=1}^{N} s_{I_y mn}\ \dot{f}_n - \frac{1}{2}\overline{\Omega}\rho \sum_{n=1}^{N} \sum_{k,l=1}^{K,L} s_{I_y mnkl}\ f_n\ f_k\ \dot{f}_l + \rho \sum_{n=1}^{N} \sum_{k,l=1}^{K,L} s_{I_z mnkl}\ f_n \dot{e}_k\ \dot{f}_l - \rho \sum_{n=1}^{N} \sum_{k,l=1}^{K,L} s_{I_y mnkl}\ f_n \dot{e}_k\ \dot{f}_l$$

$$+ \rho \sum_{n=1}^{N} \sum_{k,l=1}^{K,L} s_{I_z mnkl}\ e_n\ \dot{f}_k\ \dot{f}_l + \frac{\rho}{g} \sum_{n=1}^{N} s_{I_z mn}\ e_n + \frac{\rho}{g} \sum_{n=1}^{N} \sum_{k=1}^{K} s'_{I_z z_\alpha z'_\alpha mnk}\ \dot{f}_n\ \dot{f}_k$$

$$\frac{d}{dt}(\frac{\partial T}{\partial \dot{e}_m}) = -\overline{\Omega}\rho\sum_{n=1}^{N} s_{I_z mn}\dot{f}_n - \overline{\Omega}\rho\sum_{n=1}^{N} s_{I_y mn}\dot{f}_n + \overline{\Omega}\rho\sum_{n=1}^{N}\sum_{k,l=1}^{K,L} s_{I_y mnkl}\dot{f}_n f_k f_l + \overline{\Omega}\rho\sum_{n=1}^{N}\sum_{k,l=1}^{K,L} s_{I_y mnkl} f_n \dot{f}_k f_l$$

$$+\overline{\Omega}\rho\sum_{n=1}^{N}\sum_{k,l=1}^{K,L} s_{I_y mnkl} f_n f_k \dot{f}_l + \rho\sum_{n=1}^{N} s_{I_y mn}\ddot{e}_n - \rho\sum_{n=1}^{N}\sum_{k,l=1}^{K,L} s_{I_y mnkl}\dot{f}_n f_k \dot{e}_l - \rho\sum_{n=1}^{N}\sum_{k,l=1}^{K,L} s_{I_y mnkl} f_n \dot{f}_k \dot{e}_l$$

$$-\rho\sum_{n=1}^{N}\sum_{k,l=1}^{K,L} s_{I_y mnkl} f_n f_k \ddot{e}_l + \rho\sum_{n=1}^{N}\sum_{k,l=1}^{K,L} s_{I_z mnkl}\dot{e}_n f_k \dot{f}_l + \rho\sum_{n=1}^{N}\sum_{k,l=1}^{K,L} s_{I_z mnkl} e_n \dot{f}_k \dot{f}_l + \rho\sum_{n=1}^{N}\sum_{k,l=1}^{K,L} s_{I_z mnkl} e_n f_k \ddot{f}_l$$

$$-\rho\sum_{n=1}^{N}\sum_{k,l=1}^{K,L} s_{I_y mnkl}\dot{e}_n f_k \dot{f}_l - \rho\sum_{n=1}^{N}\sum_{k,l=1}^{K,L} s_{I_y mnkl} e_n \dot{f}_k \dot{f}_l - \rho\sum_{n=1}^{N}\sum_{k,l=1}^{K,L} s_{I_y mnkl} e_n f_k \ddot{f}_l + \rho\sum_{n=1}^{N} s_{I_z mn}\ddot{e}_n + \rho\sum_{n=1}^{N}$$

$$s'_{I_z z_\alpha mn}\ddot{f}_n$$

$$\frac{\partial T}{\partial f_m} = -\overline{\Omega}^2\rho\sum_{n=1}^{N} s_{I_z mn} f_n - \overline{\Omega}^2\rho\sum_{n=1}^{N}\sum_{k,l=1}^{K,L} s_{I_y mnkl} e_n e_k f_l + \frac{1}{2}\overline{\Omega}^2\rho\sum_{n=1}^{N}\sum_{k,l=1}^{K,L} s_{I_z mnkl} f_n f_k f_l + \overline{\Omega}\rho\sum_{n=1}^{N} s_{I_z mn}\dot{e}_n$$

$$-\overline{\Omega}\rho\sum_{n=1}^{N} s_{I_y mn}\dot{e}_n + \frac{3}{2}\overline{\Omega}\rho\sum_{n=1}^{N}\sum_{k,l=1}^{K,L} s_{I_y mnkl} f_n f_k \dot{e}_l - \rho\sum_{n=1}^{N}\sum_{k,l=1}^{K,L} s_{I_y mnkl} f_n \dot{e}_k \dot{e}_l - \overline{\Omega}\rho\sum_{n=1}^{N}\sum_{k,l=1}^{K,L} s_{I_z mnkl} e_n \dot{f}_k f_l$$

$$-\overline{\Omega}\rho\sum_{n=1}^{N}\sum_{k,l=1}^{K,L} s_{I_y mnkl} e_n \dot{f}_k f_l + \rho\sum_{n=1}^{N}\sum_{k,l=1}^{K,L} s_{I_z mnkl} e_n \dot{e}_k \dot{f}_l - \rho\sum_{n=1}^{N}\sum_{k,l=1}^{K,L} s_{I_y mnkl} e_n \dot{e}_k \dot{f}_l - \Omega^2\sum_{n=1}^{N} S_{xMz_\alpha mn} b_n$$

$$-\Omega^2\sum_{n=1}^{N} S_{xMz_\alpha{}^2 mn} f_n - \Omega^2\sum_{n=1}^{N} S_{xMy_\alpha mn} c_n - \Omega^2\sum_{n=1}^{N} S_{xMy_\alpha{}^2 mn} f_n$$

$$\frac{d}{dt}(\frac{\partial T}{\partial \dot{f}_m}) = \rho\sum_{n=1}^{N} {}'s_{D_1 mn}\ddot{a}_n + \rho\sum_{n=1}^{N} S_{D_2 mn}\ddot{f}_n + \rho\sum_{n=1}^{N} s_{I_p mn}\ddot{f}_n + \overline{\Omega}\rho\sum_{n=1}^{N} s_{I_z mn}\dot{e}_n + \overline{\Omega}\rho\sum_{n=1}^{N} s_{I_y mn}\dot{e}_n$$

$$-\overline{\Omega}\sum_{n=1}^{N}\sum_{k,l=1}^{K,L} s_{I_z mnkl}\dot{e}_n f_k f_l - \overline{\Omega}\sum_{n=1}^{N}\sum_{k,l=1}^{K,L} s_{I_z mnkl} e_n \dot{f}_k f_l - \overline{\Omega}\sum_{n=1}^{N}\sum_{k,l=1}^{K,L} s_{I_z mnkl} e_n f_k \dot{f}_l - \frac{1}{2}\overline{\Omega}\rho\sum_{n=1}^{N}\sum_{k,l=1}^{K,L}$$

$$s_{I_y mnkl}\dot{e}_n f_k f_l - \frac{1}{2}\overline{\Omega}\rho\sum_{n=1}^{N}\sum_{k,l=1}^{K,L} s_{I_y mnkl} e_n \dot{f}_k f_l - \frac{1}{2}\overline{\Omega}\rho\sum_{n=1}^{N}\sum_{k,l=1}^{K,L} s_{I_y mnkl} e_n f_k \dot{f}_l + \rho\sum_{n=1}^{N}\sum_{k,l=1}^{K,L} s_{I_z mnkl}\dot{e}_n f_k \dot{e}_l$$

$$+\rho\sum_{n=1}^{N}\sum_{k,l=1}^{K,L} s_{I_z mnkl} e_n \dot{f}_k \dot{e}_l + \rho\sum_{n=1}^{N}\sum_{k,l=1}^{K,L} s_{I_z mnkl} e_n f_k \ddot{e}_l - \rho\sum_{n=1}^{N}\sum_{k,l=1}^{K,L} s_{I_y mnkl}\dot{e}_n f_k \dot{e}_l - \rho\sum_{n=1}^{N}\sum_{k,l=1}^{K,L} s_{I_y mnkl} e_n \dot{f}_k \dot{e}_l$$

$$-\rho\sum_{n=1}^{N}\sum_{k,l=1}^{K,L} s_{I_y mnkl} e_n f_k \ddot{e}_l + \rho\sum_{n=1}^{N} s_{I_z mn}\ddot{f}_n + \rho\sum_{n=1}^{N} s_{I_y mn}\ddot{f}_n + \rho\sum_{n=1}^{N}\sum_{k,l=1}^{K,L} s_{I_z mnkl}\dot{e}_n e_k \dot{f}_l + \rho\sum_{n=1}^{N}\sum_{k,l=1}^{K,L}$$

$$s_{I_z mnkl}\, e_n\, \dot{e}_k\, \dot{f}_l + \rho \sum_{n=1}^{N} \sum_{k,l=1}^{K,L} s_{I_z mnkl}\, e_n\, e_k\, \ddot{f}_l + \sum_{n=1}^{N} s_{Mz_\alpha mn}\, \ddot{b}_n + \sum_{n=1}^{N} s_{Mz_\alpha{}^2 mn}\, \ddot{f}_n + \sum_{n=1}^{N} s_{My_\alpha mn}\, \ddot{c}_n + \sum_{n=1}^{N} s_{My_\alpha{}^2 mn}\, \ddot{f}_n$$

$$+ \rho \sum_{n=1}^{N} {}'s_{I_z z_\alpha mn}\, \ddot{e}_n + \rho \sum_{n=1}^{N} S_{I_z z_\alpha{}^2 mn}\, \ddot{f}_n + \rho \sum_{n=1}^{N} {}'s_{I_y y_\alpha mn}\, \ddot{d}_n + \rho \sum_{n=1}^{N} S_{I_y y_\alpha{}^2 mn}\, \ddot{f}_n + \frac{\rho}{g} \sum_{n=1}^{N} {}'s_{I_z z_\alpha mn}\, \dot{e}_n + \frac{\rho}{g} \sum_{n=1}^{N} s_{I_z z_\alpha{}' mn}\, \dot{e}_n$$

$$+ \frac{\rho}{g} \sum_{n=1}^{N} S_{I_z z_\alpha{}^2 mn}\, \ddot{f}_n + \frac{\rho}{g} \sum_{n=1}^{N} s_{I_z z_\alpha{}'^2 mn}\, \ddot{f}_n + \frac{\rho}{g} \sum_{n=1}^{N} {}'s_{I_y y_\alpha mn}\, \dot{d}_n + \frac{\rho}{g} \sum_{n=1}^{N} s_{I_y y_\alpha{}' mn}\, \dot{d}_n + \frac{\rho}{g} \sum_{n=1}^{N} S_{I_y y_\alpha{}^2 mn}\, \ddot{f}_n$$

$$+ \frac{\rho}{g} \sum_{n=1}^{N} s_{I_y y_\alpha{}'^2 mn}\, \ddot{f}_n$$

Table A

VALUES OF D'S AS FUNCTION OF X

$D(x)$	$Equivalent$	$D(x)$	$Equivalent$
$A(x)$	$= \iint_A dydz$	$D_{11}(x)$	$= \psi \frac{\partial \psi}{\partial x} \iint_A r^2 \, dydz$
$D_1(x)$	$= \psi \iint_A dydz$	$D_{12}(x)$	$= \frac{\partial \psi}{\partial x} \iint_A r^2 \, dydz$
$D_2(x)$	$= \psi^2 \iint_A dydz$	$D_{13}(x)$	$= (\frac{\partial \psi}{\partial y})^2 \iint_A dydz = 0$
$D_3(x)$	$= \psi^3 \iint_A dydz$	$D_{14}(x)$	$= (\frac{\partial \psi}{\partial y})^2 \psi \iint_A dydz = 0$
$D_4(x)$	$= \psi^4 \iint_A dydz$	$D_{15}(x)$	$= (\frac{\partial \psi}{\partial y})^2 \frac{\partial \psi}{\partial x} \iint_A dydz = 0$
$D_5(x)$	$= \frac{\partial \psi}{\partial x} \iint_A dydz$	$D_{16}(x)$	$= (\frac{\partial \psi}{\partial y})^2 (\frac{\partial \psi}{\partial x})^2 \iint_A dydz = 0$
$D_6(x)$	$= (\frac{\partial \psi}{\partial x})^2 \iint_A dydz$	$D_{17}(x)$	$= (\frac{\partial \psi}{\partial y})^2 \psi \frac{\partial \psi}{\partial x} \iint_A dydz = 0$
$D_7(x)$	$= (\frac{\partial \psi}{\partial x})^3 \iint_A dydz$	$D_{18}(x)$	$= \psi^2 \frac{\partial \psi}{\partial x} (\frac{\partial \psi}{\partial y})^2 \iint_A dydz = 0$
$D_8(x)$	$= (\frac{\partial \psi}{\partial x})^4 \iint_A dydz$	$D_{19}(x)$	$= z_1 (\frac{\partial \psi}{\partial y}) \iint_A dydz = 0$
$D_9(x)$	$= \psi \frac{\partial \psi}{\partial x} \iint_A dydz$	$D_{20}(x)$	$= z_1 (\frac{\partial \psi}{\partial y}) \frac{\partial \psi}{\partial x} \iint_A dydz = 0$
$D_{10}(x)$	$= \psi^2 \frac{\partial \psi}{\partial x} \iint_A dydz$	$D_{21}(x)$	$= z_1 (\frac{\partial \psi}{\partial y}) \psi \iint_A dydz = 0$
$D_{22}(x)$	$= \psi (\frac{\partial \psi}{\partial x})^2 \iint_A dydz$	$D_{31}(x)$	$= (\frac{\partial \psi}{\partial z})^2 \iint_A dydz = 0$
$D_{23}(x)$	$= (\psi \frac{\partial \psi}{\partial x})^2 \iint_A dydz$	$D_{32}(x)$	$= (\frac{\partial \psi}{\partial z})^2 \psi \iint_A dydz = 0$
$D_{24}(x)$	$= \psi (\frac{\partial \psi}{\partial x})^3 \iint_A dydz$	$D_{33}(x)$	$= (\frac{\partial \psi}{\partial z})^2 \psi^2 \iint_A dydz = 0$
$D_{25}(x)$	$= \psi^3 \frac{\partial \psi}{\partial x} \iint_A dydz$	$D_{34}(x)$	$= (\frac{\partial \psi}{\partial z})^2 \frac{\partial \psi}{\partial x} \iint_A dydz = 0$
$D_{26}(x)$	$= \iint_A r^2 \, dydz = I_p$	$D_{35}(x)$	$= (\frac{\partial \psi}{\partial z})^2 (\frac{\partial \psi}{\partial x})^2 \iint_A dydz = 0$
$D_{27}(x)$	$= \iint_A r^4 \, dydz$	$D_{36}(x)$	$= (\frac{\partial \psi}{\partial z})^2 \psi \frac{\partial \psi}{\partial x} \iint_A dydz = 0$

$D_{28}(x)$	$= \psi \iint_A r^2 \, dydz$	$D_{37}(x)$	$= y_1 \left(\frac{\partial \psi}{\partial z}\right) \iint_A dydz = 0$
$D_{29}(x)$	$= \psi^2 \iint_A r^2 \, dydz$	$D_{38}(x)$	$= y_1 \left(\frac{\partial \psi}{\partial z}\right) \frac{\partial \psi}{\partial x} \iint_A dydz = 0$
$D_{30}(x)$	$= \left(\frac{\partial \psi}{\partial x}\right)^2 \iint_A r^2 \, dydz$	$D_{39}(x)$	$= y_1 \left(\frac{\partial \psi}{\partial z}\right) \psi \iint_A dydz = 0$

Table B

ALL S INTEGRAL DEFINITIONS

S $(integral)$	$Equivalent$	S $(integral)$	$Equivalent$
s_{Amn}	$=\int_0^L A(x)\phi_n(x)\phi_m(x)dx$	s_{Mmn}	$=\int_0^L m(x)\phi_n(x)\phi_m(x)dx$
$s_{I_y mn}$	$=\int_0^L I_y(x)\phi_n(x)\phi_m(x)dx$	$s_{I_z mn}$	$=\int_0^L I_z(x)\phi_n(x)\phi_m(x)dx$
$s_{I_p mn}$	$=\int_0^L I_p(x)\phi_n(x)\phi_m(x)dx$	$s_{y_\alpha' I_y mn}$	$=\int_0^L y_\alpha'(x) I_y(x)\phi_n(x)\phi_m(x)dx$
$s_{z_\alpha' I_z mn}$	$=\int_0^L z_\alpha'(x) I_z(x)\phi_n(x)\phi_m(x)dx$	$s_{I_y y'^2_\alpha mn}$	$=\int_0^L I_y(x) y_\alpha'^{\,2}(x)\phi_n(x)\phi_m(x)dx$
$s_{My_\alpha mn}$	$=\int_0^L m(x) y_\alpha(x)\phi_n(x)\ \phi_m(x)dx$	$s_{Mz_\alpha mn}$	$=\int_0^L m(x) z_\alpha(x)\phi_n(x)\ \phi_m(x)dx$
$s_{I_z z'^2_\alpha mn}$	$=\int_0^L I_z(x) z_\alpha'^{\,2}(x)\phi_n(x)\phi_m(x)dx$	$s'_{D_1 mn}$	$=\int_0^L D_1(x)\phi_{nx}(x)\phi_m(x)dx$
s'_{Amn}	$=\int_0^L A(x)\phi_{nx}(x)\phi_m(x)dx$	$s'_{y_\alpha I_y mn}$	$=\int_0^L y_\alpha(x) I_y(x)\phi_{nx}(x)\phi_m(x)dx$
$s'_{z_\alpha I_z mn}$	$=\int_0^L z_\alpha(x) I_z(x)\phi_{nx}(x)\phi_m(x)dx$	$'s_{Amn}$	$=\int_0^L A(x)\phi_n(x)\phi_{mx}(x)dx$
$'s_{D_1 mn}$	$=\int_0^L D_1(x)\phi_n(x)\phi_{mx}(x)dx$	$'s_{I_y y_\alpha mn}$	$=\int_0^L I_y(x) y_\alpha(x)\phi_n(x)\phi_{mx}(x)dx$
$'s_{I_z z_\alpha mn}$	$=\int_0^L I_z(x) z_\alpha(x)\phi_n(x)\phi_{mx}(x)dx$	$'s_{I_y y_\alpha y'_\alpha mn}$	$=\int_0^L I_y(x) y_\alpha(x) y'_\alpha(x)\phi_n(x)\phi_{mx}(x)dx$
$'s_{I_z z_\alpha z'_\alpha mn}$	$=\int_0^L I_z(x) z_\alpha(x) z'_\alpha(x)\phi_n(x)\phi_{mx}(x)dx$	S_{Amn}	$=\int_0^L A(x)\phi_{nx}(x)\phi_{mx}(x)dx$
S_{Pmn}	$=\int_0^L P(x)\phi_{nx}(x)\phi_{mx}(x)dx$	$S_{K_1 mn}$	$=\int_0^L K_1(x)\phi_{nx}(x)\phi_{mx}(x)dx$
$S_{K_2 mn}$	$=\int_0^L K_2(x)\phi_{nx}(x)\phi_{mx}(x)dx$	$S_{I_y mn}$	$=\int_0^L I_y(x)\phi_{nx}(x)\phi_{mx}(x)dx$
$S_{I_z mn}$	$=\int_0^L I_z(x)\phi_{nx}(x)\phi_{mx}(x)dx$	$S_{I_{yz} mn}$	$=\int_0^L I_{yz}(x)\phi_{nx}(x)\phi_{mx}(x)dx$
$S_{I_p mn}$	$=\int_0^L I_p(x)\phi_{nx}(x)\phi_{mx}(x)dx$	$S_{D_2 mn}$	$=\int_0^L D_2(x)\phi_{nx}(x)\phi_{mx}(x)dx$

S_{D_5mn}	$=\int_0^L D_5(x)\phi_{nx}(x)\phi_{mx}(x)dx$	S_{D_6mn}	$=\int_0^L D_6(x)\phi_{nx}(x)\phi_{mx}(x)dx$
$S_{Py_\alpha mn}$	$=\int_0^L P(x)y_\alpha(x)\phi_{nx}(x)\phi_{mx}(x)dx$	$S_{Pz_\alpha mn}$	$=\int_0^L P(x)z_\alpha(x)\phi_{nx}(x)\phi_{mx}(x)dx$
$S_{I_y y_\alpha y'_\alpha mn}$	$=\int_0^L I_y(x)y_\alpha(x)y'_\alpha(x)\phi_{nx}(x)\phi_{mx}(x)dx$	$S_{I_z z_\alpha z'_\alpha mn}$	$=\int_0^L I_z(x)z_\alpha(x)z'_\alpha(x)\phi_{nx}(x)\phi_{mx}(x)dx$
$S_{I_y y_\alpha^2 mn}$	$=\int_0^L I_y(x)y_\alpha^2(x)\phi_{nx}(x)\phi_{mx}(x)dx$	$S_{I_z z_\alpha^2 mn}$	$=\int_0^L I_z(x)z_\alpha^2(x)\phi_{nx}(x)\phi_{mx}(x)dx$
$S_{(PI_p/M)mn}$	$=\int_0^L [P(x)I_p(x)/m(x)]\phi_{nx}(x)\phi_{mx}(x)dx$	S'_{D_1mn}	$=\int_0^L D_1(x)\phi_{nxx}(x)\phi_{mx}(x)dx$
S'_{D_9mn}	$=\int_0^L D_9(x)\phi_{nxx}(x)\phi_{mx}(x)dx$	S''_{D_2mn}	$=\int_0^L D_2(x)\phi_{nxx}(x)\phi_{mxx}(x)dx$
S''_{I_pmn}	$=\int_0^L I_p(x)\phi_{nxx}(x)\phi_{mxx}(x)dx$	$'S_{D_1mn}$	$=\int_0^L D_1(x)\phi_{nx}(x)\phi_{mxx}(x)dx$
$'S_{D_9mn}$	$=\int_0^L D_9(x)\phi_{nx}(x)\phi_{mxx}(x)dx$	S_{Amnk}	$=\int_0^L A(x)\phi_{nx}(x)\phi_{kx}(x)\phi_{mx}(x)dx$
S_{D_2mnk}	$=\int_0^L D_2(x)\phi_{nx}(x)\phi_{kx}(x)\phi_{mx}(x)dx$	S_{D_5mnk}	$=\int_0^L D_5(x)\phi_{nx}(x)\phi_{kx}(x)\phi_{mx}(x)dx$
S_{D_6mnk}	$=\int_0^L D_6(x)\phi_{nx}(x)\phi_{kx}(x)\phi_{mx}(x)dx$	S_{D_7mnk}	$=\int_0^L D_7(x)\phi_{nx}(x)\phi_{kx}(x)\phi_{mx}(x)dx$
$S_{D_{12}mnk}$	$=\int_0^L D_{12}(x)\phi_{nx}(x)\phi_{kx}(x)\phi_{mx}(x)dx$	S_{I_pmnk}	$=\int_0^L I_p(x)\phi_{nx}(x)\phi_{kx}(x)\phi_{mx}(x)dx$
S'_{D_1mnk}	$=\int_0^L D_1(x)\phi_{nxx}(x)\phi_{kx}(x)\phi_{mx}(x)dx$	S'_{D_9mnk}	$=\int_0^L D_9(x)\phi_{nxx}(x)\phi_{kx}(x)\phi_{mx}(x)dx$
$S'_{D_{22}mnk}$	$=\int_0^L D_{22}(x)\phi_{nxx}(x)\phi_{kx}(x)\phi_{mx}(x)dx$	$S'_{D_{28}mnk}$	$=\int_0^L D_{28}(x)\phi_{nxx}(x)\phi_{kx}(x)\phi_{mx}(x)dx$
S''_{D_2mnk}	$=\int_0^L D_2(x)\phi_{nxx}(x)\phi_{kxx}(x)\phi_{mx}(x)dx$	$S''_{D_{10}mnk}$	$=\int_0^L D_{10}(x)\phi_{nxx}(x)\phi_{kxx}(x)\phi_{mx}(x)dx$
S'''_{D_3mnk}	$=\int_0^L D_3(x)\phi_{nxx}(x)\phi_{kxx}(x)\phi_{mxx}(x)dx$	S_{Amnkl}	$=\int_0^L A(x)\phi_{nx}(x)\phi_{kx}(x)\phi_{lx}(x)\phi_{mx}(x)dx$
S_{D_5mnkl}	$=\int_0^L D_5(x)\phi_{nx}(x)\phi_{kx}(x)\phi_{lx}(x)\phi_{mx}(x)dx$	S_{D_6mnkl}	$=\int_0^L D_6(x)\phi_{nx}(x)\phi_{kx}(x)\phi_{lx}(x)\phi_{mx}(x)dx$
S_{D_7mnkl}	$=\int_0^L D_7(x)\phi_{nx}(x)\phi_{kx}(x)\phi_{lx}(x)\phi_{mx}(x)dx$	S_{D_8mnkl}	$=\int_0^L D_8(x)\phi_{nx}(x)\phi_{kx}(x)\phi_{lx}(x)\phi_{mx}(x)dx$

$S_{D_{12}mnkl}$	$=\int_0^L D_{12}(x)\phi_{nx}(x)\phi_{kx}(x)\phi_{lx}(x)\phi_{mx}(x)dx$	$S_{D_{27}mnkl}$	$=\int_0^L D_{27}(x)\phi_{nx}(x)\phi_{kx}(x)\phi_{lx}(x)\phi_{mx}(x)dx$
$S_{D_{30}mnkl}$	$=\int_0^L D_{30}(x)\phi_{nx}(x)\phi_{kx}(x)\phi_{lx}(x)\phi_{mx}(x)dx$	$S_{I_p mnkl}$	$=\int_0^L I_p(x)\phi_{nx}(x)\phi_{kx}(x)\phi_{lx}(x)\phi_{mx}(x)dx$
S'_{D_1mnkl}	$=\int_0^L D_1(x)\phi_{nxx}(x)\phi_{kx}(x)\phi_{lx}(x)\phi_{mx}(x)dx$	S'_{D_9mnkl}	$=\int_0^L D_9(x)\phi_{nxx}(x)\phi_{kx}(x)\phi_{lx}(x)\phi_{mx}(x)dx$
$S'_{D_{11}mnkl}$	$=\int_0^L D_{11}(x)\phi_{nxx}(x)\phi_{kx}(x)\phi_{lx}(x)\phi_{mx}(x)dx$	$S'_{D_{22}mnkl}$	$=\int_0^L D_{22}(x)\phi_{nxx}(x)\phi_{kx}(x)\phi_{lx}(x)\phi_{mx}(x)dx$
$S'_{D_{24}mnkl}$	$=\int_0^L D_{24}(x)\phi_{nxx}(x)\phi_{kx}(x)\phi_{lx}(x)\phi_{mx}(x)dx$	$S'_{D_{28}mnkl}$	$=\int_0^L D_{28}(x)\phi_{nxx}(x)\phi_{kx}(x)\phi_{lx}(x)\phi_{mx}(x)dx$
S''_{D_2mnkl}	$=\int_0^L D_2(x)\phi_{nxx}(x)\phi_{kxx}(x)\phi_{lx}(x)\phi_{mx}(x)dx$	$S''_{D_{10}mnkl}$	$=\int_0^L D_{10}(x)\phi_{nxx}(x)\phi_{kxx}(x)\phi_{lx}(x)\phi_{mx}(x)dx$
$S''_{D_{23}mnkl}$	$=\int_0^L D_{23}(x)\phi_{nxx}(x)\phi_{kxx}(x)\phi_{lx}(x)\phi_{mx}(x)dx$	$S''_{D_{29}mnkl}$	$=\int_0^L D_{29}(x)\phi_{nxx}(x)\phi_{kxx}(x)\phi_{lx}(x)\phi_{mx}(x)dx$
S'''_{D_3mnkl}	$=\int_0^L D_3(x)\phi_{nxx}(x)\phi_{kxx}(x)\phi_{lxx}(x)\phi_{mx}(x)dx$	$S'''_{D_{25}mnkl}$	$=\int_0^L D_{25}(x)\phi_{nxx}(x)\phi_{kxx}(x)\phi_{lxx}(x)\phi_{mx}(x)dx$
S''''_{D_4mnkl}	$=\int_0^L D_4(x)\phi_{nxx}(x)\phi_{kxx}(x)\phi_{lxx}(x)\phi_{mxx}(x)dx$	S_{xMmn}	$=\int_0^L xm(x)\phi_{nx}(x)\phi_{mx}(x)dx$
$S_{xy_\alpha Mmn}$	$=\int_0^L xm(x)y_\alpha(x)\phi_{nx}(x)\phi_{mx}(x)dx$	$S_{xz_\alpha Mmn}$	$=\int_0^L xm(x)z_\alpha(x)\phi_{nx}(x)\phi_{mx}(x)dx$

REFERENCES

[1] Zayas, J., Technology Innovation for Wind Energy: Carbon Fiber. Sandia National Laborateries.

[2] Rand, J., Wind Turbine Blade Design. KidWind project.

[3] Thomsen, O. T., Sandwich Materials for Wind Turbine Blades- Present and Future. Journal of Sandwich Structures and Materials 2009.

[4] Layton, J., Turbine Aerodynamics. How Stuff Works, 2006.

*[5] Griffin, D. A., Infused Carbon Fiber Spar Demonstration in Megawatt-Scale Wind Turbine Blades. . SAMPE, 2009. **45**(5).*

[6] Langtangen, H. P., A. T., Advanced Topics in a Computational Partial Differential Equations.

*[7] Jureczko, M., Pawlak, M., and Mezyk, A., Optimization of wind turbine blades. Journal of Materials Processing Technology, 2005. **167**: p. PP 463-471.*

[8] Ingram, G., Wind Turbine Blade Analysis using the Blade Element Momentum Method. 2005.

[9] Bisplinghoff, R. L., Ashley, H., and Halfman, R. L., Aeroelasticity. 1955: Dover.

[10] Veers, P., Bir, G., and Lobitz, D., Aeroelastic Tailoring in Wind turbine Blade Applications. 1998.

[11] Campos, T. S., Fernando, S., and Piggot, H., Wind rotor blade construction (Small Wind Systems for Battery Charging). Department for International Development, UK, 2001.

*[12] Xu, X. S., Wu, X. Z., and Zhang, H. W., The Saint-Venant problem and principle in elasticity. International Journal of Solids and Structures 1997. **34**(22): p. 2815–2827.*

[13] Sokolnikoff, I. S., Mathematical Theory of Elasticity. 1956: McGraw- HillBook Company.

[14] Timoshenko, G., Theory of Elasticity. McGraw-Hill, New York.

[15] Young, W. C., Roark's Formulas for Stress & Strain. 1989: McGraw-Hill, USA.

[16] Herrera, A. N., and J. M., Torsional rigidity of non-circular bars in mechanisms and machines. 2004.

*[17] Rosen, A., Structural and dynamic behaviour of pretwisted rods and beams. Applied Mechanics Review 1991. **44**(12): p. 483–515*

*[18] Carnegie, W., Vibration of pre-twisted cantilever blading allowing for rotary inertia and shear deflection. Journal of, Mechanical Engineering Science 1964. **6**: p. 105–109.*

[19] Yardimoglu, B, and T. Y., Finite element model for vibration analysis of pre-twisted Timoshenko beam. 2003.

[20] Kaya, M. O., and Ozgumus, O. O., Flexural–torsional-coupled vibration analysis of axially loaded closed-section composite Timoshenko beam by using DTM. 2007.

[21] Ozgumus, O. O., and Kaya, M. O., Energy expressions and free vibration analysis of a rotating double tapered Timoshenko beam featuring bending-torsion coupling. 2007.

[22] Kuang- Chen Liu, J. F., Leslie Yeo, The axial–torsional vibration of pretwisted beams. 2008.

[23] Amabili, M., Non-linear vibrations of doubly curved shallowshells. 2004.

[24] Subrahmanyam, K. B., S. V. K., and .J.S.R., Coupled bending-torsion vibrations of rotating blades of asymmetric aerofoil cross section with allowance for shear deflection and rotary inertia by use of the Reissner method. 1980.

[25] Fung, Y. C., Foundations of Solid Mechanics. 1965: Prentice-Hall, Englewood Cliffs NJ.

[26] Shames, I. H., and C. L. D., Solid Mechanics: A variational Approach. 1973: , McGraw-Hill, New York.

[27] *Habali, S. M., and Saleh, I. A. , Local design, testing and manufacturing of small mixed airfoil wind turbine blades of glass fiber reinforced plastics. Part I: Design of the blade and root. 1999.*

[28] *Younsi, R., El-Batanony, I., Tritsch, J. B., Naji, H., and Landjerit, B., Dynamic study of a wind turbine blade with horizontal axis. 2000.*

[29] *Pournaras, C., V. R., and Kladas, A., Dynamic wind turbine model including blade oscillation effects for control strategy enabling mechanical stress reduction*

[30] *Svacek, P., M. F., and Horacek, J., Numerical simulation of flow induced airfoil vibrations with large amplitudes. 2006.*

[31] *(Submitted) Mohammad , F.M., and Ayorinde, E. , Linear Dynamic Study of a Wind Turbine Blade Considering Airfoil Warping and All Aeroelastic Load Couplings. 2012.*

[32] *Anderson, R. A., Flexural vibrations in uniform beams according to the Timoshenko theory. Journal of Applied Mechanics 1953.* ***20****: p. 504–510.*

[33] *Carnegie, W., Vibration of pre-twisted cantilever blading. Proceedings of the Institution of Mechanical Engineers, 1959.* ***173****: p. 343–374.*

[34] *Dawson, B., N. G. G., Carnegie, W., Effect of slenderness ratio on the natural frequencies of pre-twisted cantilever beams of uniform rectangular cross-section. Journal of Mechanical Engineering Science 1971.* ***13****: p. 51–59.*

[35] *Carnegie, W., J. T., The effects of shear deformation and rotary inertia on the lateral frequencies of cantilever beams in bending. Journal of Engineering for Industry Transactions of the American Society of Mechanical Engineers 1972.* ***94****: p. 267–278.*

[36] *Nam-II Kima, C. C. F., Moon-Young Kim, Stiffness matrices for flexural–torsional/lateral buckling and vibration analysis of thin-walled beam. 2006.*

[37] *Banerjee, J. R., Free vibration analysis of a twisted beam using the dynamic stiffness method. 2001.*

[38] Banerjee, J. R., Development of an exact dynamic stiffness matrix for free vibration analysis of a twisted Timoshenko beam. 2002.

[39] Williams, J. R. B., and F. W., Coupled bending-torsional dynamic stiffness matrix of an axially loaded Timoshenko beam element. 1993.

[40] Subrahmanyam, K. B., S. V. K., and J. S. R., Coupled bending-bending vibrations of pretwisted cantilever blading allowing for shear deflection and rotary inertia by the Reissner method. 1981.

[41] Rao, K. B. S., and J. S., Coupled bending-bending vibrations of pretwisted tapered cantilver beams treated by the Reissner method. 1981.

[42] Chu, C., The effect of initial twist on the torsional rigidity of thin prismatical bars and tubular members. Proceedings of the First US National Congress of Applied Mechanics, 1951: p. 265–269.

*[43] Rosen, A., The effect of initial twist on the torsional rigidity of beams- another point of view. Journal of Applied Mechanics 1980. **47** p. 389–392.*

*[44] Rosen, A., Theoretical and experimental investigation of the nonlinear torsion and extension of initially twisted bars. Journal of Applied Mechanics 1983. **50**: p. 321–326.*

*[45] Hodges, A. H., Torsion of pretwisted beams due to axial loading. Journal of Applied Mechanics 1980. **47**: p. 393–397.*

*[46] Krenk, S., A linear theory for pretwisted elastic beams. Journal of Applied Mechanics, 1983. **50**: p. 137–142.*

*[47] Tsuiji, T., Free vibrations of thin-walled pretwisted beams. Bulletin of JSME 1985. **28**(239): p. 894–898.*

[48] Bathe, K. J., Finite Element Procedures. 1982.

[49] Subbaraj, K., and M. A. D., A survey of direct time-integration methods in computational structural dynamics. 1988.

[50] Panda, S. K., and B. N. S., Nonlinear free vibration of spherical shell panel using higher order shear deformation theory – A finite element approach.

[51] Eisley, J. G., Nonlinear Vibration of Beams and Rectangular Plates.

[52] Subbaraj, K., and Dokainish, M. A., A survey of direct time-integration methods in computational structural dynamics-I. Explicit methods. . 1988.

[53] Remseth, S. N., Non linear static and dynamic analysis of framed structures. 1979.

[54] Dokainish, M. A., and Subbaraj, K., A Survey of direct time integration methods in computational structural dynamics-I Explicit methods. Computational Structures, 1989. ***32****.*

[55] Subbaraj, K., and Dokainish, M. A., A survey of direct time-integration methods in computational structural dynamics-III. Recent developments in implicit methods. Computational Structures.

[56] Subbaraj, K., and Dokainish, M. A., A survey of direct time-integration methods in computational structural dynamics-IV. Mixed implicit-explicit methods and operator-splitting methods. Computational Structural.

[57] Katona, M. G., and Zienkiewicz, A unified set of unit step algorithms- Part3: the beta-m method, a presentation of the Newmark scheme. International Journal of Numerical Methods, 1985. ***21****(345-1359).*

[58] Penry, S.N., and Wood, W. L., Comparison of some single step methods for the numerical solution of the structural dynamic equation. International Journal of Numerical Methods, 1985. ***21****(1941-1955).*

[59] Thomas, R. M., Properties and extensions of a single atep algorithm for dynamic problem. 1982.

[60] Wood, W. L., Aunified set of single step algorithms-Part 2: theory. 1984.

[61] Zienkiewicz, O. C., Wood, W. L., and Taylor, R. L. , An alternative single step algorithm for dynamic problems. 1980.

[62] Zienkiewicz, O. C., Wood, W. L., and Hine, N. W., and Taylor, R. L. , A unified set of single step algorithms. Part 1: general formulation and applications. 1984.

[63] Subbaraj, K., and Dokainish, M. A., A Survey of Direct Time-Integration Methods in Computational Structural Dynamics-II Imlicit Methods. 1988.

[64] Newmark, N. M., A method of computation for structural dynamics. Journal of Engineering Mechanics, 1949.

[65] Warburton, G. R., Some recent advances in structural vibrations. In. Vibrations of Engineering Structures, Lecture Notes in Engineering, No. 10, Springer, Berlin, 1985.

*[66] Chan, S. P., Cox, H. L., and Benfield, W. A., Transient analysis of forced vibrations of complex structural mechanical systems. J. R. Aeronaut Soc., 1962. **66**(457-460).*

*[67] Zienkiewicz, O. C., A new look at the Newmark, Houbolt and other time stepping formulae, a weighted residual approach. Earthq. Enging. Struct. Dyn., 1977. **5**(413-418).*

[68] Chaix, M., and Leleus, F., France Private communication to O. C. Zienkiewicz. 1975.

*[69] Goudreau, G. L., and Taylor, R. L., Evaluation of numerical integration methods in elastodynamics Computational Methods applications, Mechanical Engineering, 1972. **2**(69-97).*

*[70] Gladwell, I., and Thomas, R. M., Stability properties of the Newmark, Houbolt and Wilson-θ methods. . International Journal of Numerical Methods, 1980. **4**: p. 143-158.*

*[71] Hughes, T. J. R., A note on the stability of Newmark's algorithm in nonlinear structural dynamics. Intrnational Journal for Numerical Methods in Engineering, 1977. **11**(2): p. 383-386.*

[72] Brown, J. M. B., The discretization error of Newmark's method for numerical integration in structural dynamics. Earthquake Engineering & Structural Dynamics, 1985. ***13****(1): p. 43-51.*

[73] Hilber, H. M., Hughes, T. J. R., and Taylor, R. L., Improved numerical dissipation for time integration algorithms in structural dynamics. Earthquake Engineering & Structural Dynamics, 1977. ***5****: p. 283-292.*

[74] Kneg, R. D., and Key, S. W., Transient shell response by numerical time integration. International Journal for Numerical Methods in Engineering, 1973. ***17****: p. 273-286.*

[75] Kneg, R. D., Unconditional stability in numerical time integration methods. Journal of Applied Mechanics, 1973. ***40****: p. 417-420.*

[76] Saleh, T., and R. A. M., Water pumping from deep wells by using Aeroman 16th international Snnenforum, 1988.

[77] Stoddard, F. S., Structural dynamics, stability and control of high aspect ratio wind turbine generators.

[78] Stoddard, D. M. E., and F. S., Wind turbine engineering design.

[79] Author: Stiesdal, H., L.-O. P., and C. N., Translation: Furze, J., and Piggott H., The Wind Turbine Components and Operation.

[80] Habali, S. M., and Saleh, I. A., Local design, testing and manufacturing of small mixed airfoil wind turbine blades of glass fiber reinforced plastics. Part II: Manufacturing of the blade and rotor. 1999.

[81] wikipedia.org.

[82] Soviet Ultralight and Homebuilt Aircraft Website.

[83] Hoffmann, M. J., Ramsay, R. Reuss, and Gregorek, G. M., Effects of Grit Roughness and Pitch Oscillations on the NACA 4415 Airfoil. 1996.

[84] UIUC Applied Aerodynamics Group, Department of Aerospace Engineering, UIUC Airfoil Data Site, UIUC Airfoil Coordinates Database Web site.

[85] Somers, D. M., Design and Experimental Results for the S809 Airfoil, Airfoils, Incorporated, State College, Pennsylvania. 1997.

[86] Delft University of Technology Low Speed Laboratory low-turbulence wind tunnel data.

[87] Simms, D. S. S., Hand M., and Fingersh, L. J., NREL Unsteady Aerodynamics Experiment in the NASA-Ames Wind Tunnel: A Comparison of Predictions to Measurements. 2001.

[88] V Ol, M., Bernal, L., Kang, C.-K., and Shyy, W., Shallow and deep dynamic stall for flapping low Reynolds number airfoils. 2009.

*[89] Carnegie, W., Vibrations of rotating cantilever blading: theoritical approaches to the frequency problem based on energy methods. Journal of Mechanical Engineering Science, 1959. **1**: p. 235-240.*

ABSTRACT

LINEAR AND NON-LINEAR DEFORMATIONS OF A WIND TURBINE BLADE CONSIDERING WARPING AND ALL AEROELASTIC LOAD COUPLINGS

by

FOUAD MOHAMMAD MOHAMMAD

May 2012

Advisor: Dr. Emmanuel Ayorinde

Major: Mechanical Engineering

Degree: Doctor of Philosophy

The structural dynamics behavior of the blade of a horizontal axis wind turbine that reacts to the different components of the aerodynamic loading were studied by many researchers using different approaches and assumptions. In the present research, the author considered all the extensional, torsional and flexural loadings acting on the blade with their couplings, variable airfoil cross sections with warping effects, shear deflection, rotary inertia and with or without blade's pretwist for both the linear small deformation case and the nonlinear large deformation case. To the best knowledge of the author the simultaneous inclusion of all these factors has not been done before. The "assumed modes method" was used, in which displacements are assumed to be an expansion of products of time-step dependent constants and polynomial functions of x (where x is the coordinate along the length of the blade) that satisfy the boundary conditions at the fixed end where x=0 (hub of the blade) and at the free end where x=L (tip of the blade). The mass matrix, linear and nonlinear stiffness matrices and the load vector (function of time step) of the dynamic equations of motion are deduced from the Lagrange equations of motion that were derived step by step. The steps of the linear and nonlinear Newmark implicit iteration schemes used for solving the linear and nonlinear dynamic equations of motion respectively were explained in detail. Numerical implementation examples for both linear and nonlinear cases were demonstrated for a 14m long blade with and without pretwisting that has specific

material and geometrical properties and a decreasing NACA4415 airfoil cross section from hub to tip. For both of the linear and nonlinear examples, the aerodynamic loadings (lift, drag and pitch moment) and the nonlinear stiffness matrices were computed at each time step utilizing a time dependent set of parameters such as angle of attack, material and air density, wind and blade speed, flow angle, yaw and pitch angles. Then the unknown displacements u, v and w in the directions of x, y and z axes respectively, the bending rotations θ_1 and θ_2 about the y and z axes respectively and the torsional rotation ϕ about the x axis, were solved using the linear and nonlinear Newmark implicit iteration schemes. The linear case displacement result plots are shown to agree with the work of Younsi et al. The nonlinear case displacement result plots are shown to agree with the Ls-Dyna code.

Keywords: aeroelasticity, Bézier surfaces, gust of wind, Lagrange equations, nonlinear Newmark procedure, wind turbine blade aerodynamic loadings

AUTOBIOGRAPHICAL STATEMENT

Fouad Mohammad Mohammad

CAREER OVERVIEW

- Over 20 years of industrial experience and many years of graduate teaching experience at Wayne State University (WSU) and Gannon University.
- Experienced in many FEA (finite element analysis) and structural optimization codes (linear, nonlinear, static, dynamic, crash and NVH).
- Managed and performed the entire design cycle from specification, development through design, prototype build, test and validation for IC engine components.
- Redesigned, validated and implemented many turbochargers rotary assembly components using Six Sigma, FEA, fatigue and fracture of material root cause analysis.
- Experienced in diesel and gasoline engine emissions and combustion flame simulation using Star CD CFD (computational fluid dynamics).
- Experienced in wind turbine blade research in the area of aerodynamic loading, composite material, implicit and explicit numerical methods, vibration, frequency and stress analysis where I created my own code and compared with Radioss (Block), Ls-Dyna results and other published models.

EDUCATION

Wayne State University, Detroit, MI
Ph.D. Candidate, Mechanical Engineering (Graduated on May 7th, 2012)

Case Western Reserve University, Cleveland, OH
Ph.D. Candidate, Mechanical & Aerospace Engineering, Jan. 2007-Dec. 2008
- Transferred course credits to WSU due to relocation

Wayne State University, Detroit, MI
MS, Mechanical Engineering, May 2005

American University of Beirut, Beirut, Lebanon
BS, Mechanical Engineering, August 1990

Laurier-McDonald Vocational Automotive, Montreal, QC
Diploma, Automotive Specialty Mechatronics, February 1997

EXPERIENCE

Part Time Faculty Member, Wayne State University, Detroit, MI, since Jan. 2012
- Teach Finite Element Methods #2 (ME 7020)

Computer Lab Instructor, Wayne State University, Detroit, MI, Jan. 2010 – May 2011
- Taught Hypermesh/Optistruct/Nastran for Finite Element Methods #1 (ME 5040)

Adjunct Instructor, Gannon University, Erie, PA, Sept. 2007– Dec. 2008
- Taught the following graduate ME courses: Design for Reliability (GENG 621), Engineering Analysis I (GENG 603), Six-Sigma Design (GME 698) and Material Plasticity (GME 643)

Lead Professional Engineer, General Electric (Rail), 2006–2009

Manager, Frank's Auto, 2001–2005

Senior Mechanical Engineer, Canpack Company, 1994–2000

Project Engineer, Moses Cranes and Heavy Equipment, 1991–1993

Mechanical Engineer, Gargour & Sons, (Mercedes Benz), 1989 –1991